BLANK PAGE

CLOSURE ANALYSIS AND TEST STUDY
VOLUME IV

SUBSCALE STATIC TEST REPORT

APPENDIX 2

TECHNICAL REPORT NO. 4171-1
31 JULY 1969

Prepared for

DEPARTMENT OF THE AIR FORCE
SPACE AND MISSILE SYSTEMS ORGANIZATION
AIR FORCE SYSTEMS COMMAND
NORTON AIR FORCE BASE, CALIFORNIA

THE RALPH M. PARSONS COMPANY
ENGINEERS-CONSTRUCTORS
LOS ANGELES
NEW YORK

FOREWORD

This final report, which is composed of Volumes I through VIII, contains the results of a research study conducted by The Ralph M. Parsons Company under the direction of John E. McCarney. The Ralph M. Parsons Company personnel making significant technical contribution to this effort include David M. Hopper, Philip R. Sands, Richard C. Mayer, and Philip Mannes.

The study was performed from 1 June 1967 to 31 July 1969 under Contract No. F04694-67-C-0105 for the Department of the Air Force, Space and Missile Systems Organization (AFSC), Norton Air Force Base, California 92409. The SAMSO project officers were Maj G. W. Barnes, Capt F. G. Harms, and 1st Lt H. S. Yoshioka. The Aerospace Corporation provided systems engineering and technical direction, with Warren Pfefferle acting as Technical Director.

This technical report has been reviewed and is approved.

Charles B. Totten
Acting Chief, Technology Section
Facilities Development Branch

Howard S. Yoshioka
Howard S. Yoshioka, 1st Lt, USAF
Project Officer, Technology Section
Facilities Development Branch

CLOSURE ANALYSIS AND TEST STUDY

INDEX OF VOLUMES

APPENDIX 2

SUBSCALE STATIC TEST REPORT

ABSTRACT

This report describes subscale static tests of composite silo closure and closure support models performed by The Ralph M. Parsons Company as a part of the Closure Analysis and Test Study. A total of 41 tests were performed in two phases. The effect on total load capacity caused by varying a broad range of design parameters including strength and relative thicknesses of steel shell material, span-to-depth ratio, support configuration, and concrete strength were investigated. Closure/closure support combinations with ultimate load capacities ranging from 1000 psi to 23,000 psi were tested.

Manual, empirical and finite-element design and analytical techniques are presented which will yield accurate predictions of the ultimate load capacities of full-scale composite closures.

TABLE OF CONTENTS

LIST OF ILLUSTRATIONS

LIST OF ILLUSTRATIONS
(CONTINUED)

LIST OF ILLUSTRATIONS
(CONTINUED)

LIST OF ILLUSTRATIONS
(CONTINUED)

LIST OF ILLUSTRATIONS
(CONTINUED)

LIST OF ILLUSTRATIONS
(CONTINUED)

LIST OF ILLUSTRATIONS
(CONTINUED)

LIST OF ILLUSTRATIONS
(CONTINUED)

LIST OF ILLUSTRATIONS
(CONTINUED)

LIST OF TABLES

1.0 INTRODUCTION

This report describes subscale static tests of composite silo closure and closure support models performed as a part of the Closure Analysis and Test (CAT) Study by The Ralph M. Parsons Company. A total of 41 tests were performed in two phases. The tests encompassed a broad range of test parameters and variables, at ultimate load capacities ranging from 1,000 to 23,000 psi. The test variables included strength and relative thicknesses of materials; span-to-depth ratios; support stiffness and friction; symmetry; and silo configurations. These variables were applied to both closure and silo support models. The predominant model scale was approximately one to six.

1.1 Background

Prior to initiation of the CAT project, only a limited amount of research had been performed in the study of response characteristics of composite concrete/steel plates. While studies exploring the strength of plain concrete under triaxial load conditions have been performed for many decades, structures had not been tested for the specific purpose of examining these phenomena until very recently. The significant efforts in this area were by the Illinois Institute of Technology Research Institute (IITRI) in 1964 and by the University of Illinois in 1967-1968. These two organizations studied the problems associated with composite closure design and explored the effects of various types of shear reinforcing on the load capacity of small-scale models.

The conclusions drawn by both groups of researchers were similar to the extent that essential agreement existed concerning the influence of the confining steel upon the apparent strength of the composite models. The extent of this influence however was not clearly defined by either effort.

In an earlier related effort, the Armour Research Foundation (ARF) performed a similar series of tests on small-scale composite support structures. Although this was a very limited test effort (three specimens), results indicated clearly that significant increases in load support capacity could be attained by laterally restraining the concrete subjected to high bearing stresses. As in the other two efforts, the conclusions were somewhat qualitative.

1.2 Scope of Analysis and Tests

Recognizing the need for definitive research to advance the technology of hardened construction, and fully aware of the interesting research into composite construction described above, SAMSO/Aerospace outlined a comprehensive and parametric plan to develop empirical design data applicable to advanced missile facility design and construction. This approach was structured (in the contract work statement) to identify the parametric nature of the necessary analytical and experimental work and specified a minimum level of effort. Implicit however was the latitude to restructure the effort to pursue significant findings. That this latitude was exercised on several occasions can be demonstrated by the fact that the proposed level of effort in the area of static tests and analysis was increased threefold following the award of the contract.

The scope of the analysis and test efforts, as amended and redirected, included the following:

a. Perform analyses of all influencing factors and design both silo closure and silo support structure models to fail at assigned loads. These loads were preliminarily established at 4000, 8000, and 12,000 psi and were later expanded to include 20,000 and 30,000 psi.

b. Examine and establish the effects of variations of material strengths on the load capacities of the various structures. Concrete strengths (f'_c) were established at 3000, 6000 and 12,000 psi. Steel strengths (f_y) were established at 36,000, 70,000, 150,000 and 180,000 psi.

c. Examine and establish the influence of steel stiffness (as opposed to strength) upon the load capacity and ductility of the structures.

d. Determine the effects of friction at the closure/support interface; μ values were arbitrarily established at < 0.1, ~ 0.02 and > 0.5. In an effort to separate the effects of friction from the interaction of the closure and the silo, the friction tests were to be performed on a nonyielding (nonsilo) support.

e. Determine the effects of closure/silo support interaction and, if favorable to the gross load capacity, develop designs to ensure this interaction under shock and vibration loads.

f. Examine the effects of structural symmetry in an effort to identify variations in load capacity, response and predictability.

g. Examine thick plate versus thin plate relationships by varying span-to-depth ratios.

h. Examine the influence of relative bearing widths, with the aim of establishing a practical minimum.

i. Examine static and dynamic test results in an effort to establish correlation and to identify (a range of) dynamic load factors.

j. From analysis of the static test results, develop a semi-empirical design technique applicable to full-scale composite structures.

2.0 DESCRIPTION OF TEST HARDWARE AND INSTRUMENTATION

As originally proposed, a maximum of 6000 psi was to have been sufficient for all static tests. At model scales of up to 1/5, this maximum allowed a rather straightforward design solution. During the proposal effort, a test fixture was designed that tested two specimens at a time (Figure 2-1). The specimens were placed back to back and the top surfaces of both were loaded with a flat jack. Reaction loads were taken, through the supports, by opposing platens connected by tie-bolts. While somewhat primitive, this was an adequate and inexpensive solution to the proposed maximum test pressures.

When the maximum test pressure was increased to 12,000 psi following contract award, this design could not be extrapolated, and parametric studies were made to develop an adequate technique. These studies are covered in Appendix 5, Test Hardware Description and Data, and require little elaboration here. As a result of these studies, the test fixture pictured in Figure 2-2

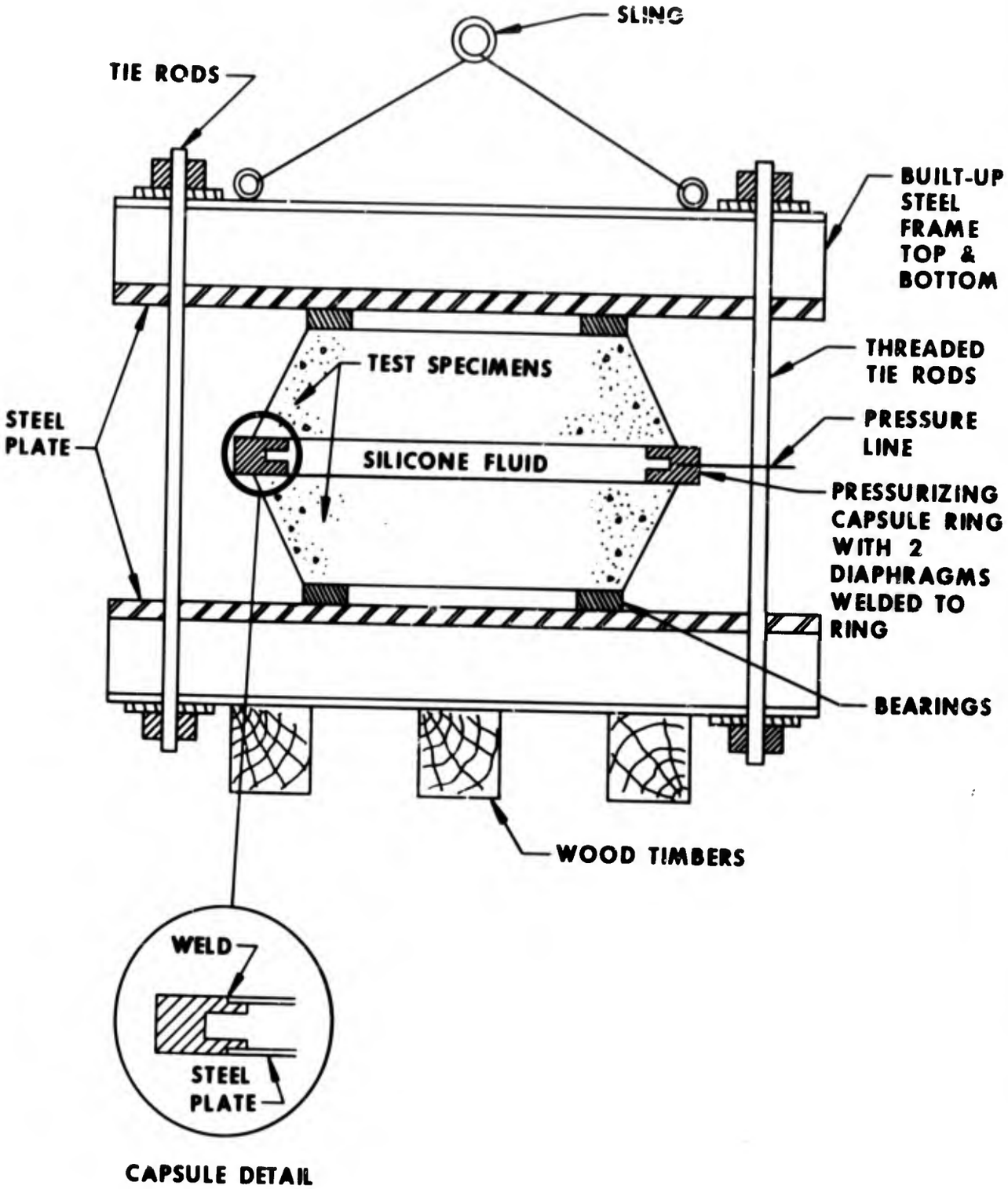

FIGURE 2-1

PROPOSED FIXTURE FOR SUBSCALE STATIC TESTS

and graphically presented in Figure 2-3 was proposed. This fixture develops 12 million pounds of force at 15,000 psi and, with the adapters available, can hydrostatically load a uniaxial test envelope of up to 55 inches diameter by 111 inches high. This diameter could be increased to 65 inches by providing one additional adapter. The fixture was designed and fabricated by Parsons and assembled by Nuclear Weapons Effects Division (NWED) personnel of the Waterways Experiment Station (WES) at Vicksburg, Mississippi. The fixture was installed in the Central Firing System at WES, which has a reaction capacity of approximately 60 million pounds.

As can be seen in Figure 2-3, the test structures were loaded by means of a contained elastomer, pressurized by the large (32-1/4-inch diameter) hydraulic cylinder. Radial forces exerted by the elastomer were resisted by a heavy "T" section ring. The elastomer was sealed against extrusion by means of 3/16-inch-diameter aluminum wire seals placed on each side of the leg of the section. Since the elastomer behaved as a fluid at pressures greater than approximately 100 psi, and was less than 6 percent compressible at 15 ksi, approximately three-eighths of the volume of the 1-inch-thick pad was available to deflect the test structures. This resulted in a centerline deflection capability of approximately 1 inch on the 32-1/4-inch-diameter models, the limiting factor being the complete compression of the seal rings. Naturally, on larger (52-inch diameter) or smaller (12-inch diameter) models, the deflection capability varied proportionally since the seal diameter was 3/16 inch for all models. On the tests with an anticipated ultimate unit

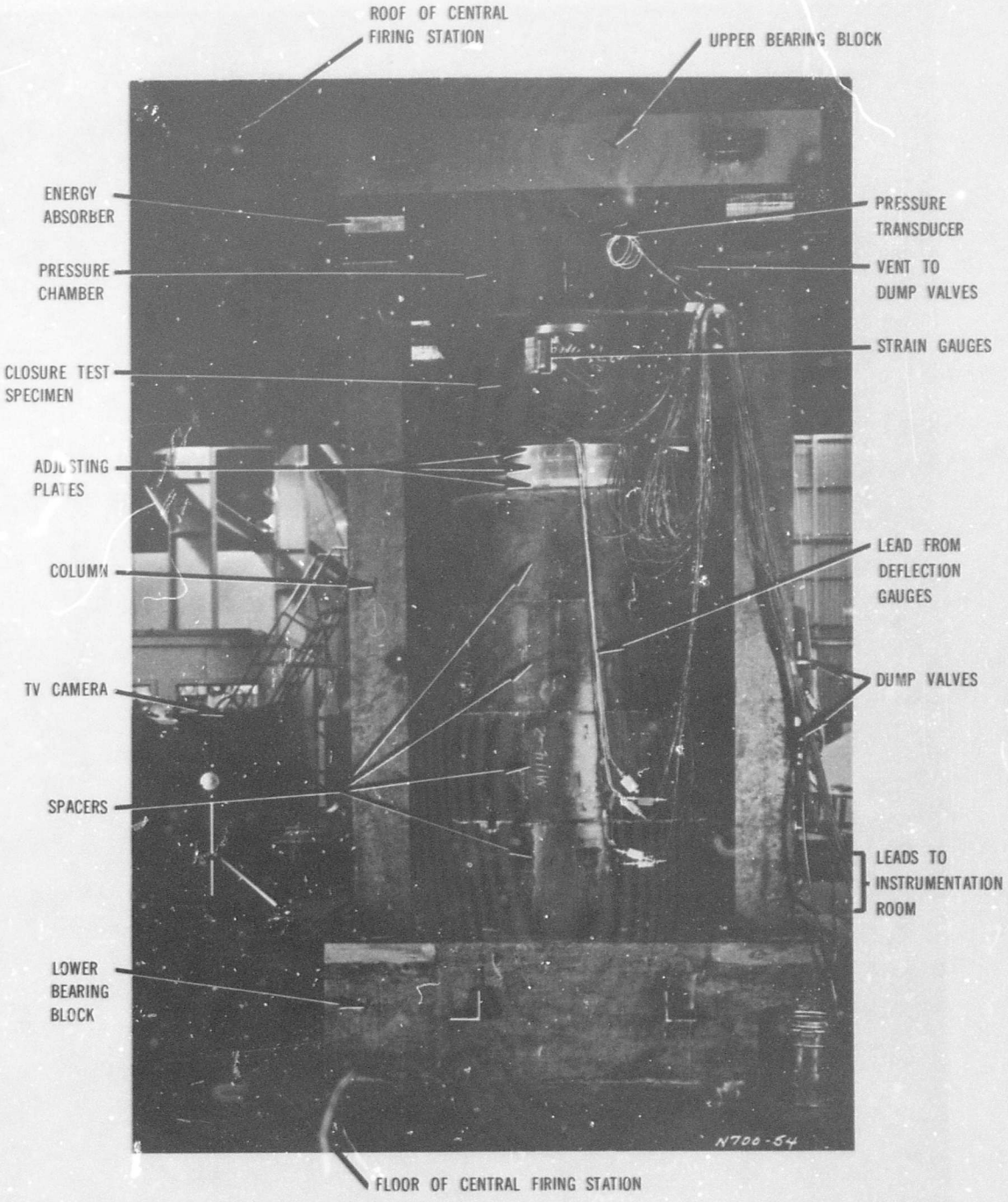

FIGURE 2-2

SUBSCALE STATIC TEST FIXTURE PHASE I ASSEMBLY - FRONT VIEW

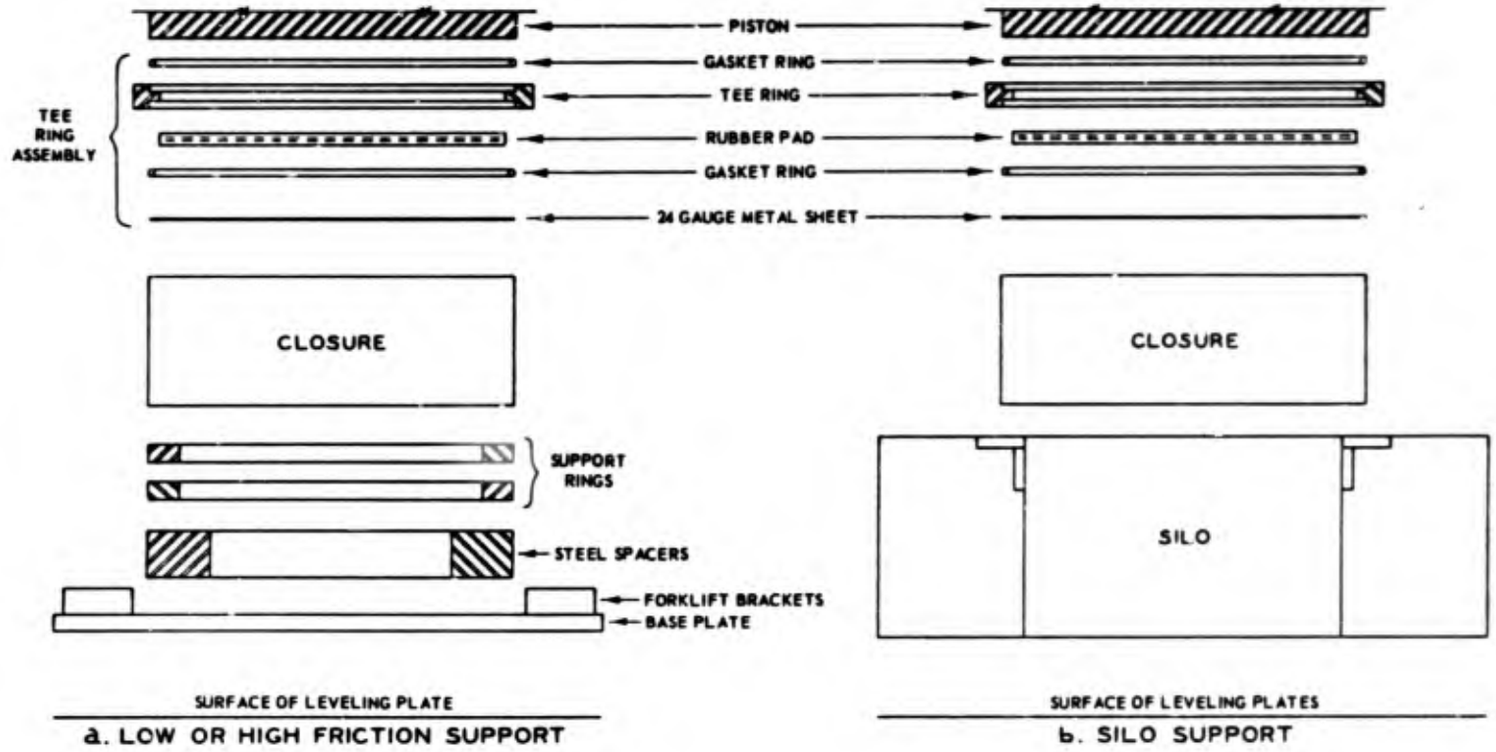

FIGURE 2-3

SCHEMATIC OF TEST ASSEMBLY

load capacity of less than 12,000 psi, full annealed (1100-0) aluminum wire was used for the seals. This wire has a yield strength of 5000 psi and made an excellent seal. At test pressures above 12,000 psi, 1100-H14 wire was used, providing a yield strength of 17,000 psi. Both types of wire were heli-arc welded into continuous rings.

2.1 Instrumentation

Prior to the start of the tests, rather ambitious plans were made concerning the instrumentation to be used. It was hoped that by accumulating masses of strain and deflection data the failure mechanisms of the various models could be pinpointed, aiding in the correlation with the analytical data. Unfortunately, this correlation proved to be no simple task. Three basic factors contribute to the problem: (1) throughout the tests, the quality of the strain data was somewhat suspect, being erratic and in some cases contrary to simple observations; (2) the responses of the various structures were relatively unknown and therefore it was difficult to range the instruments properly; and (3) receipt of the data rather late in the project left insufficient opportunity for a comprehensive evaluation.

However, so that others may benefit from our experience, the instrumentation schemes used in the test project are described following. In the test descriptions (Section 3.0) it will be noted that primary emphasis is placed on the centerline load-deflection curves which proved to be the most useful data collected.

2.1.1 Phase I Instrumentation

Strain Measurements

Table 2-1 gives the number of strain measurements made for each of the first 15 tests (Phase I). The arrangement for the closure models is shown in Figure 2-4. The arrangement for the silo models is shown in Figure 2-5. As shown in these two figures, strain measurements were recorded on the exterior of the steel shell and on 1/4-inch-diameter deformed instrumentation bars placed on the concrete fill.

The strain gauges used in all tests were 120-ohm, epoxy foil backed gauges made by Micro-Measurements, Model No. EA-06-250BG120. These had a length of 1/4 inch and a gauge factor of 2.095. Figure 2-6 shows a typically instrumented closure model being set up for testing.

Deflection Measurements

Model deflections were measured across the closure bottom, vertically at the support bearing, and laterally on the inner silo wall (Figure 2-7). The large gauges shown in the lower photograph are Bourns Model 156 with 2-1/2 inches of travel, and the smaller gauges are Bourns Model 141 with 1/2 inch of travel. Both are linear potentiometers, with the smaller gauge of 5000-ohm resistance and the larger at 10,000 ohm. The gauge shafts were spring-loaded against the test specimen.

Pressure Measurements

Test pressures at the hydraulic cylinder were measured with a 20,000-psi Statham transducer, Model Pa-822-20M. This proved to be an excellent instrument, almost perfectly linear to 10,000 psi, the capacity of the WES

TABLE 2-1

NUMBER AND TYPE OF INSTRUMENTATION CHANNELS

Test No.	Closure	Support	Instrumentation Channels							Total Channels
			Closure			Support			Pressure	
			Strain		Deflection	Strain		Deflection		
			Internals	Externals		Internals	Externals			
1	M120-1A	Low friction	11	14	5	--	--	--	1	31
2	M120-1B	Low friction	--	14	5	--	--	--	2	21
3	M120-2A	Low friction	22	16	5	--	--	--	2	45
4	M120-2B	Low friction	22	16	5	--	--	--	2	45
5	M120-2C	M121-1A	22	16	5	16	14	8	1	82
6	M120-2C	M121-1B	--	16	5	--	14	8	1	44
7	M120-2C	M121-2A	--	16	5	16	14	8	1	60
8	M120-3A	M121-2A	22	16	5	16	14	8	1	82
9	M120-3B	M121-3A	--	16	5	16	14	8	1	60
10	M120-5A	M121-2B	22	16	5	--	14	8	1	66
11	M120-5B	M121-3B	--	--	5	--	10	8	1	24
12	M120-4A	Low friction	29	16	5	--	--	--	1	51
13	M120-5B	Low friction	22	16	5	--	--	--	1	44
14	M120-2D	High friction	22	16	5	--	--	--	1	44
15	M120-4B	High friction	29	16	5	--	6	--	1	57

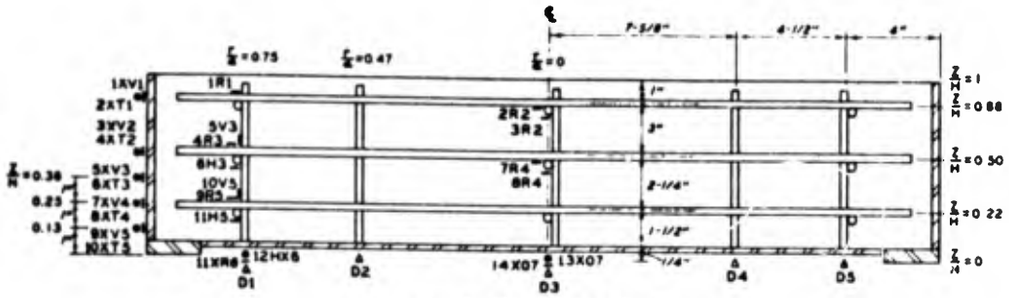

a. CLOSURE M120-1

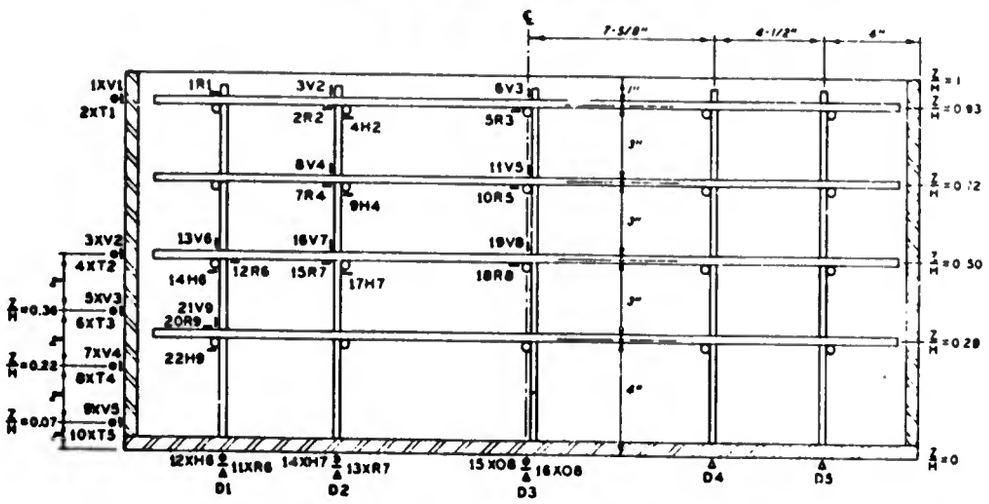

b. CLOSURES M120-2, M120-3 AND M120-5

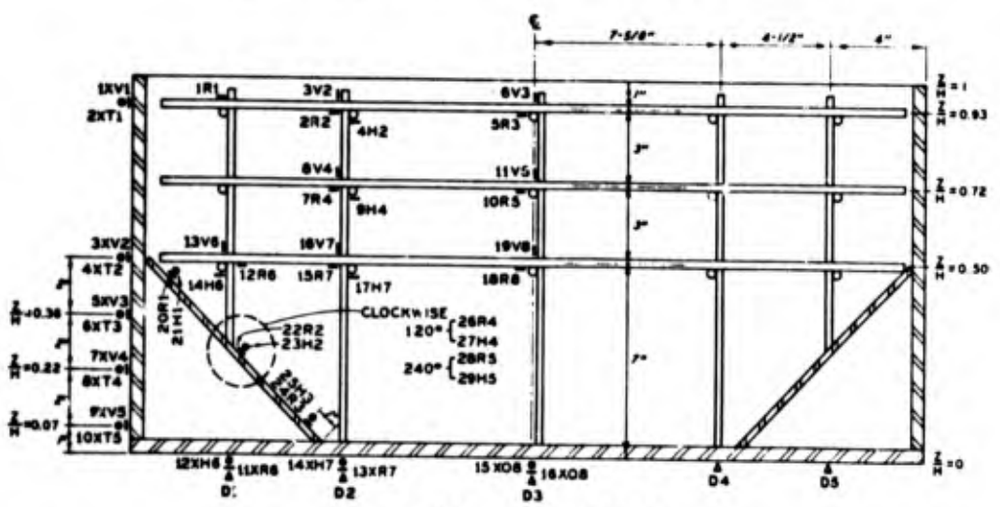

c. CLOSURE M120-4

LEGEND

	SYMBOL		SYMBOL
V - VERTICAL	|	T - TANGENTIAL	•
R - RADIAL	—	X - EXTERNAL	
H - HOOP	—& •	D - DEFLECTION	

FIGURE 2-4

CLOSURE INSTRUMENTATION ARRAY

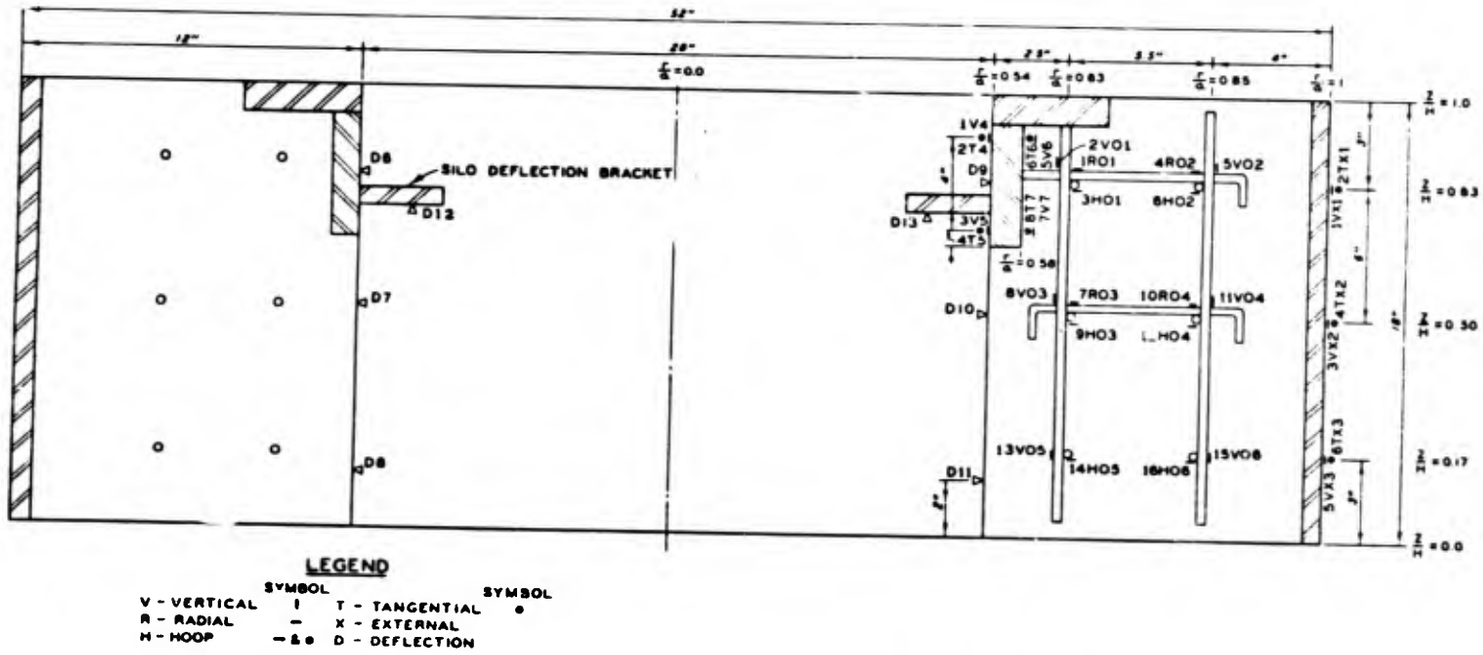

FIGURE 2-5

SILO INSTRUMENTATION ARRAY

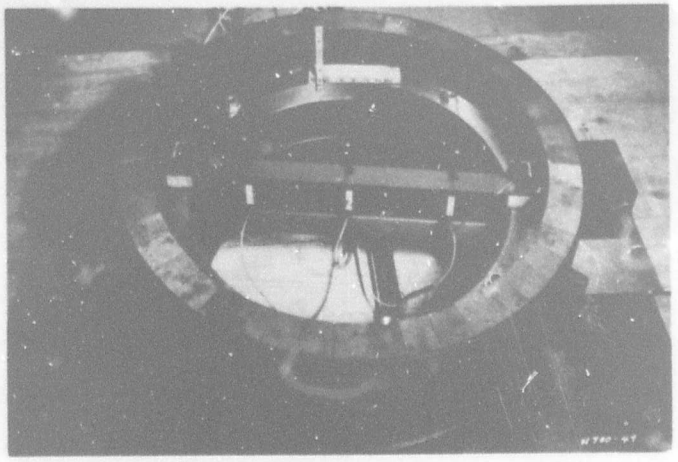

(a) Low-friction segmented support rings

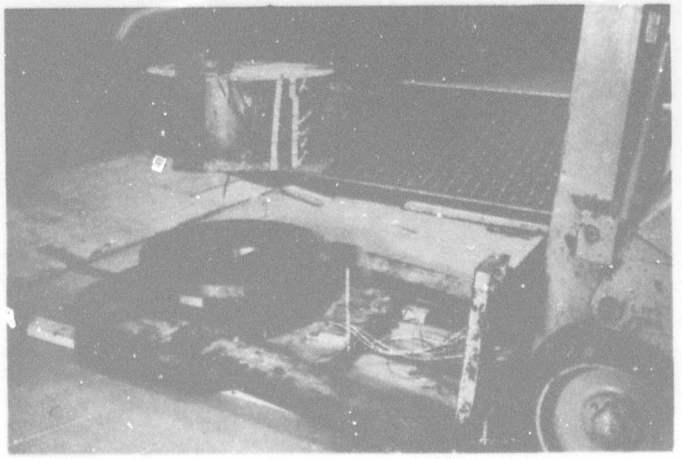

(b) Placement of closure on support

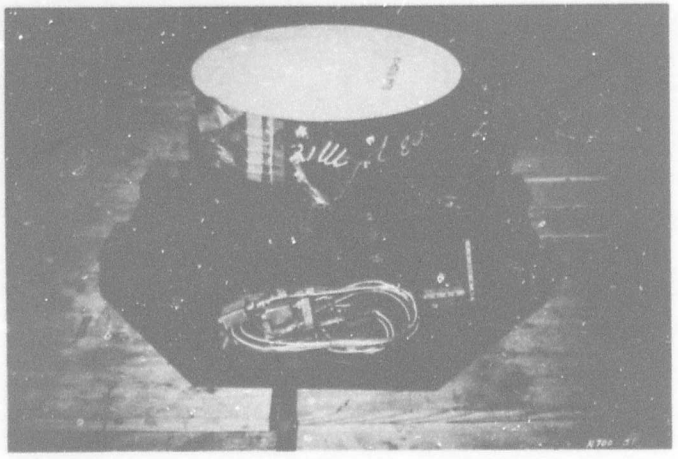

(c) Positioned closure with clamp

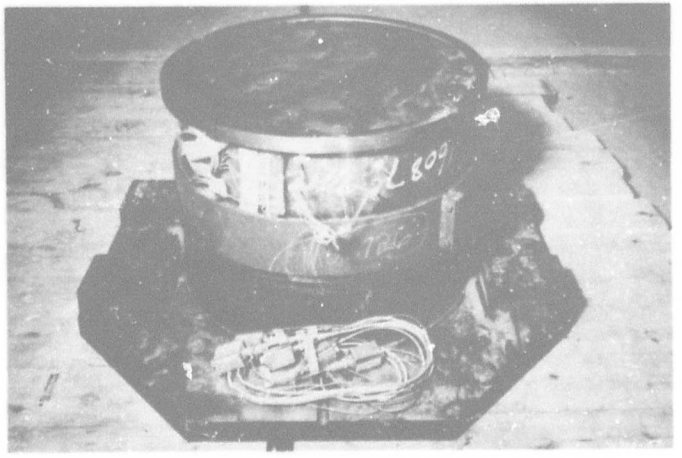

(d) Completed closure setup prior to placement in static test fixture

FIGURE 2-6

LOW-FRICTION SUPPORT TEST SETUP

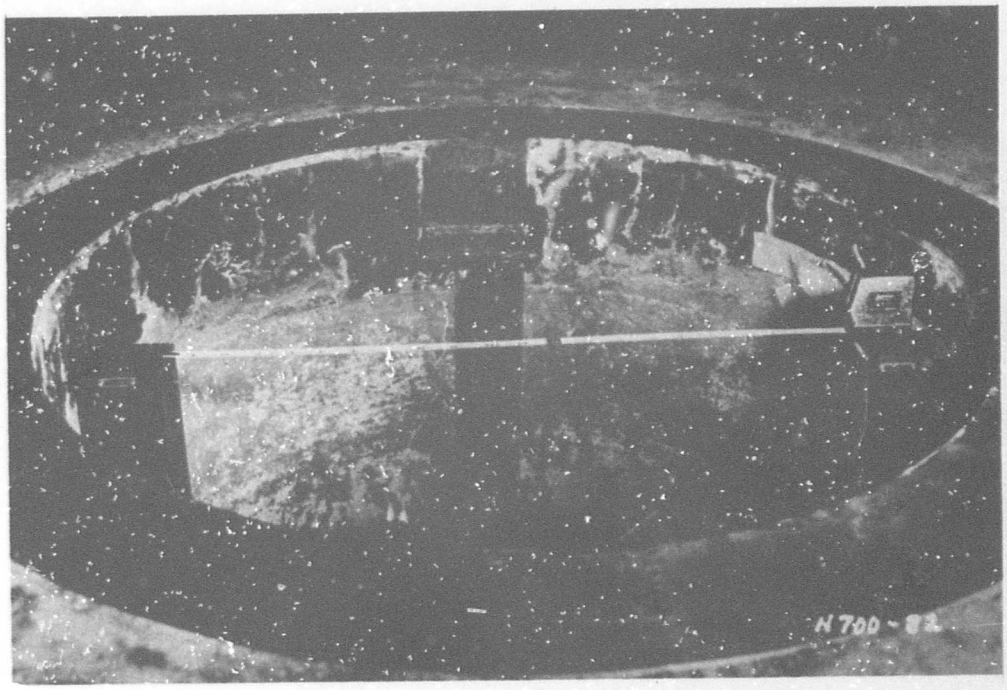

(a) Silo side wall and inner bearing ring

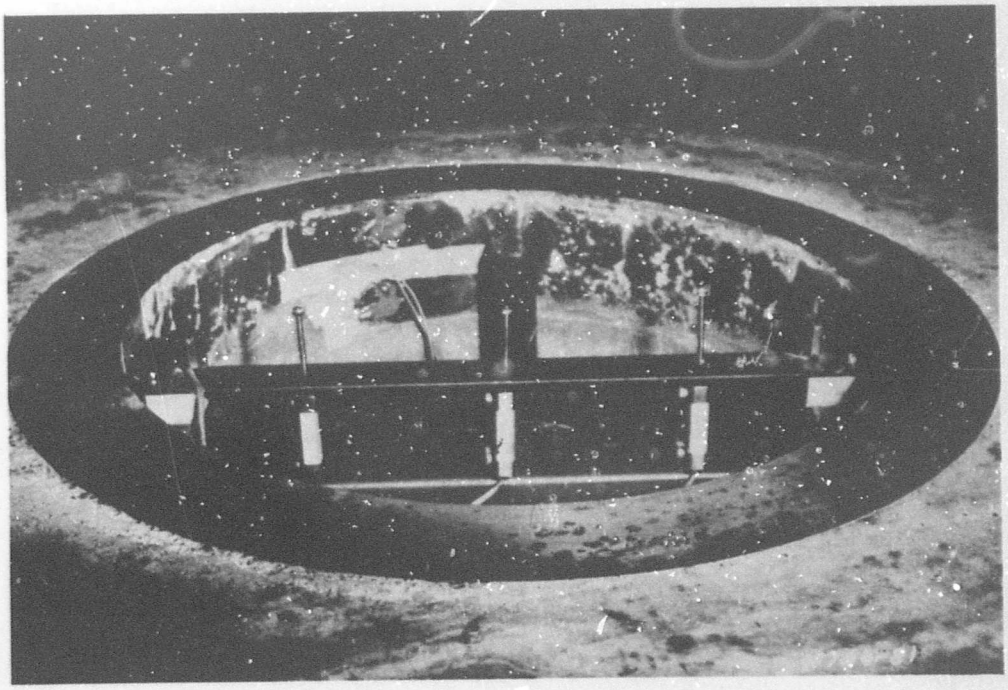

(b) Closure center line

FIGURE 2-7

SILO DEFLECTION GAUGE MOUNTINGS

A2-15

dead-weight tester, and in good agreement with a 20,000-psi bourdon gauge of test quality above 10,000 psi. The bourdon gauge was used in most of the tests to verify the pressure traces read out on an X-Y plotter.

Recording Equipment

Analog test data was recorded on 36-channel CEC oscillographs and/or 14-channel FM tape recorders. Signal conditioning was through SAM and DANA dc amplifiers, coupled with galvo drivers. Quick-look data was recorded on X-Y or X-Y-Y plotters.

2.1.2 Phase II Instrumentation

The pause between the first and second phase tests gave us time to redesign the model instrumentation in an attempt to provide more useful data. The number of internal strain gauges was reduced drastically and the number of deflection measurements was increased (see Table 2-2). Figures 2-8 and 2-9 depict the instrument arrays used in Tests 16 through 31 and Test 34. The arrays for Tests 32, 33, and 35 are shown on Figures 2-10, 2-11 and 2-12, respectively. Closure bottom deflections only were recorded in Tests 36 through 41. All Phase II instrumentation was of the same type as that used for Phase I; the only revision was the redesign of the deflection gauge mounts to facilitate instrumentation setup (Figure 2-13).

In the test descriptions (Section 3), it will be noted that selected data plots have been included for Tests 16 through 35. These plots result directly from the Phase II instrumentation plan and were received from WES in May 1969. Examination of these plots, as time permitted, gave us some

TABLE 2-2

NUMBER AND TYPE OF INSTRUMENTATION CHANNELS

Test No.	Closure	Support	Instrumentation Channels							Total Channels
			Closure			Support			Pressure	
			Strain		Deflection	Strain		Deflection		
			Internals	Externals		Internals	Externals			
16	M120-2a	Low friction	--	14	4	--	--	--	1	19
17	M130-1-7	Low friction	3	14	4	--	--	--	1	22
18	M130-1-6	Low friction	3	14	4	--	--	--	1	22
19	M130-2-2	Low friction	3	14	4	--	--	--	1	22
20	M130-2-1	Low friction	3	14	4	--	--	--	1	22
21	M130-3	Low friction	3	14	4	--	--	--	1	22
22	M130-4	Low friction	3	14	4	--	--	--	1	22
23	M130-7	Low friction	3	14	4	--	--	--	1	22
24	M130-1-3	Low friction	3	14	4	--	--	--	1	22
25	M130-5	Low friction	3	14	4	--	--	--	1	22
26	M133-1	Low friction	3	14	4	--	--	--	1	22
27	M133-2	Low friction	3	14	4	--	--	--	1	22
28	M130-6	Low friction	3	14	4	--	--	--	1	22
29	M130-14	Low friction	2	4	4	--	--	--	1	11
30	M130-13	Low friction	2	4	4	--	--	--	1	11
31	M130-7-1	M131-1	2	4	4	2	8	3	1	24
32	M130-9	M129-0	3	4	4	2	8	3	1	25
33	M130-8	M128-0	3	4	1	2	2	3	1	16
34	M130-7-2	M131-2	2	4	4	2	8	3	1	24
35	M127-0	M127-05	2	4	1	2	8	3	1	21
36	M130-10	M131-4	--	--	1	--	--	1	1	3
37	M130-7-3	M131-3	--	--	1	--	--	1	1	3
38	M130-11	M131-7	--	--	1	--	--	1	1	3
39	M130-12	M131-6	--	--	1	--	--	1	1	3
40	M130-7-6	M131-10	--	--	1	--	--	1	1	3
41	M130-7-5	M131-9	--	--	1	--	--	1	1	3
42	M140-1	High friction	--	--	1	--	--	--	1	2
43	M140-2	High friction	--	--	1	--	--	--	1	2

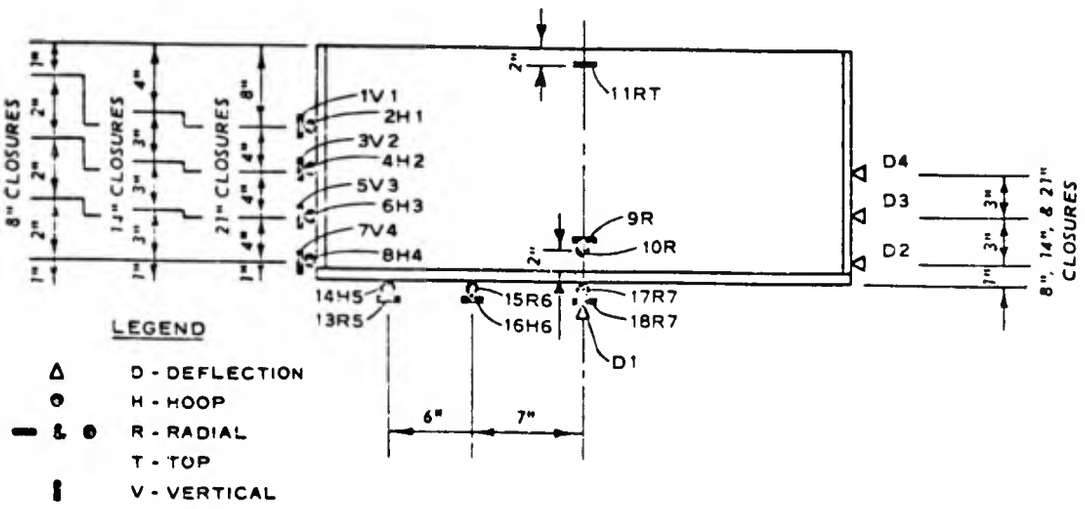

FIGURE 2-8

INSTRUMENTATION ARRAY FOR CLOSURES - TESTS 16 THROUGH 28

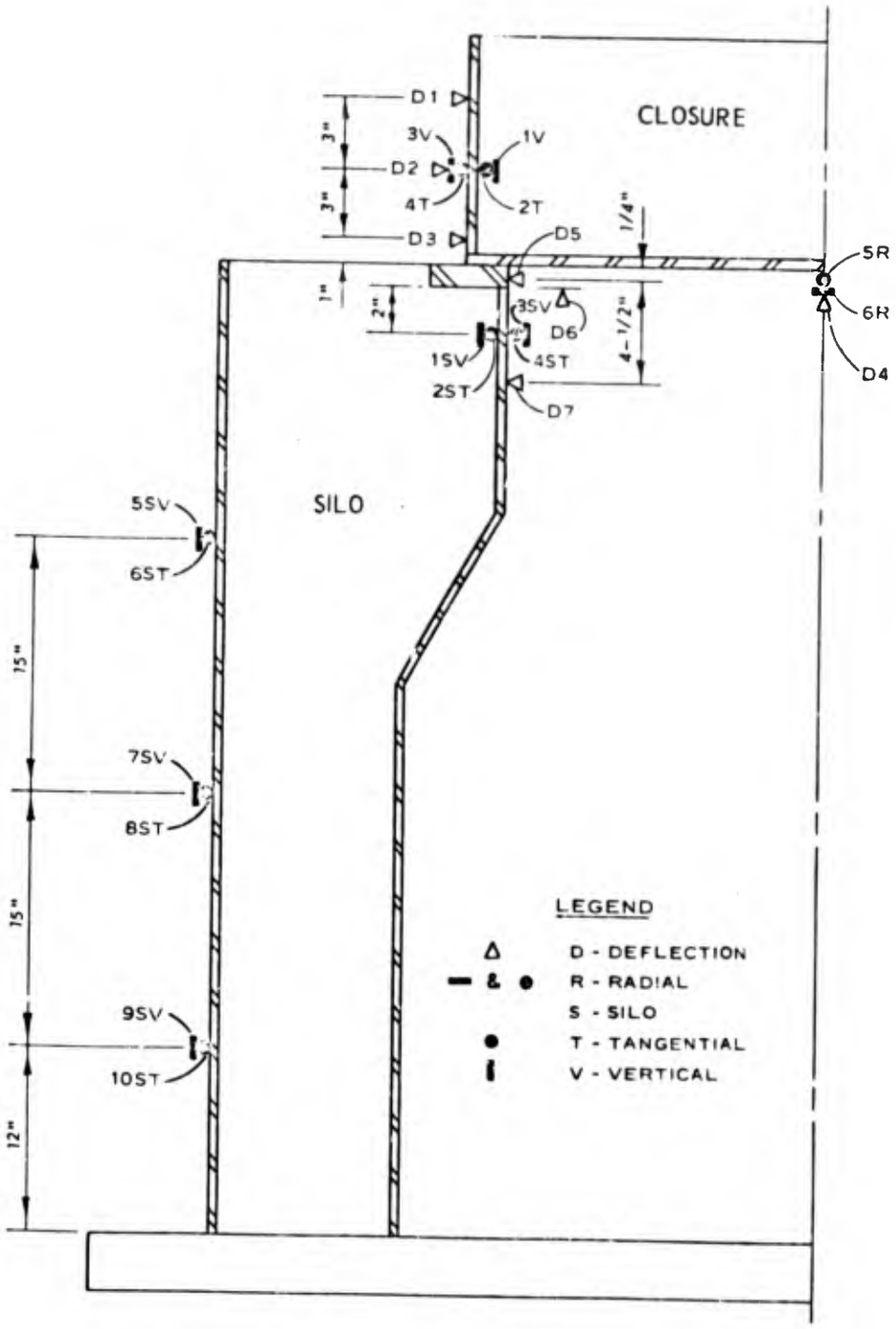

FIGURE 2-9

INSTRUMENTATION ARRAY FOR CLOSURES AND SILOS - TESTS 29,30,31 AND 34

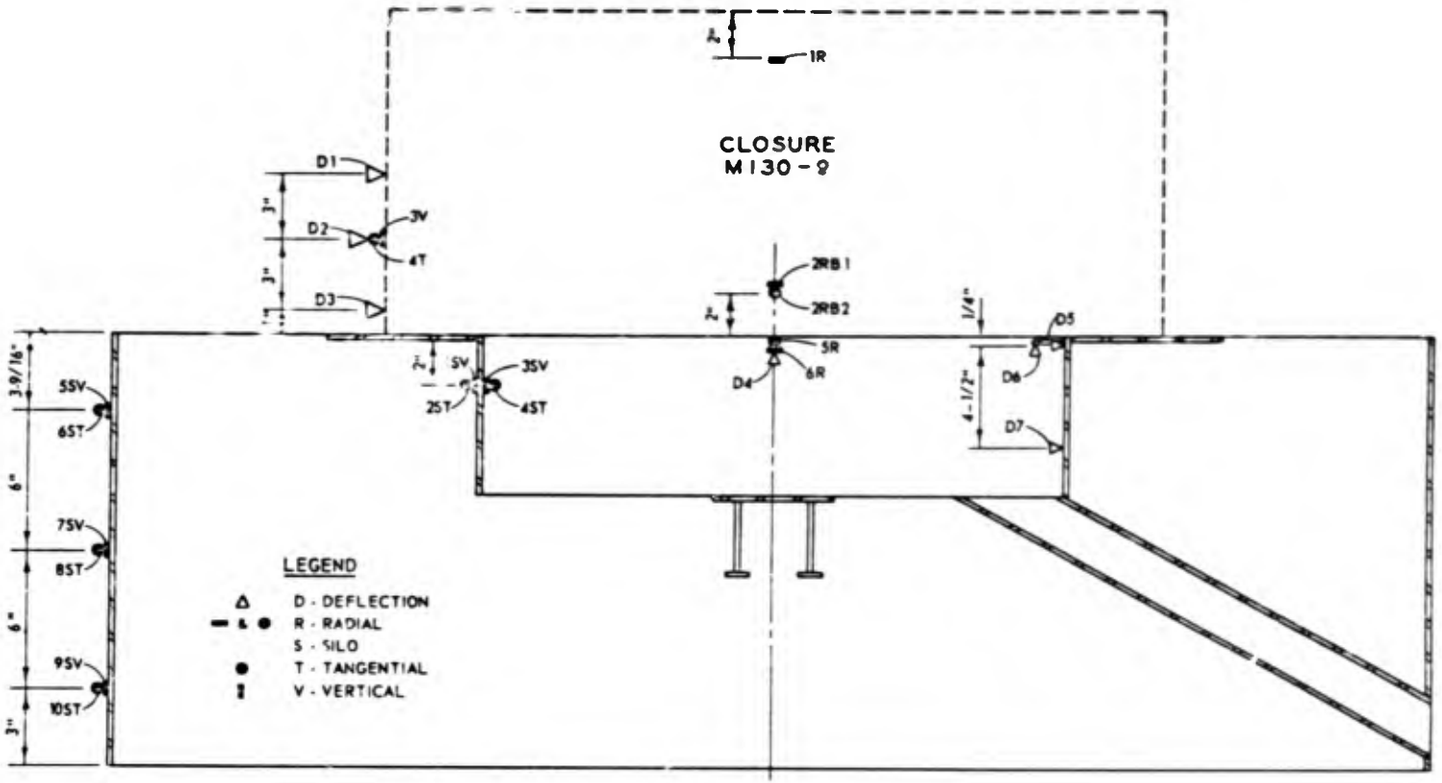

FIGURE 2-10

INSTRUMENTATION ARRAY FOR CLOSURE M130-9 AND SILO M129-0 - TEST 32 (HERCULES)

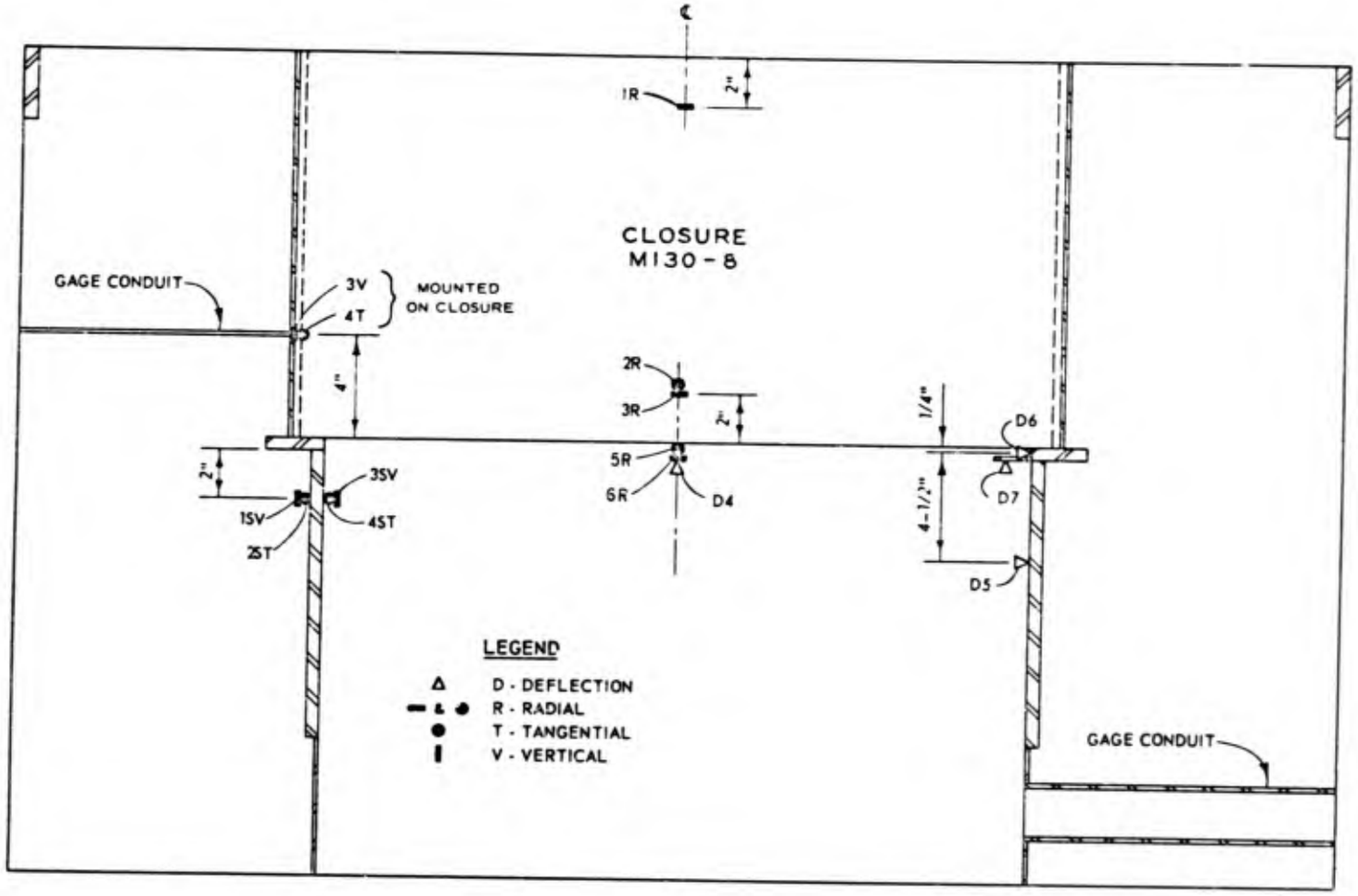

FIGURE 2-11

INSTRUMENTATION ARRAY FOR CLOSURE M130-8 AND SILO M128-0 - TEST 33 (ROCK TEST I)

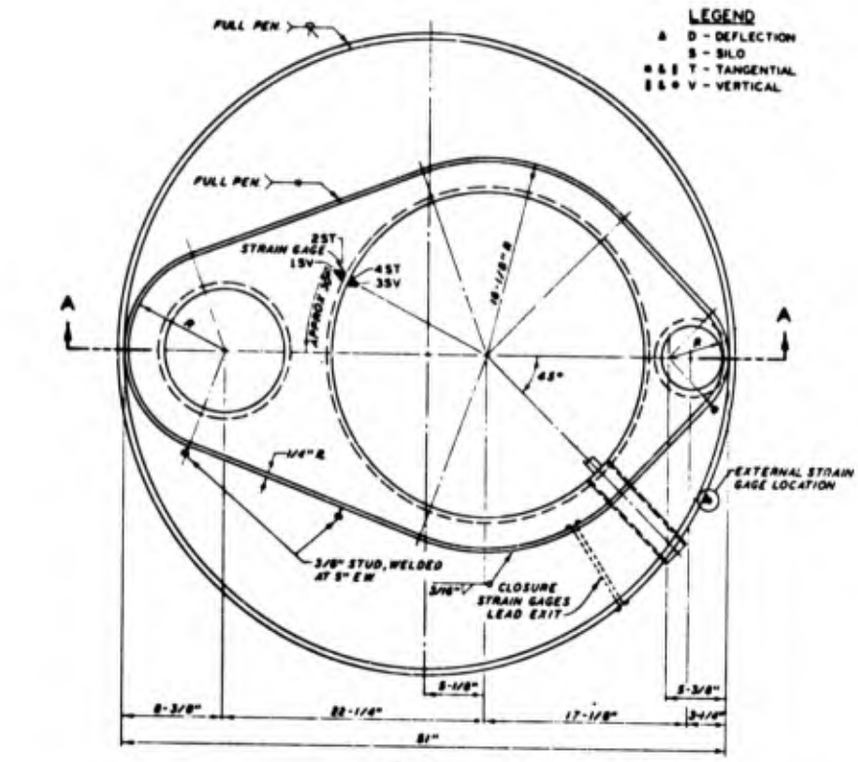

FIGURE 2-12

DESIGN GEOMETRY AND INSTRUMENTATION GAUGE ARRAY FOR SILO M127-OS - TEST 35 (RISE AND ROTATE)

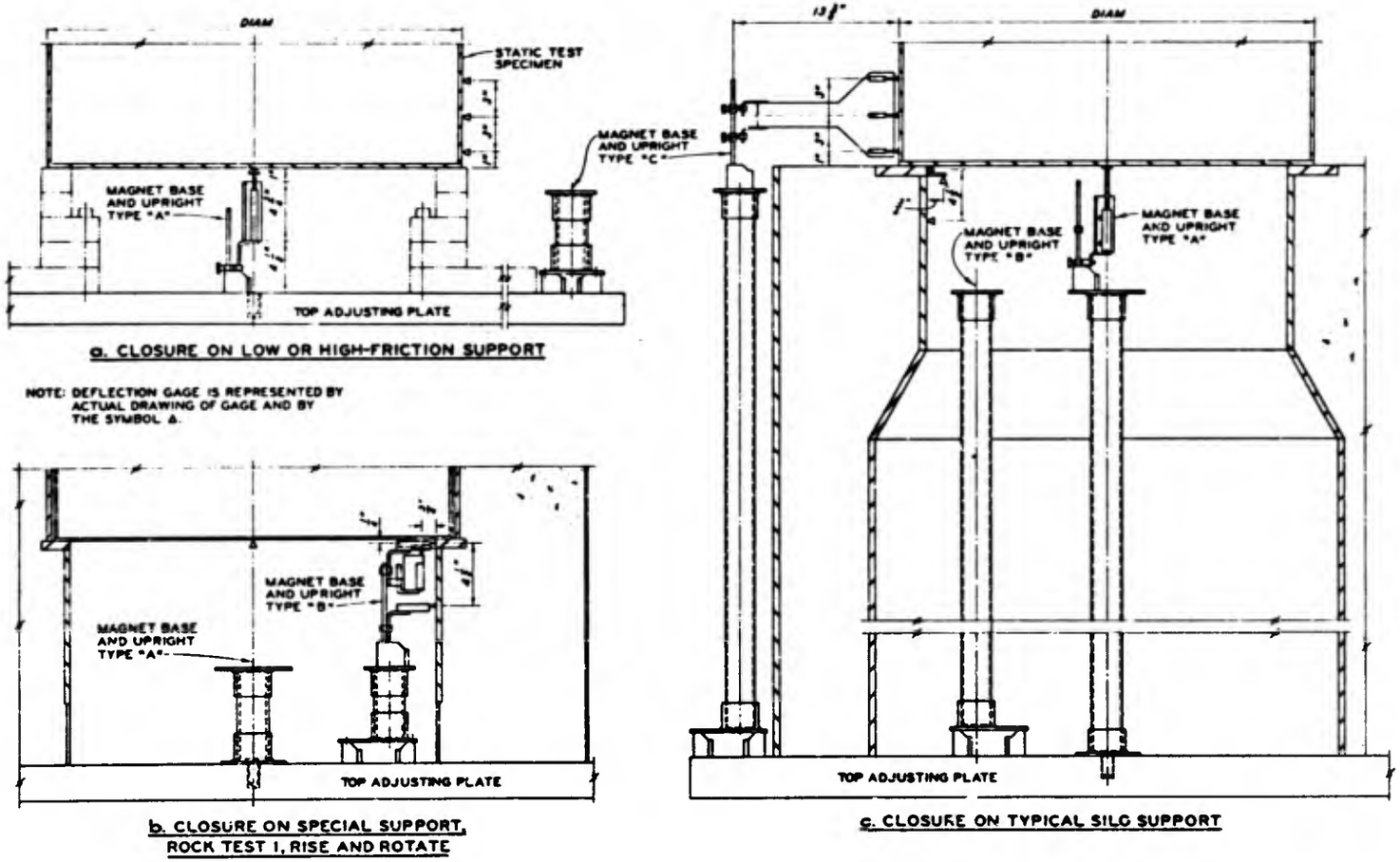

FIGURE 2-13

DEFLECTION GAUGE MOUNTS

assurance that the conclusions drawn throughout this report are correct. Of particular interest are the deflections of the side shell of the closure. It will be seen that the applied load increased steadily until relatively minor deflections occurred in the side shell, and as the deflections increased the primary load/deflection curve bent over sharply.

2.2 Model Construction

All test specimens were designed and fabricated by Parsons and were then turned over to WES for instrumentation and concrete placement. Welding of the models was in accordance with Section VIII of the ASME code. It is significant that only two weld failures were experienced and these occurred in two high strength steel models constructed of 4130 chrome molybdenum steel of 69-ksi and 180-ksi yield strengths and at test pressures of 16+ ksi and 23 ksi, respectively.

The Phase I (Tests 1 through 15) closure models are shown in Figure 2-14; the support models are shown in Figure 2-15. The Phase II (Tests 16 through 41) nominal closure and nominal silo models are shown in Figures 2-16 and 2-17, respectively. Table 2-3 gives a composite view of both closure and silo design parameters, by test.

In an effort to correlate with previous HEST results, two specimens were constructed to model structures tested in the Hercules (Test 32) test and in Rock Test I (Test 33). The silo supports for these tests are shown in Figures 2-18 and 2-19, respectively.

Test 35 represented the test of a prototype configuration of the rise and rotate closure concept and is shown on Figure 2-20.

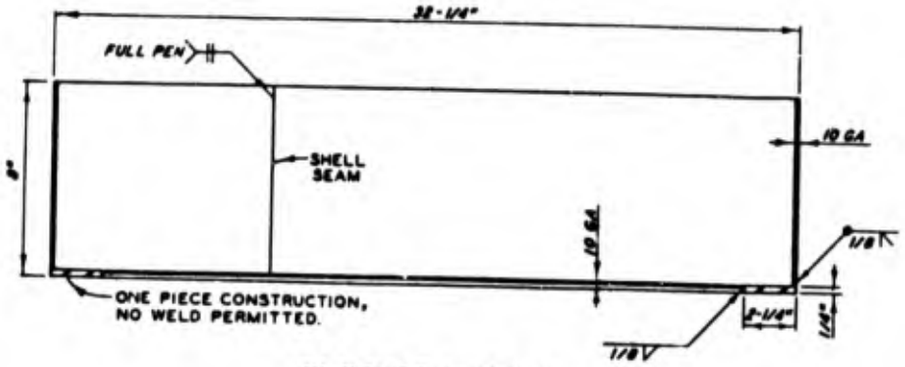

CLOSURE M120-1

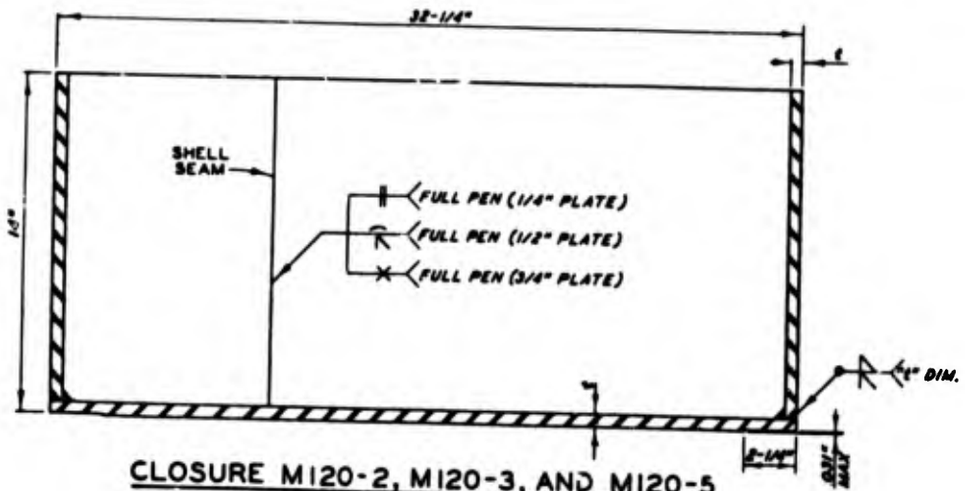

CLOSURE M120-2, M120-3, AND M120-5
WITH VARYING SHELL THICKNESS
t = 1/4, 1/2, AND 3/4 IN. RESPECTIVELY

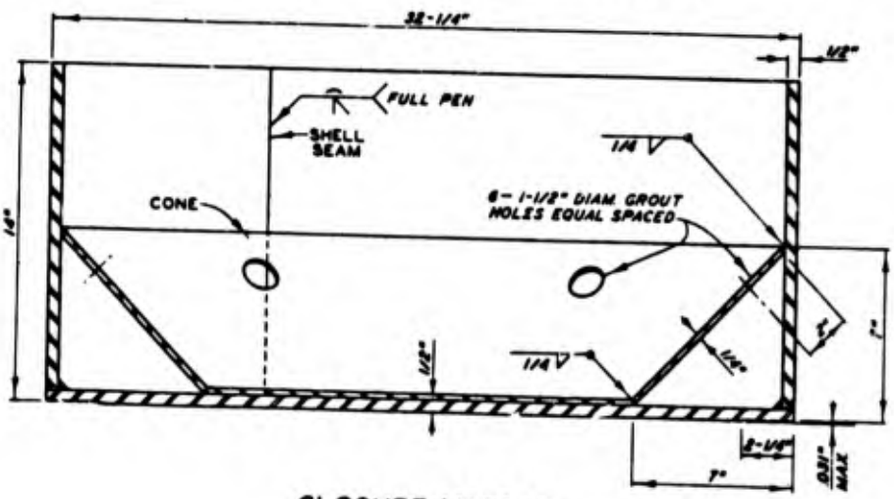

CLOSURE M120-4

FIGURE 2-14

CLOSURE SHELL DESIGN

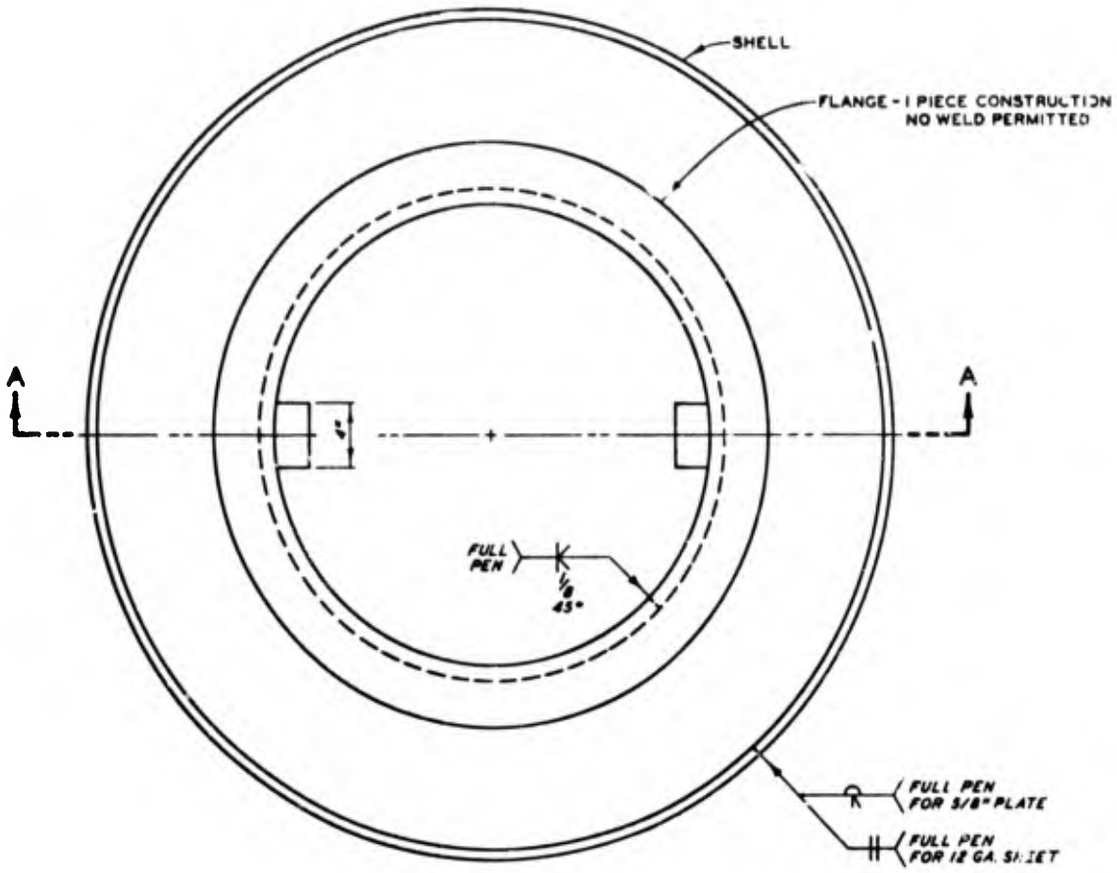

PLAN

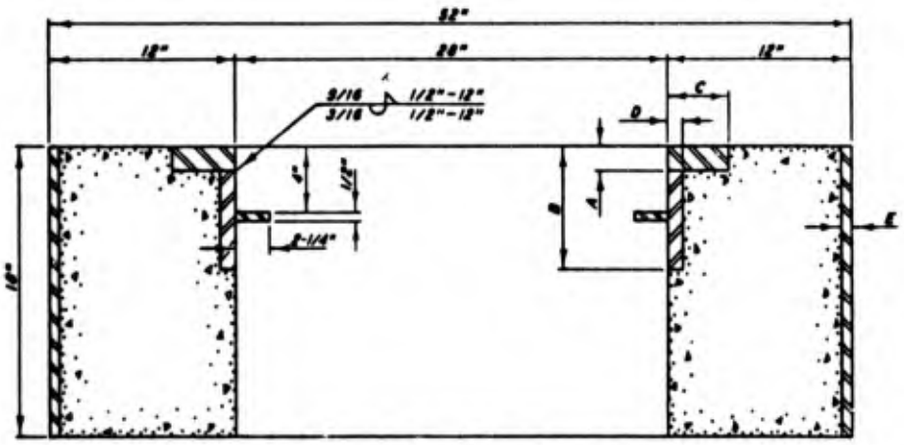

SECTION A-A

SILO DESIGN					
MODEL	A	B	C	D	E
M121-1	1/2"	6-1/2"	4"	1"	12 GAGE
M121-2	1-1/2"	7-1/2"	4"	1"	5/8"
M121-3	1-1/2"	7-1/2"	4"	1"	12 GAGE

FIGURE 2-15

SILO DESIGN

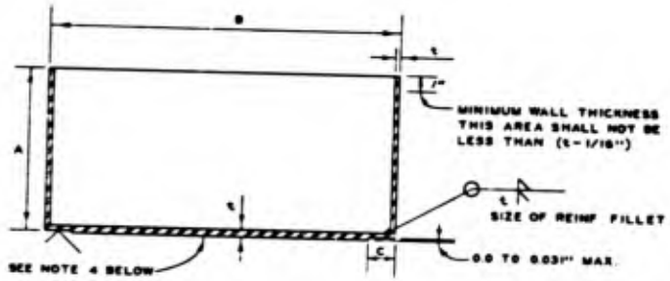

a. CLOSURES M120-2E, M130-1 — M130-14, AND M140-1

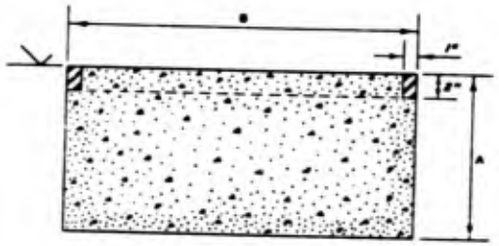

b. CLOSURES M133-1 AND M133-2

CLOSURE	STEEL SHELL THICKNESS t, IN	A DEPTH IN	B DIAMETER IN	C MACHINED BEARING AREA, IN	STEEL STRENGTH f_y
M120-2E*	1/4	14.00	32.25	2-1/4	36,000
M130-1	1/4	14.00	32.25	2-1/4	36,000
M130-2	1/4	14.00	32.25	2-1/4	70,000
M130-3	1/4	14.00	32.25	2-1/4	150,000
M130-4	1/2 SIDE 1/4 BOTTOM	14.00	32.25	2-1/4	36,000
M130-5	1/4	8.00	32.25	2-1/4	36,000
M130-6	1/4	21.00	32.25	2-1/4	36,000
M130-7*	1/2	14.00	32.25	2-1/4	36,000
M130-8	5/16	14.00	32.25	2-1/4	50,000
M130-9	1/8	14.00	32.25	4-1/4	36,000
*M130-10	1/2	14.00	32.25	2-1/4	50,000
M130-11	1/2	14.25	22.00	1-9/16	180,000
M130-12	1/2	9.50	22.00	1-9/16	60,000
M130-13	3/4	8.00	32.25	2-1/4	36,000
M130-14	3/4	21.00	32.25	2-1/4	36,000
M133-1	PLAIN CONC	8.00	32.25	—	—
M133-2	PLAIN CONC	21.00	32.25	—	—
M140-1	3/16	5.25	11.50	—	—

GENERAL NOTES:

1. DIMENSIONING AND TOLERANCING ARE PER MIL-STD-8C.
2. BREAK ALL SHARP CORNERS AND REMOVE ALL BURRS.
3. FABRICATION AND WELDING PER SECTION VIII ASME CODE. NO CODE STAMP REQUIRED.
4. ONE PIECE CONSTRUCTION, NO WELD PERMITTED.
5. INSIDE SURFACES TO BE SANDBLASTED TO WHITE METAL AFTER FABRICATION.
6. OIL MACHINED SURFACES ONLY.
7. ALL TOLERANCES TO APPLY IN THE UNRESTRAINED CONDITION.

FIGURE 2-16

STEEL SHELL DESIGN SPECIFICATIONS FOR CLOSURES M120-2E AND M130-1 THROUGH M130-14

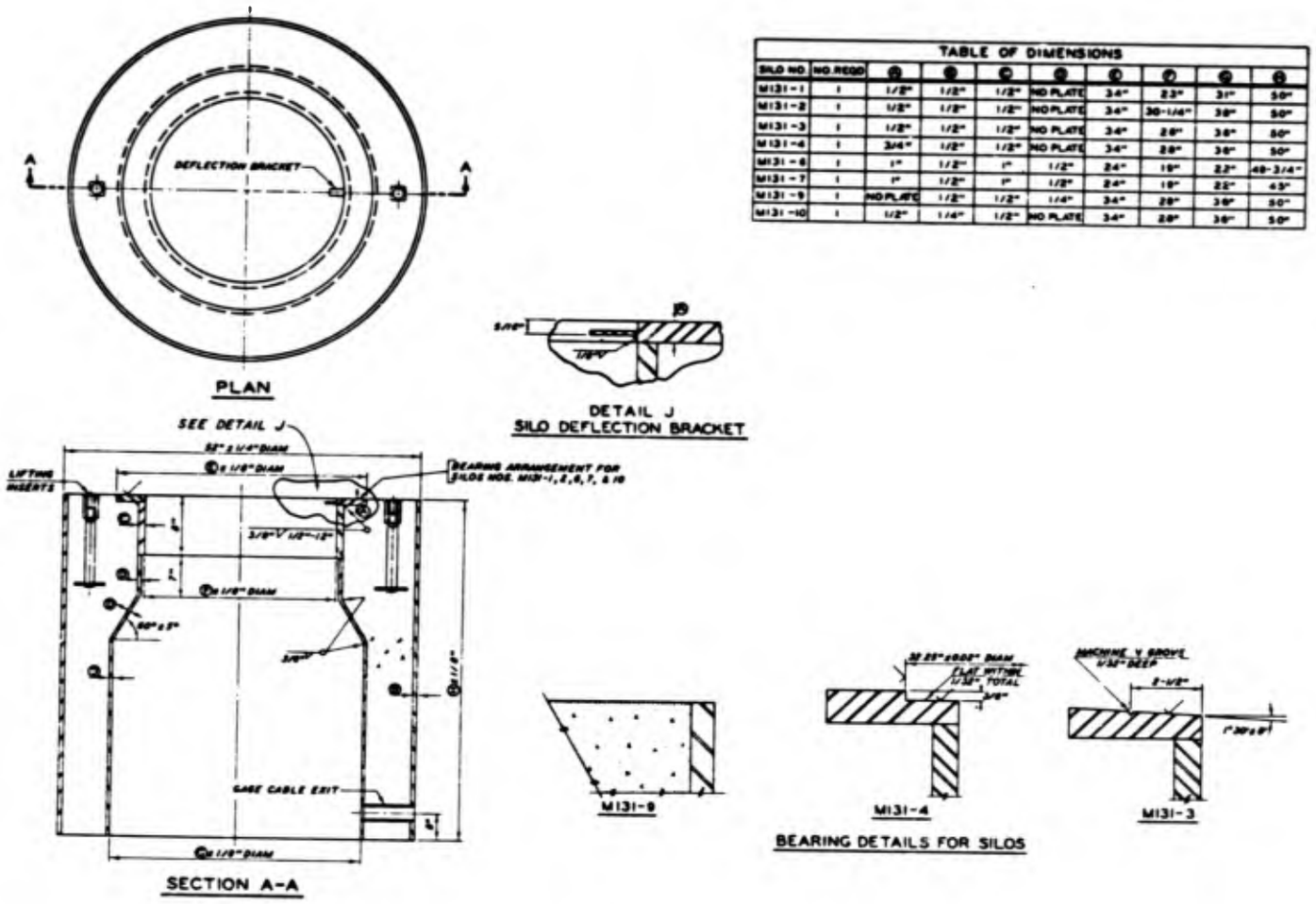

TABLE OF DIMENSIONS									
SILO NO.	NO. REQD	A	B	C	D	E	F	G	H
M131-1	1	1/2"	1/2"	1/2"	NO PLATE	34"	23"	31"	50"
M131-2	1	1/2"	1/2"	1/2"	NO PLATE	34"	30-1/16"	38"	50"
M131-3	1	1/2"	1/2"	1/2"	NO PLATE	34"	28"	36"	50"
M131-4	1	3/4"	1/2"	1/2"	NO PLATE	34"	28"	36"	50"
M131-6	1	1"	1/2"	1"	1/2"	24"	19"	27"	48-3/4"
M131-7	1	1"	1/2"	1"	1/2"	24"	19"	27"	43"
M131-9	1	NO PLATE	1/2"	1/2"	1/4"	34"	28"	36"	50"
M131-10	1	1/2"	1/4"	1/2"	NO PLATE	34"	28"	36"	50"

FIGURE 2-17

DESIGN GEOMETRIES OF SILOS M131-1 THROUGH -4 AND M131-6, -7, -9, AND -10

TABLE 2-3
PHASE II, CLOSURE AND SILO DESIGN PARAMETERS

Test No.	Closure								Friction Rings and Silo Support								
	Identification No.	L'	L	t	L/t Ratio	Concrete f'_c	Steel f_y	Shell Thickness	Identification No.	Concrete f'_c	Steel f_y	Steel Thicknesses (inches) A	B	C	D	F
		inch	inch	inch		psi	psi	inch		psi	psi					
16	M130-2E	32.25	28	14	2.0	12,000	36,000	1/4	(Low friction segmented rings)							
17	M130-1-7	32.25	28	14	2.0	Nonshrink 6,000	36,000	1/4								
18	M130-1-6	32.25	28	14	2.0	3,000	36,000	1/4								
19	M130-2-2	32.25	28	14	2.0	3,000	70,000	1/4								
20	M130-2-1	32.25	28	14	2.0	12,000	70,000	1/4								
21	M130-3	32.25	28	14	2.0	6,000	150,000	1/4	(Low friction segmented rings with steel shims)							
22	M130-4	32.25	28	14	2.0	6,000	36,000	1/2 sides 1/4 bottom								
23	M130-7	32.25	28	14	2.0	6,000	36,000	1/2								
24	M130-1-3	32.25	28	14	2.0	6,000	36,000	1/4	(Low friction segmented rings with steel shims and teflon)							
25	M130-5	32.25	28	8	3.5	6,000	36,000	1/4	(Low friction segmented rings with steel shims)							
26	M133-1	32.25	28	8	3.5	6,000	Plain concrete		(Low friction segmented rings)							
27	M133-2	32.25	28	21	1.33	6,000	Plain concrete									
28	M130-6	32.25	28	21	1.33	6,000	36,000	1/4								
29	M130-14	32.25	28	21	1.33	6,000	36,000	3/4								
30	M130-13	32.25	28	8	3.5	6,000	36,000	3/4								
31	M130-7-1	32.25	28	14	1.4	6,000	36,000	1/2	M131-1	6,000	36,000	5.5	1/2	1/2	1/2	No plate
32	M130-9	32.25	28.1875	14	1.73	6,000	36,000	1/8	M129-0 (Hercules)	6,000	36,000	6.4	1/8	1/8	1/8	"
33	M130-8	32.25	28.375	14	2.02	6,000	50,000	5/16	M128-0 (Rock Test I)	6,000	50,000	2.25	1/2	1/2	No plate	"
34	M130-7-2	32.25	30.25	14	2.16	6,000	36,000	1/2	M131-2	6,000	36,000	1.875	1/2	1/2	1/2	No plate
35	M127-0	32.25	36.50	13.25	2.0	6,000	36,000	1/4	M127-08 (Rise and rotate)	6,000	36,000	*	--	--	--	--
36	M130-10	32.25	28	14	2.0	6,000	50,000	1/2	M131-4	6,000	36,000	3.0	*	1/2	1/2	No plate
37	M130-7-3	32.25	28	14	2.0	6,000	36,000	1/2	M131-3	6,000	36,000	3.0	*	1/2	1/2	No plate
38	M130-11	22.00	19	14.25	1.33	12,000	180,000	1/2	M131-7	12,000	180,000	2.5	1.0	1.0	1/2	1/2
39	M130-12	22.00	19	9.50	2.0	12,000	60,000	1/2	M131-6	12,000	60,000	2.5	1.0	1.0	1/2	1/2
40	M130-7-4	32.25	28	14	2.0	6,000	36,000	1/2	M131-10	6,000	36,000	3.0	1/2	1/2	1/4	No plate
41	M130-7-5	32.25	28	14	2.0	6,000	36,000	1/2	M131-9	6,000	36,000	3.0	*	1/2	1/2	1/4
42	M140-1	11.50	10	5.25	1.91	--	--	3/16	(High friction solid ring)	(Closure previously tested dynamically--retested statically)						
43	M140-2	11.50	10	5.25	1.91	--	--	3/16	(High friction solid ring)	(Virgin closure tested statically)						

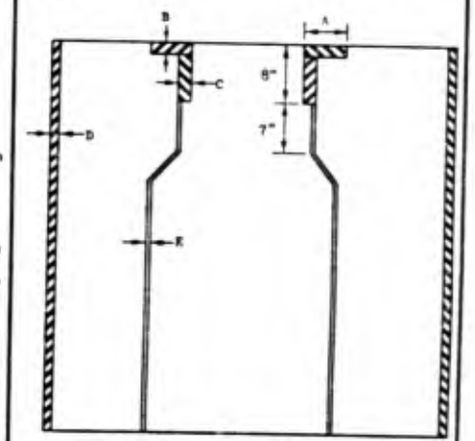

* See design.

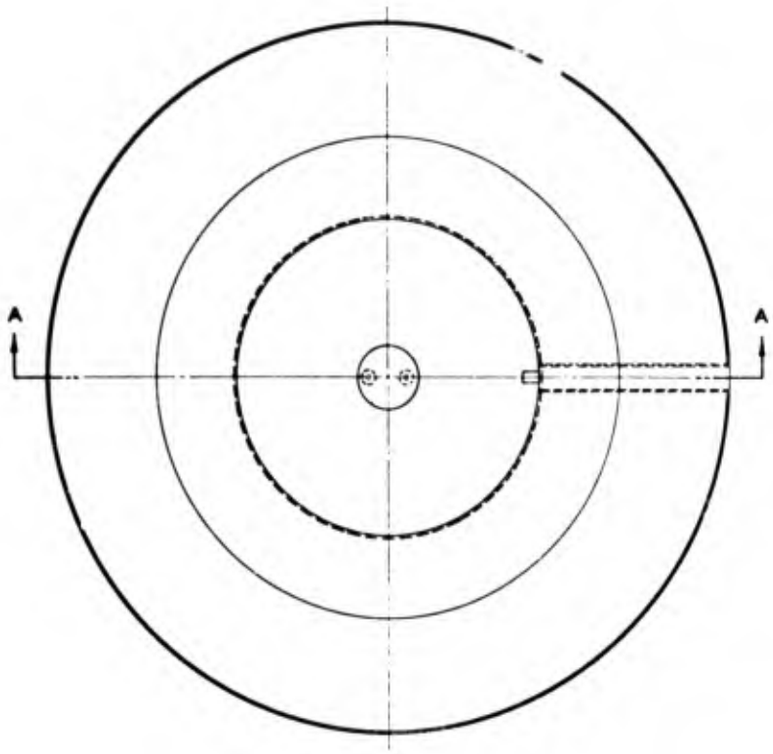

PLAN

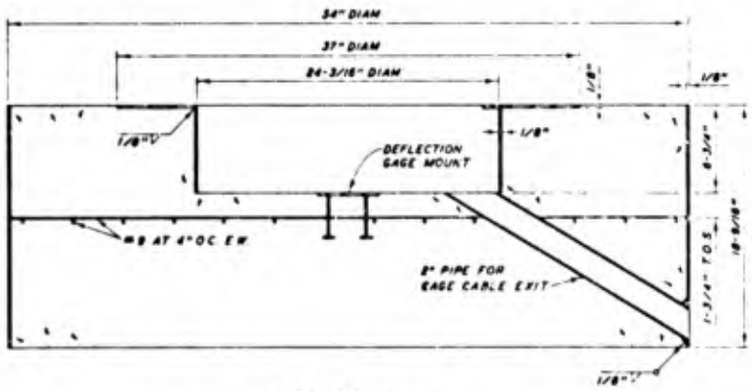

SECTION A-A

FIGURE 2-18

DESIGN GEOMETRY OF SILO

M129-0 - TEST 32 (HERCULES)

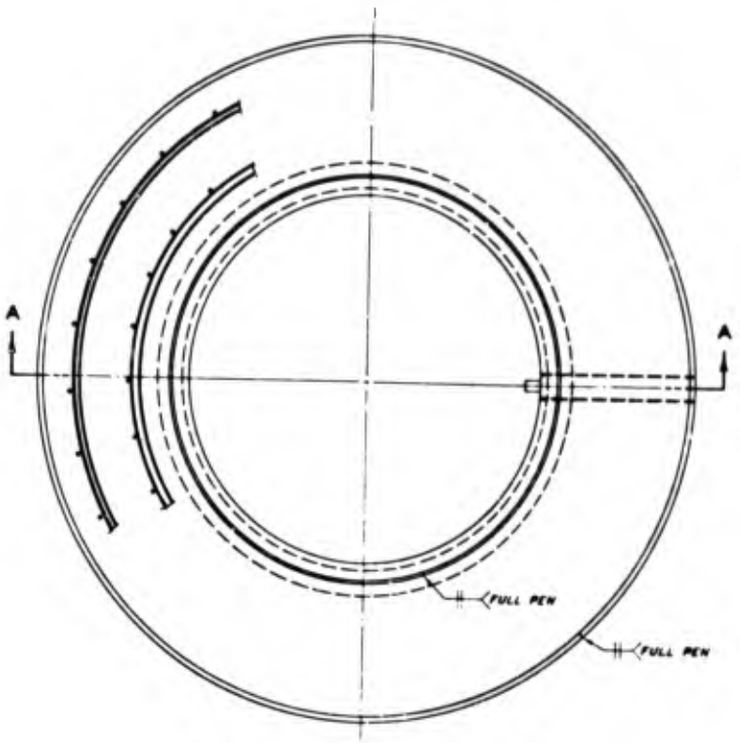

PLAN

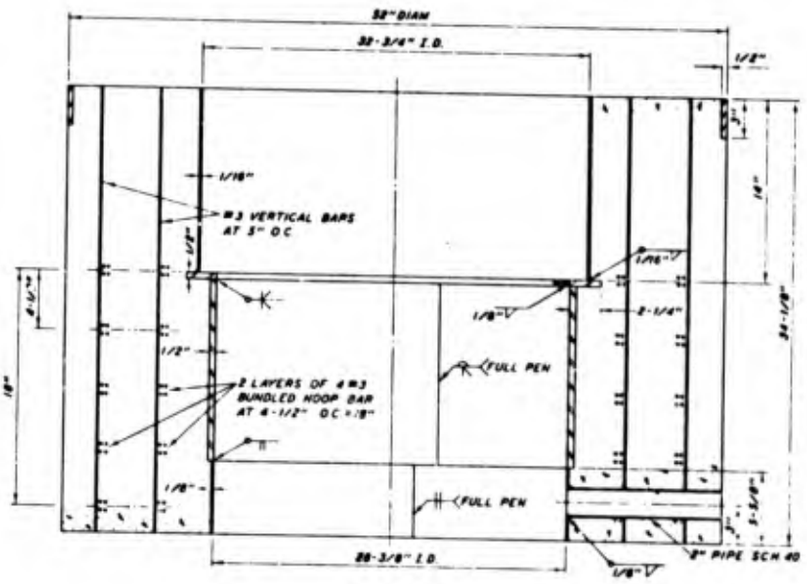

SECTION A-A

FIGURE 2-19

DESIGN GEOMETRY OF SILO M128-0 - TEST 33 (ROCK TEST I)

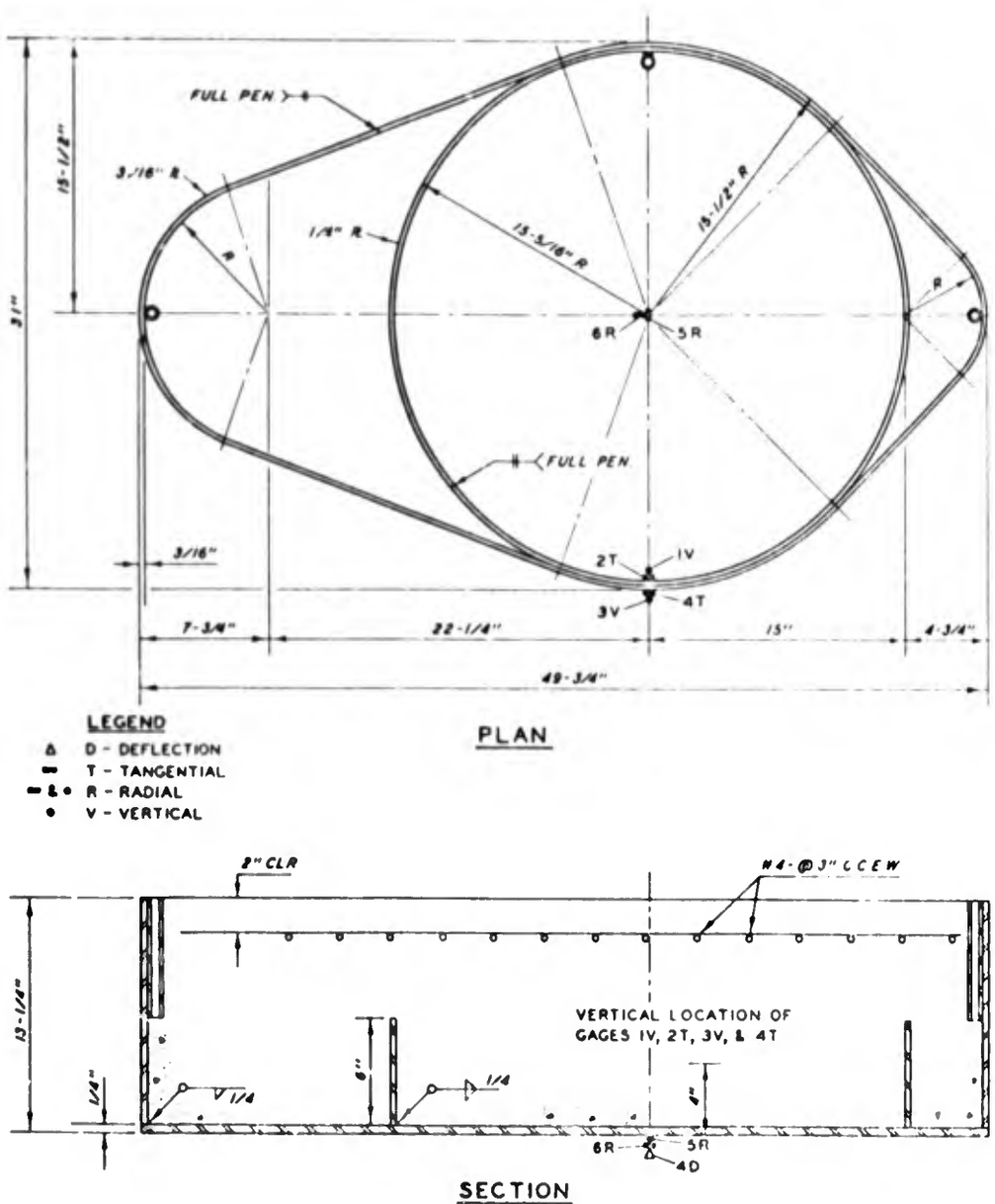

FIGURE 2-20

DESIGN GEOMETRY AND INSTRUMENTATION GAUGE ARRAY FOR CLOSURE M127-0 - TEST 35 (RISE AND ROTATE)

3.0 SUBSCALE STATIC TESTS

Table 3-1 defines the geometry, material strength, and load capacity of the models tested. Low friction and high friction tests are also indicated. For the convenience of the reader, a typical cross section of a test model is included as part of this table.

3.1 Phase I

The first fifteen static tests, designated as Phase I, were conducted to provide a baseline for future tests, to validate the test hardware, and to allow us to check our design approach.

Our initial plan was to duplicate all tests in the series. However, after the first four tests, where two pairs of identical models were tested with nearly equivalent load capacities and failure modes, it was decided to expend test effort in examination of closure/support variables rather than in duplication of test results. Thus, a great variety of variables were examined in Phase II of the series.

Full-size structures were designed and scaled down for testing purposes in the preliminary effort. It was necessary to consider the closure and the closure support as uncoupled since little was known about interaction phenomena. The variables examined were closure plate thickness, closure geometry, closure support plate thicknesses, and bearing restraint. Two models containing conical sections across the predicted shear plane were also included to determined if additional strength could be achieved with this type of section.

The Phase I tests are described in the following paragraphs.

LEGEND - TABLE 3-1

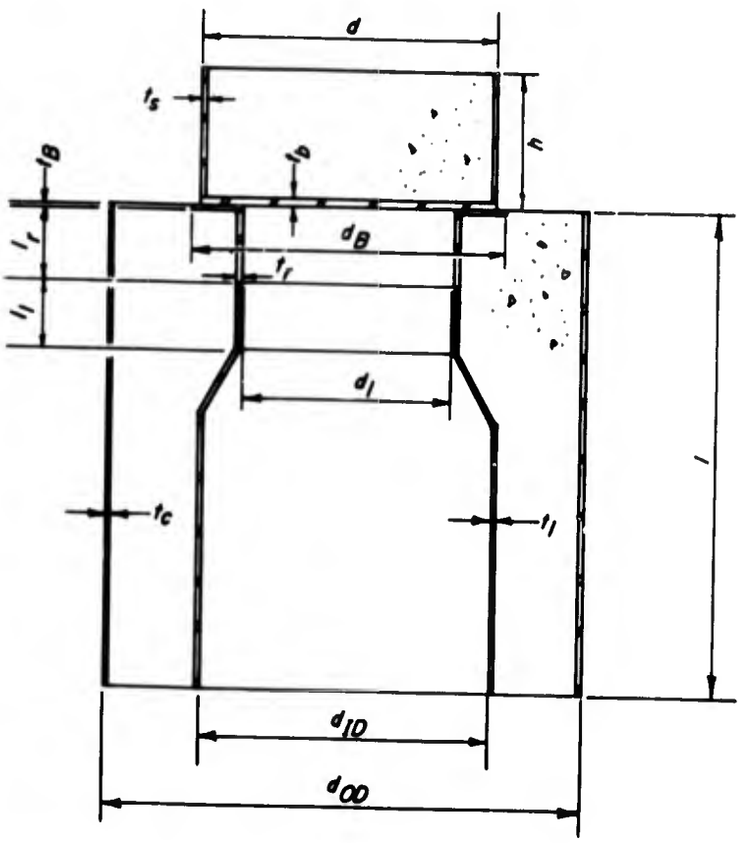

CLOSURE

- d DIAMETER
- h DEPTH
- t_s SIDE SHELL THICKNESS
- t_b BOTTOM PLATE THICKNESS

CLOSURE SUPPORT

FOUNDATION

- d_l CLEAR INSIDE DIAMETER OF SUPPORT UNDER CLOSURE
- l TOTAL DEPTH
- d_{OD} OUTSIDE DIAMETER
- d_{ID} CLEAR INSIDE DIAMETER OF LOWER PORTION

BEARING ASSEMBLY

- d_B OUTSIDE DIAMETER OF BEARING RING
- t_B BEARING PLATE THICKNESS
- l_r VERTICAL DIMENSION OF BEARING SHELL
- t_r BEARING SHELL THICKNESS

LINER AND CONFINING SHELL

- t_l LINER PLATE THICKNESS
- l_L VERTICAL DIMENSION OF LINER PLATE
- t_c OUTER SHELL THICKNESS

TABLE

STATIC TEST SPECIMEN GEOME

Test No.	Model Identification		Specimen Dimension, Inch									
			Closure				Closure Supp					
							Concrete Foundation				Bearin	
	Closure	Support	d	h	t_s	t_b	d_1	ℓ	d_{OD}	d_{ID}	d_B	
1	M120-1A	LF[b]	32.3	8	0.13	0.13	28					
2	M120-1B	LF	32.3	8	0.13	0.13	28					
3	M120-2A	LF	32.3	14	0.25	0.25	28					
4	M120-2B	LF	32.3	14	0.25	0.25	28					
5	M120-2C	M121-1A	32.3	14	0.25	0.25	28	18	52	28	36	0
6	M120-2C	M121-1B	32.3	14	0.25	0.25	28	18	52	28	36	0
7	M120-2C	M121-2A	32.3	14	0.25	0.25	28	18	52	28	36	1
8	M120-3A	M121-2A	32.3	14	0.50	0.50	28	18	52	28	36	1
9	M120-3B	M121-3A	32.3	14	0.50	0.50	28	18	52	28	36	1
10	M120-5A	M121-2B	32.3	14	0.75	0.75	28	18	52	28	36	1
11	M120-5B	M121-3B	32.3	14	0.75	0.75	28	18	52	28	36	1
12	M120-4A	LF	32.3	14	0.25	0.25	28					
13	M120-5B	LF	32.3	14	0.75	0.75	28					
14	M120-2D	HF[c]	32.3	14	0.25	0.25	28					
15	M120-4B	HF	32.3	14	0.25	0.25	28					
16	M120-2E	LF	32.3	14	0.25	0.25	28					
17	M130-1-7	LF	32.3	14	0.25	0.25	28					
18	M130-1-6	LF	32.3	14	0.25	0.25	28					
19	M130-2-2	LF	32.3	14	0.25	0.25	28					
20	M130-2-1	LF	32.3	14	0.25	0.25	28					
21	M130-3	LF	32.3	14	0.25	0.25	28					
22	M130-4	LF	32.3	14	0.50	0.25	28					
23	M130-7	LF	32.3	14	0.50	0.50	28					
24	M130-1-3	LF	32.3	14	0.25	0.25	28					
25	M130-5	LF	32.3	8	0.25	0.25	28					
26	M133-1	LF	32.3	8			28					

a/ For definition of terms, see page A2-34.

b/ LF = low friction support as discussed in Appendix 2, Section 2.

c/ HF = high friction support as discussed in Appendix 2, Section 2.

d/ Expansive concrete.

TABLE 3-1

N GEOMETRY AND LOAD CAPACITIES [a]

on, Inches							Strength, ksi		Load Capacity, ksi	Remarks
ure Support										
Bearing Assembly			Liner and Confining Shell							
d_B	t_B	ℓ_r	t_r	t_ℓ	ℓ_ℓ	t_c	f'_c	f_s		
							8	36	2.6	
							8	36	2.6	
							7	36	3.4	
							7	36	3.6	
36	0.50	6	1.0	1.0		0.10	7	36	3.2	
36	0.50	6	1.0	1.0		0.10	7	36	3.0	
36	1.50	6	1.0	1.0		0.62	8	36	4.7	
36	1.50	6	1.0	1.0		0.62	7	36	6.4	
36	1.50	6	1.0	1.0		0.10	8	36	3.8	
36	1.50	6	1.0	1.0		0.62	7	36	6.8	
36	1.50	6	1.0	1.0		0.10	8	36	4.1	
							8	36	2.9	1/4-in. shear cone in closure model
							7	36	8.8	
							7	36	4.2	
							8	36	2.8	1/4-in. shear cone in closure model
							13	36	5.5	
							7 [d]	36	3.7	
							3	36	2.8	
							3	70	5.5	
							11	70	6.6	
							6	150	7.3	Shims
							8	36	4.9	Shims
							8	36	6.4	Shims
							6	36	3.4	Teflon on supports
							7	36	3.3	Shims
							7		1.0	

TABLE 3-1 (CONTI

Test No.	Model Identification		Specimen Dimension, Inches									
			Closure				Closure Support					
							Concrete Foundation				Bearing	
	Closure	Support	d	h	t_s	t_b	d_1	ℓ	d_{OD}	d_{ID}	d_B	t_B
27	M133-2	LF	32.3	21			28					
28	M130-6	LF	32.3	21	0.25	0.25	28					
29	M130-14	LF	32.3	21	0.75	0.75	28					
30	M130-13	LF	32.3	8	0.75	0.75	28					
31	M130-7-1	M131-1	32.3	14	0.50	0.50	23	8	52	31	34	0.5
32	M130-9	M129-0	32.3	13.4	0.12	0.12	23.5	6.38	54	24.2	37	0.1
33	M130-8	M128-0	32.3	14.2	0.31	0.31	28	12.4	51.9	28.4	32.9	0.5
34	M130-7-2	M131-2	32.3	14	0.50	0.50	30.2	8	52	38	34	0.5
35	M127-0	M127-0	31.0	13.2	0.25	0.25	26.5	20.9	52	26.5	52	0.5
36	M130-10	M131-4	32.3	14	0.50	0.50	28	8	52	36	34	0.7
37	M130-7-3	M131-3	32.3	14	0.50	0.50	28	8	52	36	34	0.5
38	M130-11	M131-7	22	14.3	0.50	0.50	19	45	52	22	24	1.0
39	M130-12	M131-6	22	9.5	0.50	0.50	19	49.8	52	22	24	1.0
40	M130-7-6	M131-10	32.3	14	0.50	0.50	28	50	52	36	34	0.5
41	M130-7-5	M131-9	32.3	14	0.50	0.50	28	50	52	36	34	No Pla

3-1 (CONTINUED)

...n, Inches								Strength, ksi		Load Capacity, ksi	Remarks
...ure Support											
	Bearing Assembly			Liner and Confining Shell							
	d_B	t_B	ℓ_r	t_r	t_ℓ	ℓ_ℓ	t_c	f'_c	f_s		
								7		1.1	
								7	36	4.1	
								8	36	8.3	
								8	36	6.8	
	34	0.50	8	0.50	No Plate	7	0.50	7	36	6.6	Wide bearing
2	37	0.12	6.38	0.12	0.12		0.12	8	36	5.3	Hercules
4	32.9	0.50	12.38	0.50	0.12		Re-bar	8	50	4.5	Rock Test I
	34	0.50	8	0.50	No Plate	7	0.50	8	36	3.9	Narrow bearing
5	52	0.50	20.88	0.50	0.50		0.50	8	36	5.8	Rise and rotate
	34	0.75	8	0.50	No Plate	7	0.50	8	50	5.3	Notched bearing
	34	0.50	8	0.50	No Plate	7	0.50	9	36	5.5	Inclined bearing
	24	1.0	8	1.0	0.50	7	0.50	12	180	22.9	
	24	1.0	8	1.0	0.50	7	0.50	12	70	15.8	
	34	0.50	8	0.50	No Plate	7	0.25	8	36	4.2	
	34	No Plate	8	0.50	0.25	7	0.50	8	36	5.0	No bearing ring

TABLE 3-1
(Cont'd)
A2-37

TESTS 1 AND 2

These tests were performed to determine if models used in past closure test activities could be scaled up, and to determine the repeatability of the failure load. The models selected for Tests 1 and 2 were scaled-up versions of static test models previously tested by University of Illinois researchers. These tests essentially doubled the 1/14 scale used by the University of Illinois. Except for the bearing width which was somewhat narrower, all test variables were scaled up by a factor of two, as can be seen in Figure 3-1. The tests were performed on a low friction support.

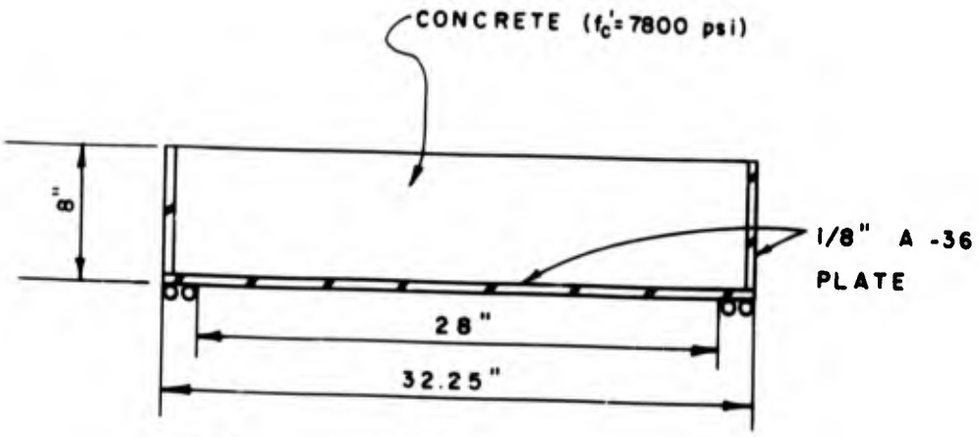

CLOSURE GEOMETRY FOR TESTS 1 AND 2
(UNIVERSITY OF ILLINOIS)

FIGURE 3-1

This section proved to be quite well proportioned since shear, bearing, and bending distress were all evident at the time of the post-test inspection, as can be seen in Figures 3-2, 3-3, and 3-4. Note the cracks starting at the bearing in both tests. The dark areas in the photographs are caused by moisture resulting from the cutting operation and are not related to the tests. The bulge that appears above the area in contact with the bearing

(Figure 3-4) is due to the yielding of the steel from the load imposed by the horizontal straining of the concrete; i.e., the outer steel ring is acting as a confinement vessel.

Originally, the University of Illinois models were designed for 1000 psi; however, failure occurred at 2150 psi. In the present tests, failure occurred at 2600 psi in both Test 1 and Test 2. The ductility of the model, as well as its ability to continue to carry a load even though high strain rates were being encountered, is evidenced in the load deflection diagrams (Figures 3-5 and 3-6).

The results of these tests established the fact that the failure load for the scaled-up models was essentially the same as that found by the University of Illinois for the smaller model. The ability to duplicate test results accurately was also established.

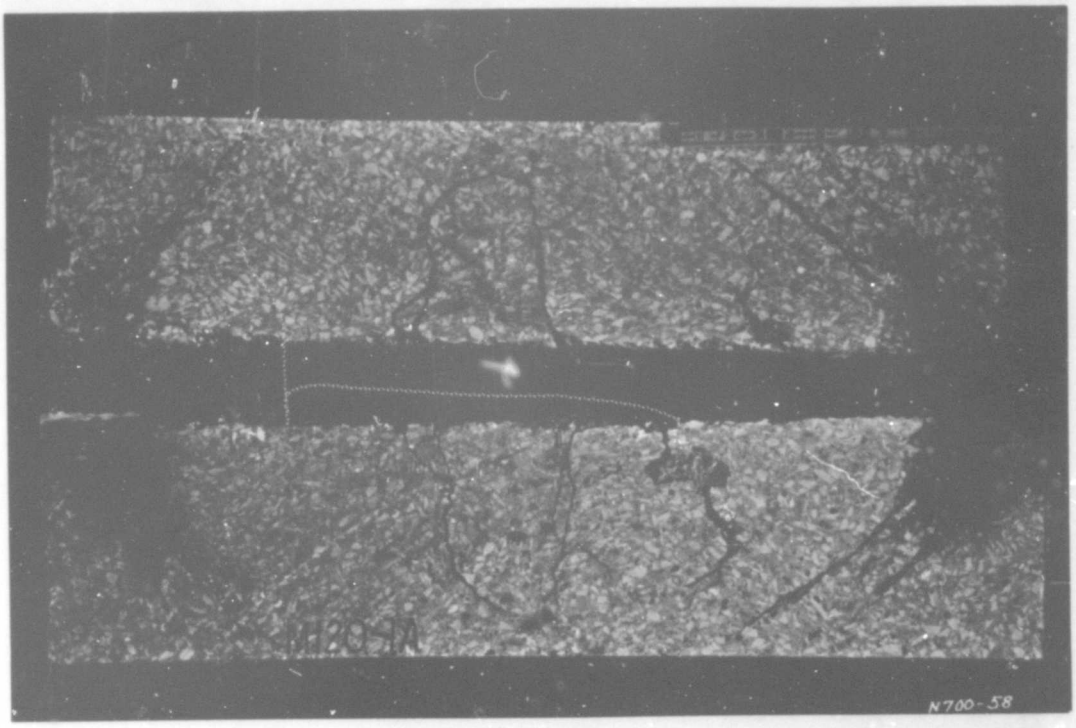

TEST 1

FIGURE 3-2

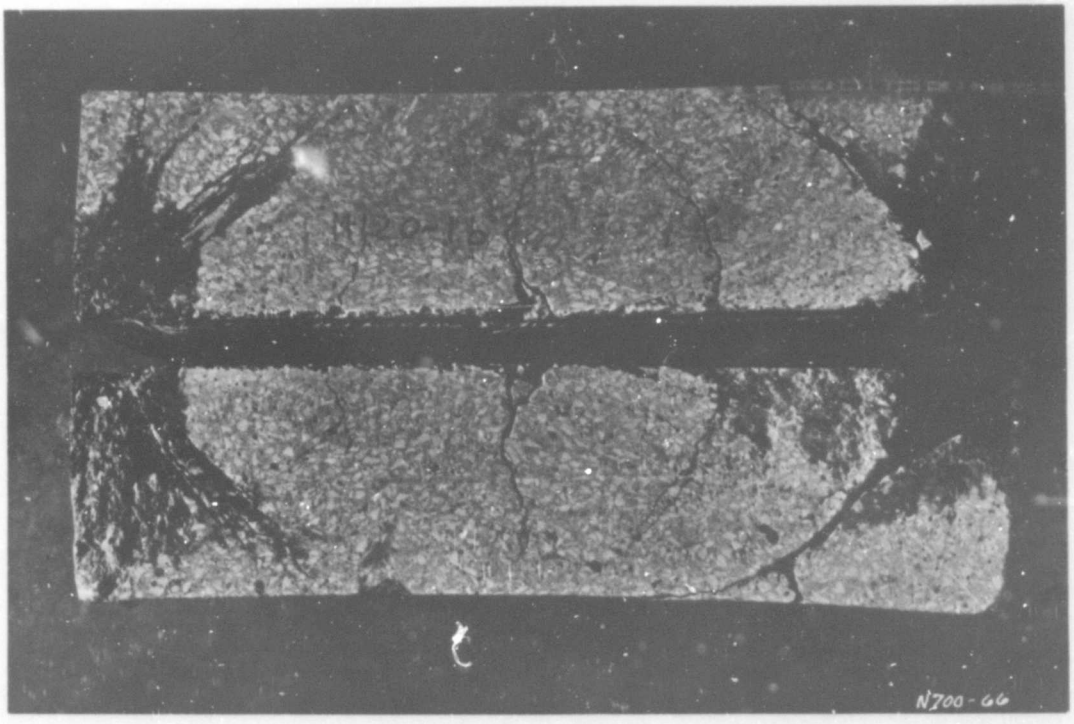

TEST 2

FIGURE 3-3

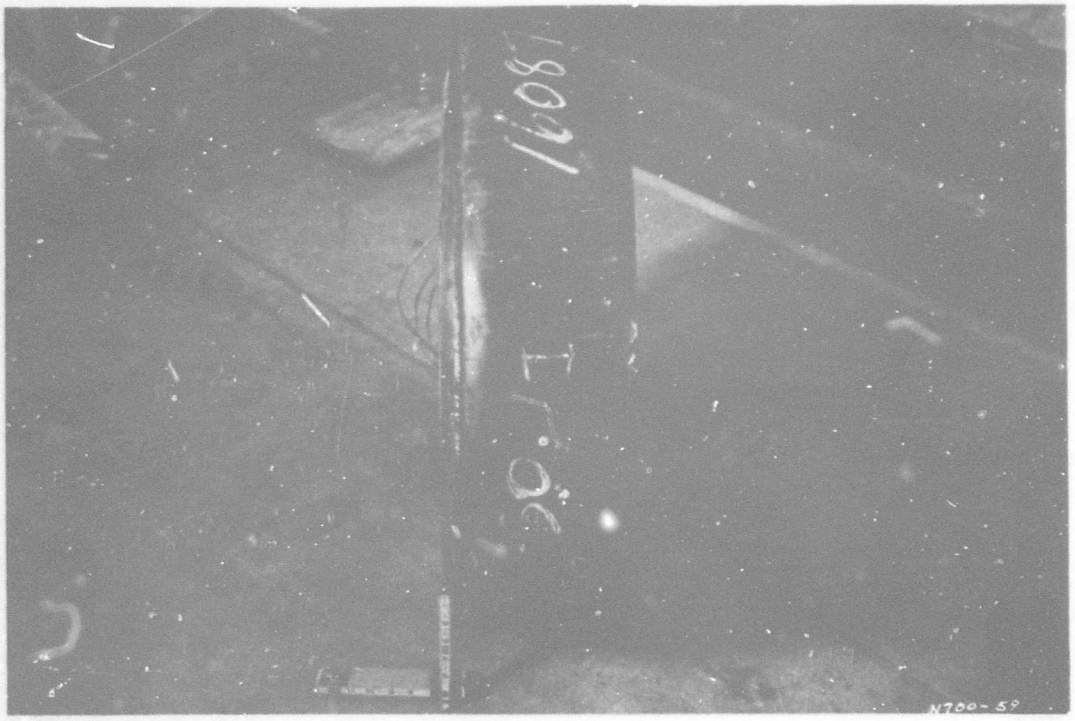

TEST 2

FIGURE 3-4

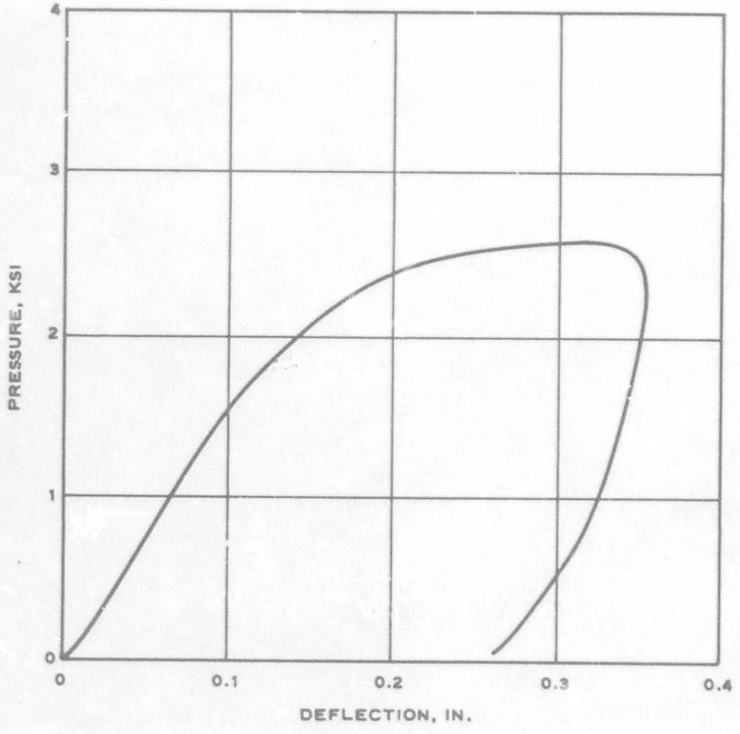

CLOSURE M120-1A TEST 1 -- PRESSURE VS. DEFLECTION

FIGURE 3-5

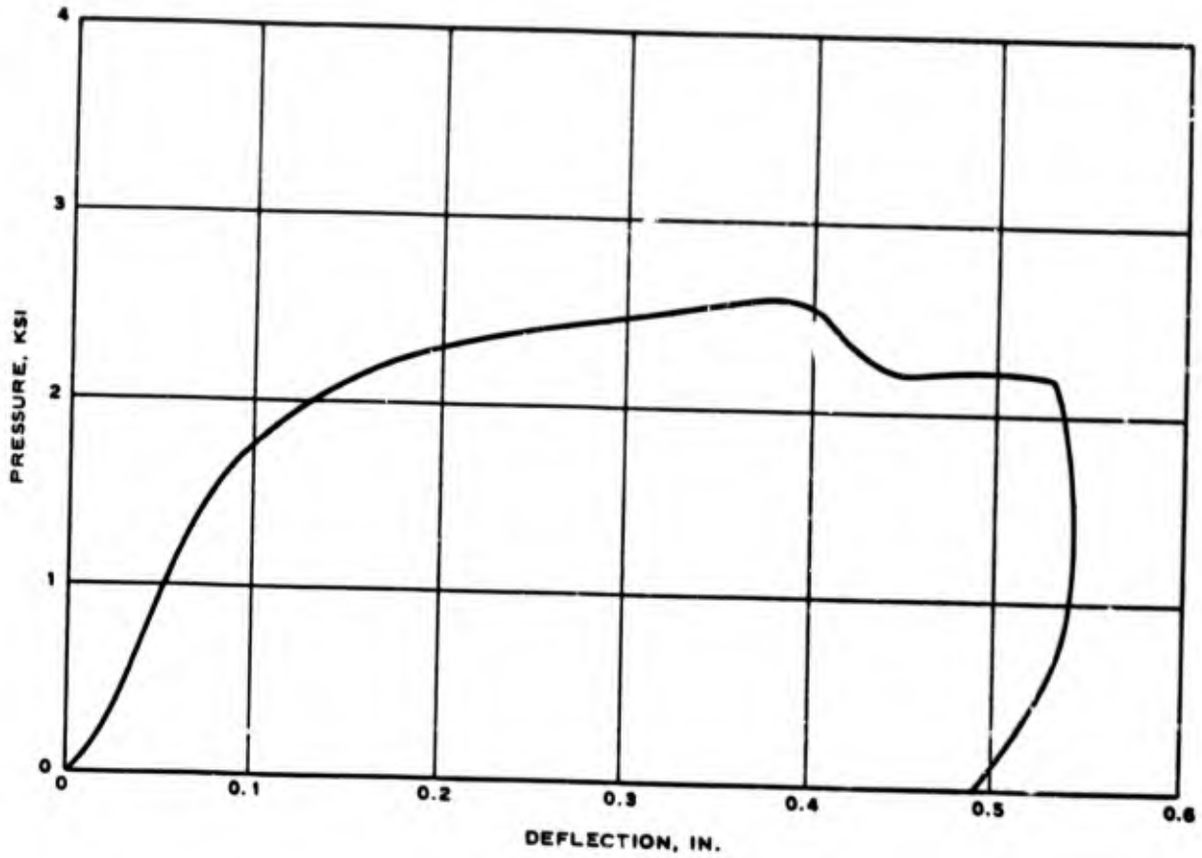

CLOSURE M120-1B TEST 2 – PRESSURE VS. DEFLECTION

FIGURE 3-6

TESTS 3 AND 4

The models in Tests 3 and 4 were designed for an ultimate load capacity of 4000 psi. These tests were performed to check the validity of the design approach, to verify the repeatibility of the test results, and to provide a point of departure for further model designs. The model geometry for Tests 3 and 4 is shown in Figure 3-7. The tests were performed on low friction supports.

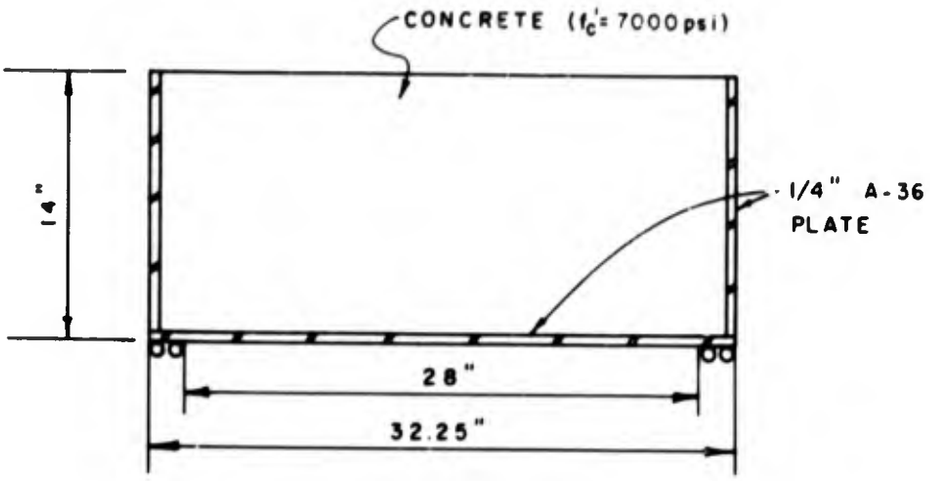

CLOSURE GEOMETRY FOR TESTS 3 AND 4

FIGURE 3-7

The section behaved as might be predicted for a deep section; steep shear cracks as well as bearing distress were observed at the time of post-test inspection. The punching of the 1/4-inch plate which can be seen in Figure 3-8 was caused by the sharp edge of the low friction bearing and is not indicative of a general-type failure mode for these models. This proved to be a test anomaly and was not evident in the models with heavier bottom plates. The maximum load capacity, however, was undoubtedly achieved before the punching action took place. In the later tests steps were taken to minimize this punching action by placing mild steel shims between the hardened bearing and the model.

Figure 3-9 shows the shell which has been cut by a cutting torch (flame cut) to expose the concrete and to allow the models to be cut in two with a diamond saw. Distress in the concrete in the area of the bearing and above the bearing is also evident. Figures 3-10 and 3-11 show close-up views of the failed area in the section.

The evident distress in the side shell supports the hypothesis that this shell acts as a confining ring and carries a sizable portion of the vertical load as well. Failure occurred at 3450 psi in Test 3 and at 3600 psi in Test 4 (see Figures 3-12 and 3-13). It should be pointed out that when the pressure deflection curves show sharp drop-off in the vertical load capacity this does not indicate a sudden failure, but is due to actually releasing the load on the model. More ductility would have been achieved had the load been carried on for a longer period of time.

The ability to duplicate test results was established as well as the ability to provide resistance to pressures as high as 3500 psi. Although the models failed below their predicted load capacity, the results were still satisfying in view of the overall structural behavior.

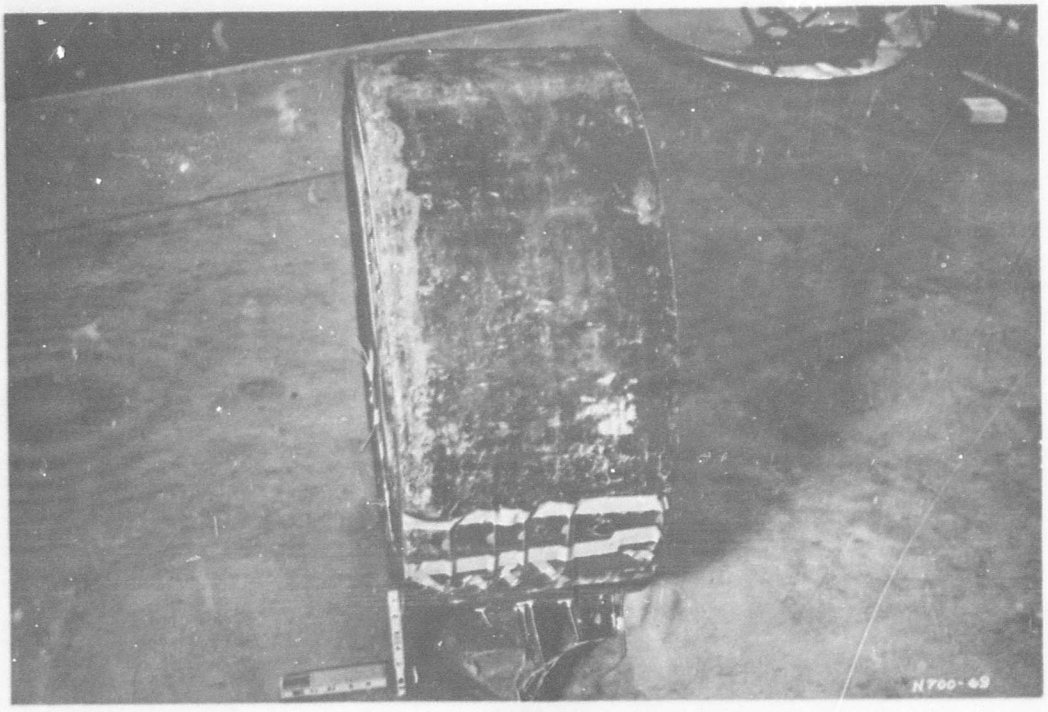

TEST 3

FIGURE 3-8

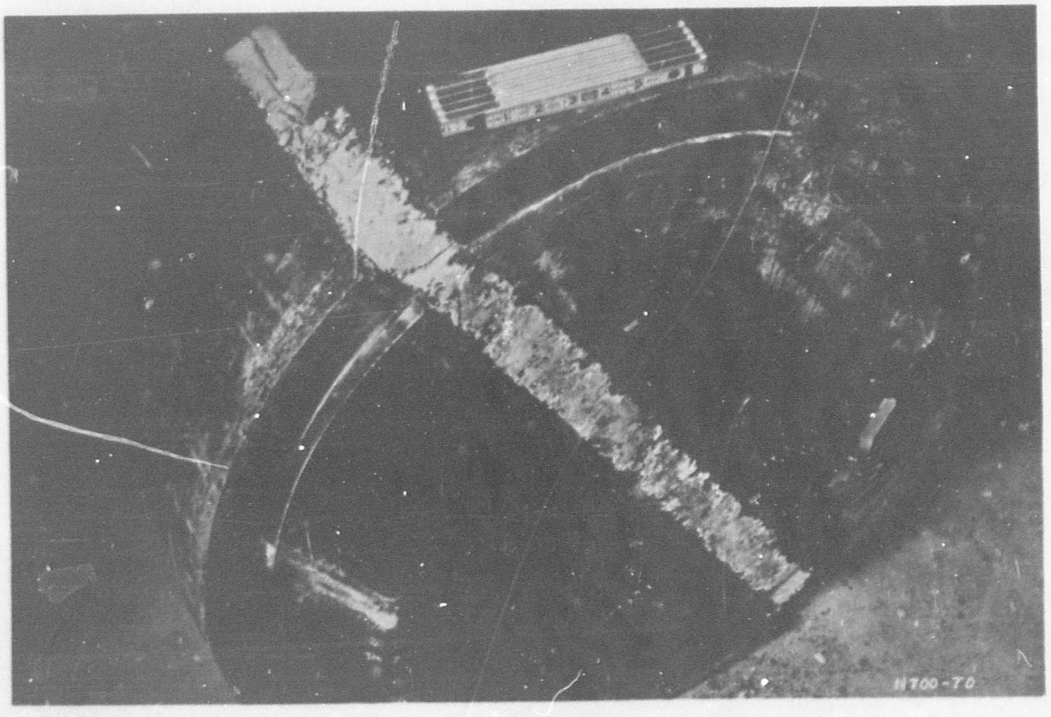

TEST 3

FIGURE 3-9

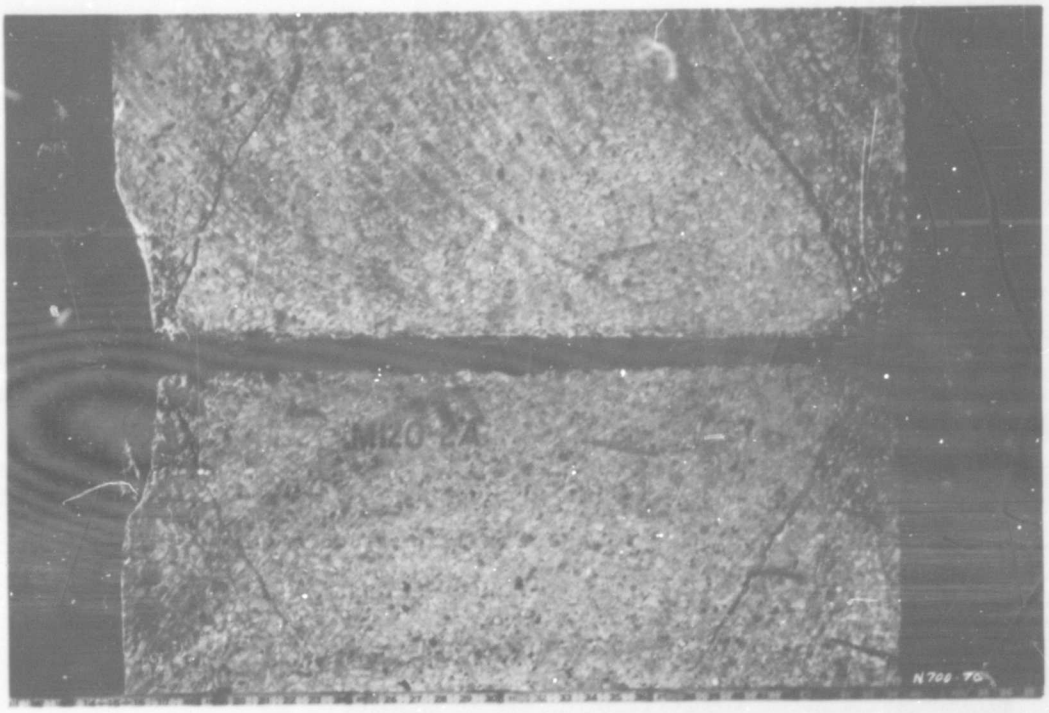

TEST 3

FIGURE 3-10

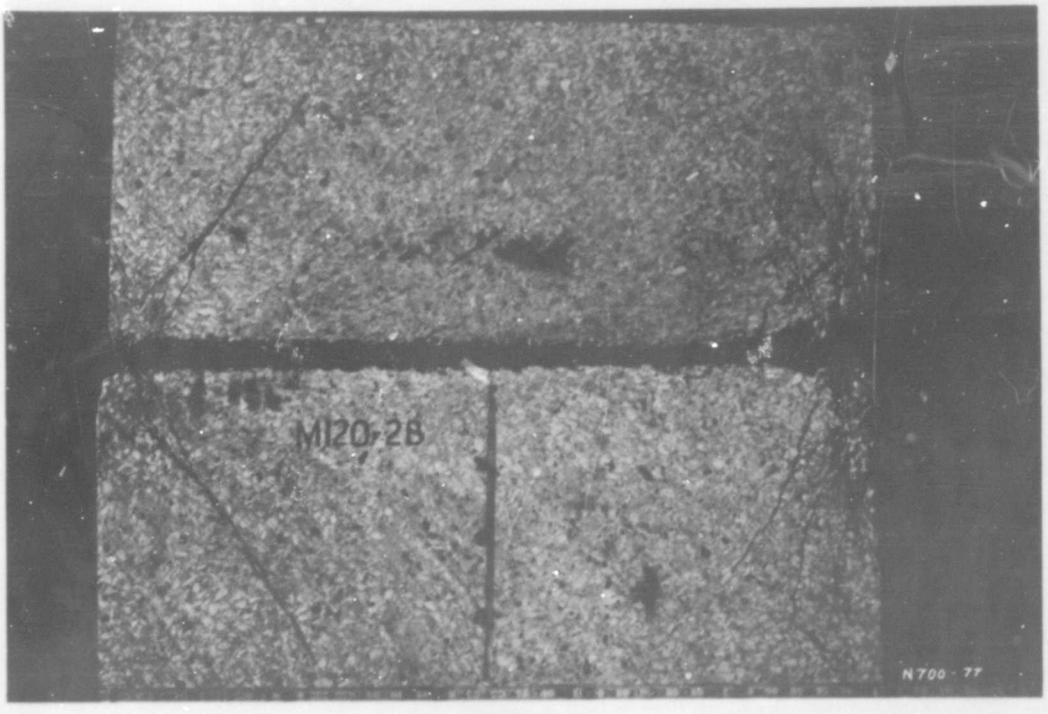

TEST 4

FIGURE 3-11

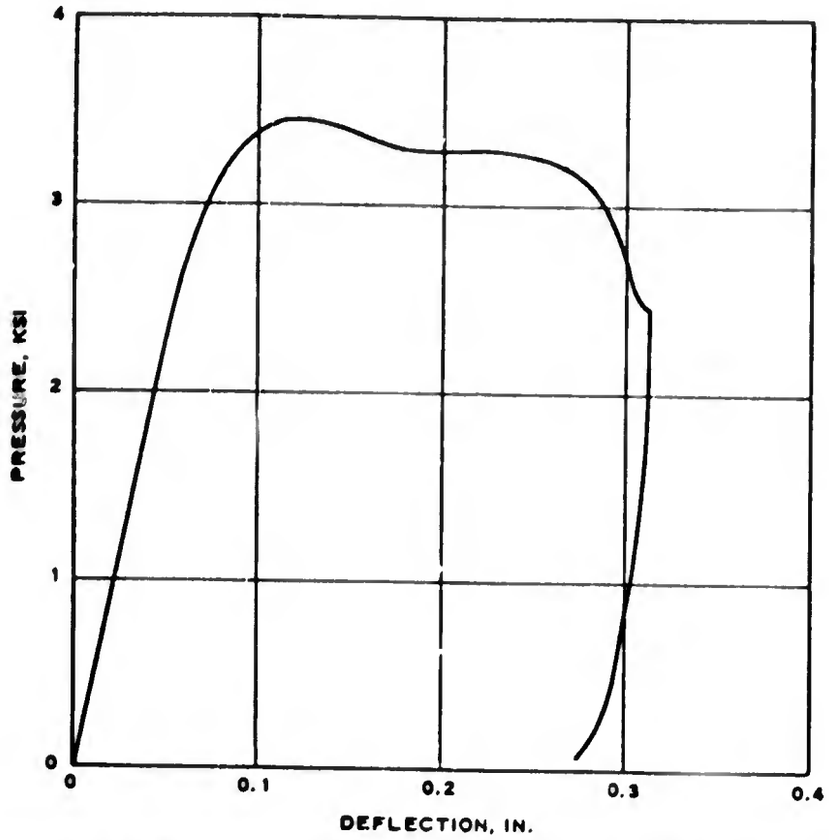

CLOSURE M120-2A TEST 3 - PRESSURE VS. DEFLECTION

FIGURE 3-12

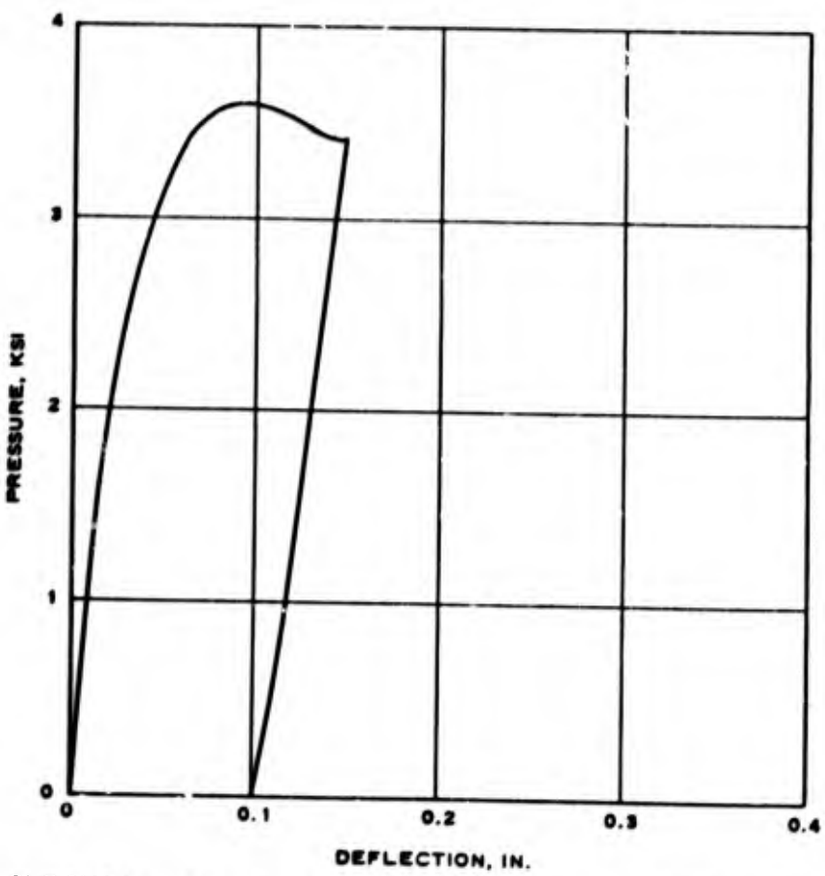

CLOSURE M120-2B TEST 4 - PRESSURE VS. DEFLECTION

FIGURE 3-13

TESTS 5 AND 6

Tests 5 and 6 represented the first attempt to test a closure model on a silo support. The silo support was proportioned to fail at 5000 psi, with the expectation that a closure could be failed on this silo and the increase in closure load capacity due to support friction could be determined.

The closure tested was identical to those used for Tests 3 and 4. The model support geometry for Tests 5 and 6 is shown in Figure 3-14.

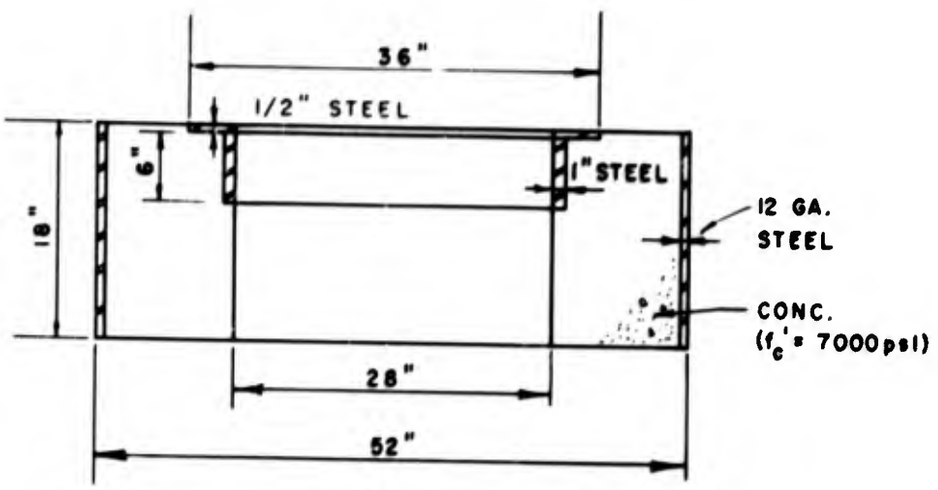

SUPPORT GEOMETRY FOR TESTS 5 AND 6

FIGURE 3-14

The radial load introduced into the support due to the expansion of the base of the closure was underestimated in initial calculations. The test failure was in the support structure which yielded an applied load of approximately 3000 psi, as is shown in the deflection curves (Figures 3-15 through 3-18). Radial cracks were evident in the concrete as well as conical cracks progressing from the bearing plate (Figures 3-19 through 3-22). The failure appeared to occur after yielding in the outer steel confining shell.

The distressed area of concrete directly under the inner confinement ring (Figure 3-20) was predicted and does not lead to failure or decrease in load capacity, but is caused by the vertical bearing of the inner confinement ring on the unconfined concrete. The spalling was expected to occur, and it did so on all the silo models tested. As can also be seen in this figure, a clip is welded to the inner confinement ring to support the displacement gauge.

Figure 3-19 shows the radial cracks in the top of the support and another view of the spalled area directly below the inner confinement ring, as well as the clip angles supporting the displacement gauge for the silo support.

It should be noted on the load displacement curve for Test 6 (Figure 3-18) that the closure did not fail but had a higher load capacity than the silo, which explains the sharp rise and return to zero on the displacement curve. The closure model remained elastic. Radial cracking was extensive in the failed support models (Figures 3-21 and 3-22). When the outer confinement ring was removed, the model fell apart.

The tests demonstrated that the assumed support failure mode was essentially correct. The contribution of the outer confining shell was vividly portrayed. However, we did not have enough outer confinement to mobilize the strength of the model and therefore did not get enough load on the closure support to load the inner confinement ring.

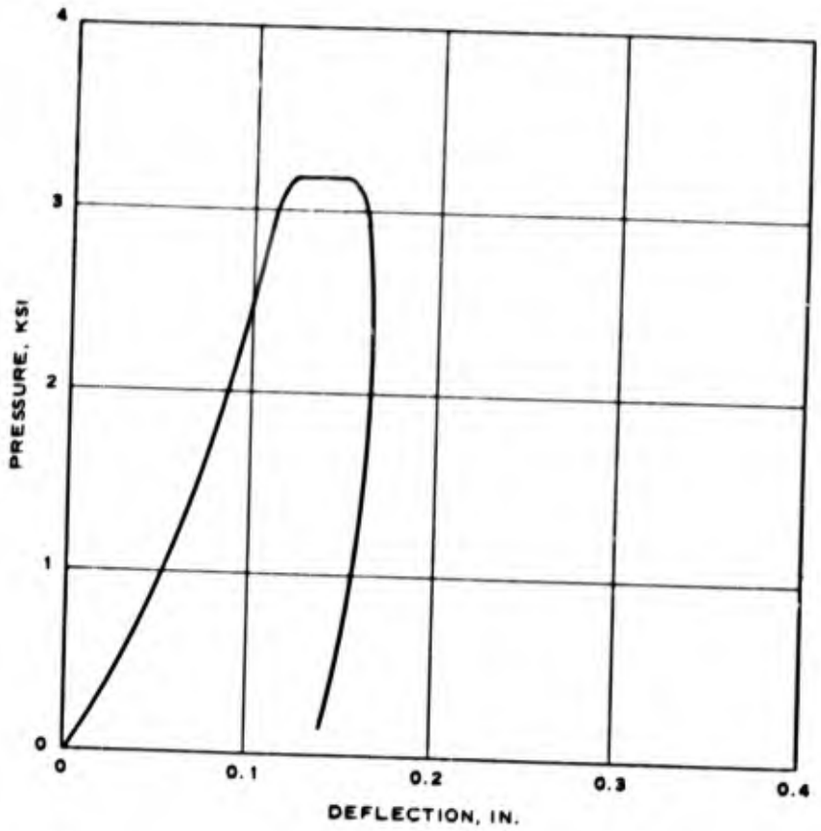

SUPPORT M121-1A TEST 5 - PRESSURE VS. DEFLECTION

FIGURE 3-15

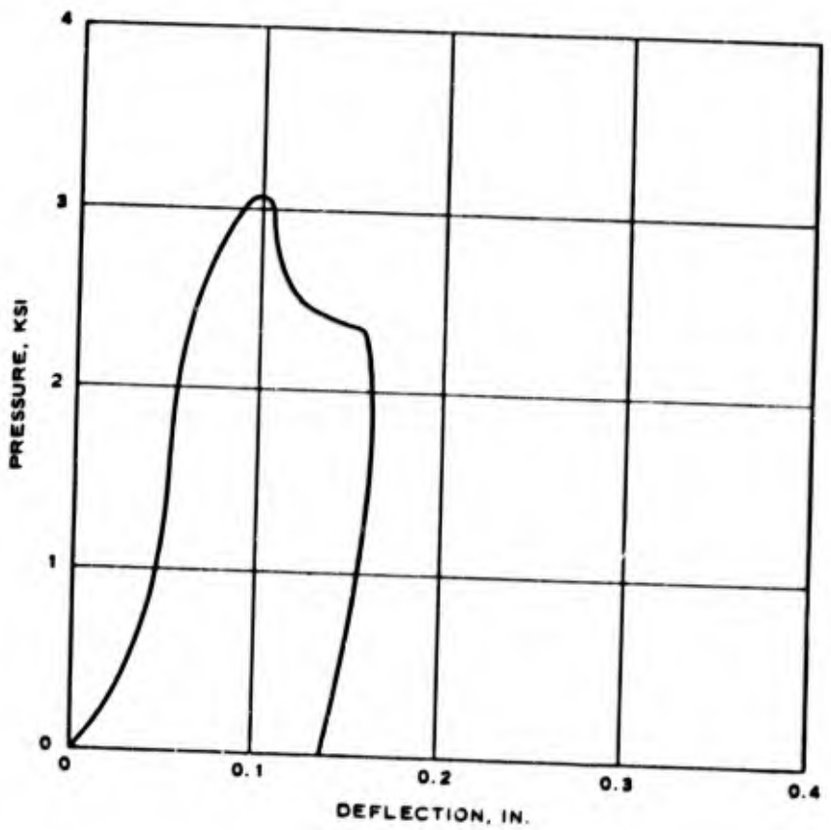

SUPPORT M121-1B TEST 6 - PRESSURE VS. DEFLECTION

FIGURE 3-16

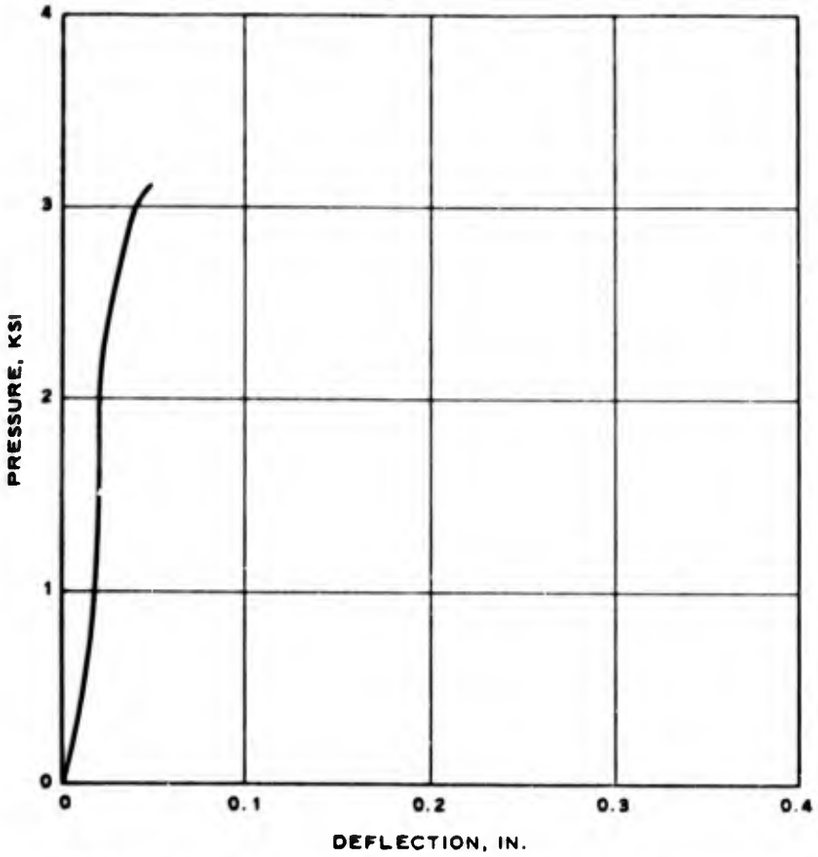

CLOSURE M120-2C TEST 5 - PRESSURE VS. DEFLECTION

FIGURE 3-17

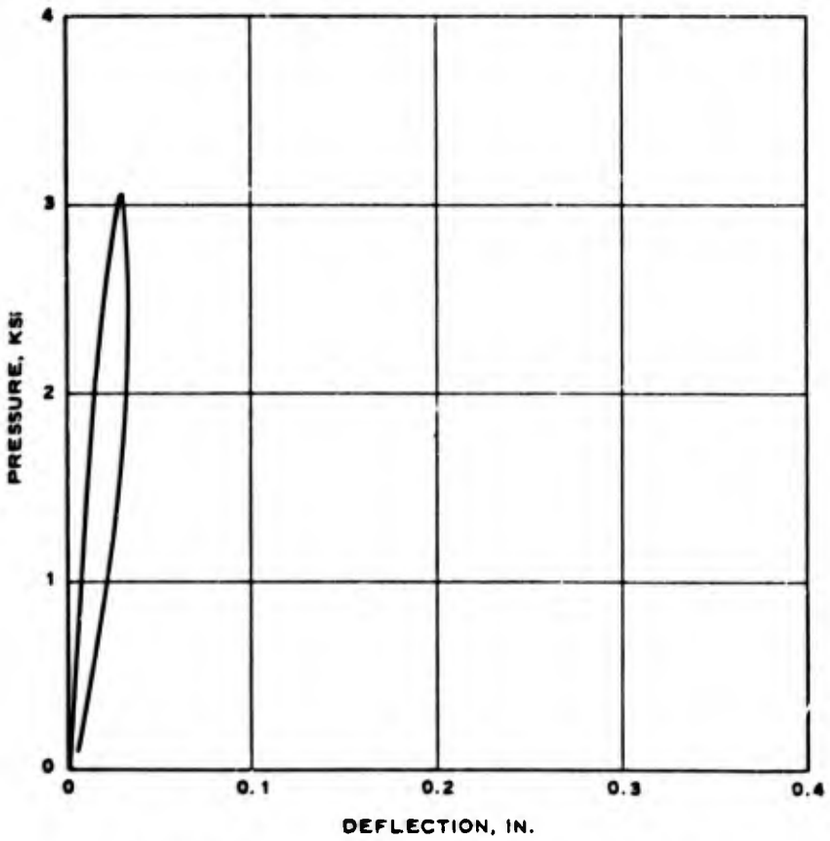

CLOSURE M120-2C TEST 6 - PRESSURE VS. DEFLECTION

FIGURE 3-18

TEST 5

FIGURE 3-19

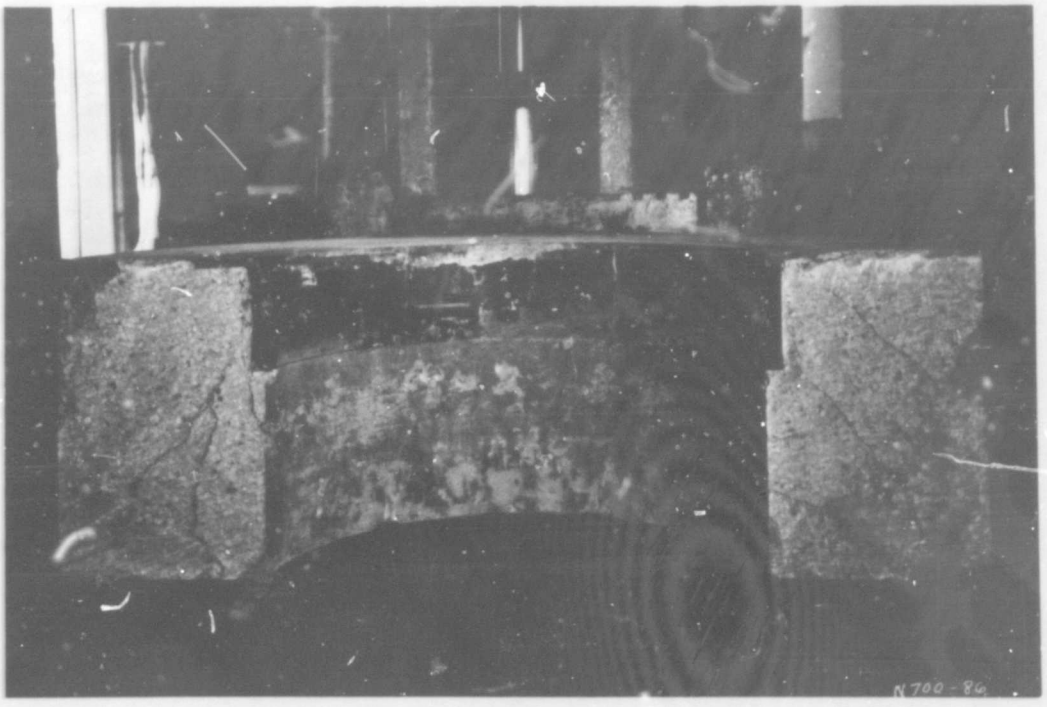

TEST 5

FIGURE 3-20

TEST 6

FIGURE 3-21

TEST 6

FIGURE 3-22

TEST 7

The closure that failed the supporting structure in Tests 5 and 6 was next tested on a support designed for a ultimate load capacity of 10,000 psi. This 10,000-psi level represents the load to be imposed on the total area of the closure; i.e., the unit load on the closure model, and not bearing stress. A 10,000-psi load on the closure would result in a load of approximately 40,000 psi on the bearings. The model support geometry for Test 7 is shown in Figure 3-23.

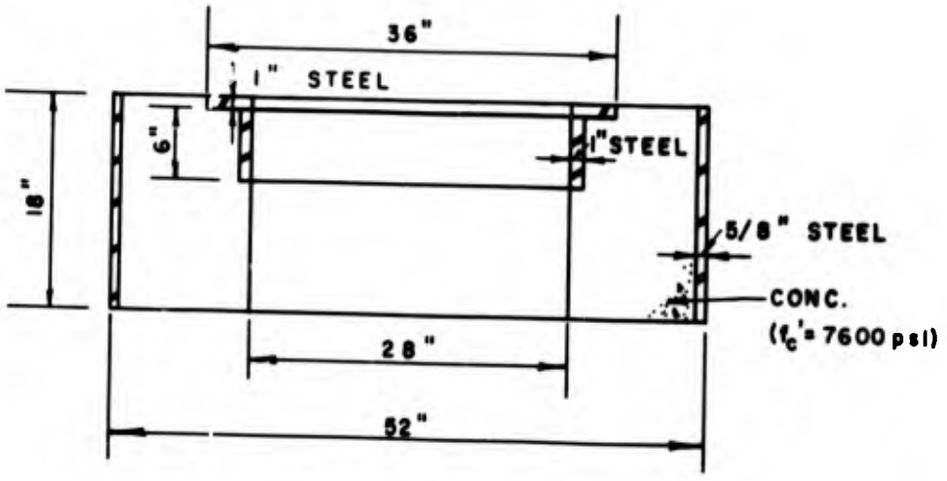

SUPPORT GEOMETRY FOR TEST 7

FIGURE 3-23

The test was undertaken to determine the increase in closure strength from high bearing friction, which could not be achieved in the earlier tests. The support had enough inherent load capacity to allow the closure model to be broken at a load of 4660 psi without visible damage to the support structure (an apparent unit bearing stress of 18,640 psi).

The pressure deflection curve for the silo (Figure 3-24) indicates essentially total recovery of the observed deflection and supports the contention that

the silo did not fail. The ductility exhibited by the closure is evident in Figure 3-25. Examination of Figure 3-26 shows that no punching action took place between the support and the bottom plate of the closure, which further substantiates the belief that the shearing was caused by the hardened low friction bearing blocks.

This test supported the contention that bearing friction could add considerable additional strength to a closure structure. In this particular situation the increased capacity was approximately 20 percent over that observed on the low friction support.

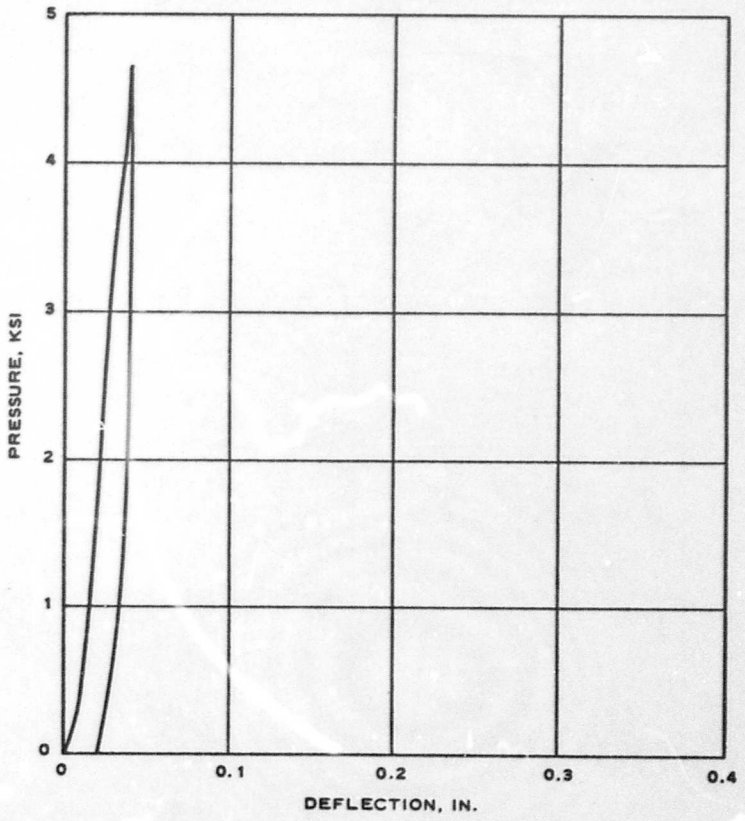

SUPPORT M121-2A TEST 7 - PRESSURE VS. DEFLECTION

FIGURE 3-24

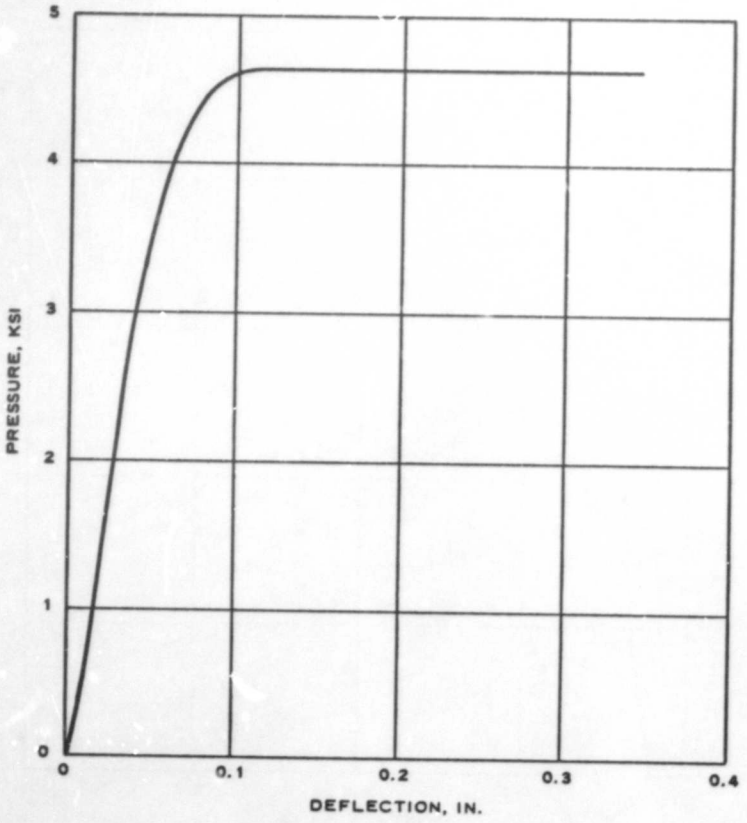

CLOSURE M120-2C TEST 7 - PRESSURE VS. DEFLECTION

FIGURE 3-25

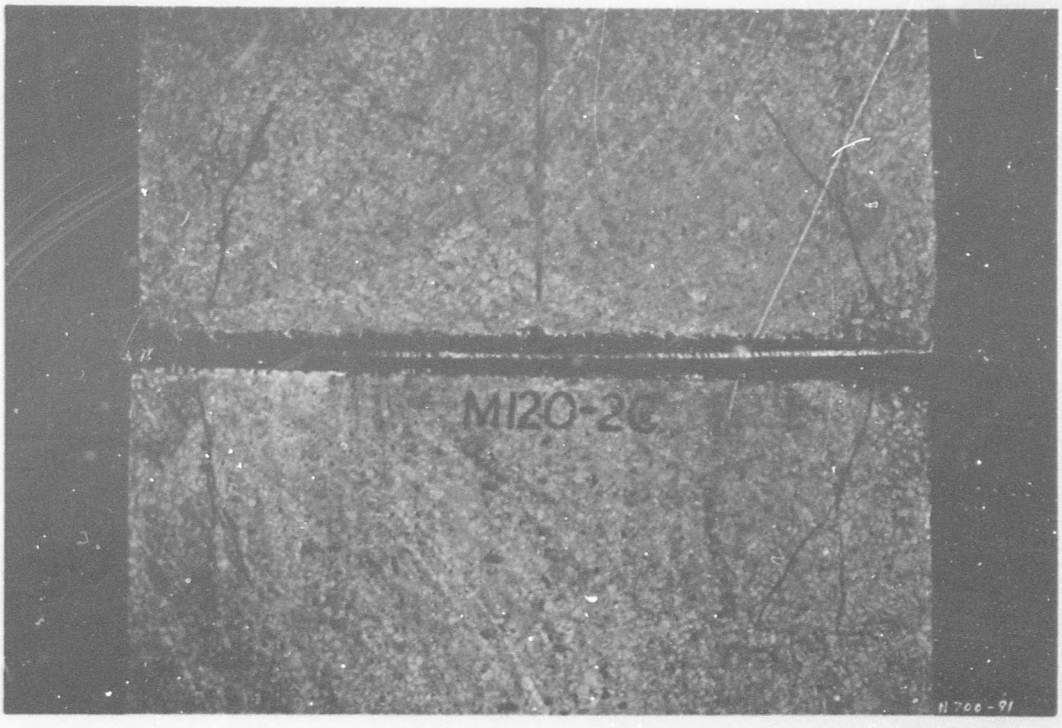

TEST 7

FIGURE 3-26
A2-59

TEST 8

The support used in Test 7 was next used to support a stronger closure model than that used in the preceding test. The closure was proportioned to fail at the 8000-psi load level. This test was intended to show the behavior of a well-matched closure and support.

The closure geometry for Test 8 is indicated in Figure 3-27. The closure support structure is shown in Figure 3-24 (Test 7).

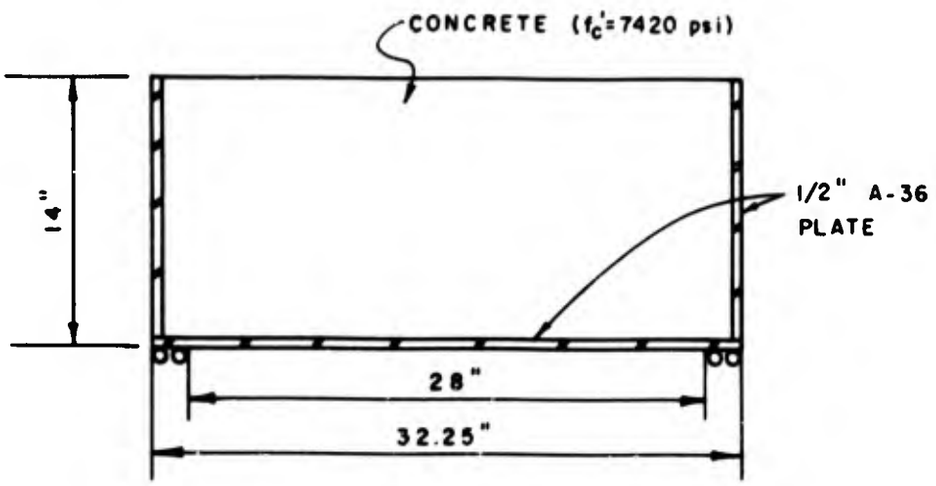

CLOSURE GEOMETRY FOR TEST 8

FIGURE 3-27

Failure was observed simultaneously in the closure and the silo at a load level of 6375 psi (an approximate bearing stress of 25,500 psi). However, examination of the load deflection curves (Figures 3-28 and 3-29) indicates that the closure could probably have taken more load, as the curve was still rising

Figure 3-30 shows only relatively minor distress in the closure, although some distress in the bearing is evident. The support shows diagonal cracking from the bearing and spalling of concrete immediately under the confinement ring, as can be seen in Figure 3-31. This appears to be a characteristic failure pattern for this support configuration. The vertical crack under the bearing of the silo (Figure 3-31) is very similar to the crack in the closure (Figure 3-30), and points out the fact that the inner confinement ring is serving the same function for the silo as that provided by the outer shell for the closure. The mode of support response was the same as previously observed. There was no shear crack in the closure model after testing. Failure appeared to be local and to have been caused by yielding of the steel shell. The silo and the closure appear to be rather closely matched in total load capacity.

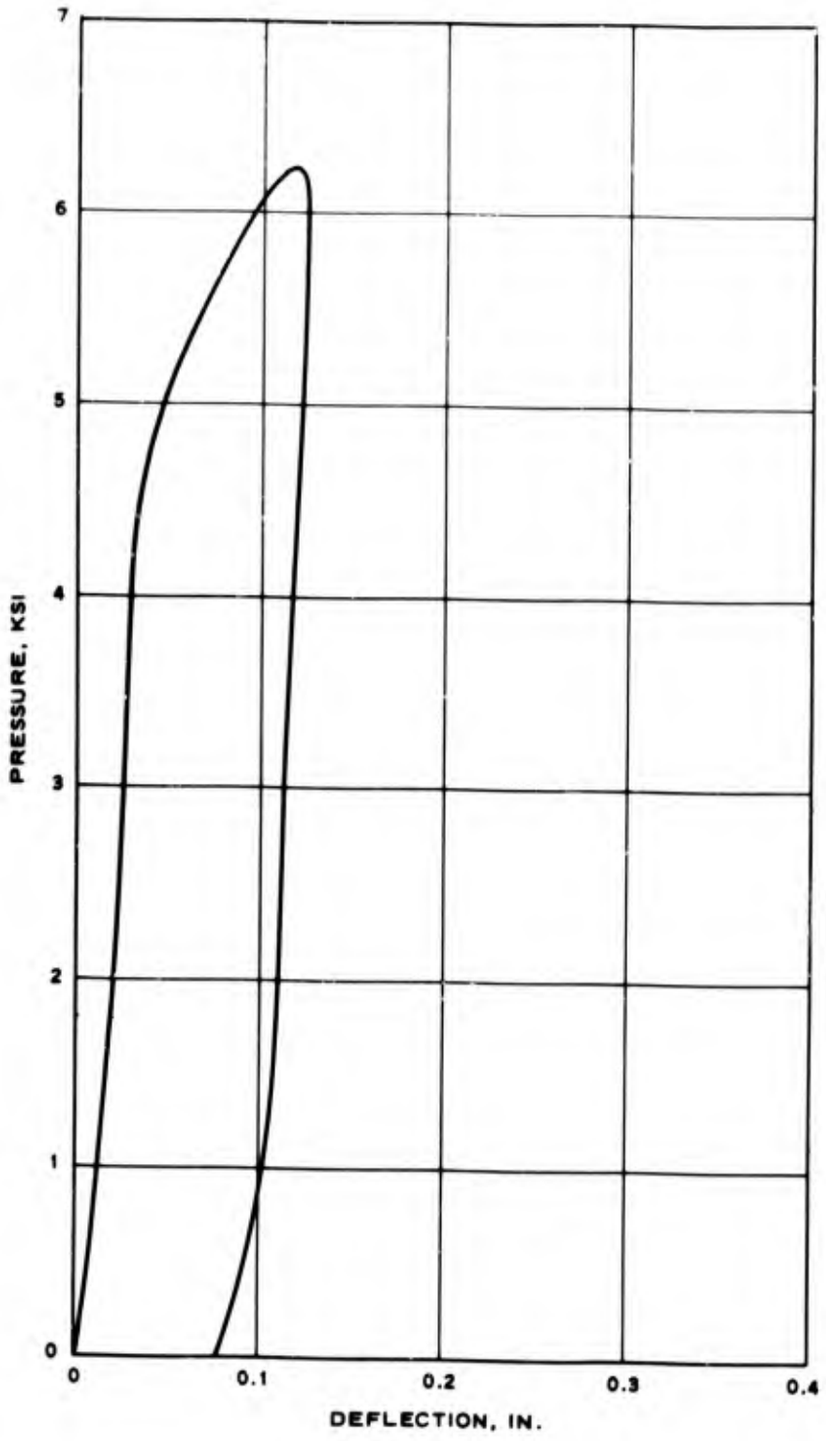

SUPPORT M121-2A TEST 8 - PRESSURE VS. DEFLECTION

FIGURE 3-28

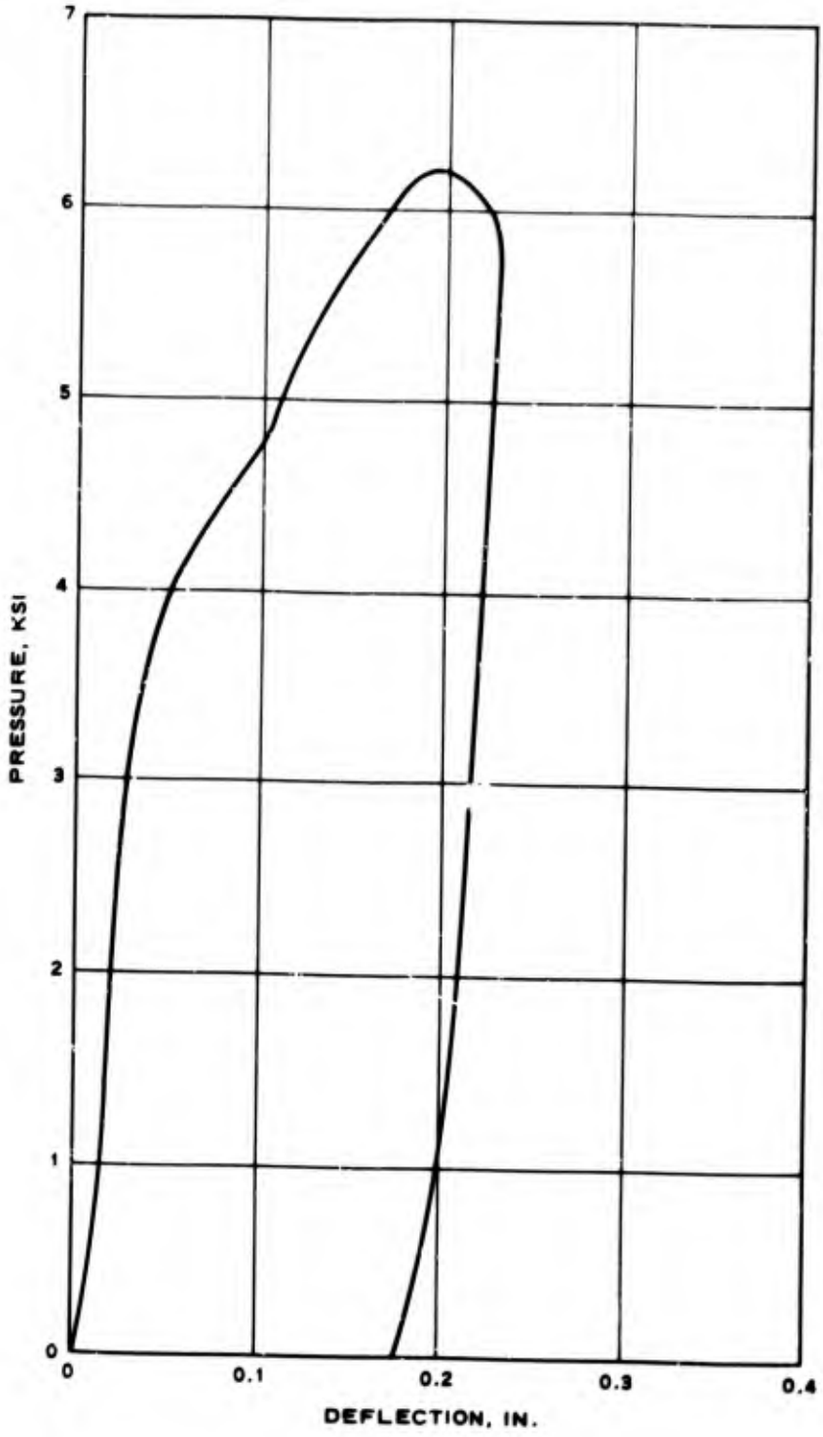

CLOSURE M120-3A TEST 8 - PRESSURE VS. DEFLECTION

FIGURE 3-29

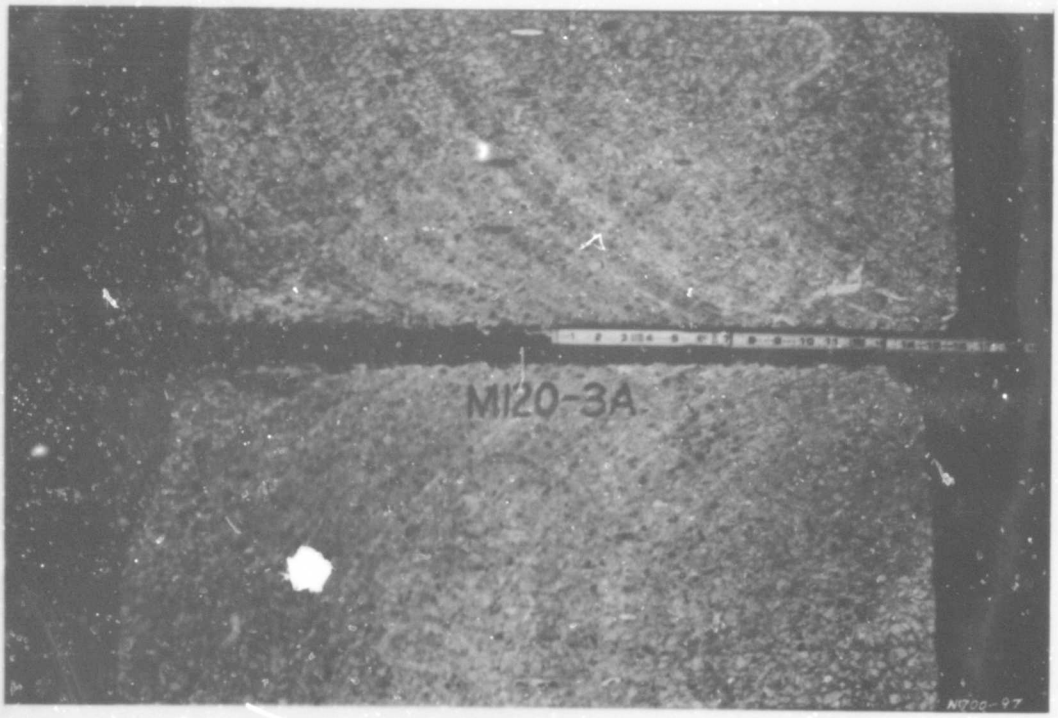

TEST 8

FIGURE 3-30

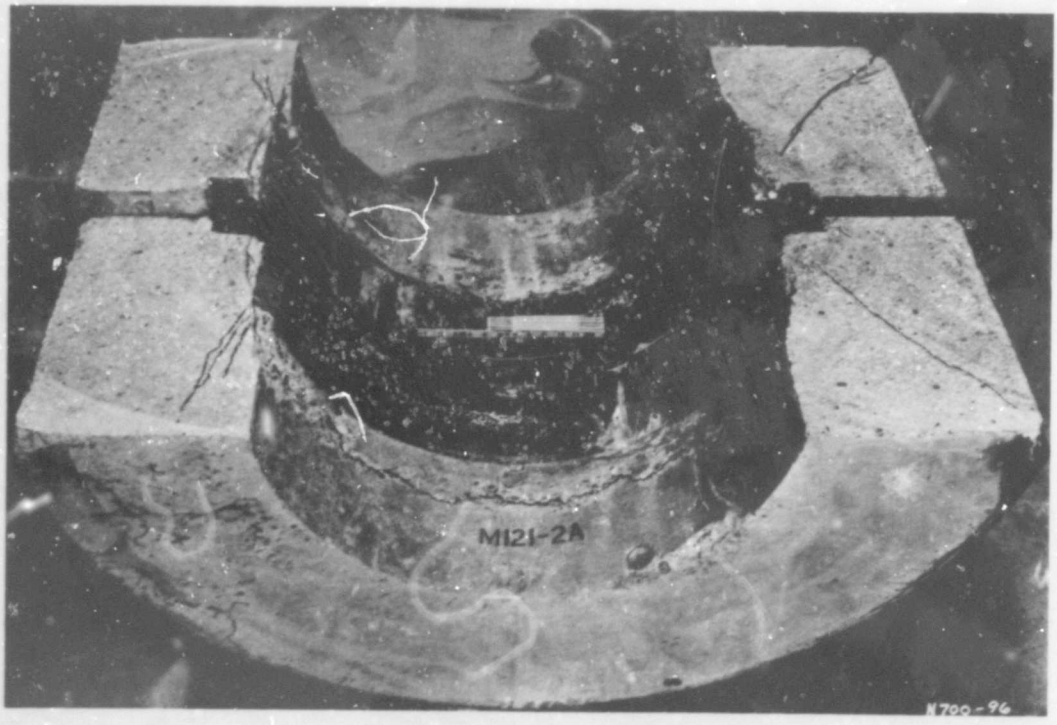

TEST 8

FIGURE 3-31

TEST 9

A closure model with 1/2-inch plates was next tested on a silo which was similar to those used in Tests 5 and 6, but with a much thicker bearing plate (1-1/2 inch, compared with 1/2 inch for Tests 5 and 6). This test was performed to determine the increase in support strength from a thicker bearing plate and a stronger closure.

The closure tested was identical to that of Test 8 (see Figure 3-27). The support geometry is shown in Figure 3-32.

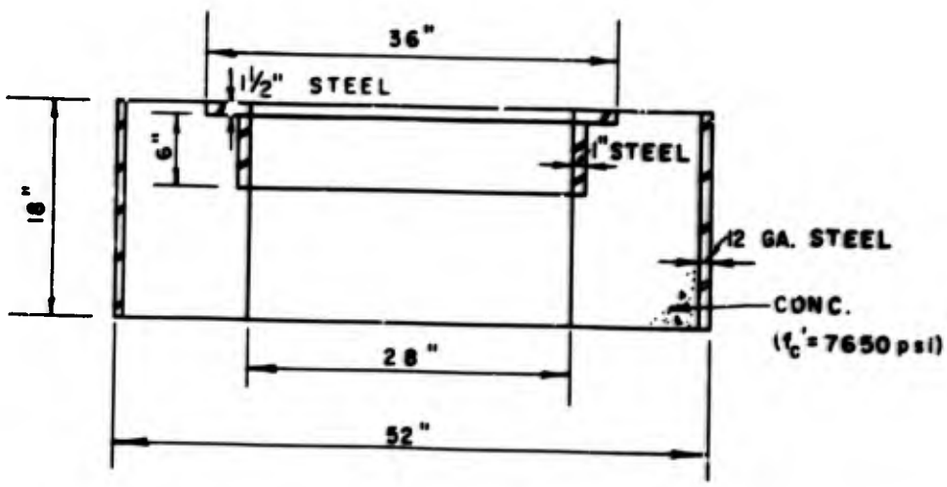

SUPPORT GEOMETRY FOR TEST 9

FIGURE 3-32

The failure occurred in the support structure, as had been predicted, at a load level of 3846 psi applied to the closure (see Figures 3-33 and 34). It should be pointed out that the slope in the load deflection curve for the closure does not represent a yielding or a reduction in load capacity, but merely models the capacity of the silo. The closure was not damaged, but the silo failed.

After the test event, the outer shell was removed from the support structure and the tendency of the structure to grow could be observed from the presence of a bend in the removed plate at its point of contact with the base of the test fixture. Note the yielded area in the lower section of the outer confinement shell of the silo (Figure 3-35). The lowest edge of the outer confinement ring was in contact with the steel base plate and could not move outward due to the friction generated between the two steel surfaces. Immediately above that a yield area can be observed - a curved section - which was caused by the horizontal loading from the concrete. This is confirmed by the crack pattern in Figure 3-36. The apparent formation of an arch (Figure 3-36) is essentially the continuation of the closure structure; the closure and the silo support actually function as a single structure.

In the crack pattern shown on the right side of Figure 3-36 there is evidence of continuation of an arch forming, which throws both vertical and horizontal loading into the outer confinement ring provided on the silo. The strength of the silo influences the apparent load capacity of the model, and vice versa to some extent, emphasizing again that the silo support and the closure are really one structure, and should be analyzed as such.

Figure 3-37 shows the closure specimen used to load the silo support in Test 9; note that it was essentially undamaged. Figure 3-38 illustrates the failed silo support.

Comparison of Test 9 with Tests 5 and 6 demonstrates that increasing the bearing plate thickness apparently accounted for a 27-percent increase in load capacity, although some increase is probably due to the heavier closure.

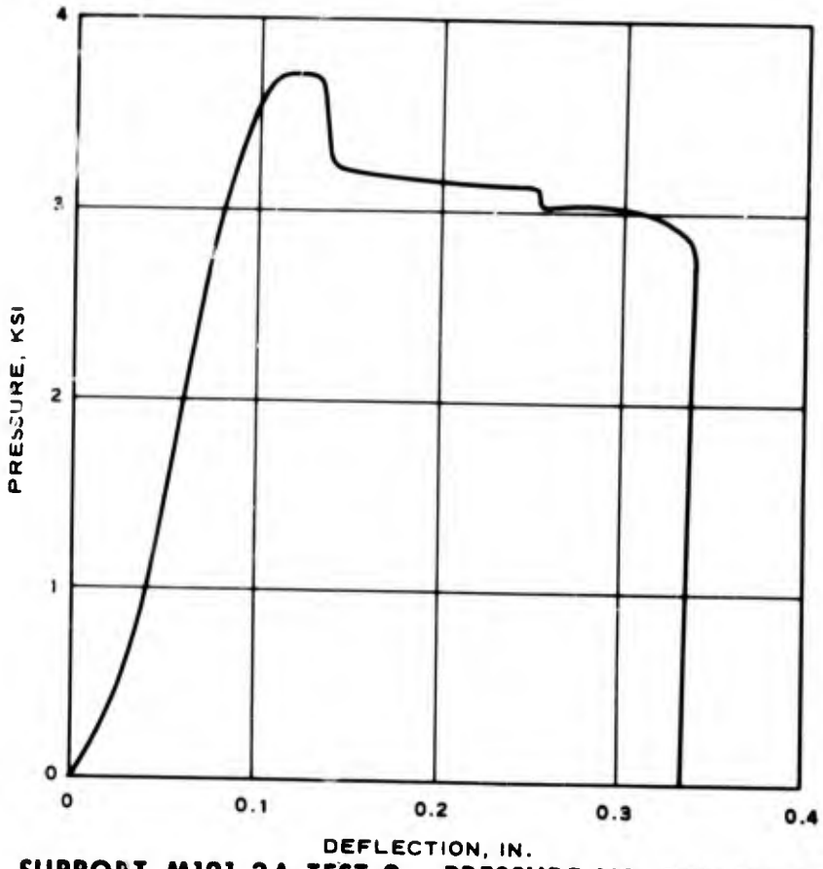

SUPPORT M121-3A TEST 9 - PRESSURE VS. DEFLECTION

FIGURE 3-33

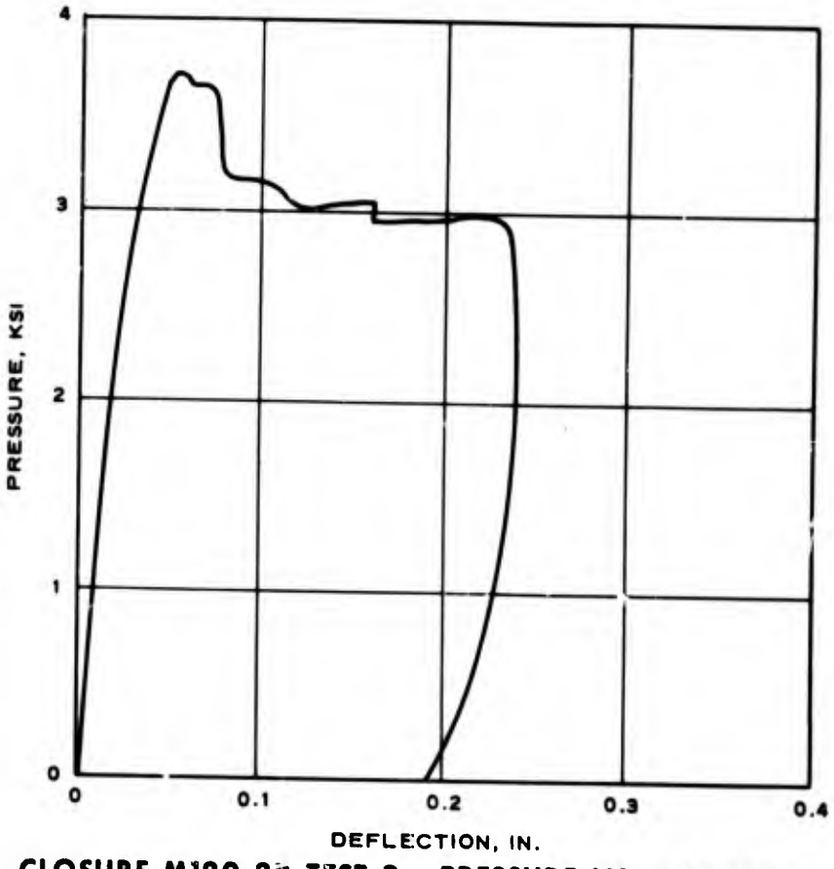

CLOSURE M120-3B TEST 9 - PRESSURE VS. DEFLECTION

FIGURE 3-34

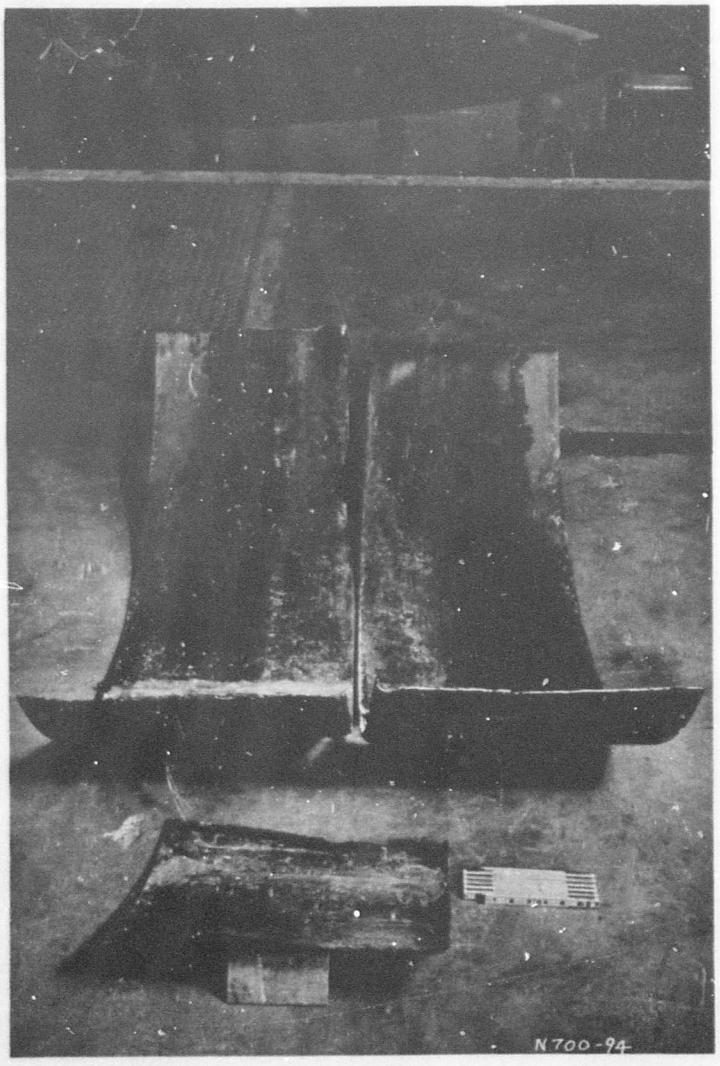

TEST 9

FIGURE 3-35

A2-68

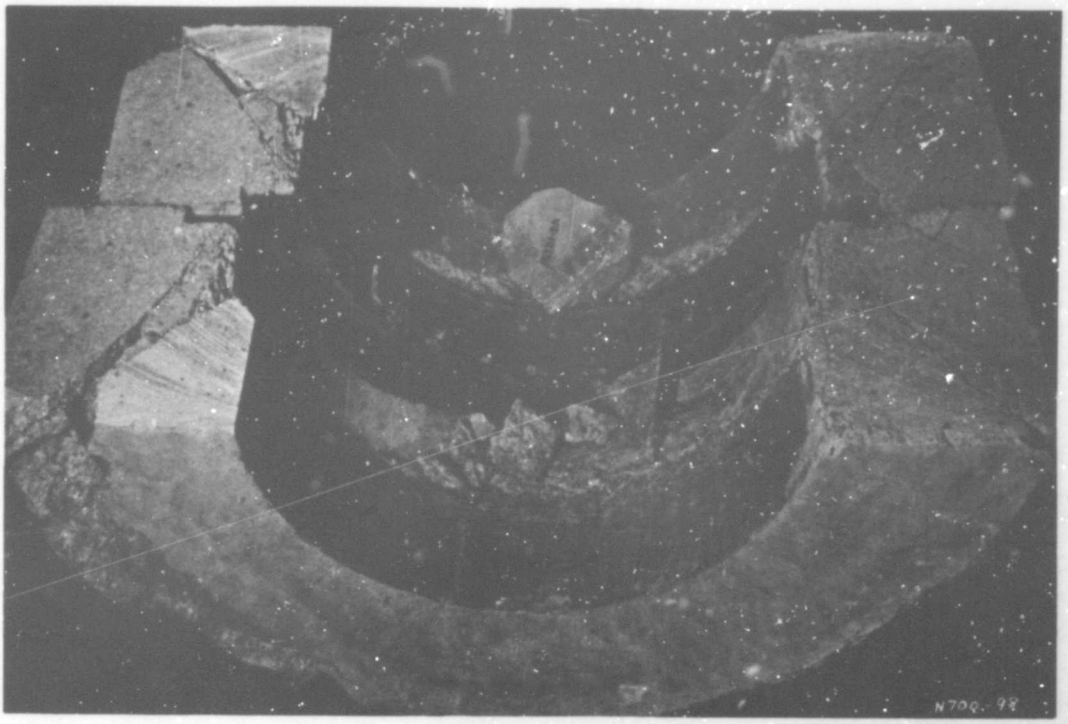

TEST 9

FIGURE 3-36

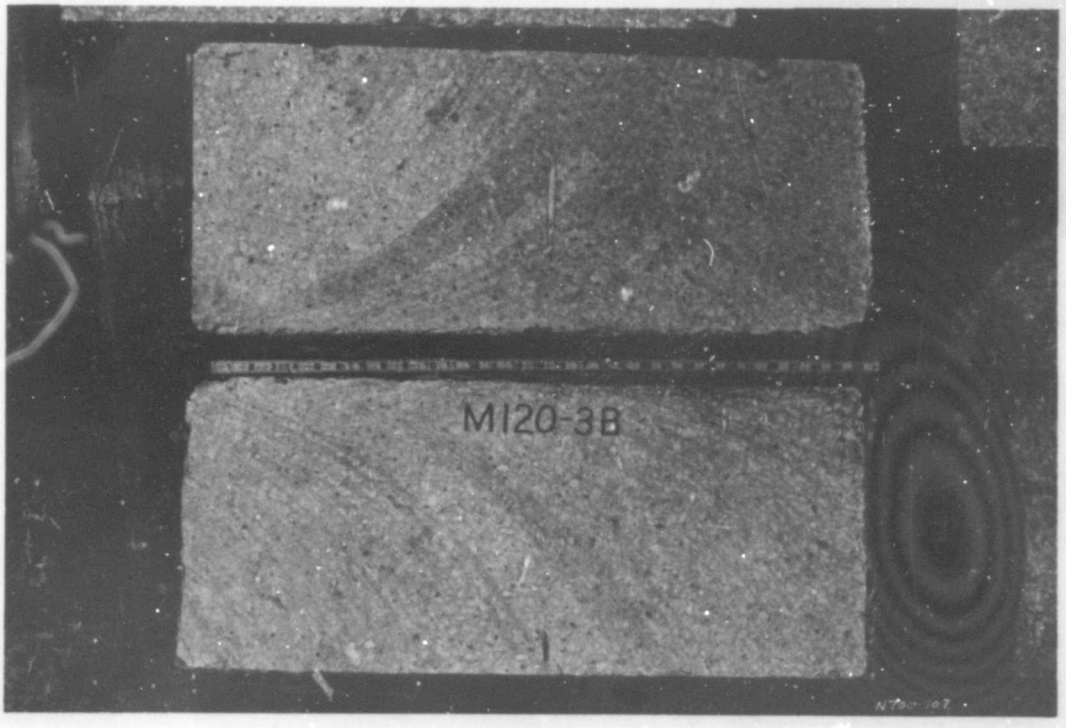

TEST 9

FIGURE 3-37

TEST 9

FIGURE 3-38
A2-70

TEST 10

This test was designed specifically to examine the interaction phenomenon. A support equivalent to that of Tests 7 and 8 was loaded by a closure specimen with 3/4-inch plates. The increased load capacity of the support structure when loaded with a stiff closure was to be examined. The closure geometry is shown in Figure 3-39.

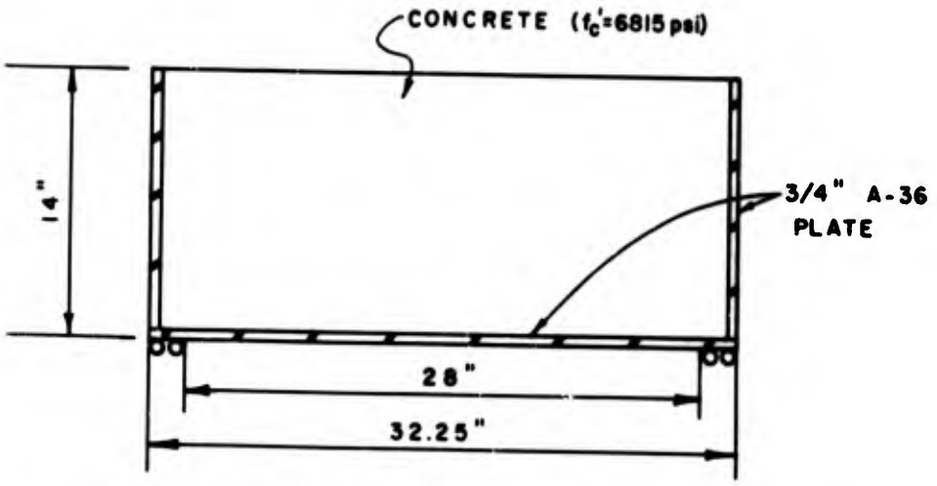

CLOSURE GEOMETRY FOR TEST 10

FIGURE 3-39

There was an anomaly in the data recovery from this test which tends to discredit the apparent results. This anomaly is seen in the silo load deflection curve (Figure 3-40), where there is a sharp rise in load capacity with no apparent displacement. This was caused by the bottoming out of the displacement gauge; therefore the vertical portion of the curve should be ignored. In the curve for the closure (Figure 3-41), none of the unloading portion of the test sequence is shown.

Evidence of silo failure, which occurred at a load level of 6800 psi, can be seen in Figures 3-42 and 3-43. The concrete in the closure does not appear to be distressed (Figure 3-44); however, significant yielding had occurred in the bottom plate. The heavy confinement ring of 3/4-inch steel has prevented a bearing failure on the closure. It appears that the strength of the combination was controlled by the silo.

Confirming the assumption that the closure probably had more load capacity is the fact that, in Test 13, a 3/4-inch closure was tested on a low friction support and attained an 8815-psi level. We are confident that this should be possible on a silo or rigid support.

Inspecting the model after the test, it was evident that the support collapsed as in previous tests and the closure distress was local due to yielding in the steel plates.

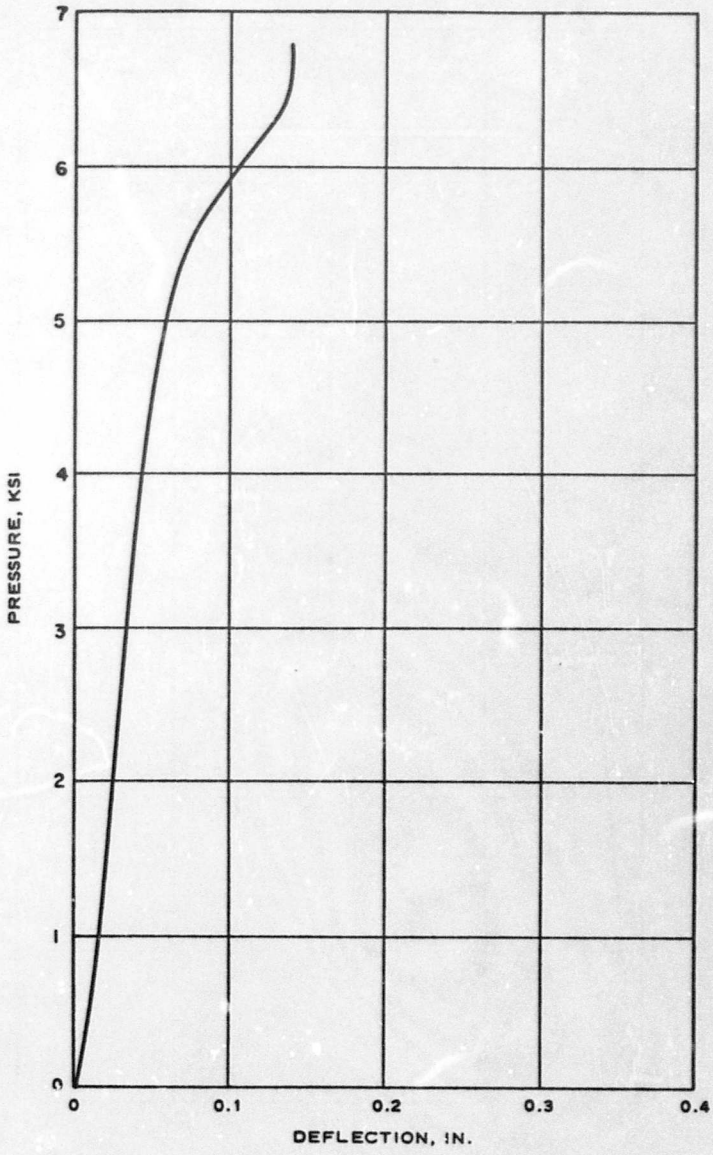

SUPPORT M121-2B TEST 10 - PRESSURE VS. DEFLECTION

FIGU[illegible]3-40

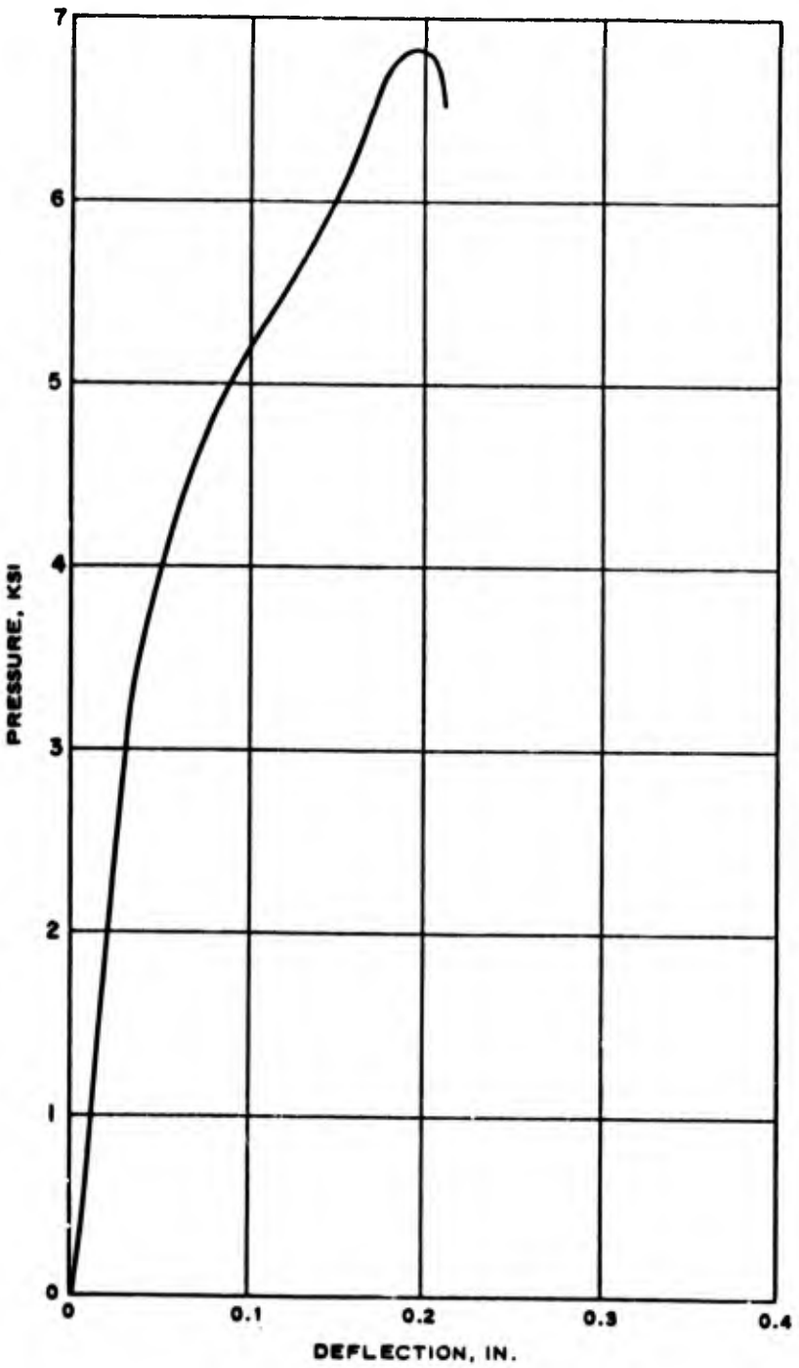

CLOSURE M120-5A TEST 10 - PRESSURE VS. DEFLECTION

FIGURE 3-41

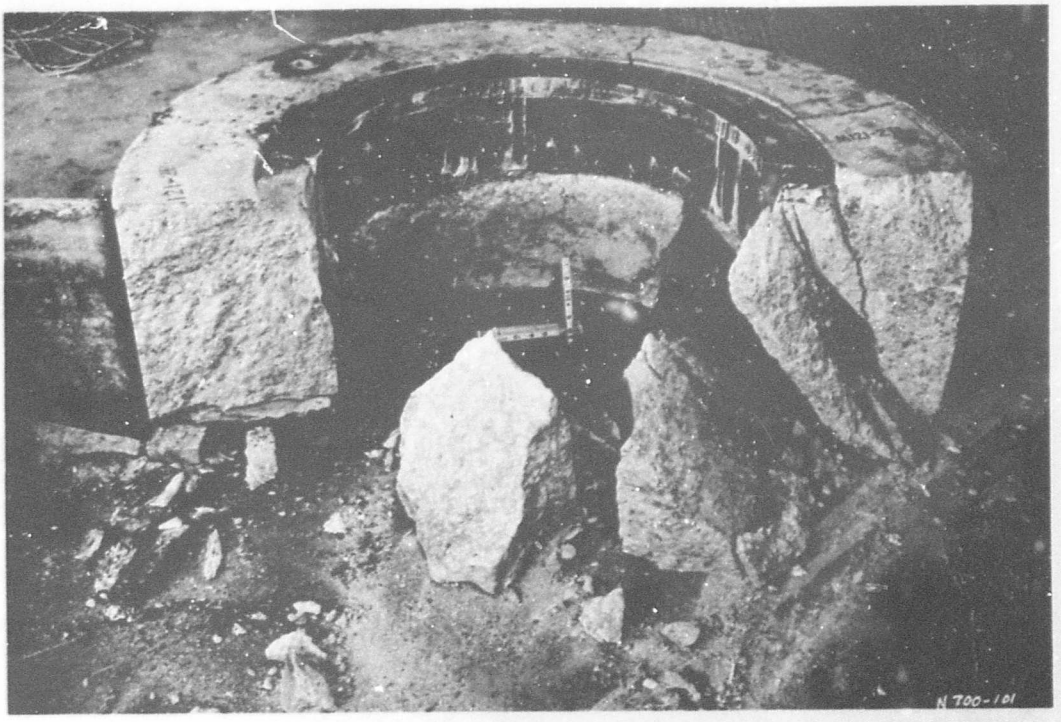

TEST 10

FIGURE 3-42

TEST 10

FIGURE 3-43

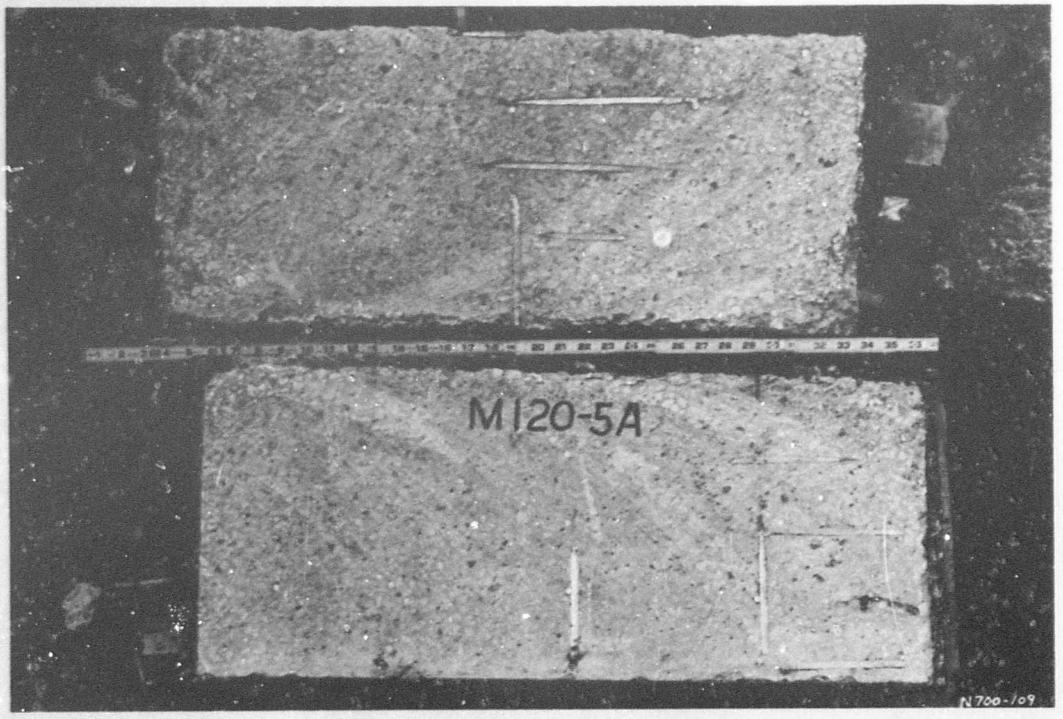

TEST 10

FIGURE 3-44
A2-76

TEST 11

To further explore the interaction phenomena, a 3/4-inch closure was next used to test a support identical to that used with a 1/2-inch closure in Test 9. The closure and the support configuration are shown in Figures 3-39 (Test 10) and Figures 3-32 (Test 9), respectively.

The pressure deflection curves (Figures 3-45 and 3-46) indicate that the support structure failed at a load of 4084 psi; no additional strength was observed over Test 9. This shows that for these particular models interaction is no more pronounced than for a less stiff closure tested on an identical support.

The general pattern of the radial cracks in Figure 3-47 is quite similar to that observed in Test 9. Figure 3-48 shows the support at the time of post-test inspection.

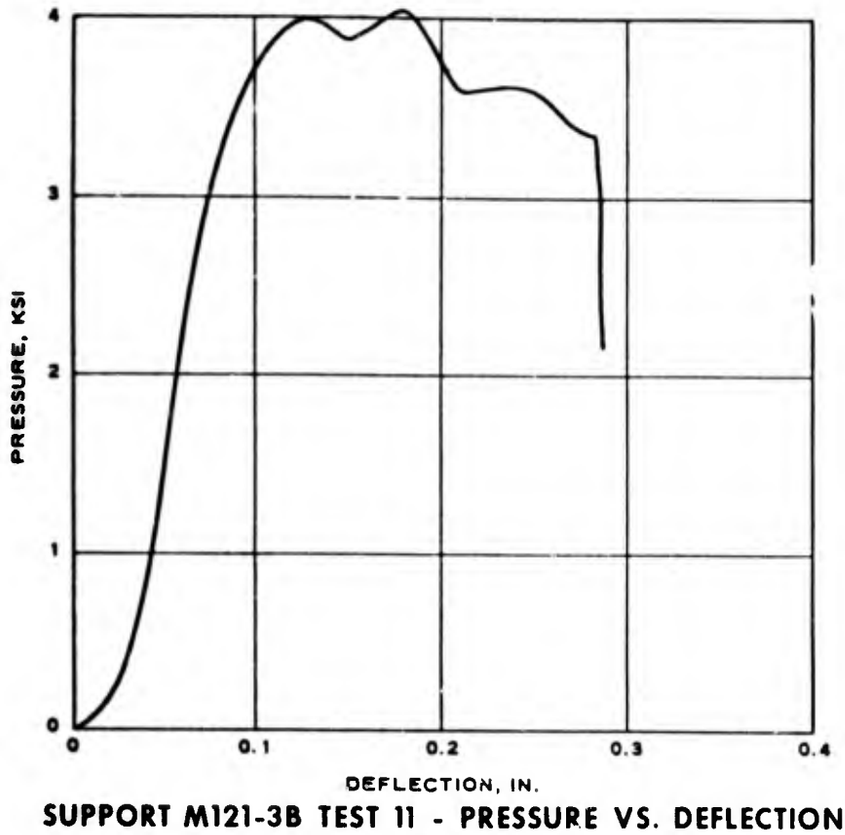

SUPPORT M121-3B TEST 11 - PRESSURE VS. DEFLECTION

FIGURE 3-45

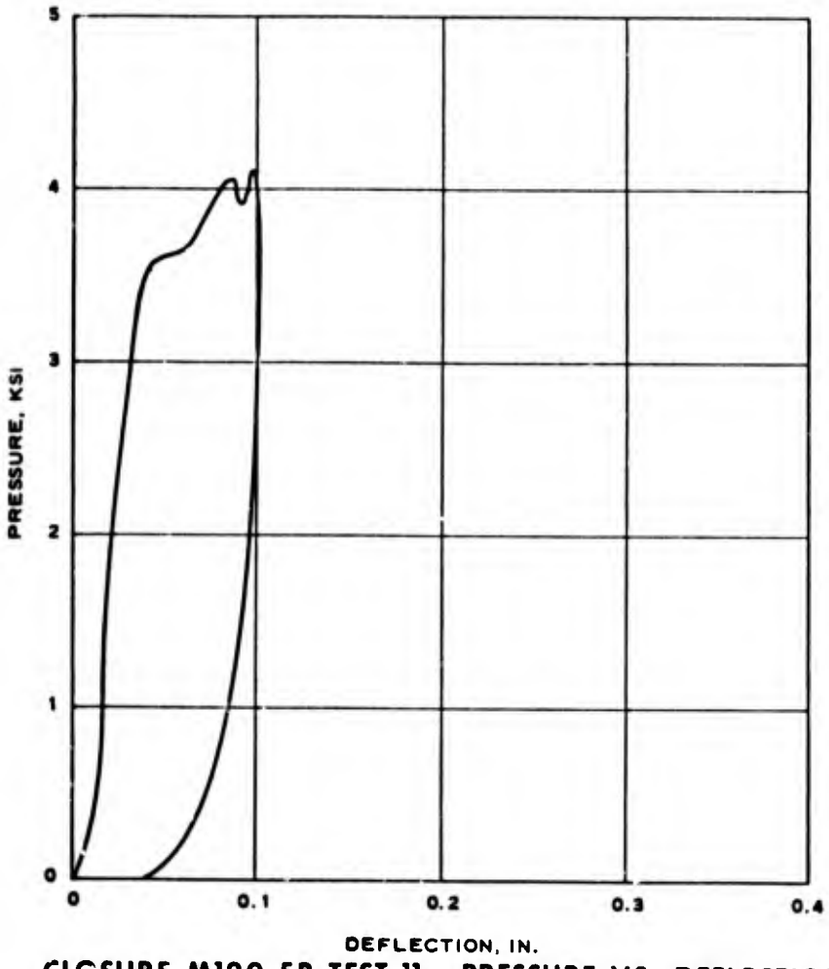

CLOSURE M120-5B TEST 11 - PRESSURE VS. DEFLECTION

FIGURE 3-46

TEST 11

FIGURE 3-47

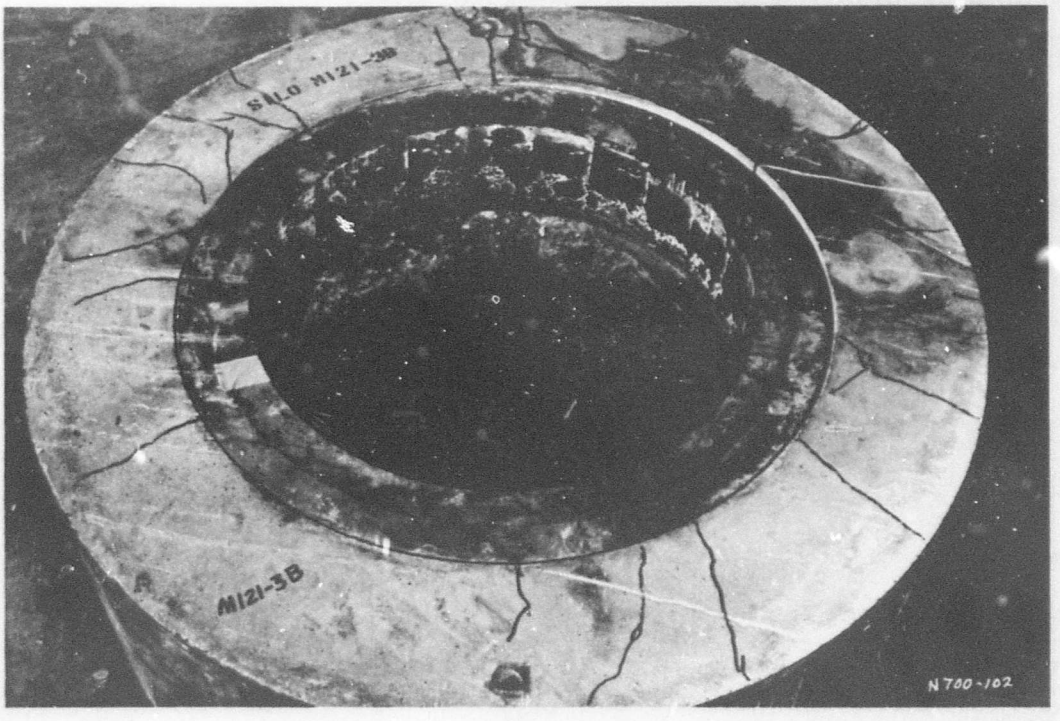

TEST 11

FIGURE 3-48

TESTS 12 AND 15

Before the test series began, there was a great deal of concern about shear failures in closures. In these tests, an attempt was made to increase the shear capacity of the models. A steel cone was placed in two of the 1/4-inch closure models, as shown in Figure 3-49.

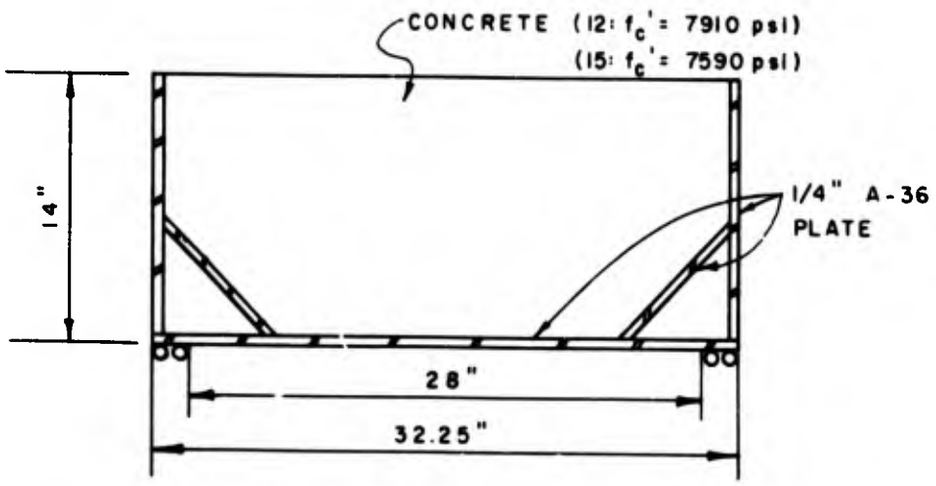

CLOSURE GEOMETRY FOR TESTS 12 AND 15

FIGURE 3-49

The models were tested on low friction and high friction (steel to steel) bearings, with identical results. The total load capacity of the models was decreased by the addition of the cone. The model on the low friction bearing failed at 2900 psi (Figure 3-50), while the model on the high friction bearing failed at 2792 psi (Figure 3-51).

The cone introduced a vertical load component directly into the outer shell and caused buckling of this element at a low load level (Figures 3-52 and 3-53). The concept could be used effectively only if the outer shell were stiffened considerably.

Since other tests have shown that a shear-type failure is not critical, this concept should be eliminated from practical consideration.

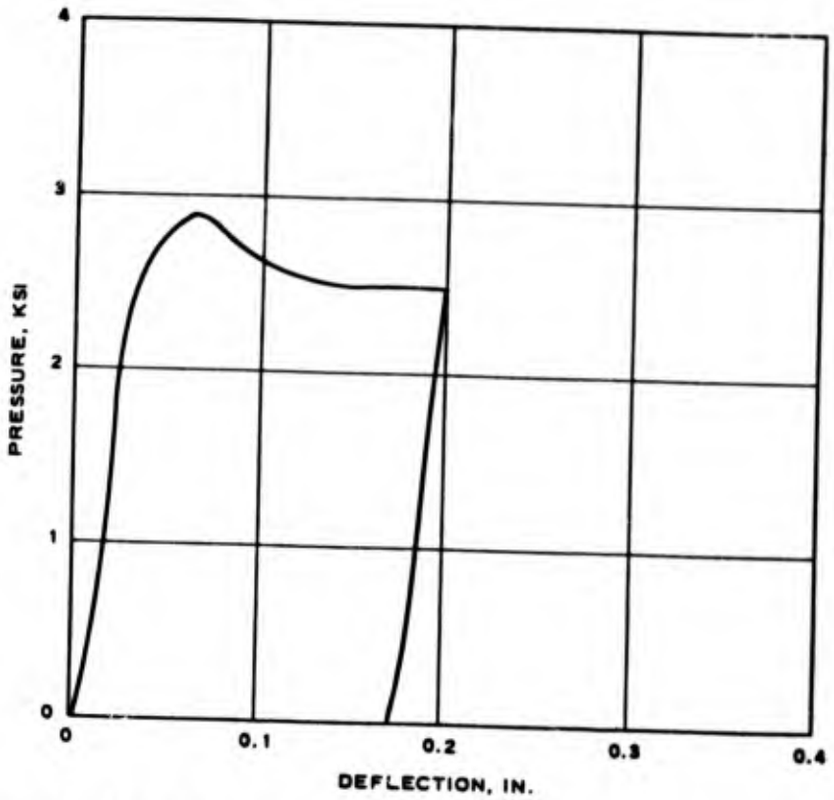

CLOSURE M120-4A TEST 12 - PRESSURE VS. DEFLECTION

FIGURE 3-50

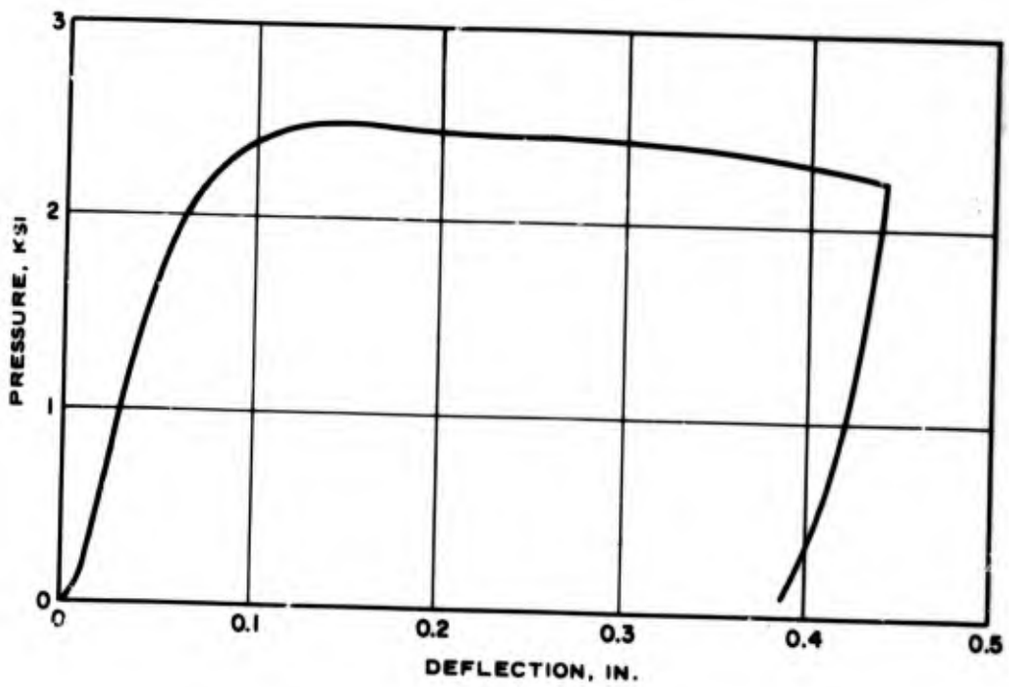

CLOSURE M120-4B TEST 15 - PRESSURE VS. DEFLECTION

FIGURE 3-51

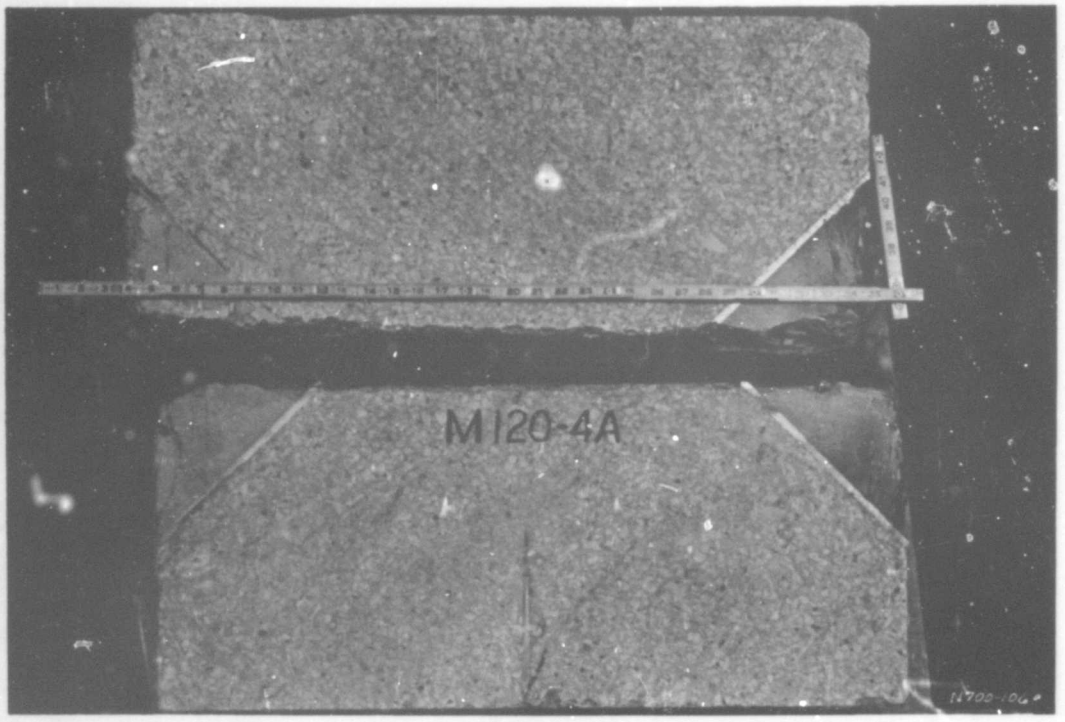

TEST 12

FIGURE 3-52

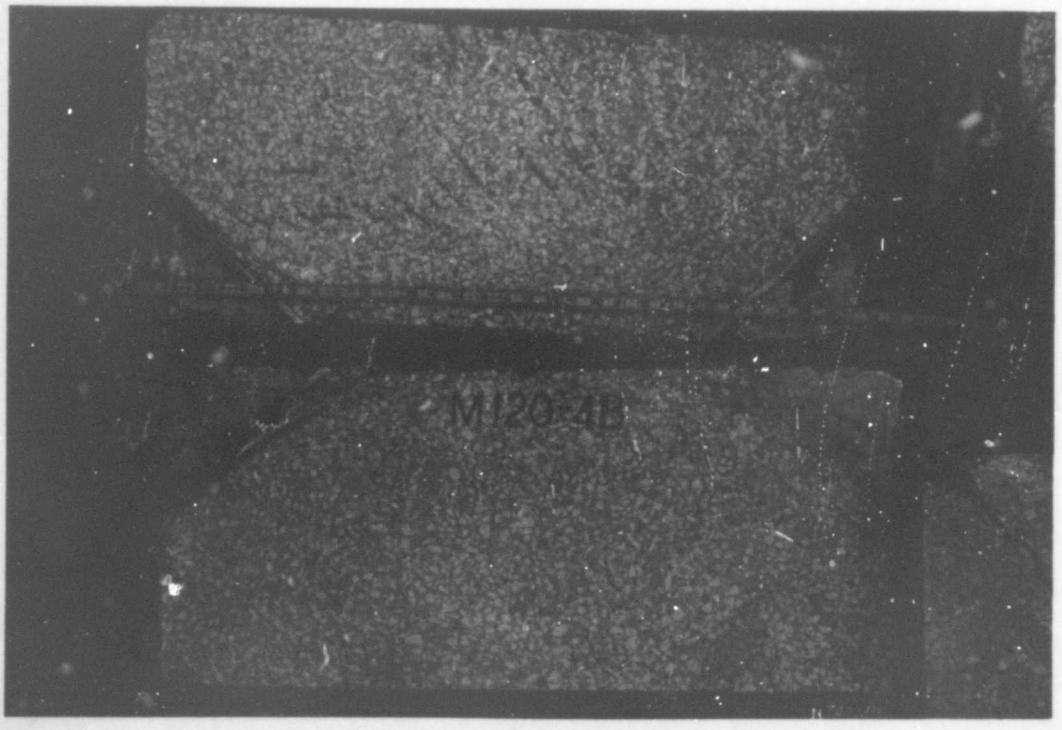

TEST 15

FIGURE 3-53

TEST 13

The Test 13 model was designed for an ultimate load capacity of 12,000 psi. This test was made to compare with the results of Test 10. The closure geometry is shown in Figure 3-54. The test was performed on a low friction support.

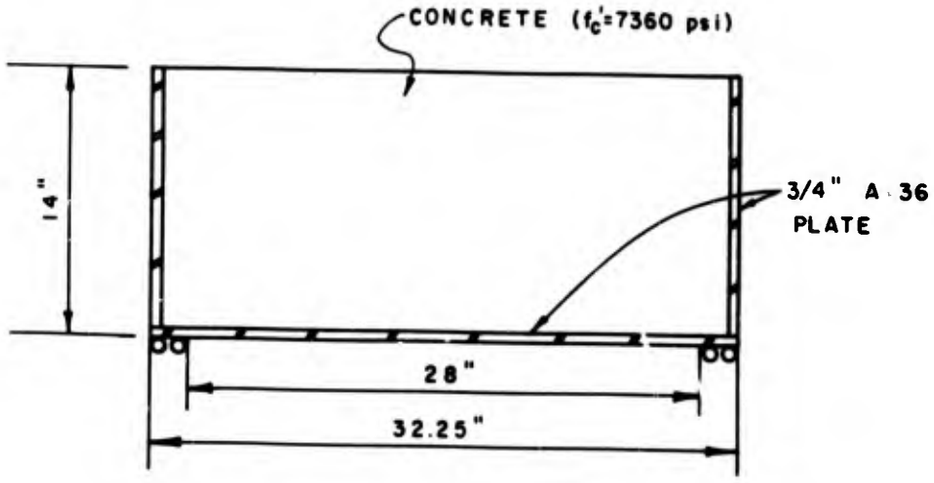

CLOSURE GEOMETRY FOR TEST 13

FIGURE 3-54

The maximum test pressure reached was 8815 psi (Figure 3-55), which lends support to the assumption that the closure in Test 10 had additional load capacity available and that the load capacity of the combination was controlled by the silo.

The test photograph shows a damaged zone of concrete extending all the way from the bearing to the top surface of the model (Figure 3-56). This is misleading since after the maximum pressure was reached vertical load was unintentionally put into the side shell from the testing apparatus. The vertical point on the deflection curve (Figure 3-55) is the point at which

the deflection gauge bottomed out. Since there was no more capacity in the gauge, it indicates zero deflection with an increase in load. Because the deflection reading was lost during the test, the test was continued to a point where the piston in the loading machine came in contact with the sidewalls of the closure model. The true collapse mode is thus not properly indicated, although it is predicted that a local failure occurred as before due to yielding of the steel plates.

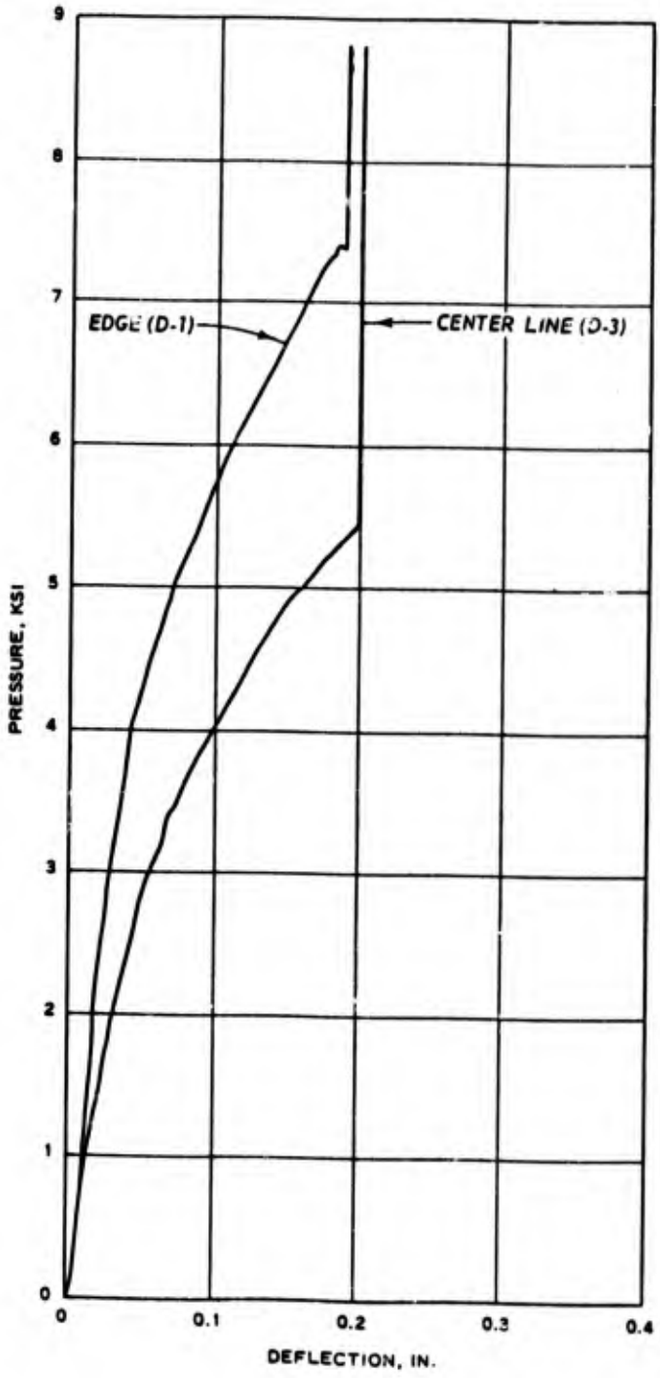

CLOSURE M120-5B TEST 13 - PRESSURE VS. DEFLECTION

FIGURE 3-55

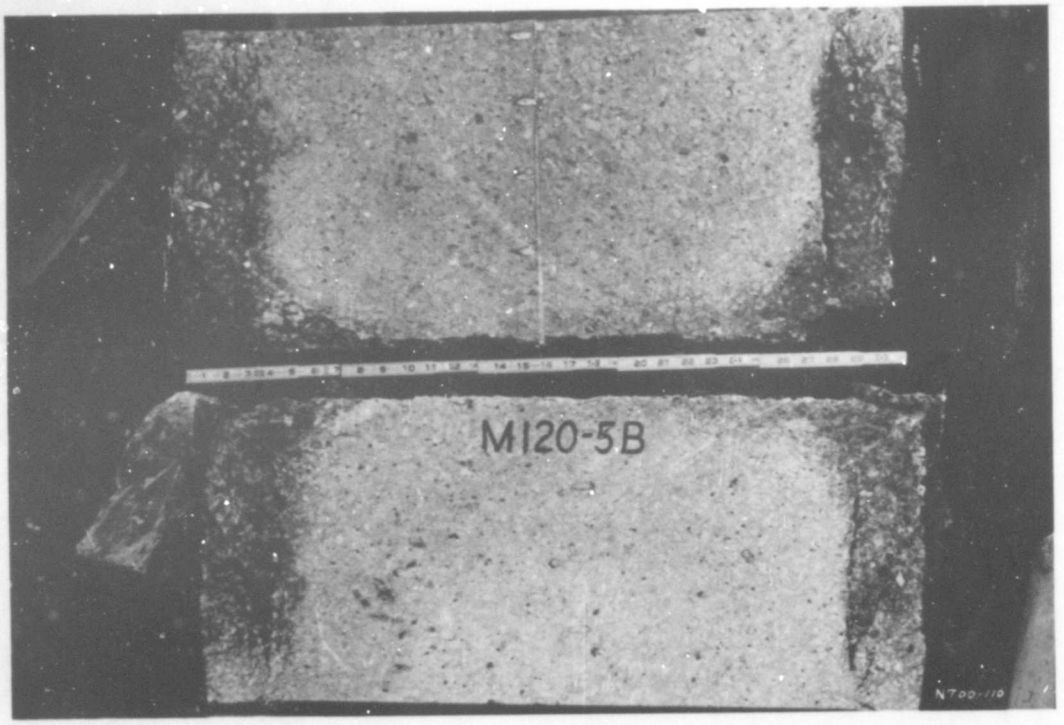

TEST 13

FIGURE 3-56

A2-86

TEST 14

A closure model identical to those used in Tests 3, 4, 5, 6, and 7 was tested on a high friction (steel-to-steel) support in order to ascertain the increased load capacity from friction and to compare this with the additional load capacity obtained when testing the model on a model support structure. The high friction support consisted of a 4-foot outside diameter by 28-inch inside diameter 2-inch-thick steel plate, which rested directly on the adjusting plates -- the steel support within the fixture. Because of the detail of the support, the stiffness of the leveling plates was actually mobilized, as was the radial stiffness of the 2-inch plate that supported the model. The closure geometry is shown in Figure 3-57.

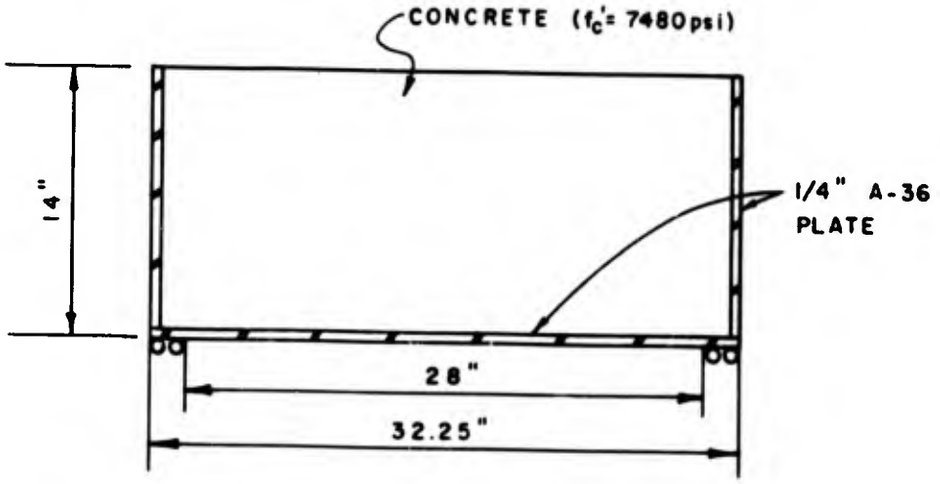

CLOSURE GEOMETRY FOR TEST 14

FIGURE 3-57

One of the effects of the increased radial stiffness and friction of the support is to increase the shear crack angle (Figure 3-58). In this test, the shear crack angles were more nearly vertical than in Tests 3 and 4. The

increased radial stiffness of the support enhances the load capacity of the model, demonstrating again the general phenomenon of the interaction between the closure and the support.

The closure failed at a pressure of 4152 psi (Figure 3-59). This test result can be compared with the results of Test 7 where an identical closure model was tested to failure on a silo support. The closure in Test 7 failed at a load of 4660 psi. After correcting the load capacity of the closure tested in Test 14 to account for the variation in concrete strength between the closure models, the apparent load capacities of the closures in Test 14 and Test 7 are 4660 psi and 4450 psi, respectively. These load capacities are in good agreement and support the assumption that support interaction through friction can increase closure load capacity by as much as 20 percent.

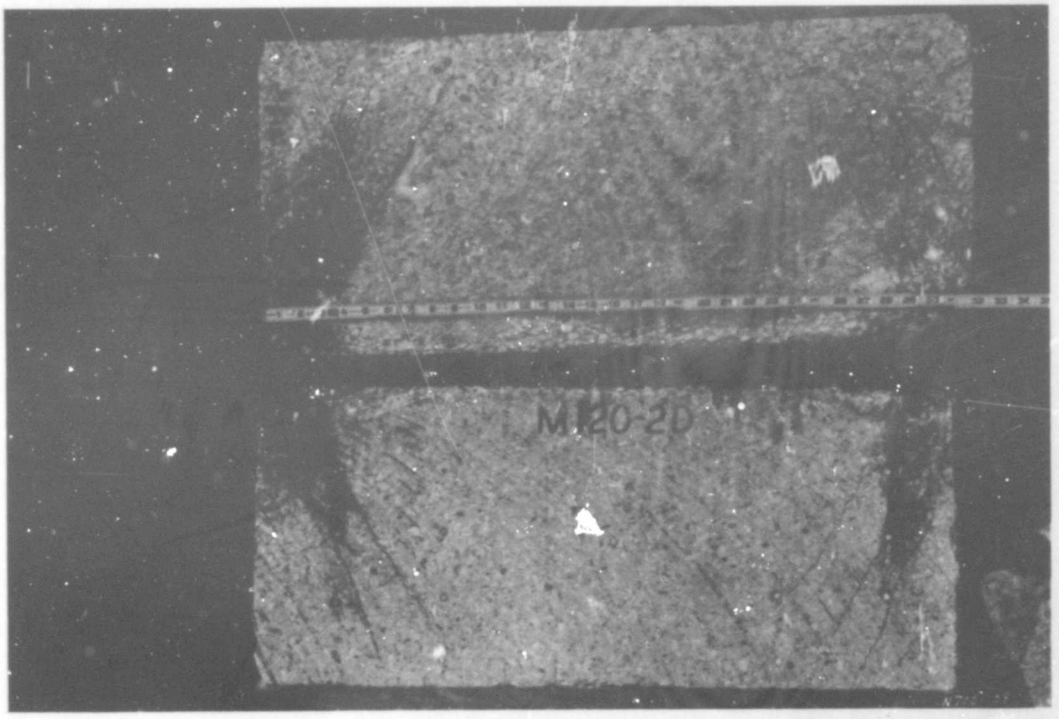

TEST 14

FIGURE 3-58

A2-89

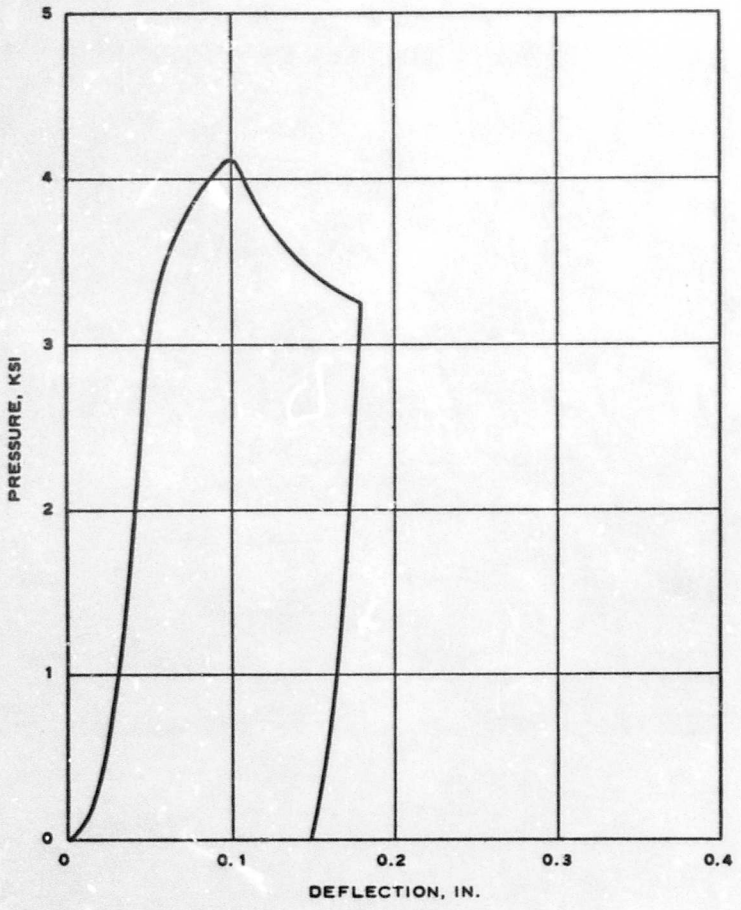

CLOSURE M120-2D TEST 14 - PRESSURE VS. DEFLECTION

FIGURE 3-59

3.2 Phase II

After the first 15 tests, there was a pause in the test sequence in order to evaluate the information obtained in the first test series and to examine critical parameters identified in Phase I. Evaluation of these tests led to the following conclusions:

1. The composite section is extremely efficient and can produce a high load capacity closure.
2. Bearing stresses are not as critical as originally imagined. Extremely high stresses can be tolerated merely by providing the effective confinement by the steel shell or the confinement ring on the silo.
3. The mode of failure apparently changes as the stiffness of the steel section is increased. As the thickness of the closure shell was increased, shear crack failure changed to a general bearing distress or steel yielding failure. With the 8 inch-deep model and thin gauge confinement, three failure modes were observed: bearing failure, shear failure and bending failure - all within one model. Shear and bearing distress were predominant in the 14-inch-deep models. In the 1/2- and 3/4-inch shells, the concrete apparently did not control the strength of the model. The stiffness prevented a bearing failure in the concrete until the steel shell had reached its yield point.

The models for the Phase II tests were modified as indicated by the results of Phase I testing. The following parameters were investigated in the second phase of the testing:

- Section depth
- Bearing width

- Closure confining shell thickness
- Closure bottom plate thickness
- Closure bearing plate thickness
- Bearing confinement shell thickness
- Support outer confining shell thickness
- Bearing haunch configuration
- Concrete strength
- Steel strength
- Reduced support friction
- Interaction phenomena

During the preparation of this report, data plots became available showing not only load versus deflection curves, but also strain data. These have been included with the Phase II test descriptions that follow.

TEST 16

Test 16 was performed to determine the increase in load capacity with the use of high strength concrete. The model geometry for this test is shown in Figure 3-60. The test was performed on a low friction support.

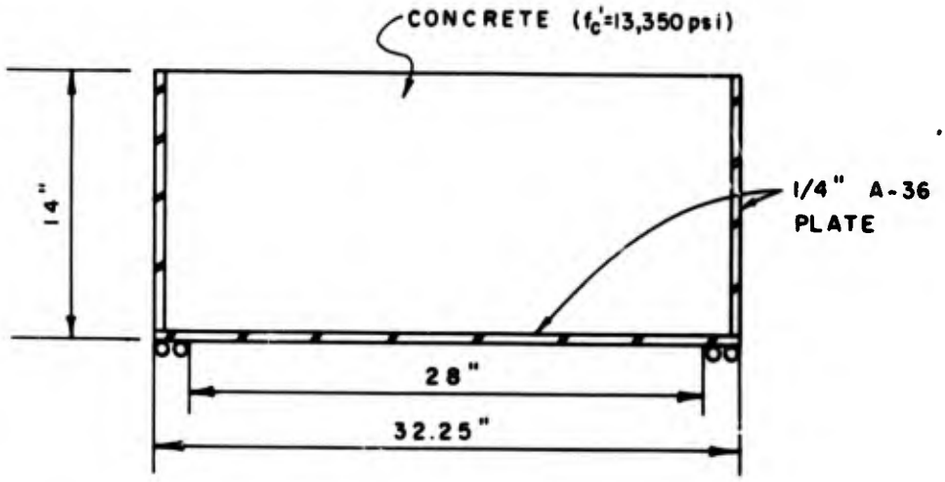

CLOSURE GEOMETRY FOR TEST 16

FIGURE 3-60

The load deflection curve shows the ductility evidenced by the model despite the relatively high strength of the concrete. The section failed at an applied pressure of 5526 psi (Figure 3-61). This represents a substantial increase in load capacity over that of Test 3 and 4 models which failed at the 3500-psi level.

The circumferential crack that can be seen just outside the bearing area (Figures 3-63 and 3-64) may be an indication that the high concrete strength is changing the failure mode. The bulging below this crack indicates that the concrete in this section has flowed plastically, thus loading and yielding the outer confinement steel.

In Figure 3-65, note the circumferential crack at the edge of the bearing; the gouges in the underside of the concrete were caused during the cutting operation and are not a result of the test loading. The apparent burnishing of the concrete in the bearing area is indicative of the applied stress, which is approximately 20,000 psi for this test. In Figure 3-66 burnishing is very evident on the bottom plate in the bearing area. The shell fell away from the model because of the deletion of the internal instrumentation bars. During Phase I of the test series, the bars had been welded to the outer confinement shell, and therefore held the concrete section and the steel shell together. No horizontal or circumferential bars were welded to the steel side shell in Phase II; the only instrumentation bars welded are the vertical bars that are welded to the bottom plate.

The results of this test support the contention that the concrete strength enhances the load capacity in approximately the same ratio as the square root of the unconfined compressive strength of the concrete.

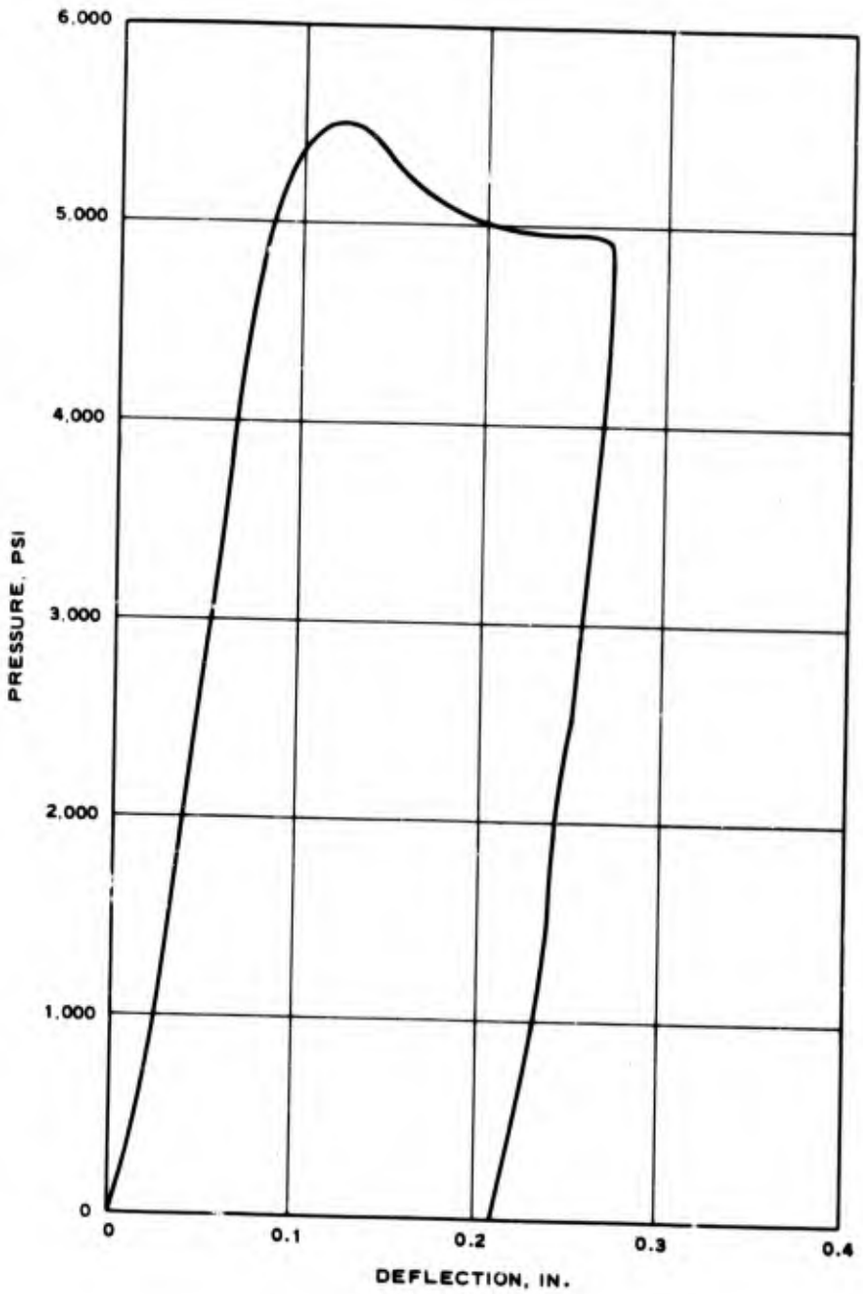

CLOSURE M120-2E TEST 16 - PRESSURE VS. DEFLECTION

FIGURE 3-61

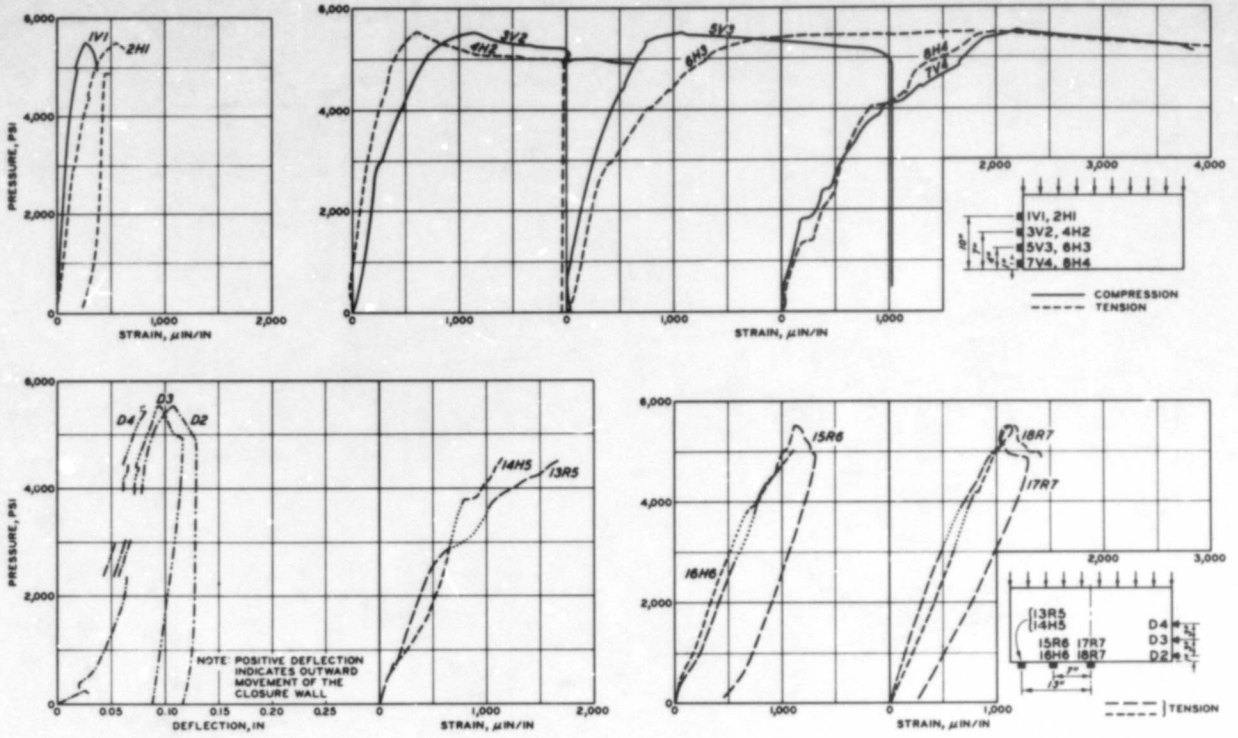

A2-96

DATA PLOT - TEST 16

FIGURE 3-62

TEST 16

FIGURE 3-63

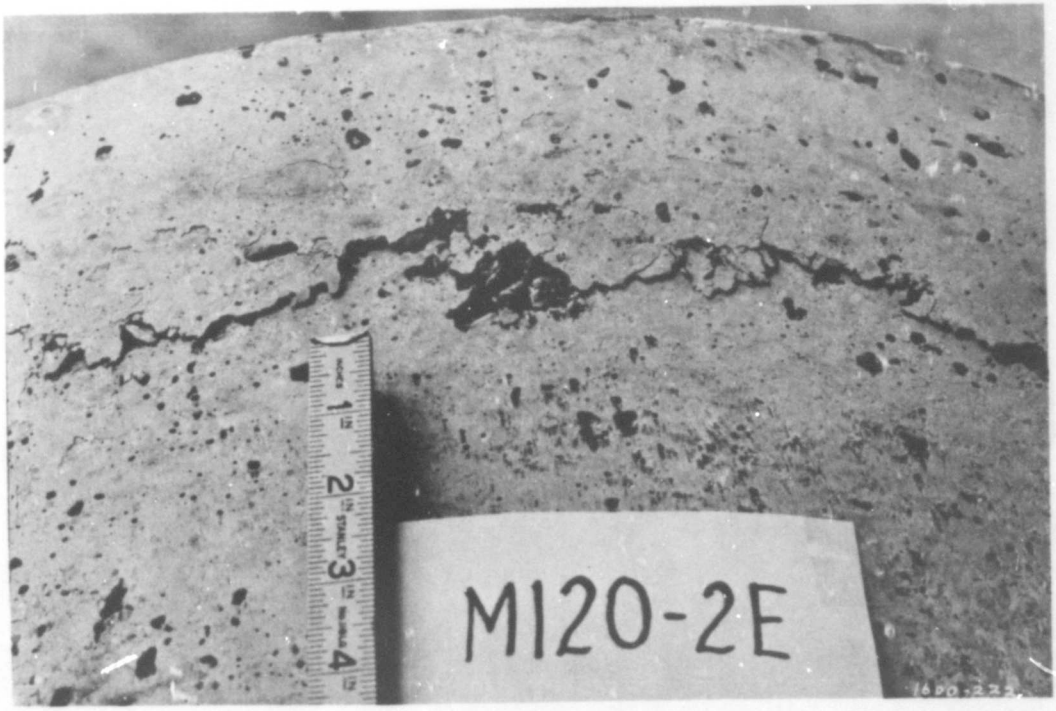

TEST 16

FIGURE 3-64

TEST 16

FIGURE 3-65

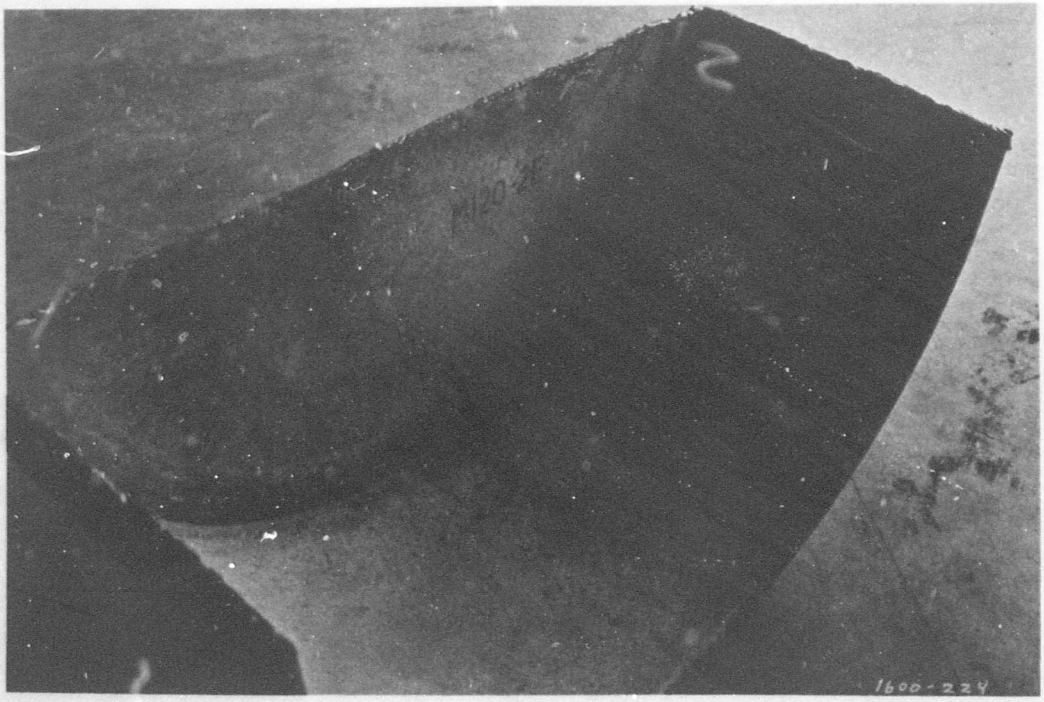

TEST 16

FIGURE 3-66

TEST 17

The effect of expansive concrete was examined in Test 17. The mix was designed so that all expected shrinkage would be overcome by the expansive admixture. It was anticipated that the concrete shear strength could be increased significantly with this procedure.

The closure geometry for Test 17 is shown in Figure 3-67. The test was performed on a low friction support.

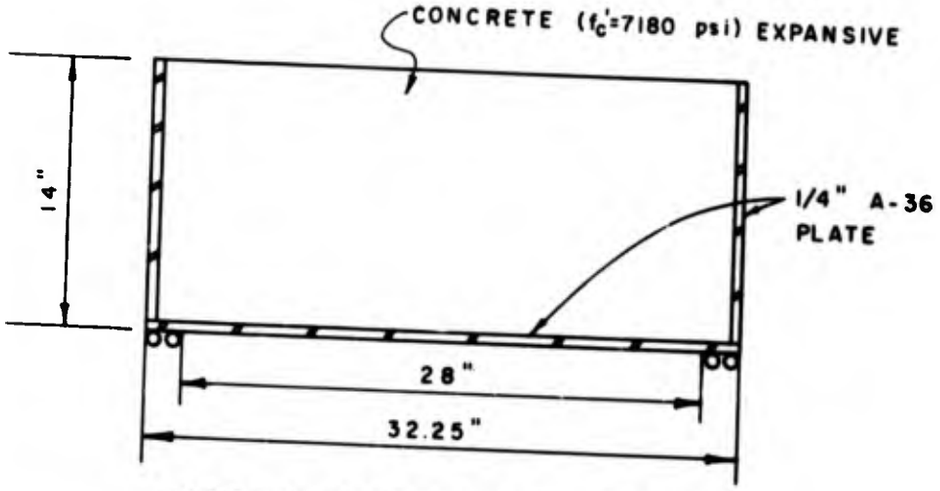

CLOSURE GEOMETRY FOR TEST 17

FIGURE 3-67

The expected increase in load capacity was not observed. The model failed at a load of 3710 psi (Figure 3-68) which compares well with the 3500-psi load capacity of the models for Tests 3 and 4. From the tests performed, there was no apparent structural advantage in using expansive concrete; however, because of increased shrinkage in full-scale structures, the use of expansive concrete may be advantageous in order to maintain the concrete in contact with the steel side shell. Figure 3-70 shows the model at the time of post-test inspection.

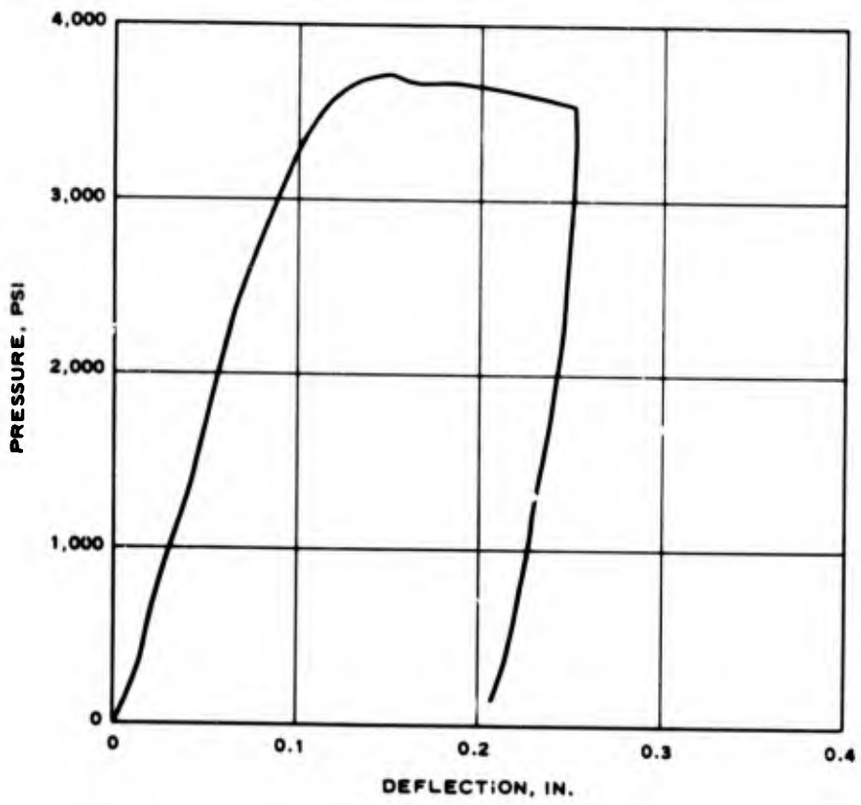

CLOSURE M130-1-7 TEST 17 - PRESSURE VS. DEFLECTION

FIGURE 3-68

A2-100

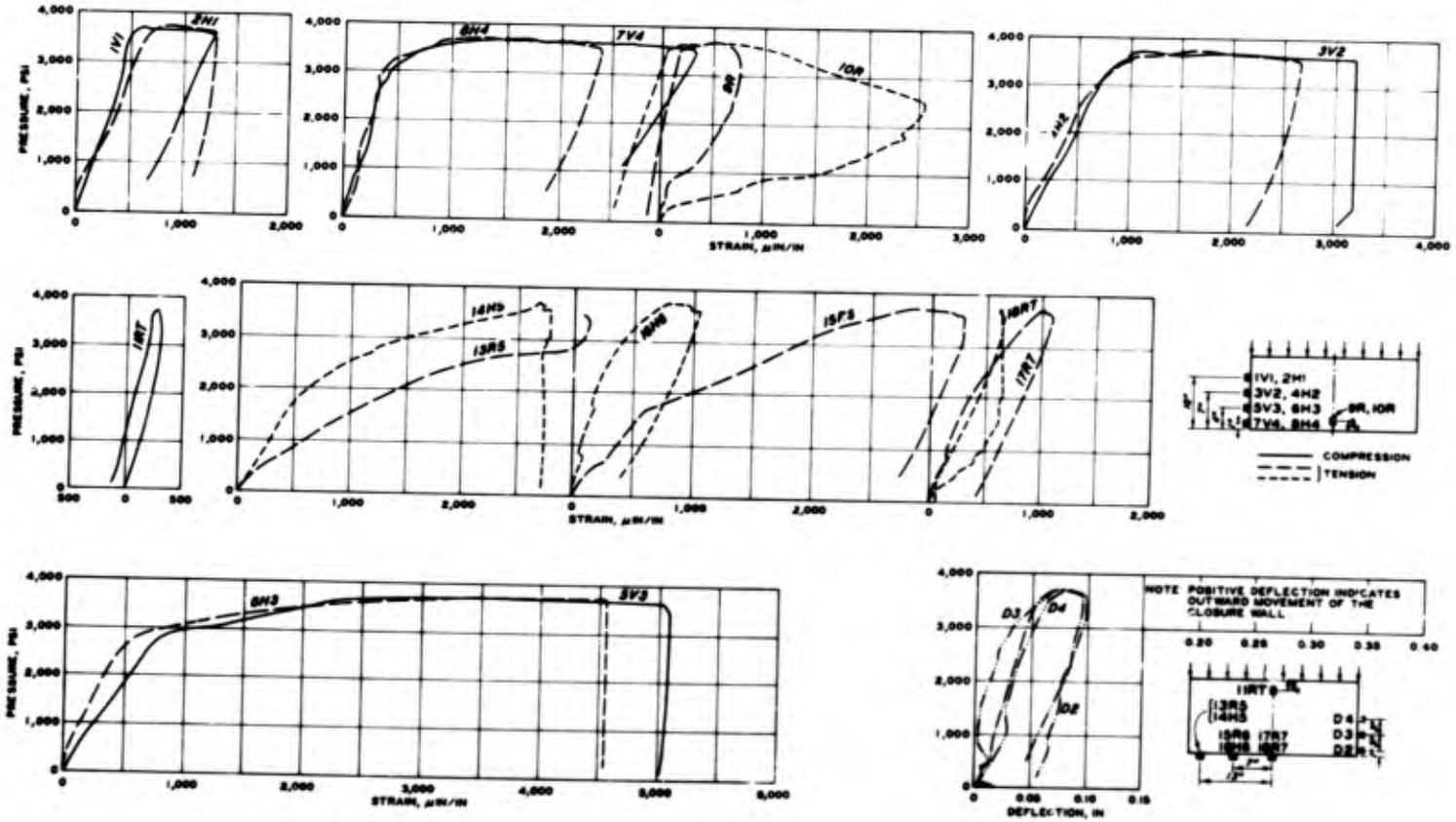

DATA PLOT - TEST 17

FIGURE 3-69

TEST 17

FIGURE 3-70

A2-102

TEST 18

The effect of concrete strength was further examined by testing a model with a lower strength concrete. The closure geometry of the model is shown in Figure 3-71. The test was performed on a low friction support.

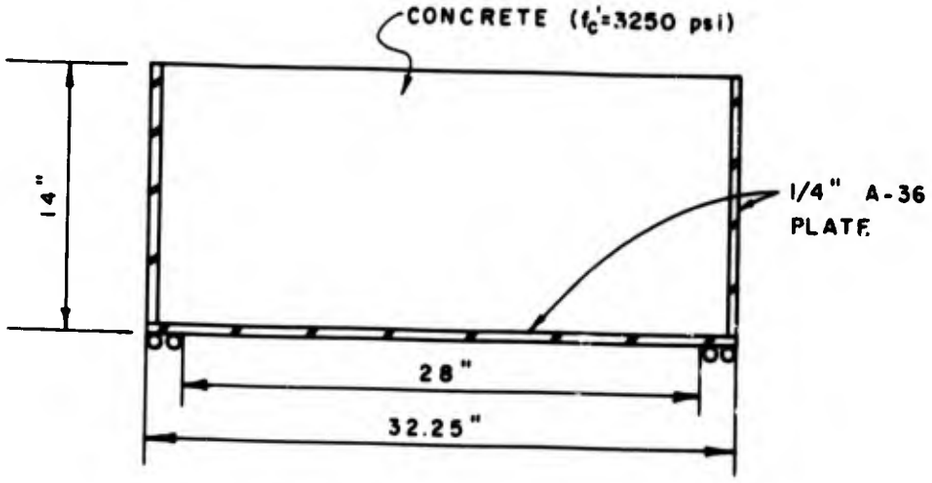

CLOSURE GEOMETRY FOR TEST 18

FIGURE 3-71

The section failed at an applied pressure of 2752 psi (Figure 3-72). The failure mode was the same as that observed in Tests 3 and 4 with the exception that greater bearing distress was observed with the lower strength concrete (Figure 3-74). This test supports the contention that the load capacity varies approximately as the square root of the unconfined compressive strength of the concrete.

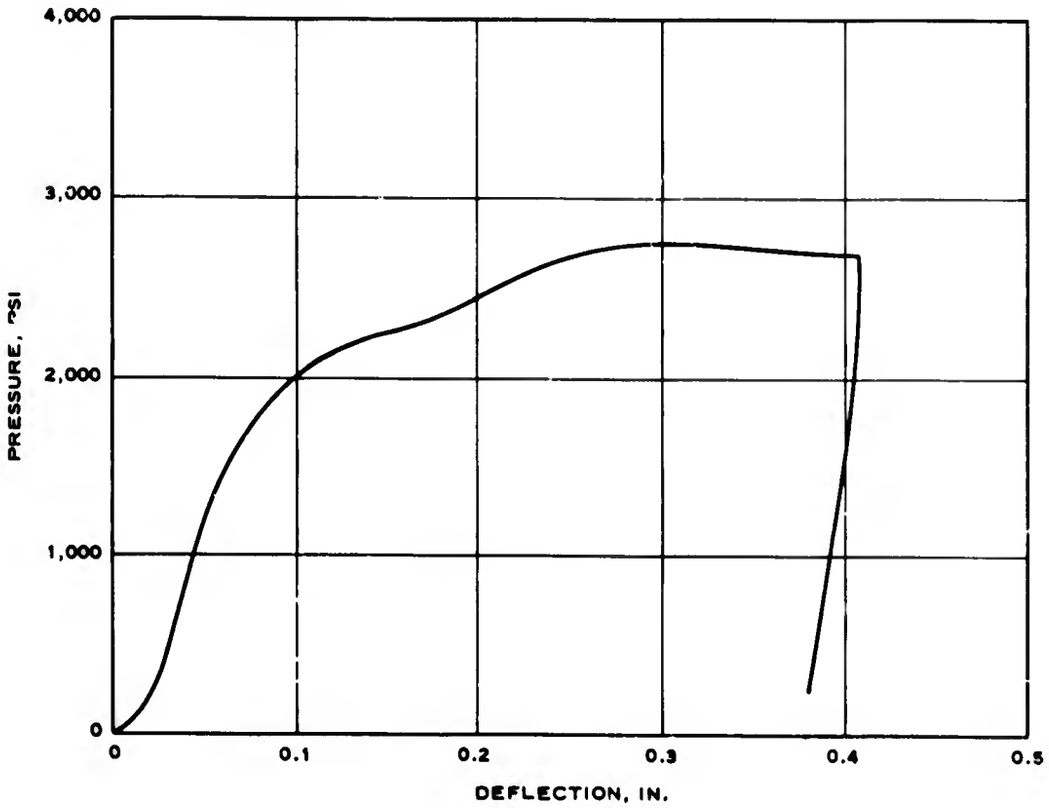

CLOSURE M130-1-6 TEST 18 - PRESSURE VS. DEFLECTION

FIGURE 3-72

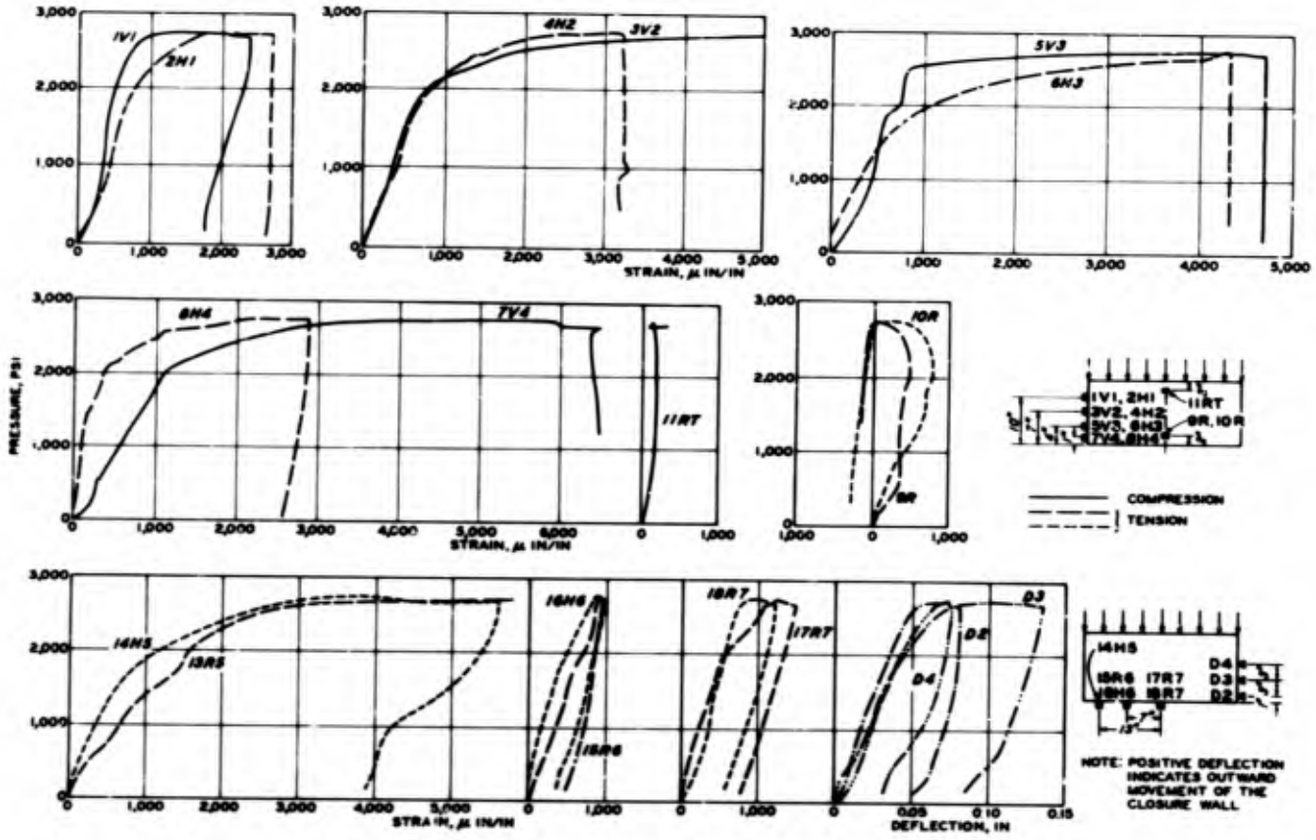

DATA PLOT - TEST 18

FIGURE 3-73

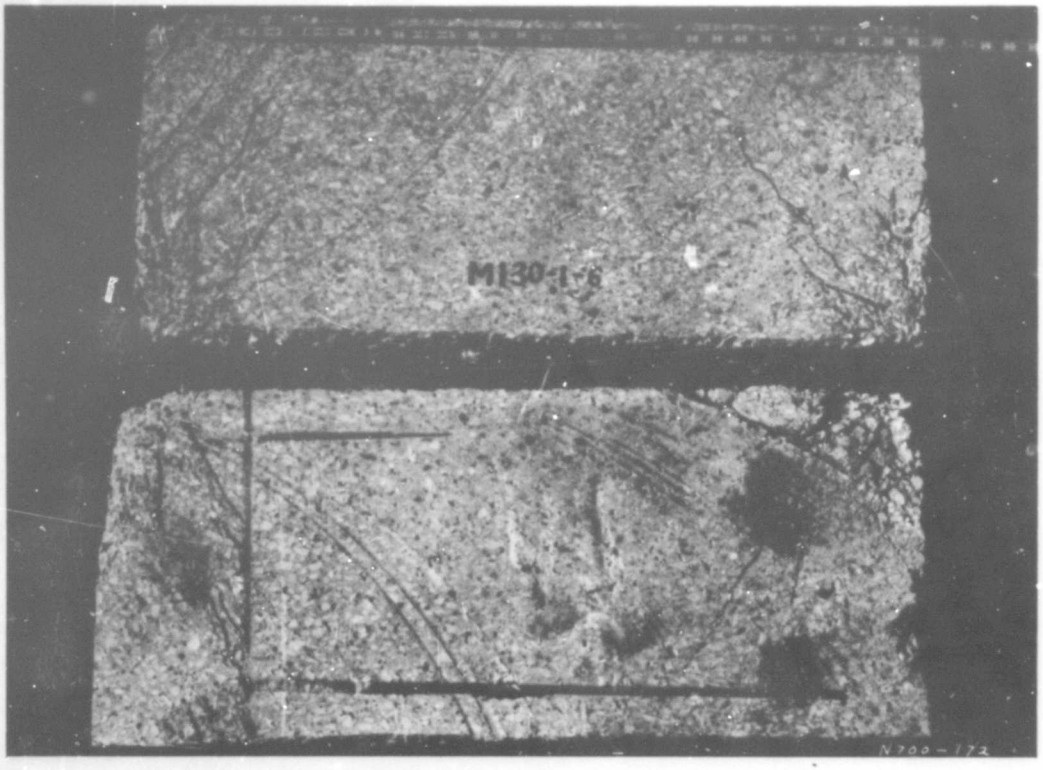

TEST 18

FIGURE 3-74
A2-106

TEST 19

In Test 19 the effect of using high strength steel was examined to determine if failure was steel strength or deformation sensitive. The model geometry is shown in Figure 3-75. The model was tested on a low friction support.

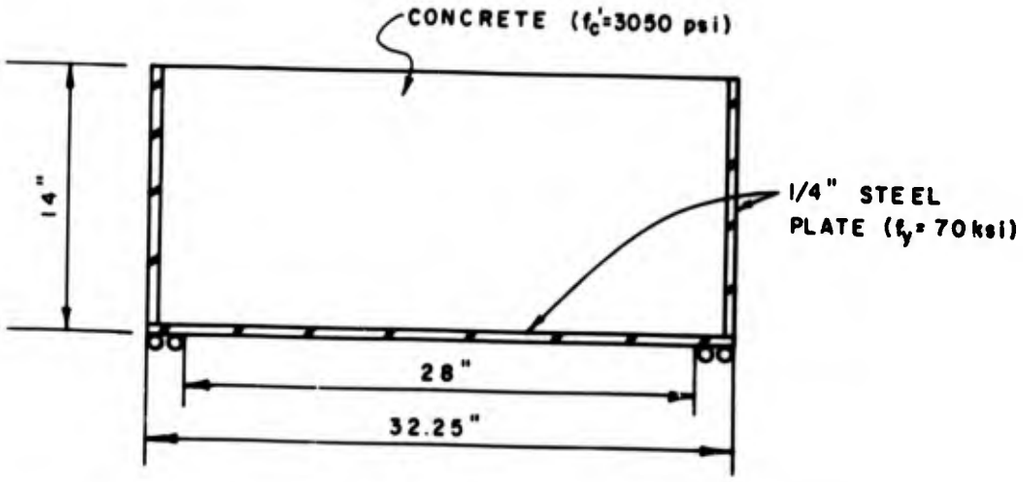

CLOSURE GEOMETRY FOR TEST 19

FIGURE 3-75

The ductility of the model, as shown on the pressure deflection curve (Figure 3-76), is attributed to the high strength steel. It appears that the total steel strength is the critical factor since the model failed at a load of 5497 psi. This compares favorably with the test of the 1/2-inch model on the support structure which failed at 6375 psi (Test 8); much greater load capacity was shown than that observed in Test 18 where an identical model constructed from A-36 steel collapsed at 2570 psi. The failure was attributed to bearing distress.

No shear crack could be observed (Figure 3-78). The increase in load capacity due to the high strength concrete noted in Test 16 was not as great as the increase noted in this test as a result of using high strength steel. It appears that a significant increase in load capacity may be attained by the use of high strength structural materials.

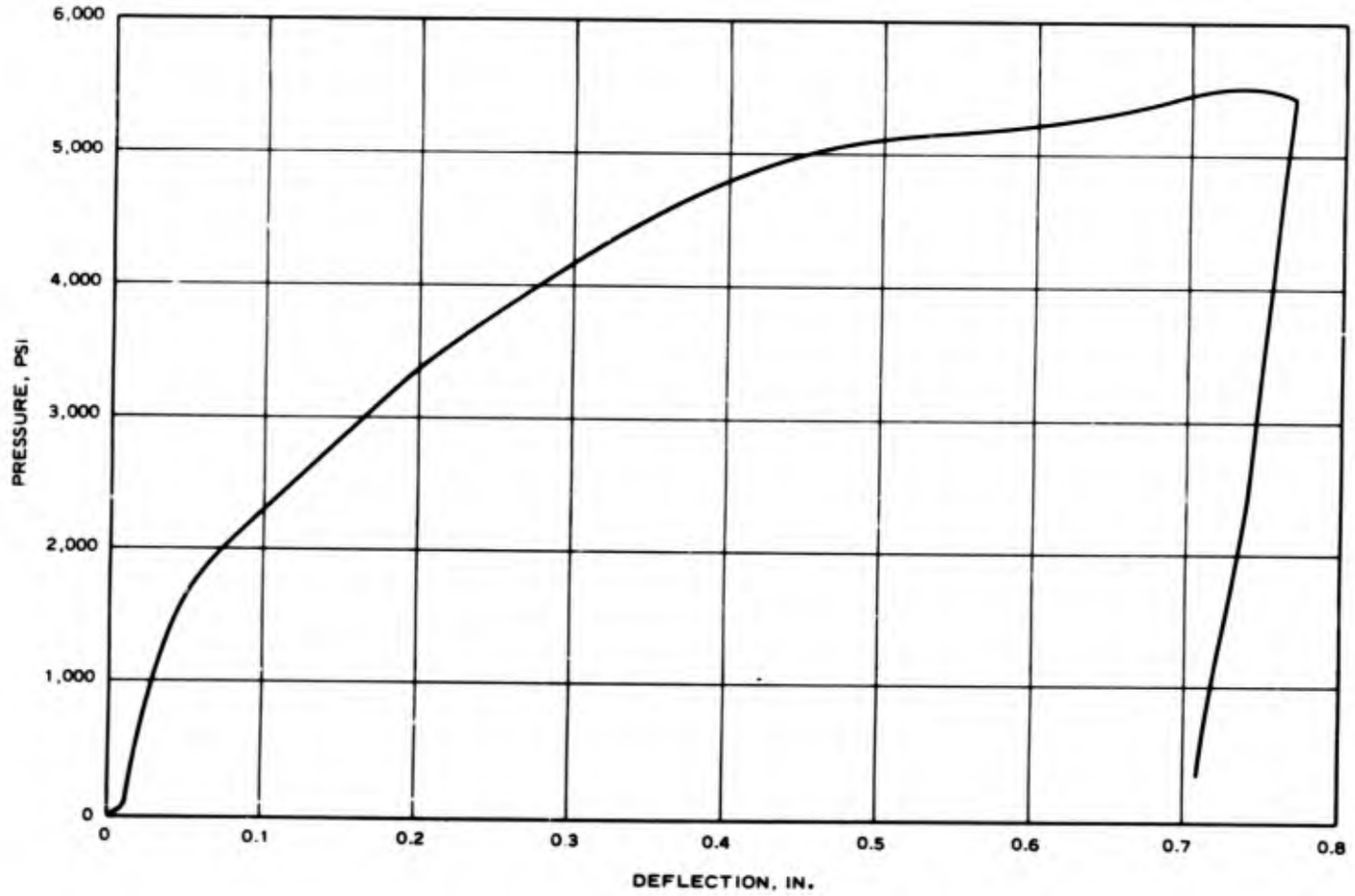

CLOSURE M130-2-2 TEST 19 - PRESSURE VS. DEFLECTION

FIGURE 3-76

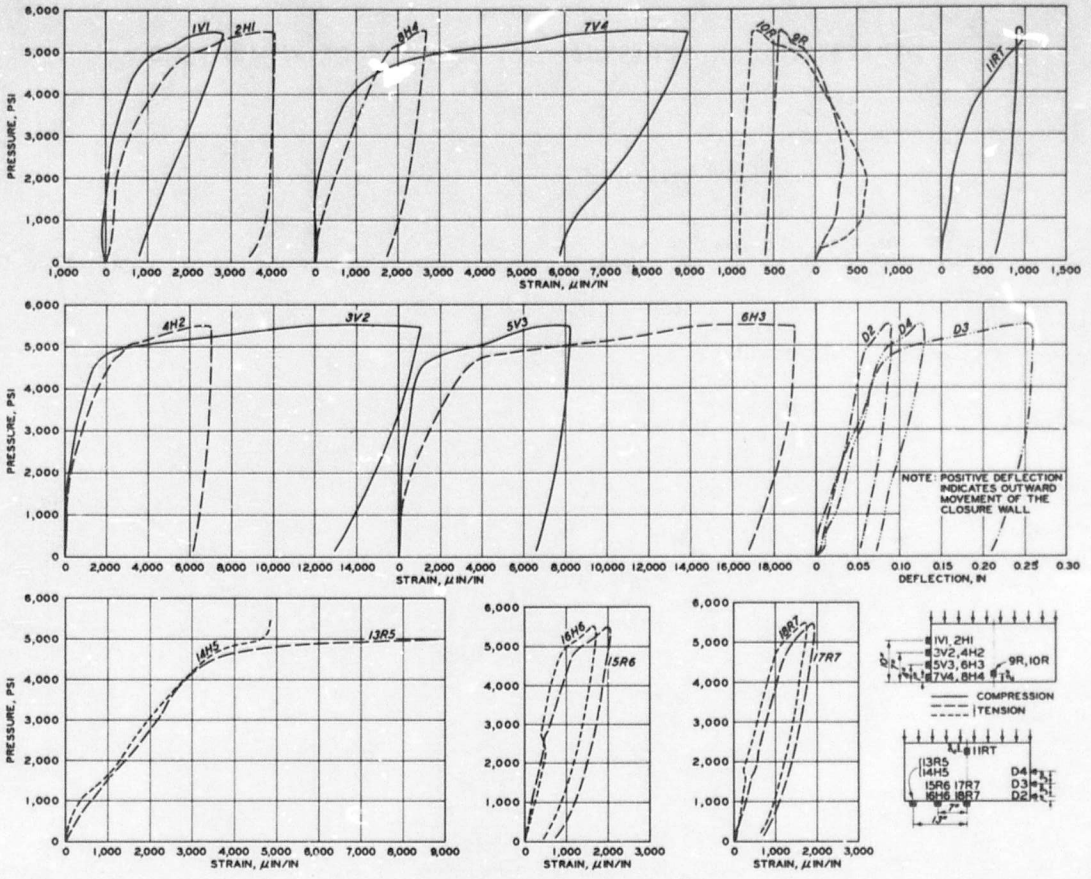

DATA PLOT - TEST 19

FIGURE 3-77

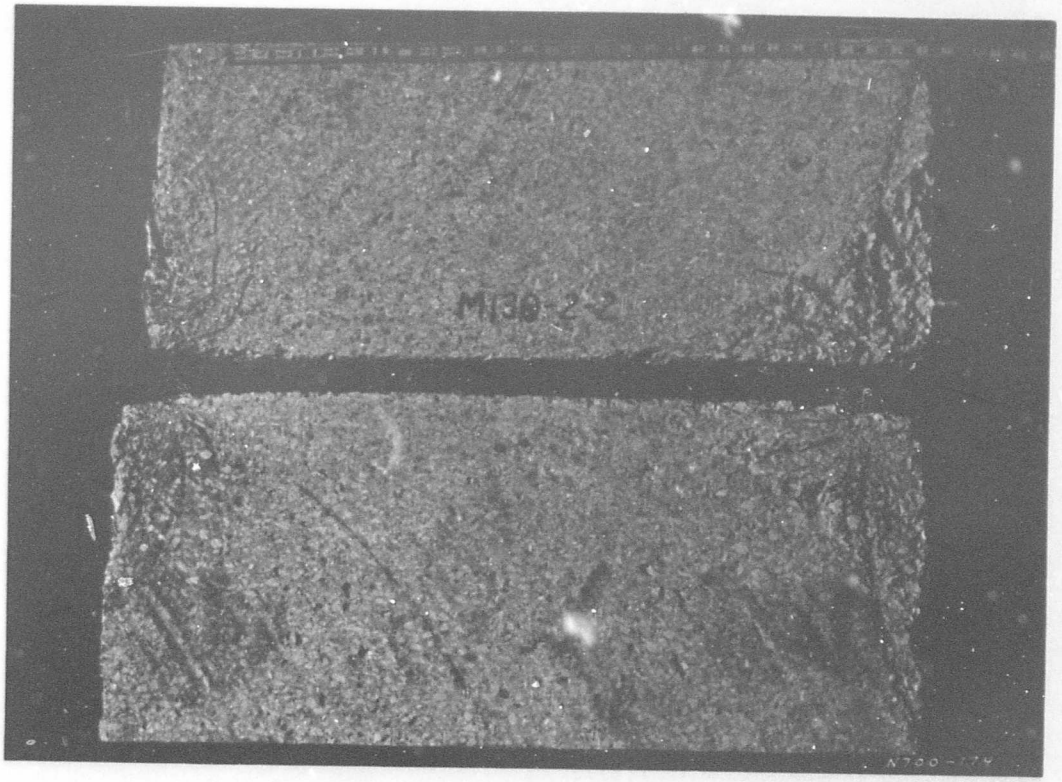

TEST 19

FIGURE 3-78

A2-111

TEST 20

In Test 20 the effect of both high strength steel and concrete was examined. The model geometry is shown in Figure 3-79; the test was performed on a low friction support.

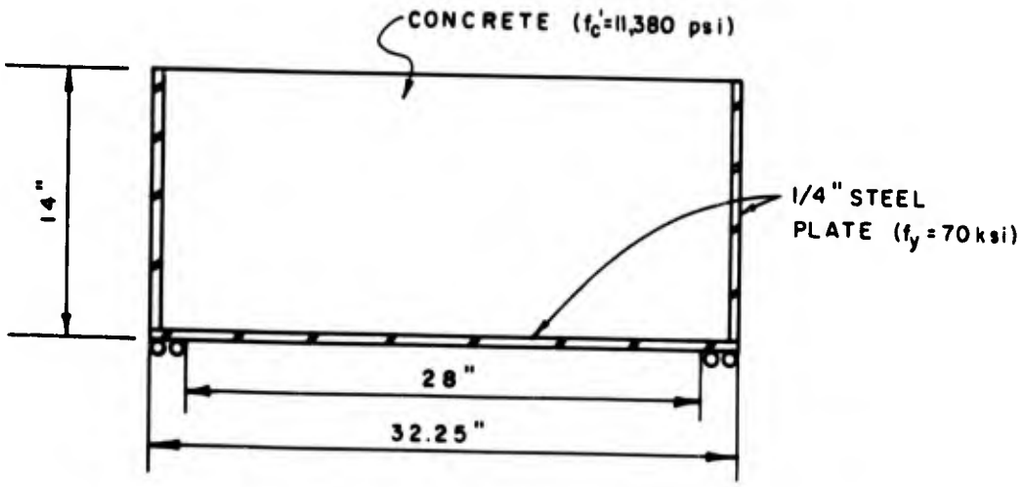

CLOSURE GEOMETRY FOR TEST 20

FIGURE 3-79

The model collapsed at a load level of 6584 psi (Figure 3-80); shear cracks were evident in the collapsed structure. There was also an unusual horizontal crack approximately 2 inches from the top surface of the model (Figure 3-82). There seems to be no explanation for the formation of these cracks, since no bearing distress was evident at the time of post-test inspection. However, these horizontal crack patterns were also noted in Test 21 (Figure 3-86). This phenomenon is undoubtedly associated with the high strength steel shell and the high strain that is being obtained in the model.

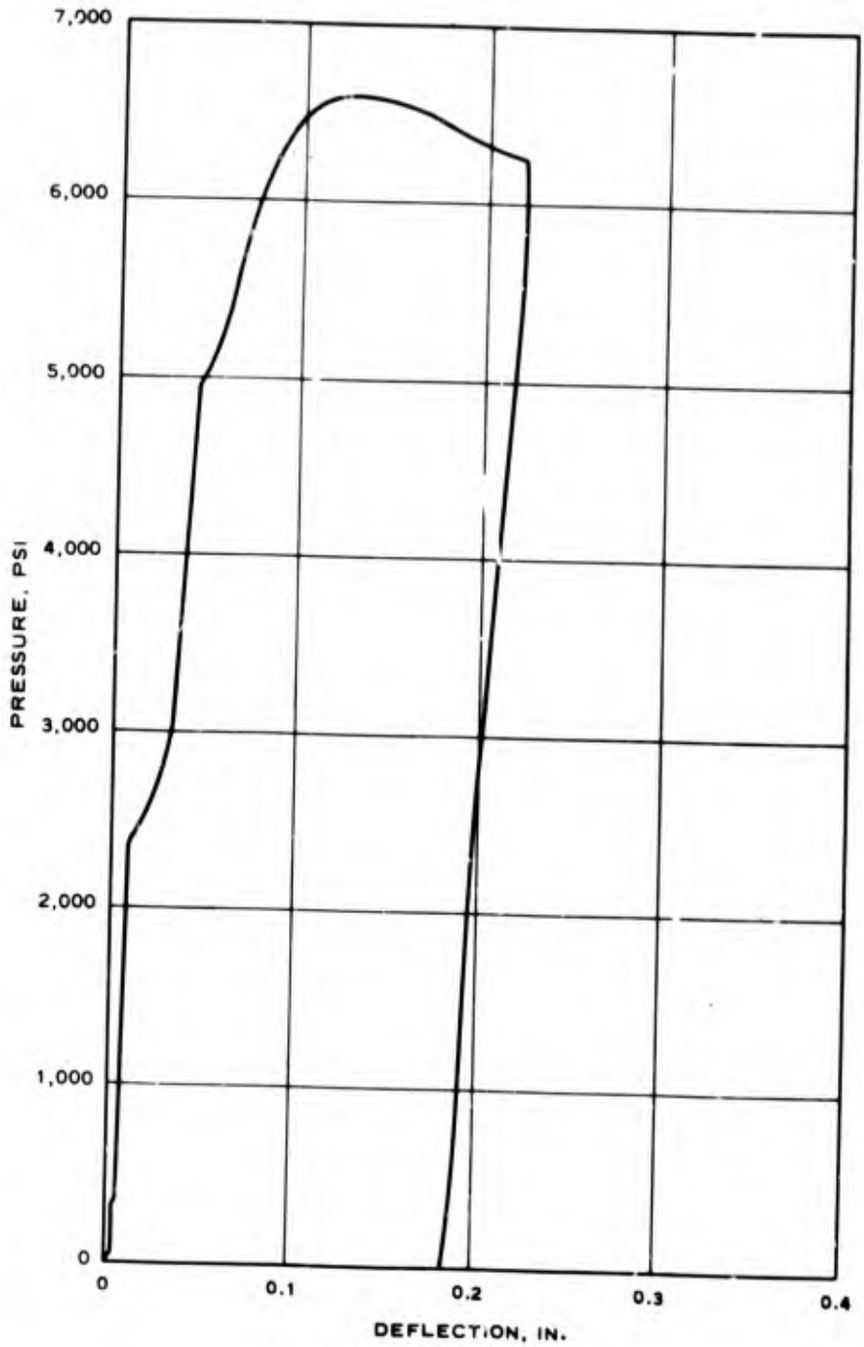

CLOSURE M130-2-1 TEST 20 - PRESSURE VS. DEFLECTION

FIGURE 3-80
A2-113

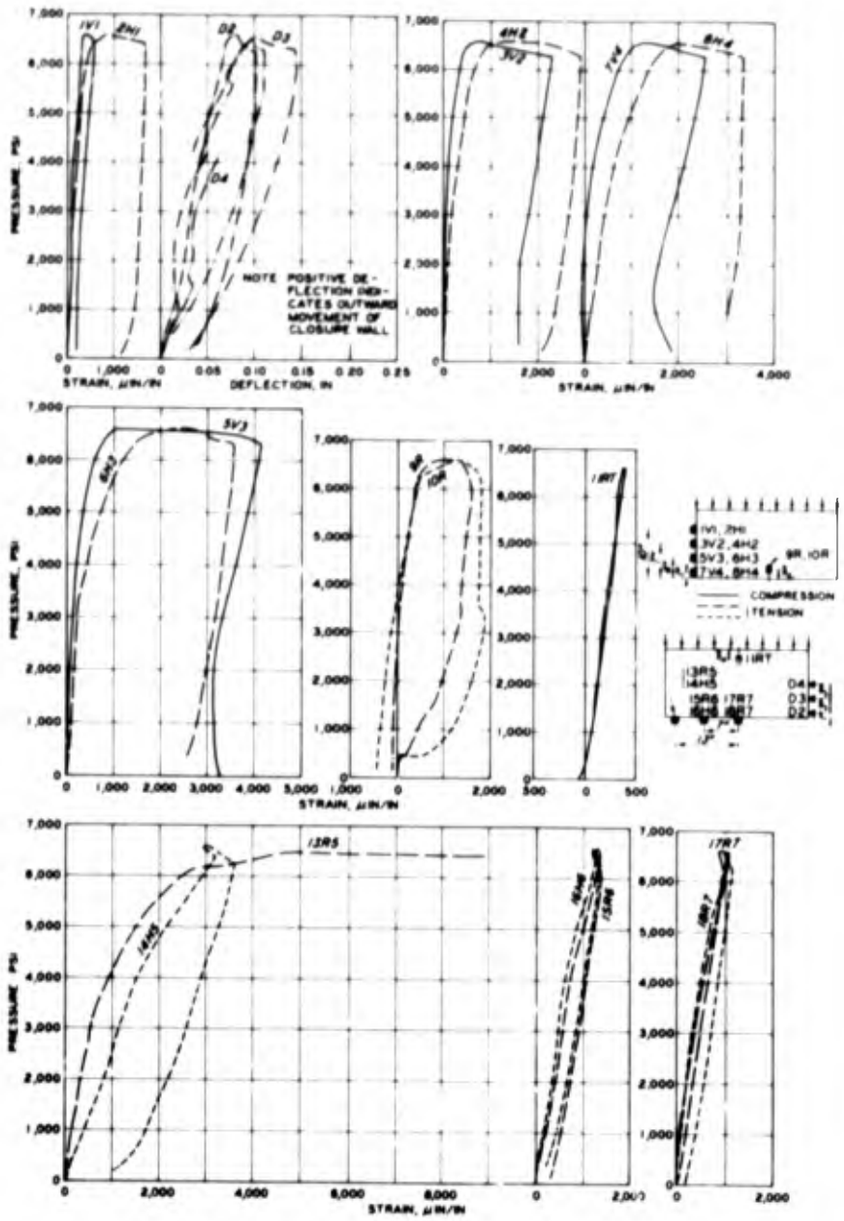

DATA PLOT - TEST 20

FIGURE 3-81

A2-114

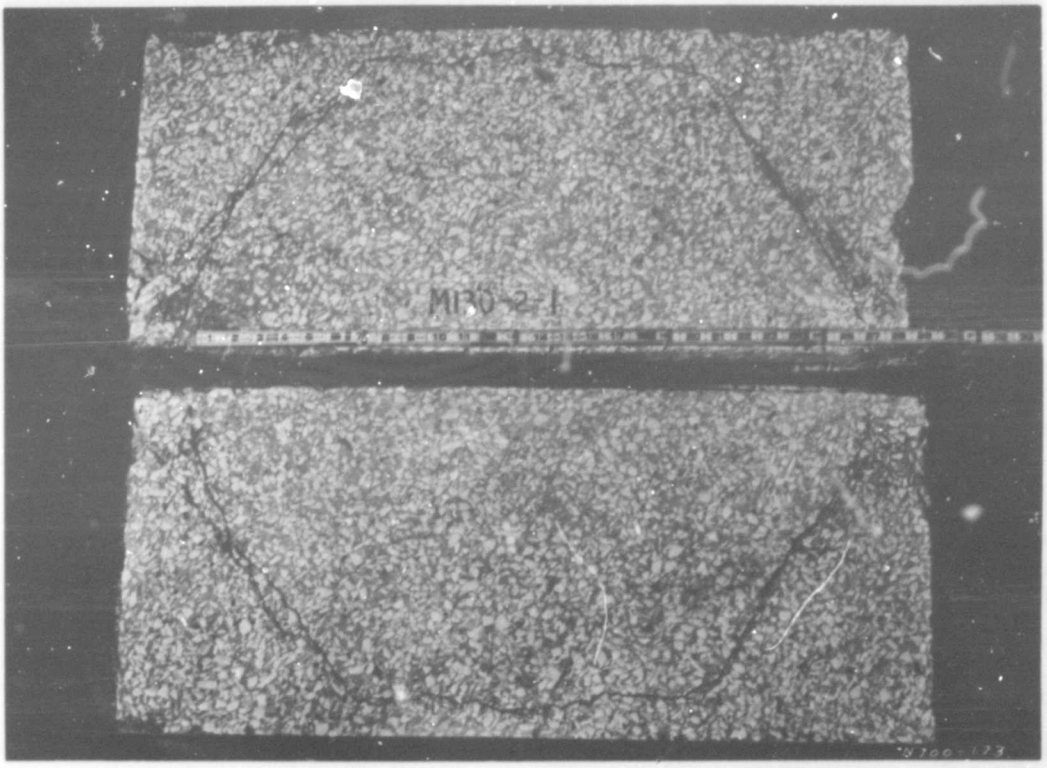

TEST 20

FIGURE 3-82
A2-115

TEST 21

The effect of ultrahigh strength steel was examined in Test 21. The model was tested on a low friction support. The closure geometry for Test 21 is shown in Figure 3-83.

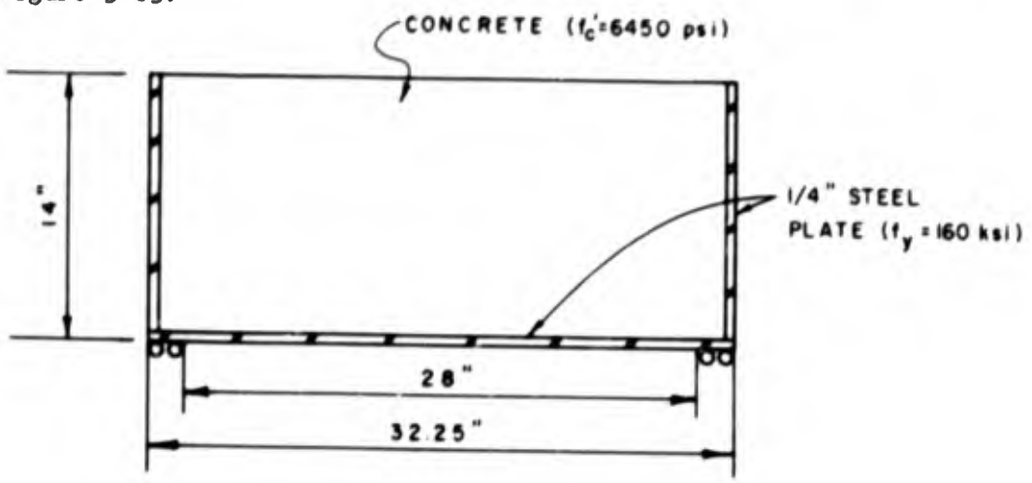

CLOSURE GEOMETRY FOR TEST 21

FIGURE 3-83

The model failed at 7300 psi (Figure 3-84), a load lower than would be expected from extrapolation of previous test results. Many horizontal cracks were observed at the time of post-test inspection (Figures 3-86 and 3-87). This indicates that a critical concrete strain situation was evidently reached. Therefore it is not possible to say that the total plate strength is the only critical design parameter.

It has been postulated that the bearing strength of the concrete may be expressed in terms of the unconfined concrete compressive strength and a linear function of the confinement pressure available from the side steel shell. In this particular test, observations of the strain records indicate that the steel remained elastic until failure. Thus the effective vertical stress in the side shell could be determined. The vertical load not carried in the side shell was assumed to be in the concrete. This indicates that the effective concrete bearing stress was approximately 15,000 psi, which implies that in this case the concrete bearing strength could be expressed as $\sigma_{concrete} = f'_c + 5.4\ \sigma_{confined}$.

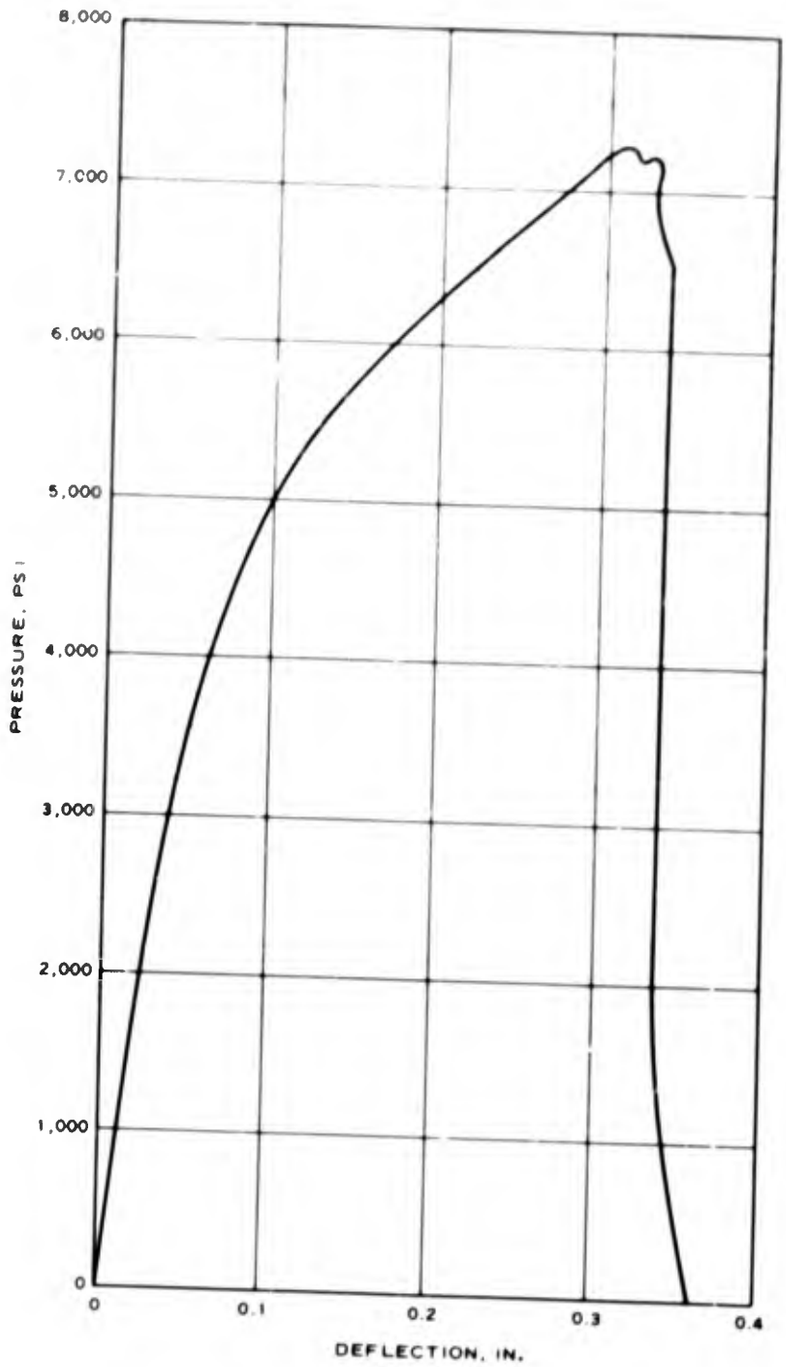

CLOSURE M130-3 TEST 21 - PRESSURE VS. DEFLECTION

FIGURE 3-84

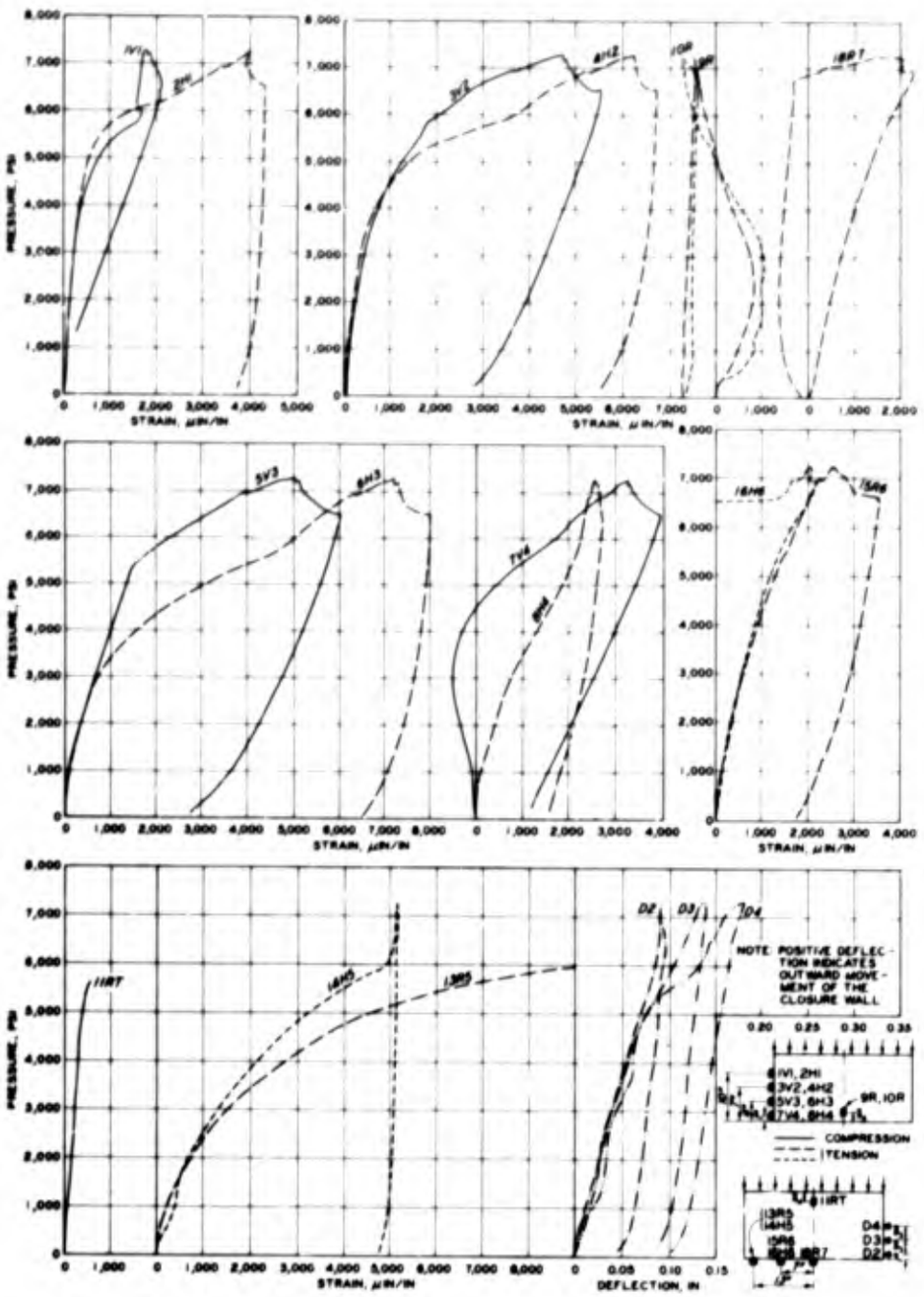

DATA PLOT - TEST 21

FIGURE 3-85

A2-118

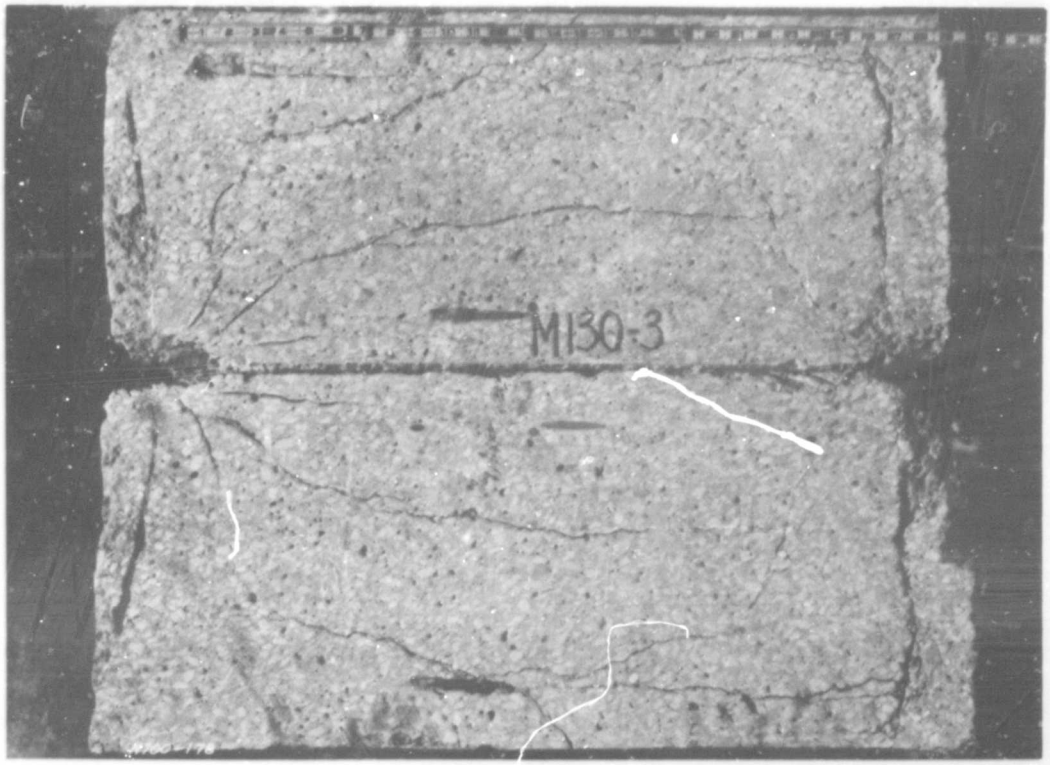

TEST 21

FIGURE 3-86

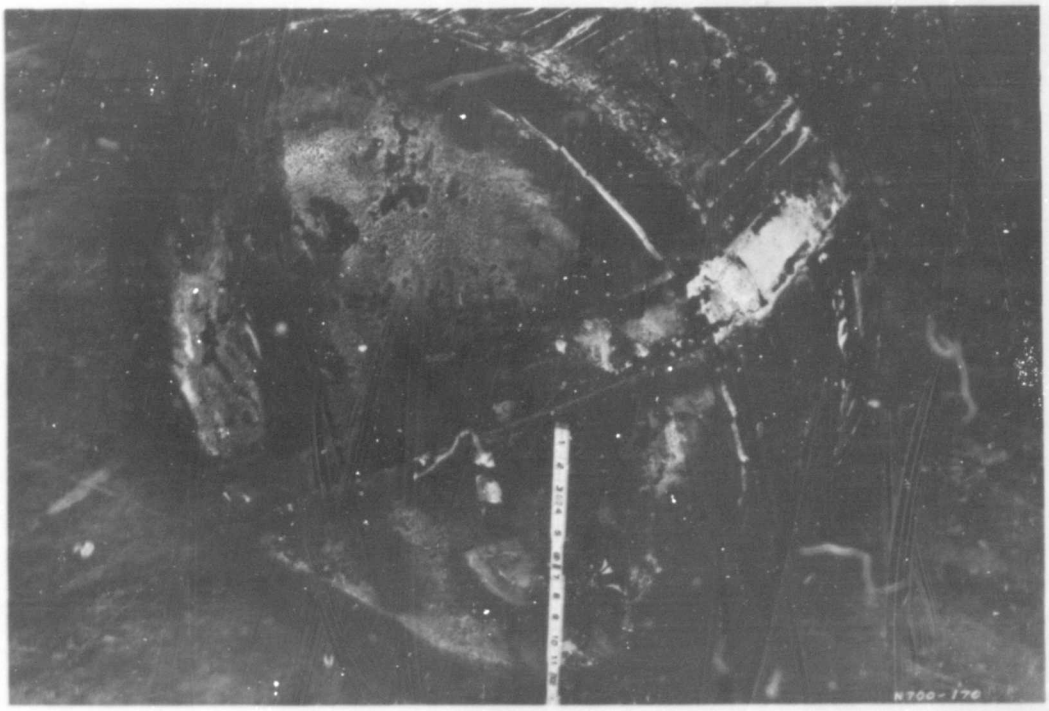

TEST 21

FIGURE 3-87

TEST 22

In Test 22 the relative contributions of the side shell and bottom plate were examined by testing a model with a thick shell and a thinner bottom plate. The model geometry is shown in Figure 3-88; the model was tested on a low friction support.

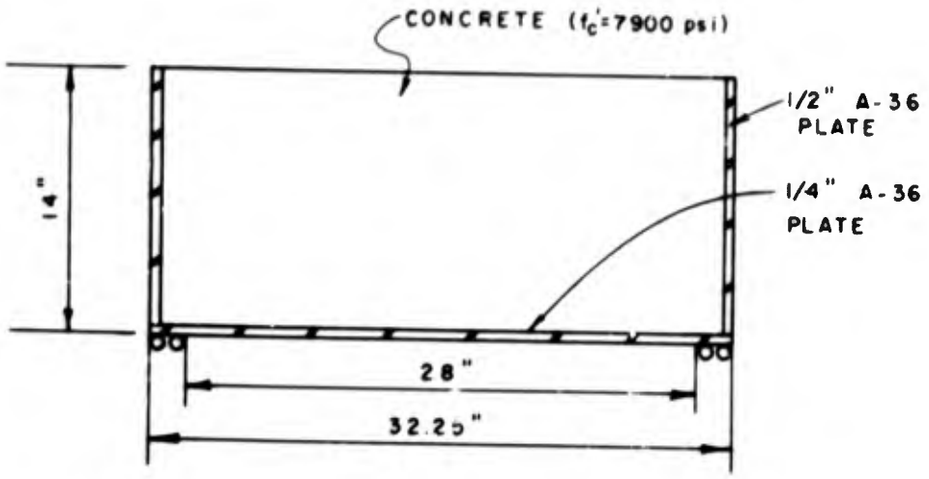

CLOSURE GEOMETRY FOR TEST 22

FIGURE 3-88

The model collapsed at 4871 psi (Figure 3-89) due to a local-type failure initiated by yielding of the steel plates. No shear crack was apparent at the time of post-test inspection (Figure 3-91). There was a 30-percent increase in load capacity over that for models with a 1/4-inch side shell and bottom plate (Tests 3 and 4), and the failure mode was similar to that observed in the 1/2-inch model tested on a support structure (Test 8).

A thicker outer shell appears advantageous from the standpoint of both failure mode and ultimate load capacity.

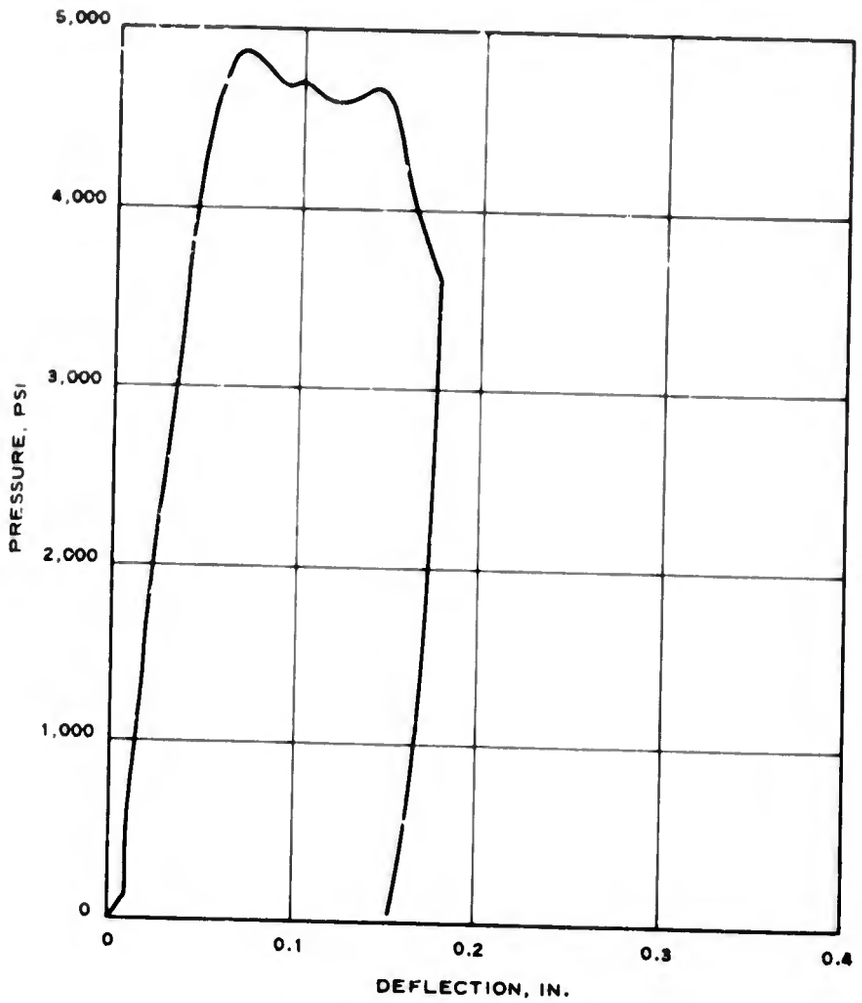

CLOSURE M130-4 TEST 22 - PRESSURE VS. DEFLECTION

FIGURE 3-89

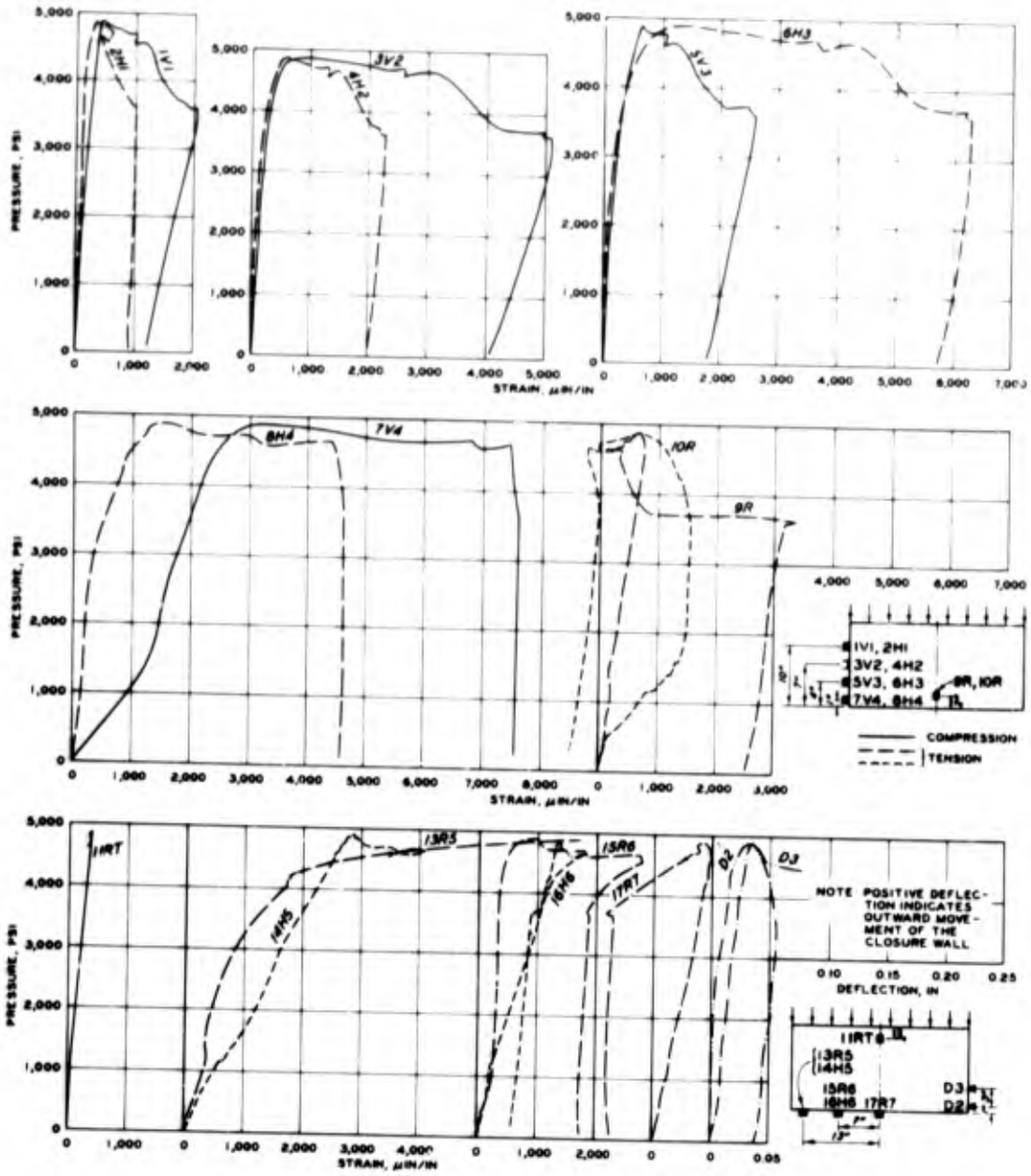

DATA PLOT - TEST 22

FIGURE 3-90

A2-122

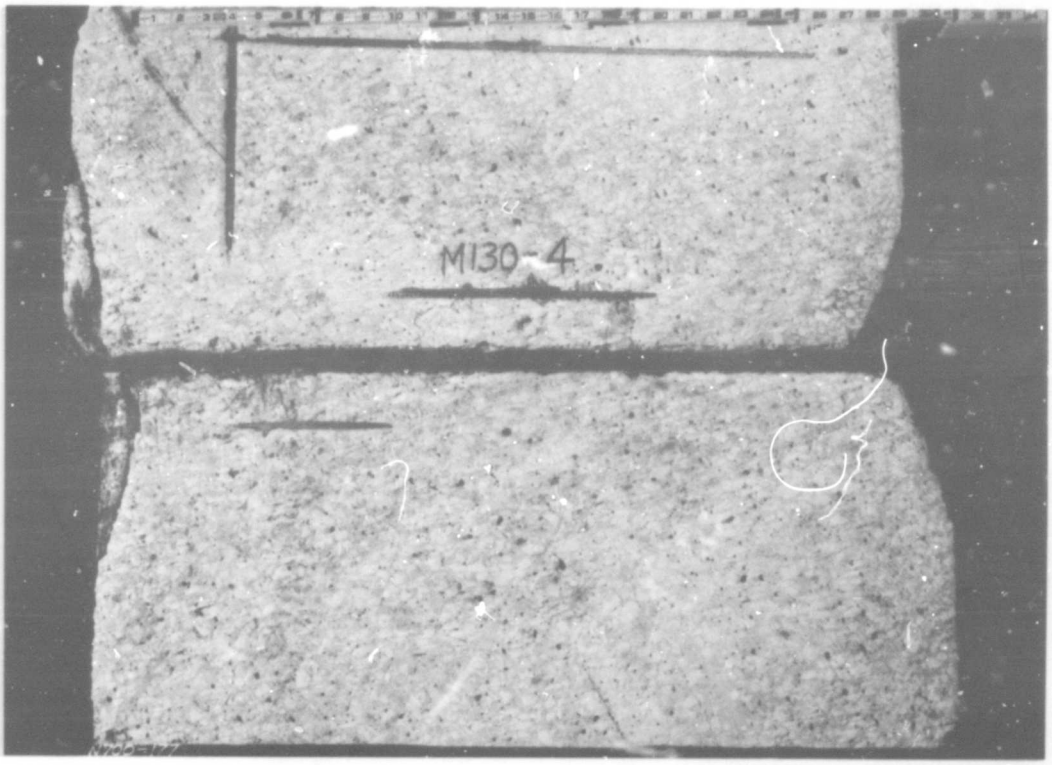

TEST 22

FIGURE 3-91

A2-123

TEST 23

Test 23 represented the first test of a 1/2-inch model on a low friction support. The results obtained were correlated with those of Tests 8, 19, 20 and 22. The model geometry for Test 23 is shown in Figure 3-92.

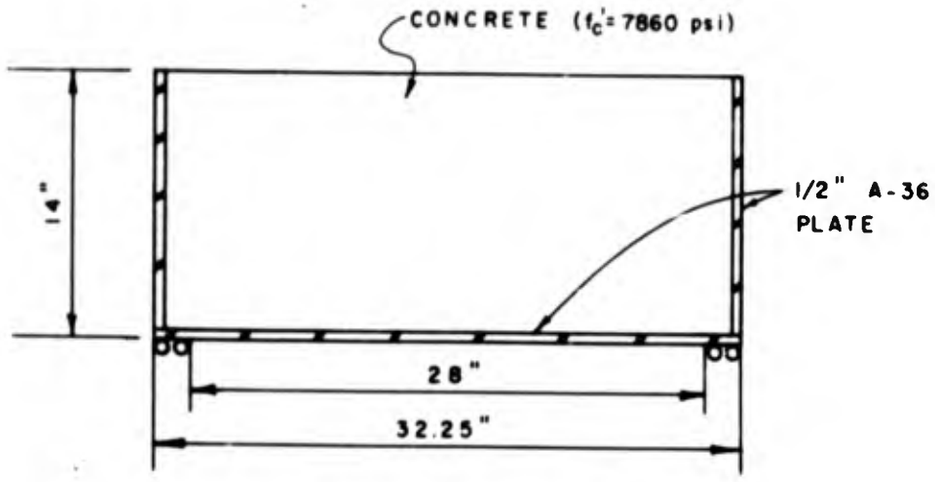

CLOSURE GEOMETRY FOR TEST 23

FIGURE 3-92

The model collapsed at a load level of 6361 psi (Figure 3-93), which is close to the 6375-psi collapse load observed on the support structure for Test 8.

Examination of Tests 19 and 20 shows that total steel strength appears to be the critical design parameter since an equivalent strength steel model with 3-ksi concrete failed at 5497 psi and one with 12-ksi concrete failed at 6584 psi.

The mode of failure was as previously observed, with shear cracks in evidence as well as severe bearing distress and the associated yielding of the steel plates (Figure 3-95). It should be noted that no shear cracks were observed with the 1/2-inch model in Test 8. In the first test series, the 1/2-inch model was tested on a silo, whereas in Test 23 the model was tested on a low-friction support, which suggests that the support condition has influenced the failure mode.

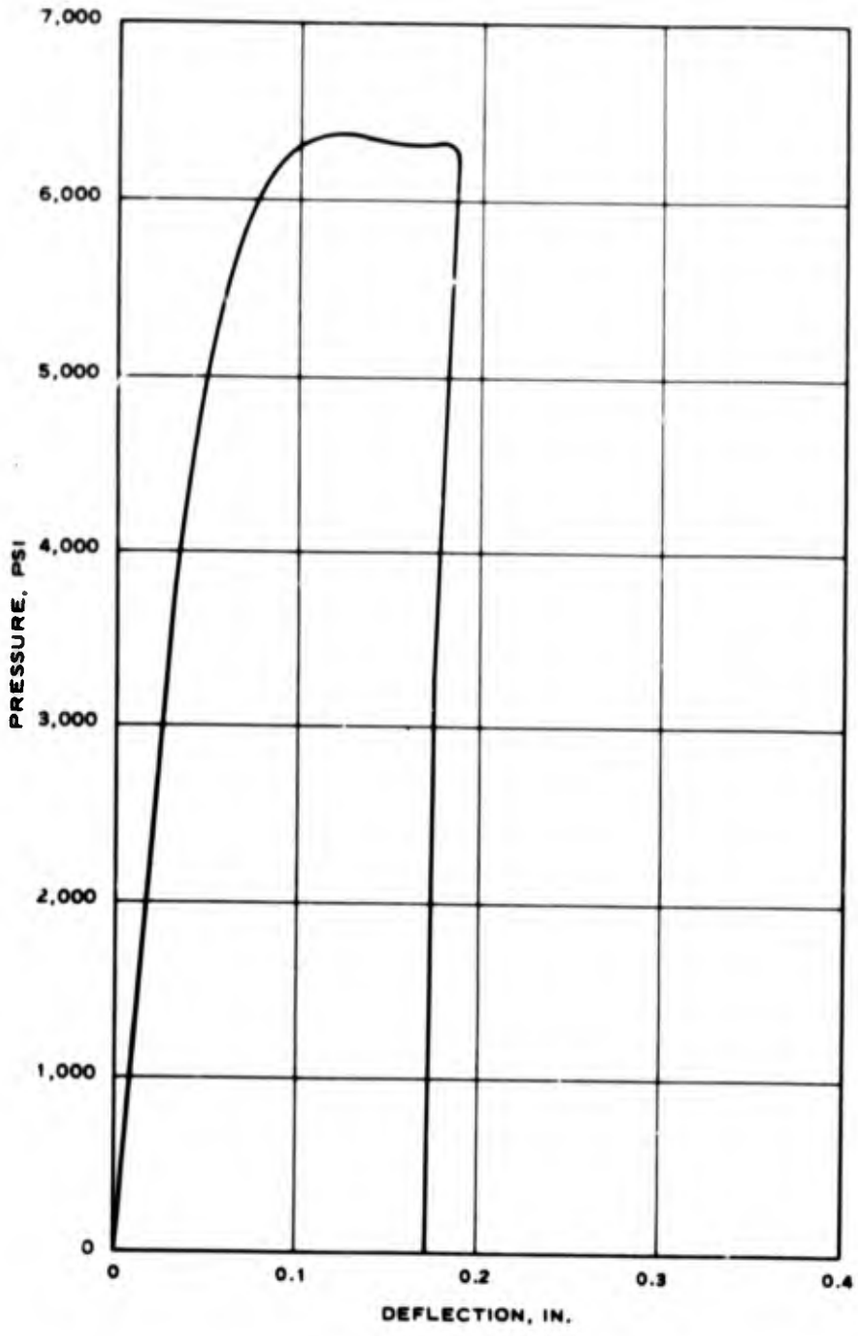

CLOSURE M130-7 TEST 23 - PRESSURE VS. DEFLECTION

FIGURE 3-93

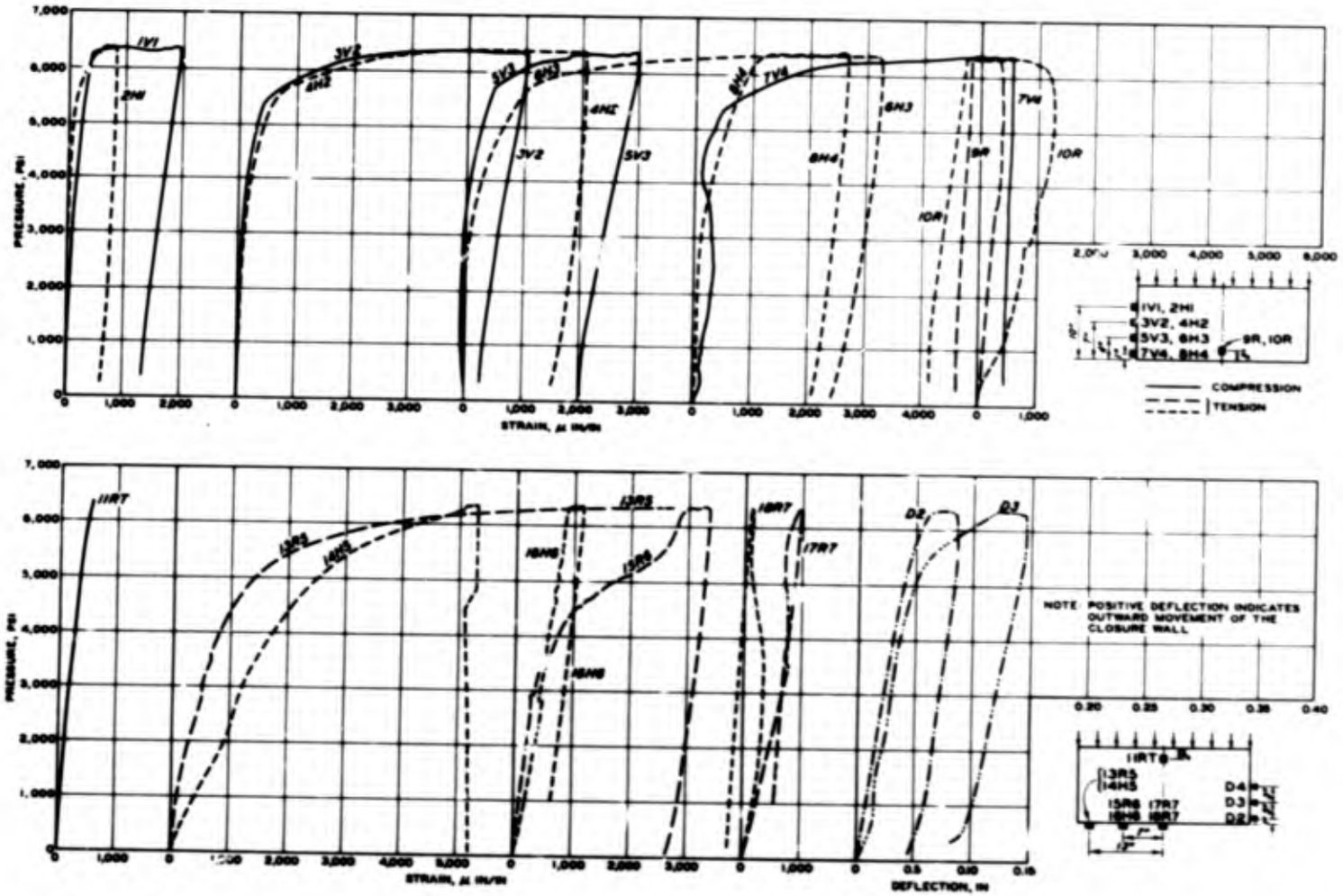

DATA PLOT - TEST 23
FIGURE 3-94

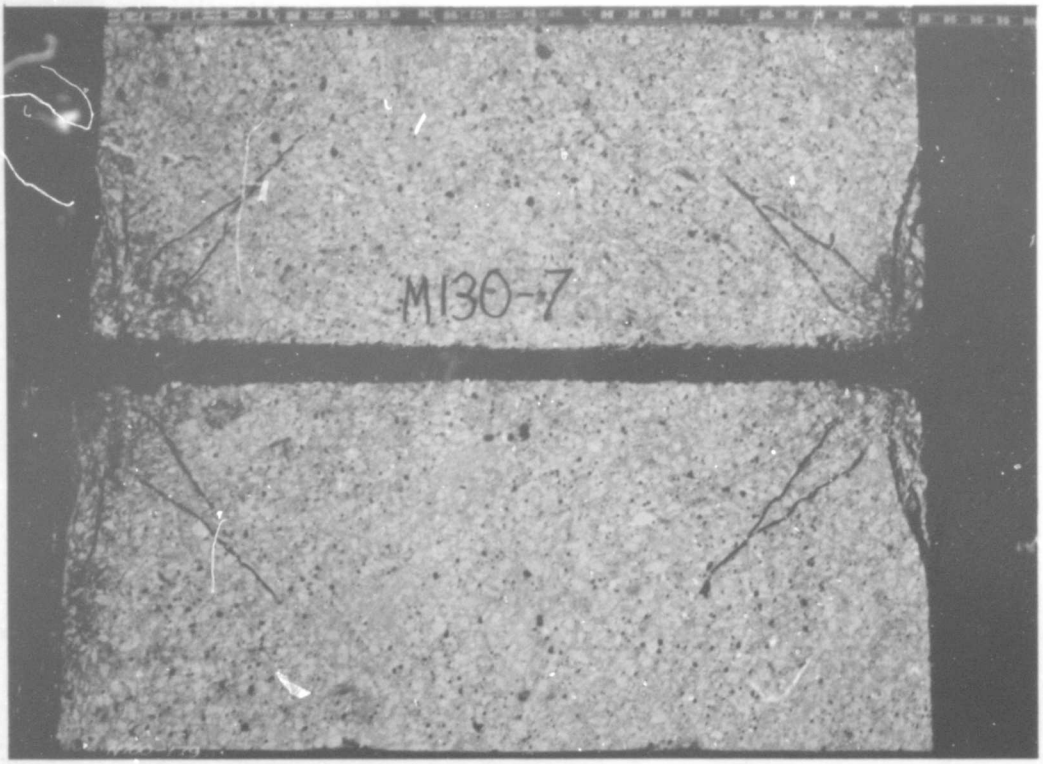

TEST 23

FIGURE 3-95
A2-128

TEST 24

A model similar to those used in Tests 3 and 4 was tested to investigate the effect of friction in the so-called low friction support. The test was performed on teflon-coated blocks with a tested coefficient of friction of 0.005, as opposed to 0.20 on the standard low friction bearing (Tests 3 and 4). The model geometry is shown in Figure 3-96.

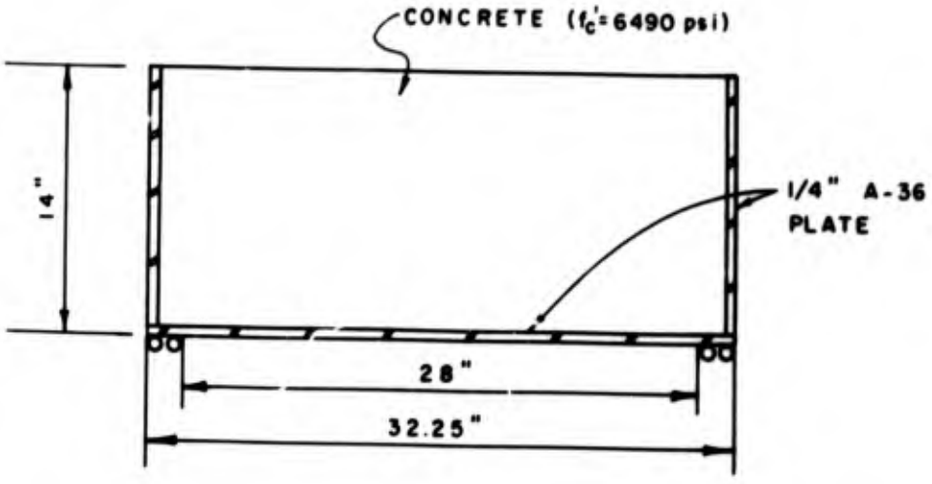

CLOSURE GEOMETRY FOR TEST 24

FIGURE 3-96

The model failed at 3409 psi (Figure 3-97), which was only a nominal decrease from the previous 3500-psi load level. The failure mode was basically the same as that previously observed (Figure 3-99). This decrease in load capacity does not appear significant in light of other uncertainties involved in the testing.

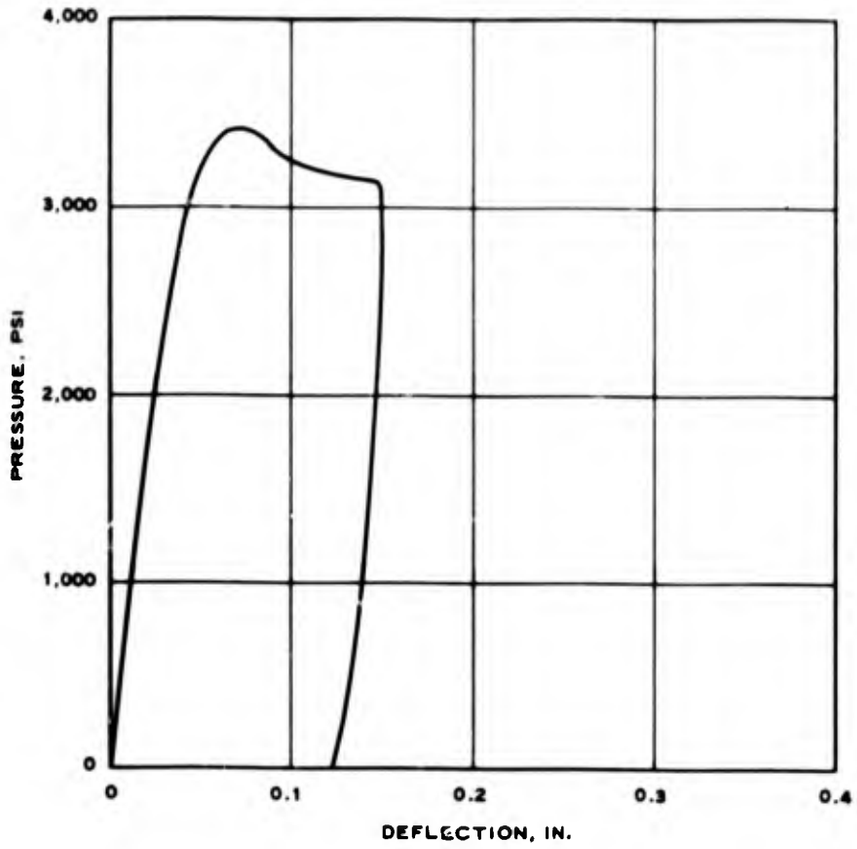

CLOSURE M130-1-3 TEST 24 - PRESSURE VS. DEFLECTION

FIGURE 3-97
A2-130

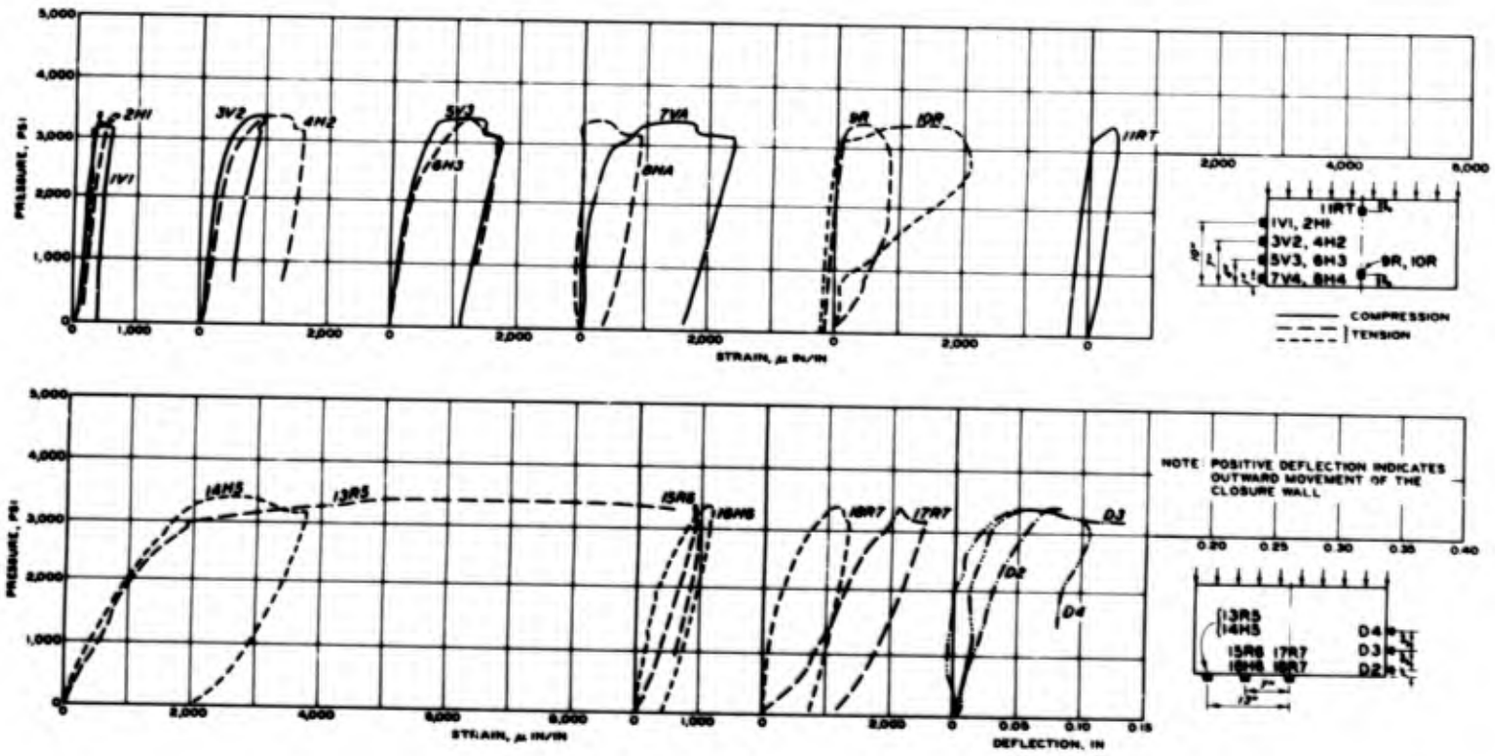

DATA PLOT - TEST 24
FIGURE 3-98

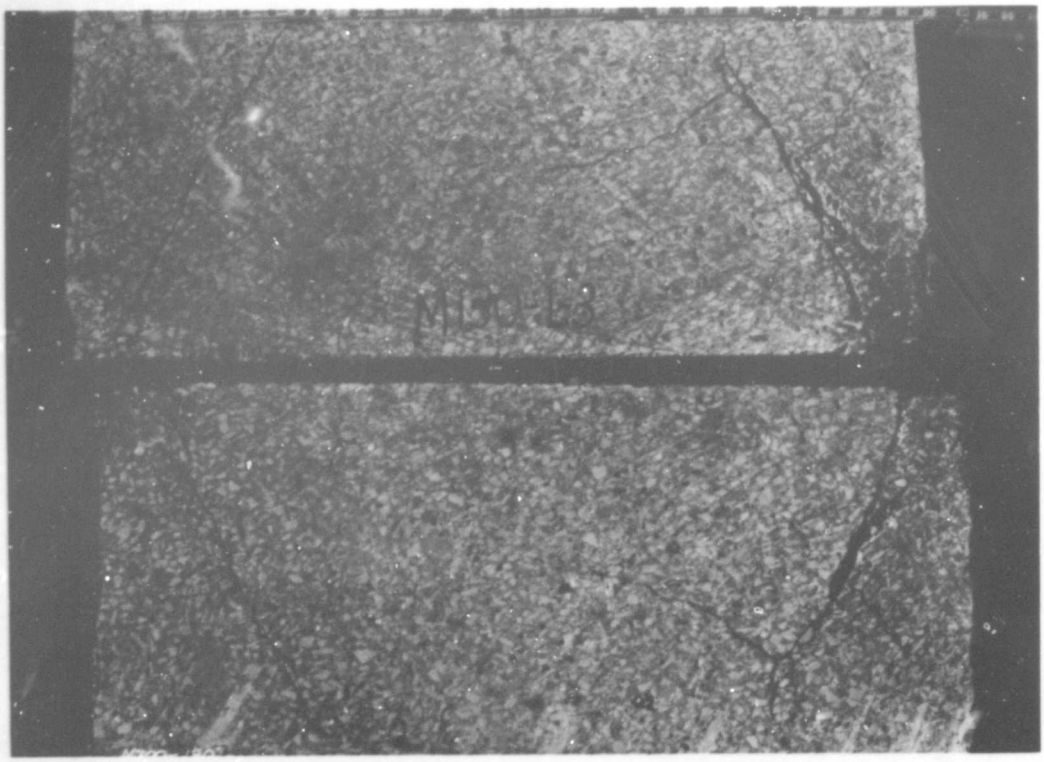

TEST 24

FIGURE 3-99

A2-132

TEST 25

In Test 25 a much thinner section than had been used in earlier tests was examined to determine the effect of the closure section depth. It was anticipated that the mode of response at this larger span-to-depth ratio would be of interest; flexural response might influence the load capacity to some degree. Since the response mode observed in Tests 1 and 2 differed significantly from that of Tests 3 and 4 in terms of flexural cracks, this test was intended to further explore the flexural response phenomenon.

The model geometry is shown in Figure 3-100. The model was tested on a low friction support.

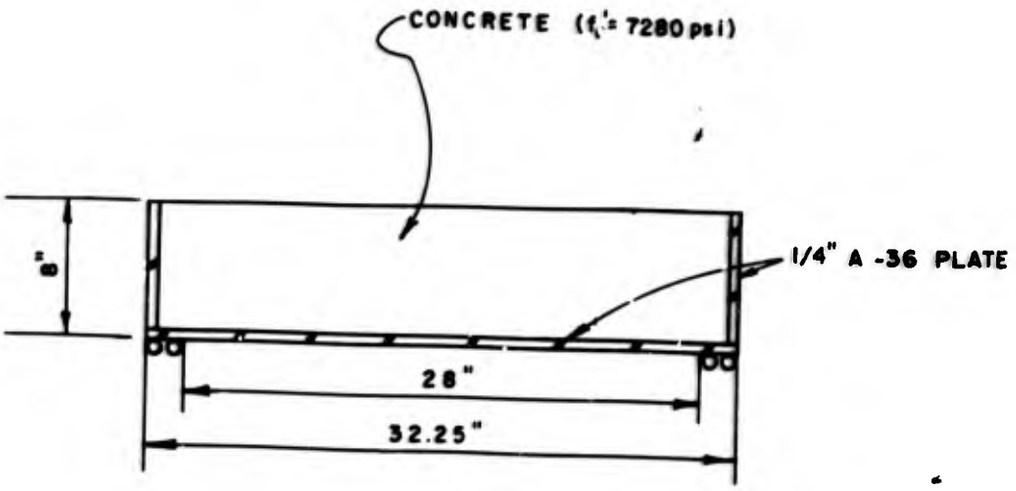

CLOSURE GEOMETRY FOR TEST 25

FIGURE 3-100

The model failed at a load of 3307 psi (Figure 3-101), which compares very favorably with the results of Tests 1, 2, 3 and 4. In Tests 1 and 2, identical models 8 inches deep with 1/8-inch plates failed at the 2600 psi level; in Tests 3 and 4, 14-inch-deep models with 1/4-inch plates failed at the 3500-psi level.

Bearing distress was evident in the model. Note the shear crack and the beginning of tensile cracks on the lower concrete surface (Figure 3-103). It is of interest to note that the load capacity of this model was only slightly less than that of the 1¼-inch-deep models in Tests 3 and 4. This tends to support the contention that the total load capacity is rather insensitive to section depth but depends rather on the steel plate thicknesses.

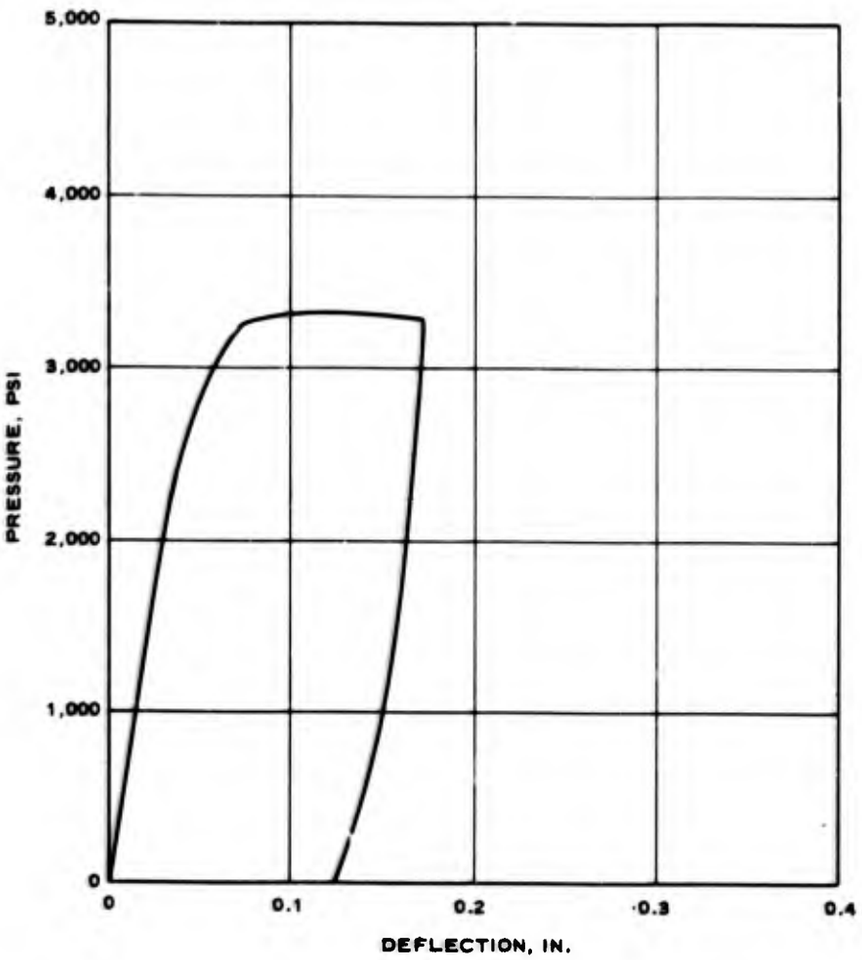

CLOSURE M130-5 TEST 25 - PRESSURE VS. DEFLECTION

FIGURE 3-101

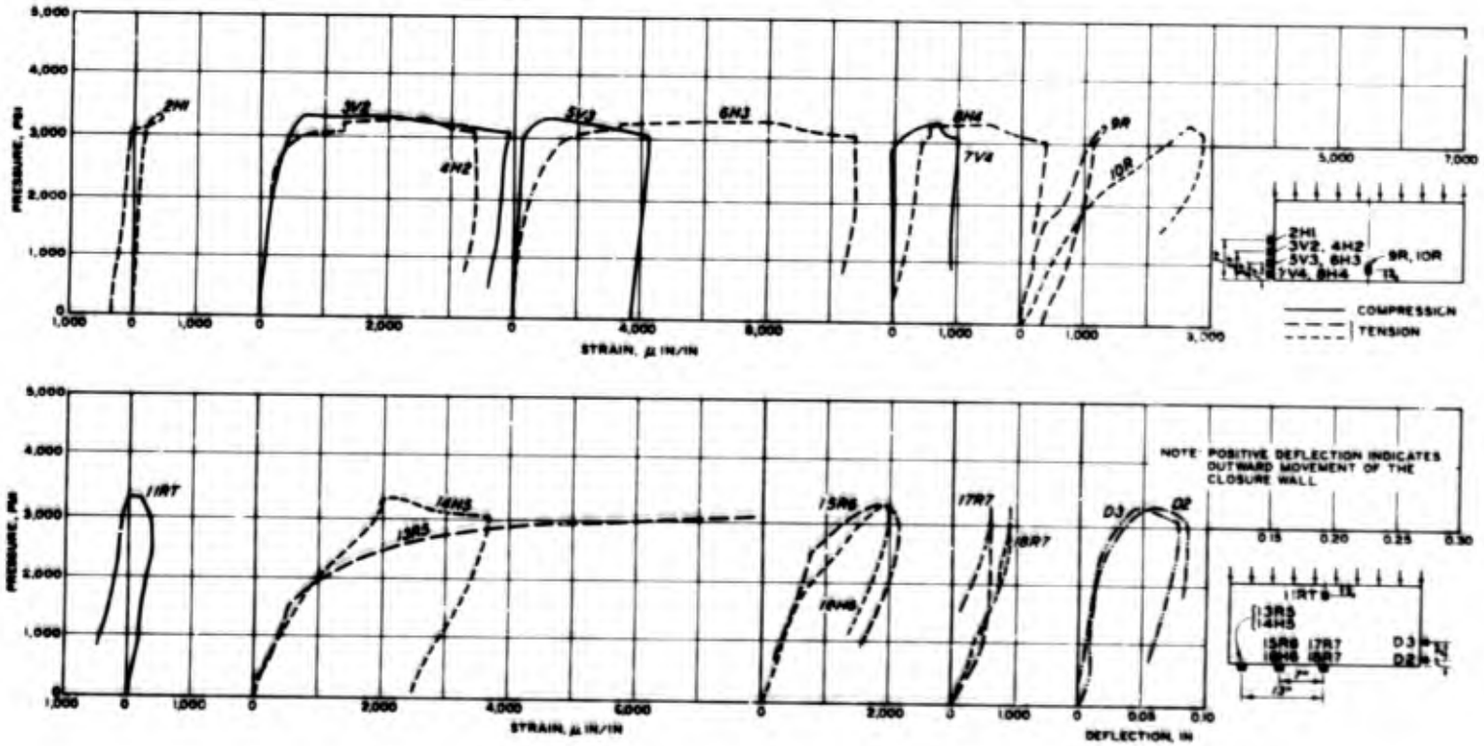

DATA PLOT - TEST 25

FIGURE 3-102

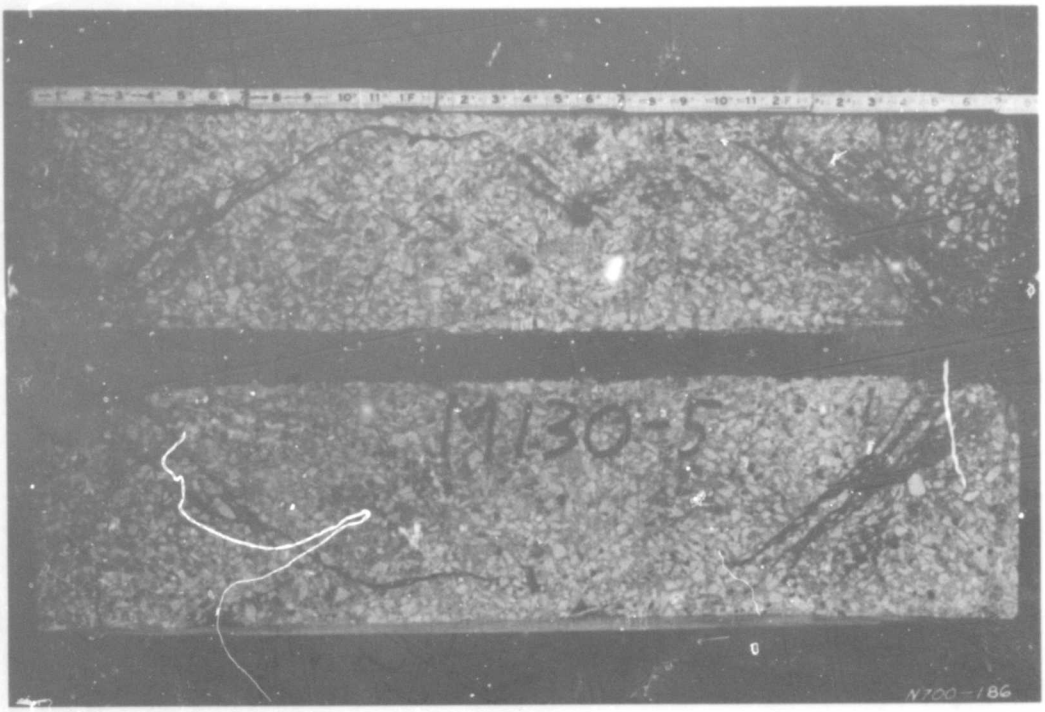

TEST 25

FIGURE 3-103

A2-136

TEST 26

Test 26 was a test of a plain concrete model with no plate reinforcing. The model tested had a clear span of 28 inches, an outside diameter of 32-1/4 inches, and a section depth of 8 inches. The model was tested on a low friction support. The concrete had an unconfined compressive strength of 7070 psi.

The model failed at the 1000-psi load level (Figure 3-104). Failure appeared to be basically due to excessive shear load. A crack formed from the inside of the bearing and ran to the outside of the closure model, causing sizable pieces of concrete to spall off the model.

The ring at the bottom of the specimen (Figure 3-106) served as an enclosure for the segmented blocks (which are just visible above the ring). The large circular steel ring at the top of the specimen is the T-ring; immediately below this is the steel which was inserted in the model to provide a seal surface for the T-ring gaskets. Tensile cracks were apparent on the bottom surface of the closure (Figure 3-107), but it is postulated that this did not influence the total load capacity of the closure.

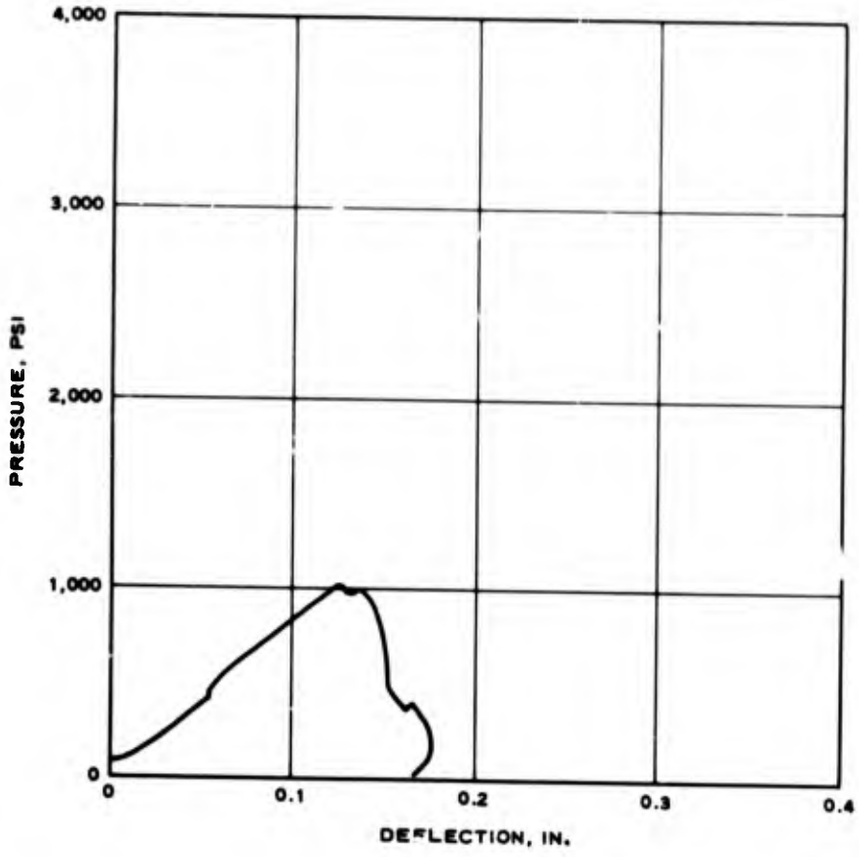

CLOSURE M133-1 TEST 26 - PRESSURE VS. DEFLECTION

FIGURE 3-104

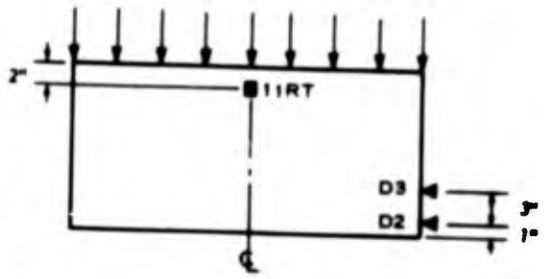

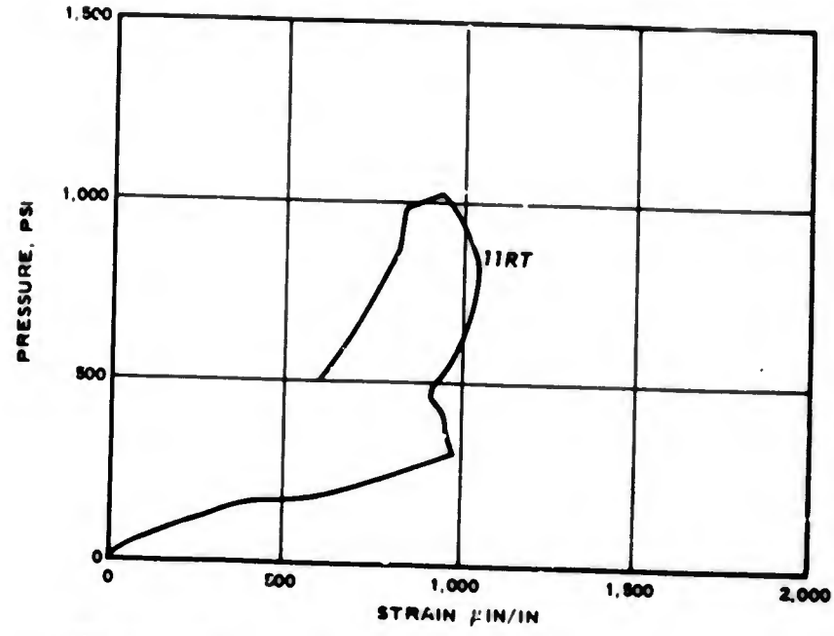

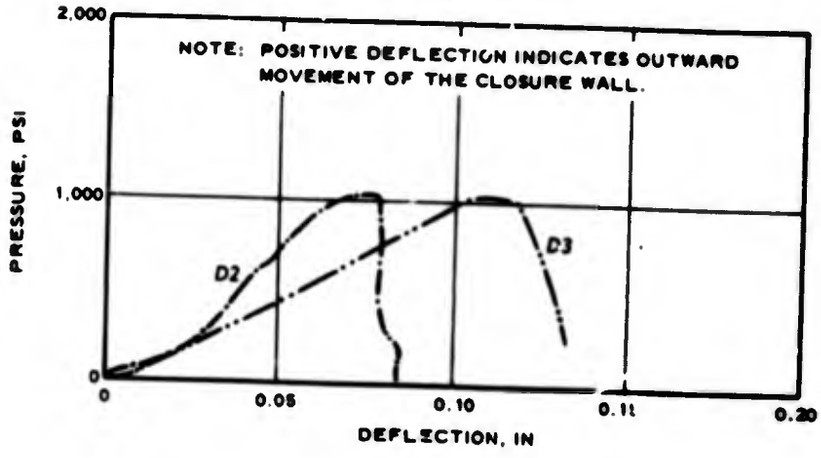

DATA PLOT - TEST 26

FIGURE 3-105

A2-139

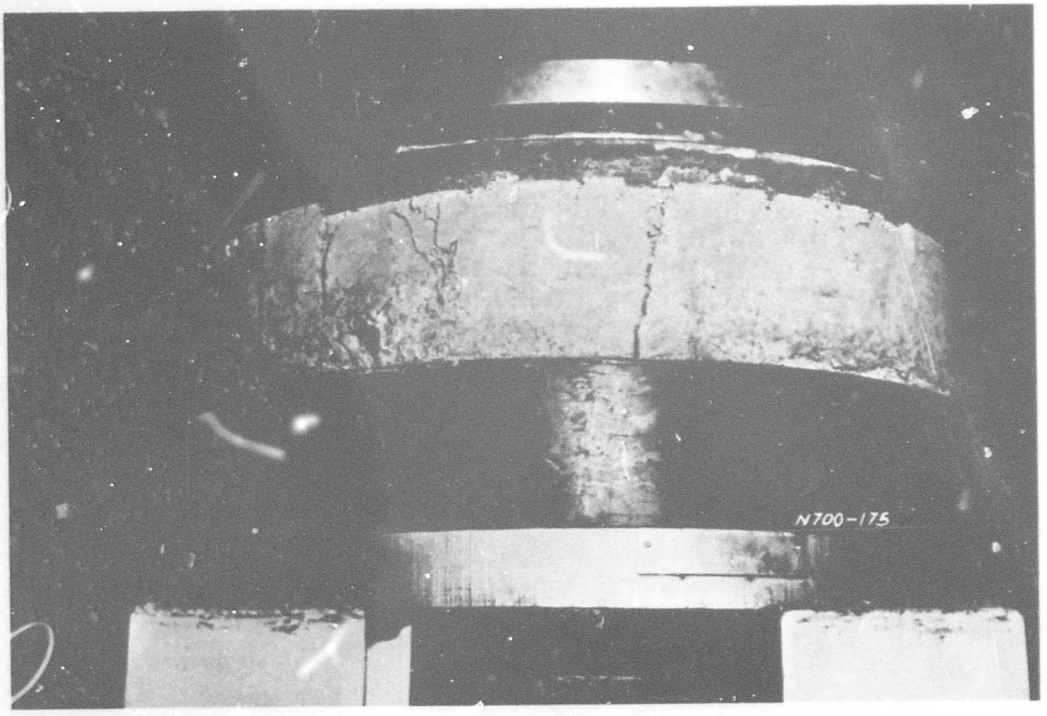

TEST 26

FIGURE 3-106

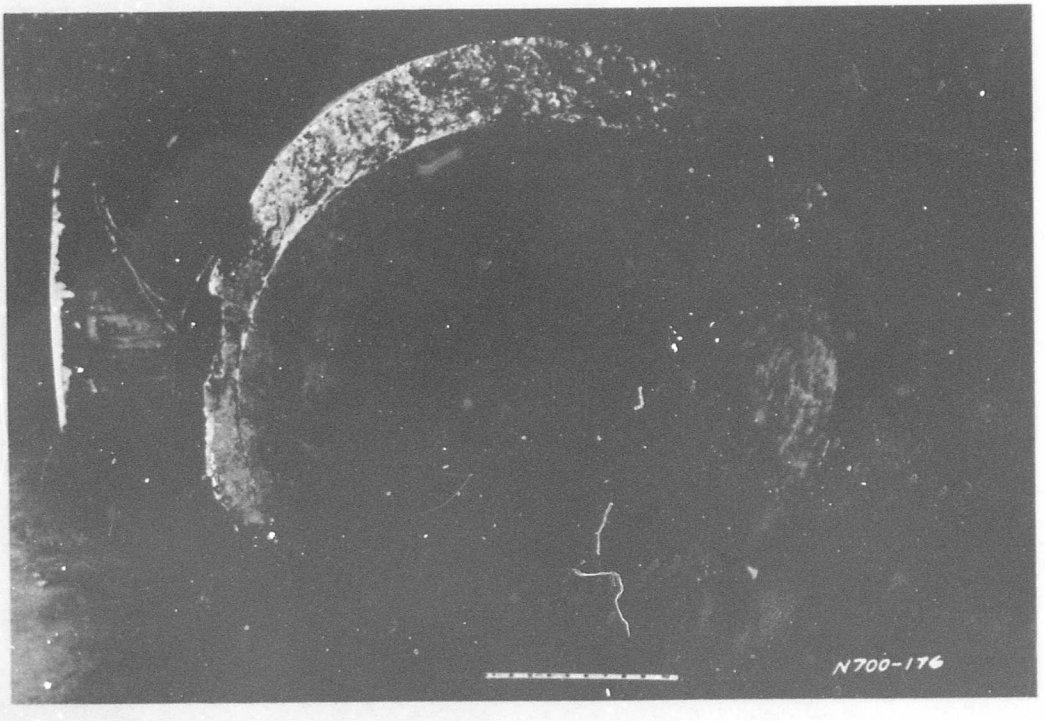

TEST 26

FIGURE 3-107

TEST 27

Test 27 was another test of a plain concrete model with no plate reinforcing. This test was performed to determine the effect of a deeper section on the total load capacity. The model tested had a clear span of 28 inches, an outside diameter of 32-1/4 inches, and a section depth of 21 inches. The model was tested on a low friction support. The concrete had an unconfined compressive strength of 6190 psi.

The model failed at 1149-psi applied load (Figure 3-108); failure again appeared to be due to excess local shear load. A crack formed from the inside of the bearing and ran vertically for some distance, causing sizable pieces of concrete to spall off the model (Figures 3-110 and 3-111). Only one tensile crack was apparent on the bottom surface of the closure, but again it is postulated that this response did not influence the total load capacity of the closure.

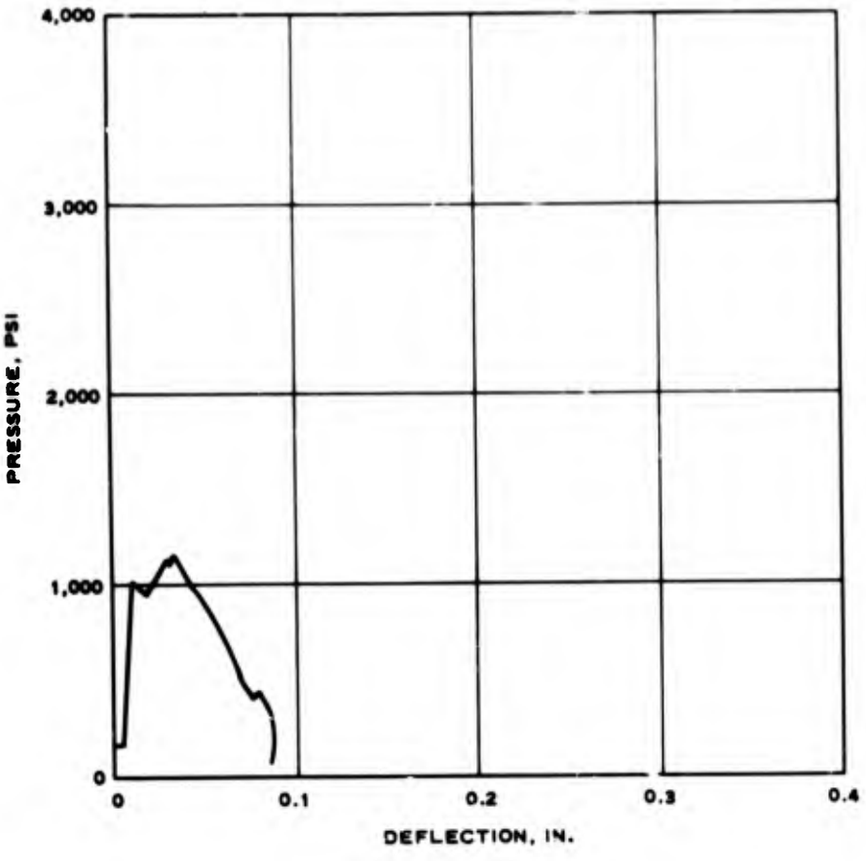

CLOSURE M133-2 TEST 27 - PRESSURE VS. DEFLECTION

FIGURE 3-108

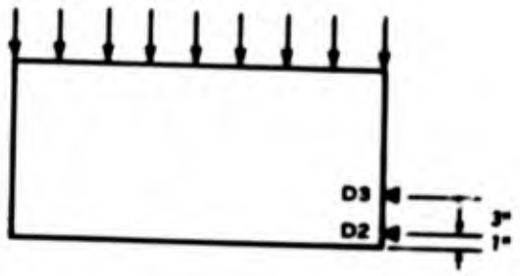

NOTE: POSITIVE DEFLECTION INDICATES OUTWARD MOVEMENT OF THE CLOSURE WALL.

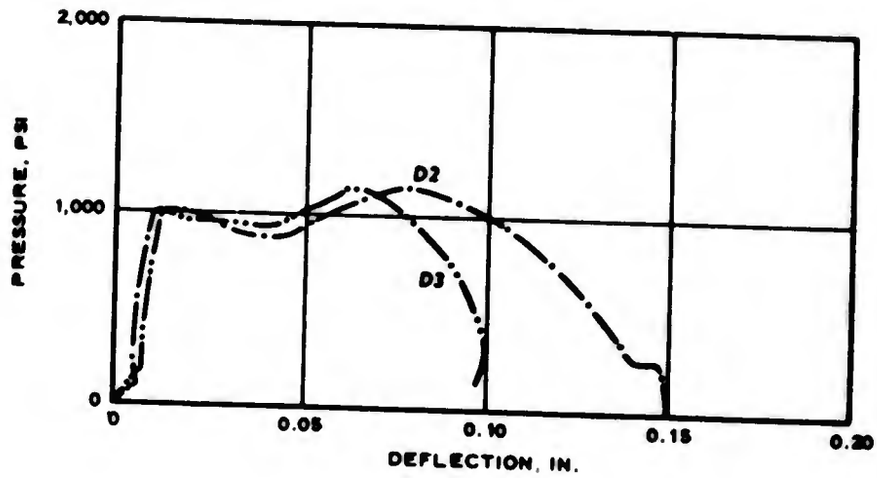

DATA PLOT - TEST 27

FIGURE 3-109

A2-143

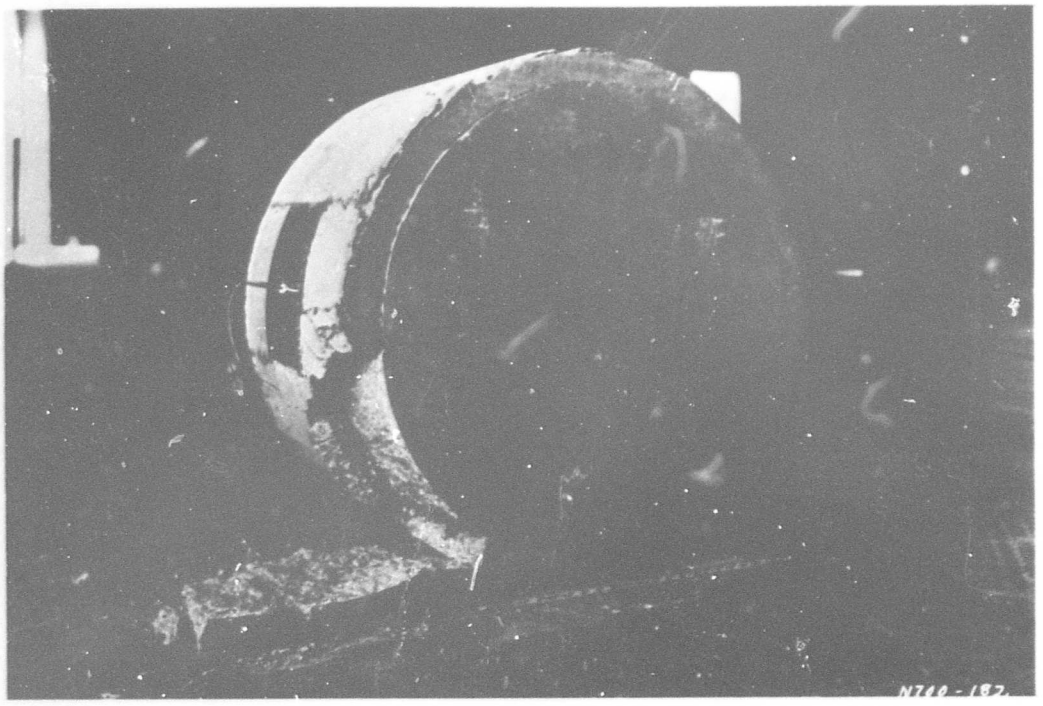

TEST 27

FIGURE 3-110

TEST 27

FIGURE 3-111

TEST 28

In Test 28 the effect of the closure section depth was further examined by testing a much thicker section than tested earlier. The mode of response was again considered to be of critical importance; flexural response might influence the load capacity. The closure geometry is shown in Figure 3-112. The model was tested on a low friction support.

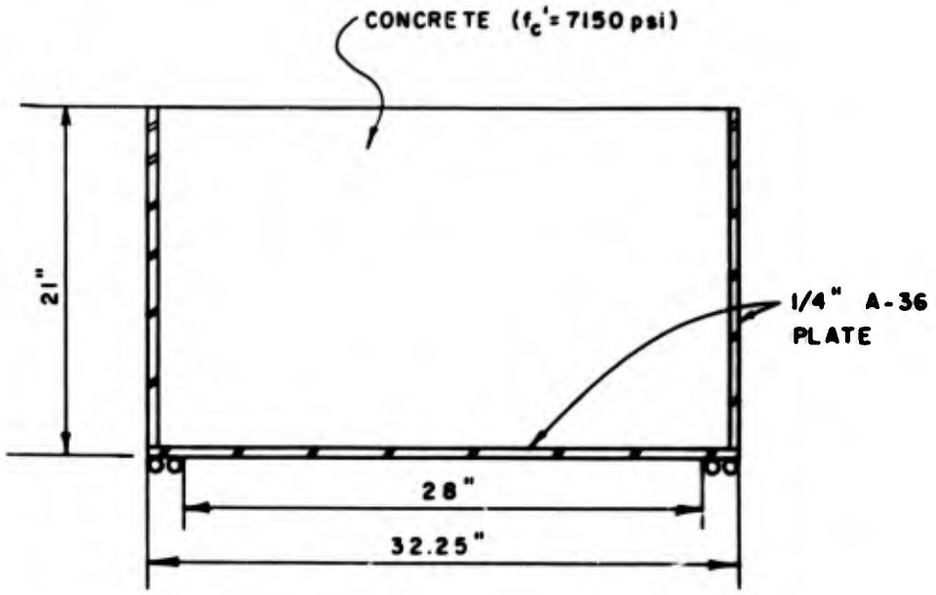

CLOSURE GEOMETRY FOR TEST 28

FIGURE 3-112

Failure was observed at 4076 psi (Figure 3-113). This was only a 12-percent increase in load capacity over the 3500 psi for Tests 3 and 4, which tends to support the assumption that load capacity is not greatly influenced by section depth.

Note the absence of cracks in the model (Figure 3-115). No distress was apparent, except in the bearing area. Results of Tests 3, 4, 25 and 28 indicate that failure is initiated by yielding of the steel plates, but that collapse is a result of the interaction of failure modes that do depend on section depth - flexure, bearing and shear.

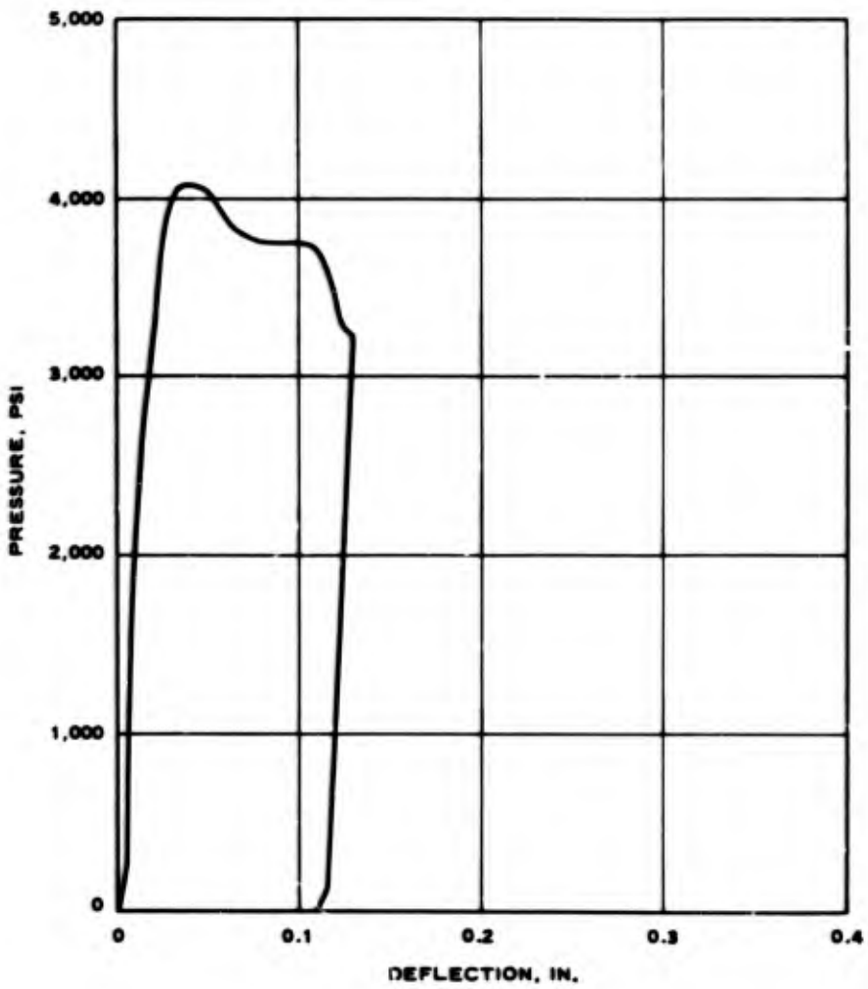

CLOSURE M130-6 TEST 28 - PRESSURE VS. DEFLECTION

FIGURE 3-113

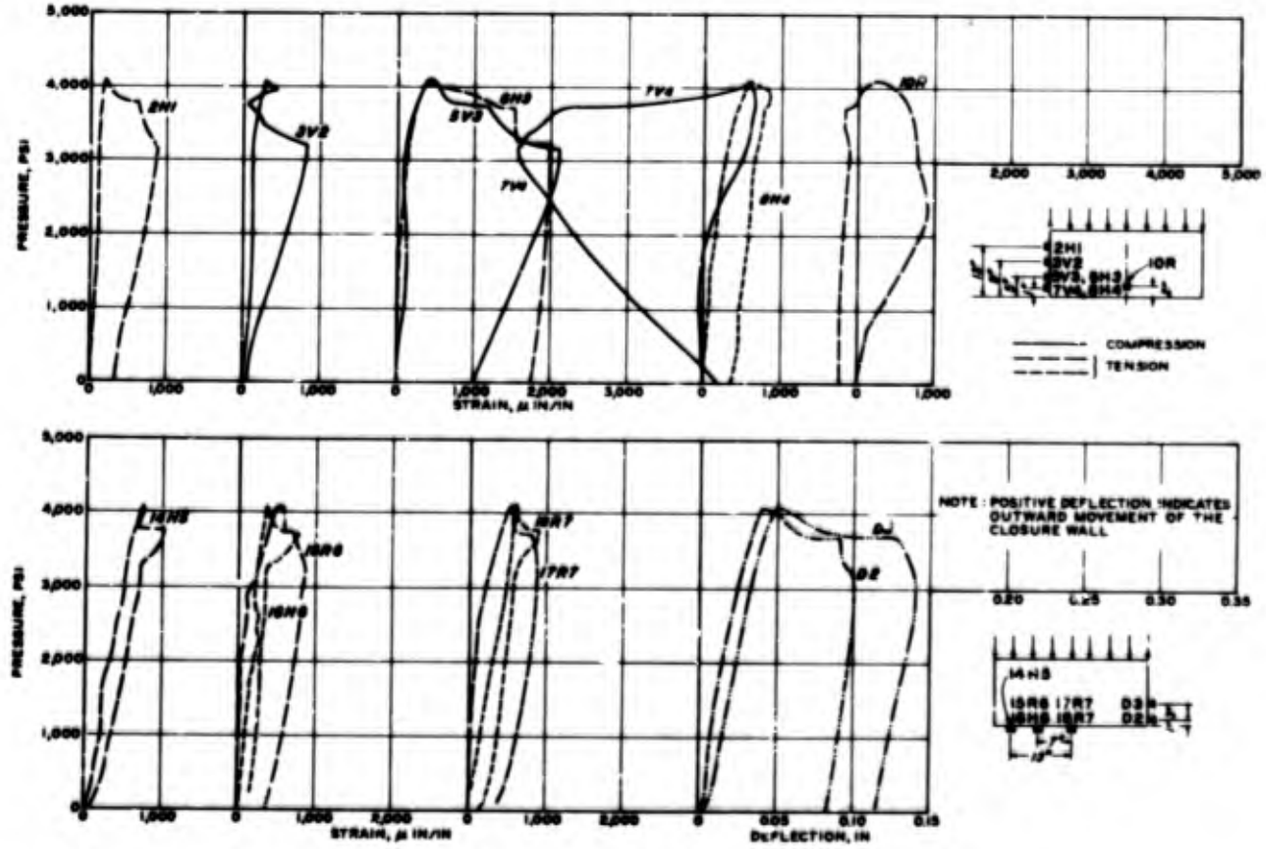

DATA PLOT - TEST 28

FIGURE 3-114

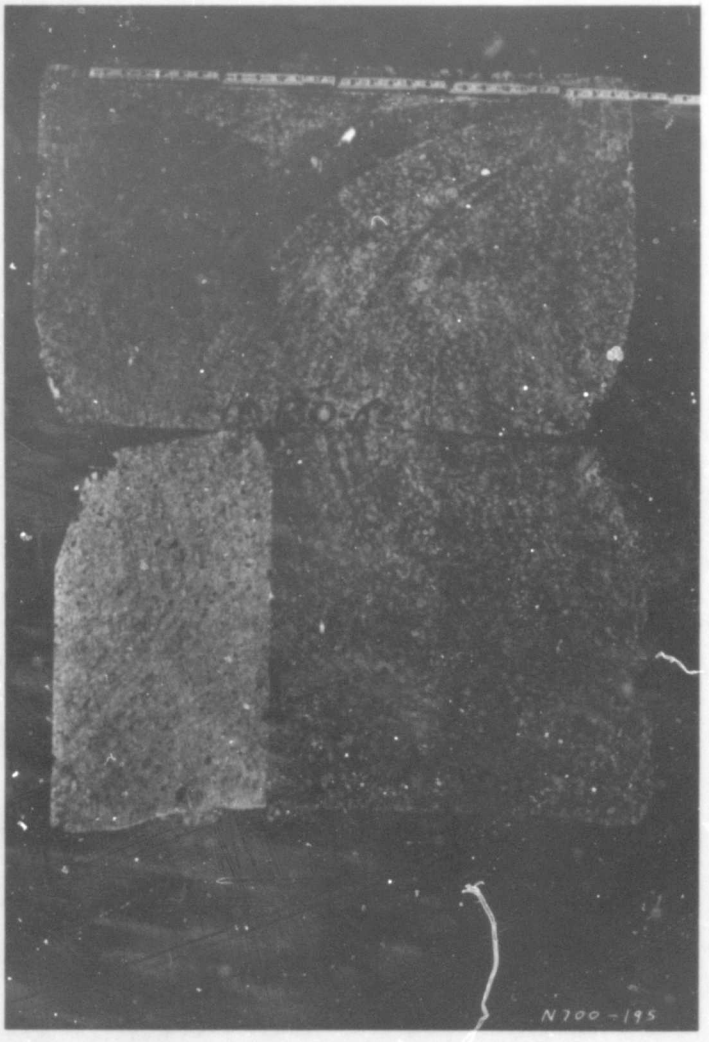

TEST 28

FIGURE 3-115

A2-148

TEST 29

Test 29 was designed to examine the effect of span-to-depth ratio on total load capacity. The results were intended to correlate with Tests 13 and 30 where similar structures were tested. Figure 3-116 shows the closure geometry for Test 29. The test was performed on a low friction support.

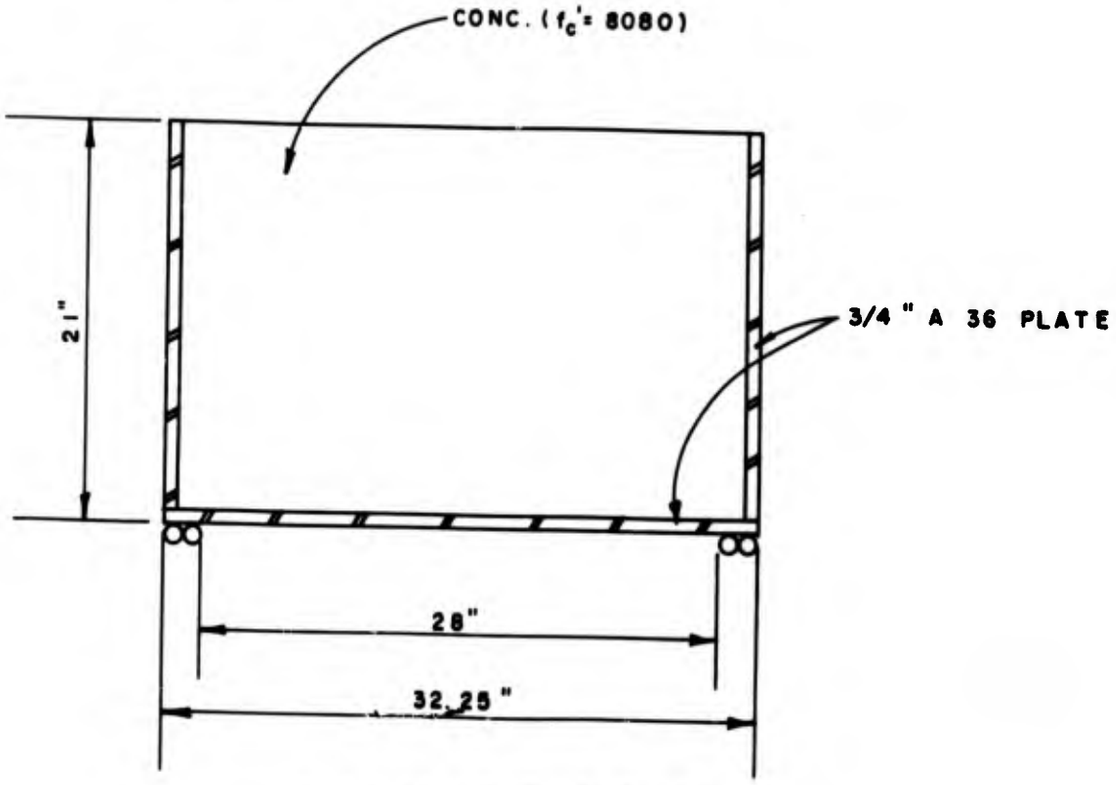

CLOSURE GEOMETRY FOR TEST 29
FIGURE 3-116

The maximum test pressure reached was 8270 psi (Figure 3-117); this compares well with the pressures observed in Tests 13 and 30. The effect of a decrease in the span-to-depth ratio is not very significant for models with the amount of confining steel used in this test. The failure mode is the same as that observed in the other similar tests, suggesting that the failure mode depends on the steel plate thickness. Here again, a local failure due to yielding of the steel plates was noted. In Figure 3-119, minor distress is evident in the concrete over the bearing where the plate yielded.

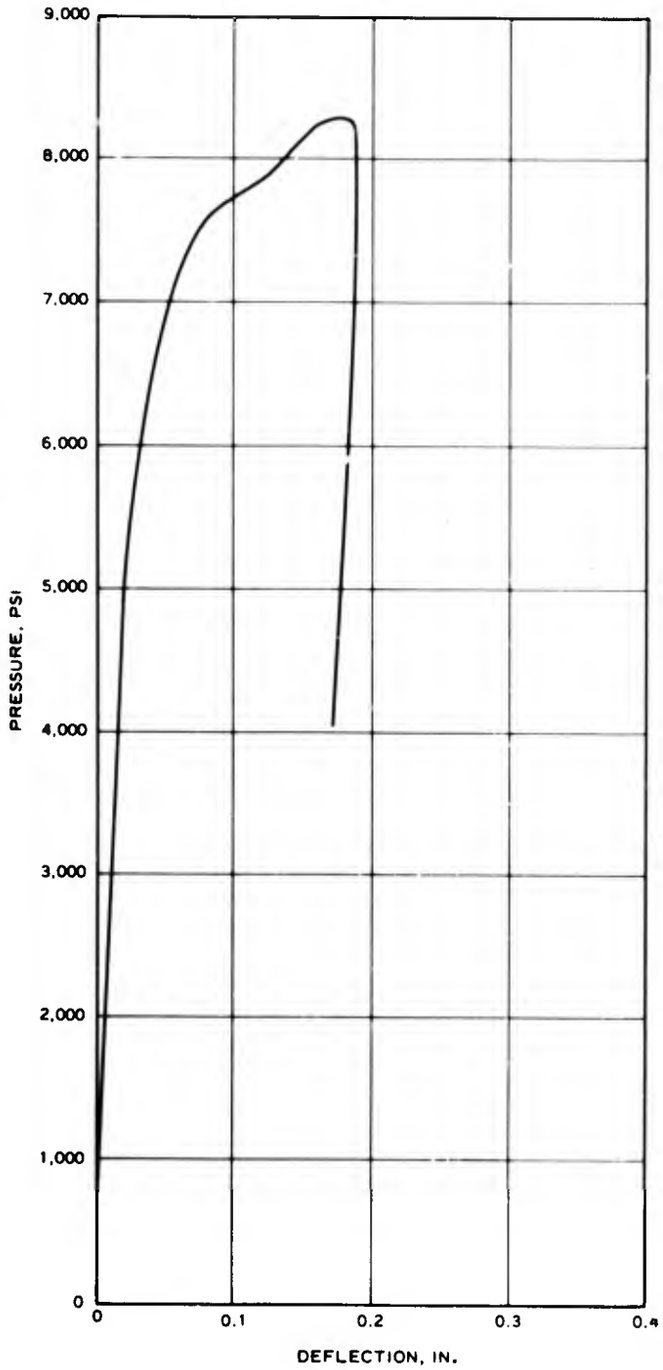

CLOSURE M130-14 TEST 29 - PRESSURE VS. DEFLECTION

FIGURE 3-117

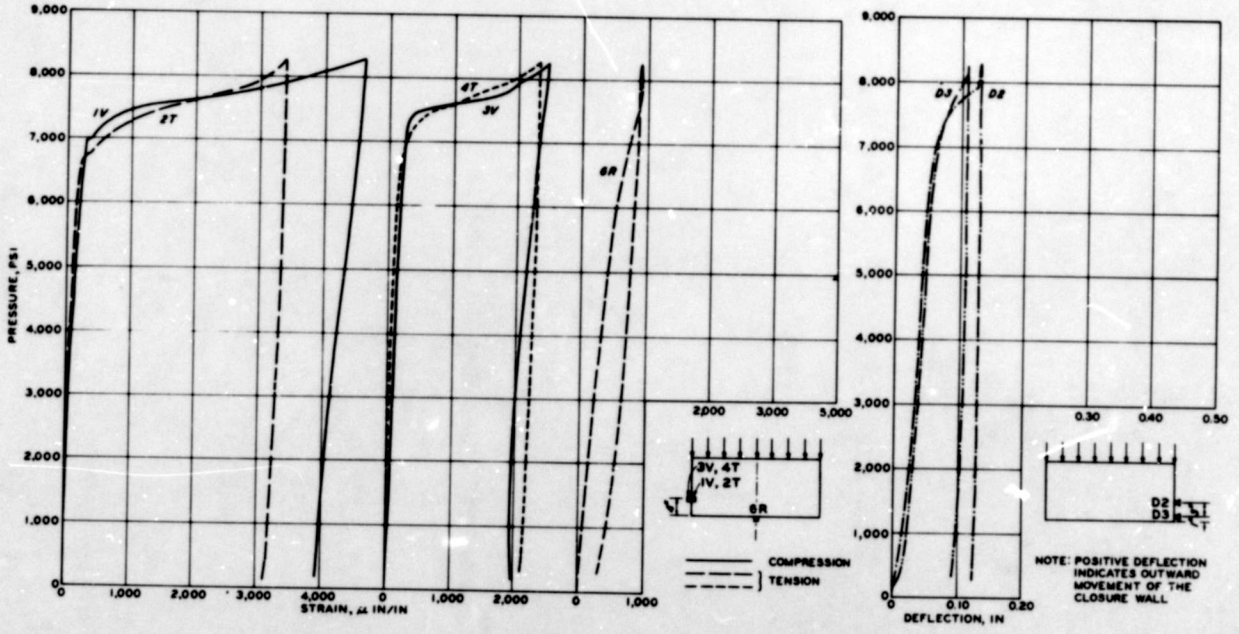

A2-151

DATA PLOT - TEST 29

FIGURE 3-118

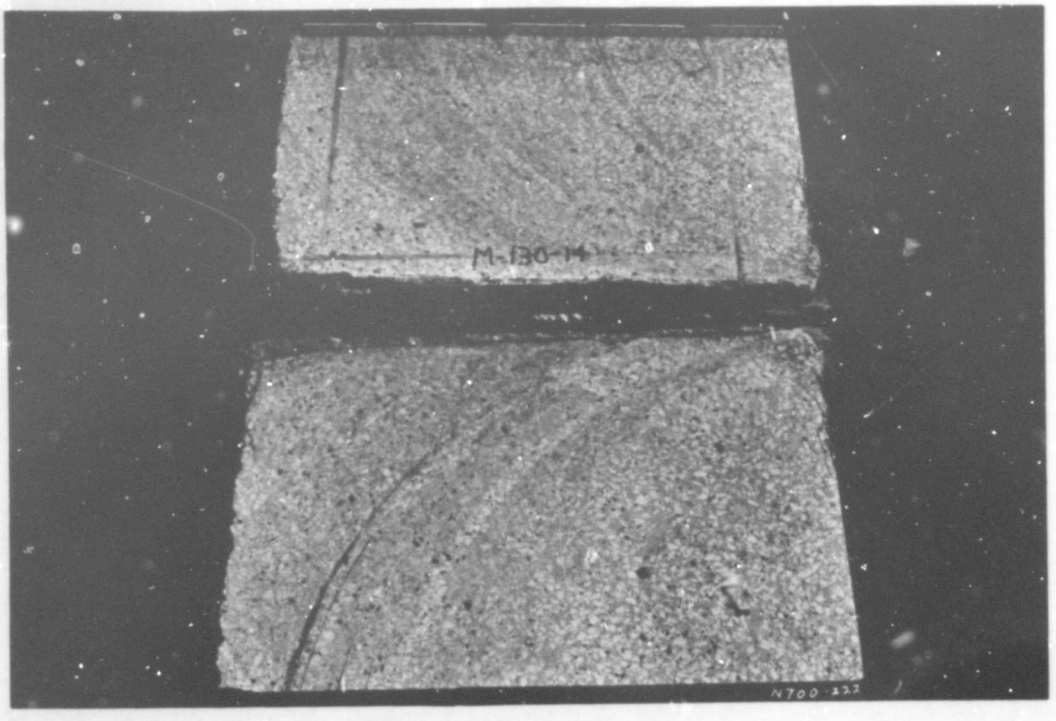

TEST 29

FIGURE 3-119

A2-152

TEST 30

Test 30 was performed to examine the effect of span-to-depth ratio on total load capacity. The results were intended to show the correlation between this test situation and Test 13 where a similar structure with a smaller span-to-depth ratio was used. Figure 3-120 shows the closure geometry for Test 30.

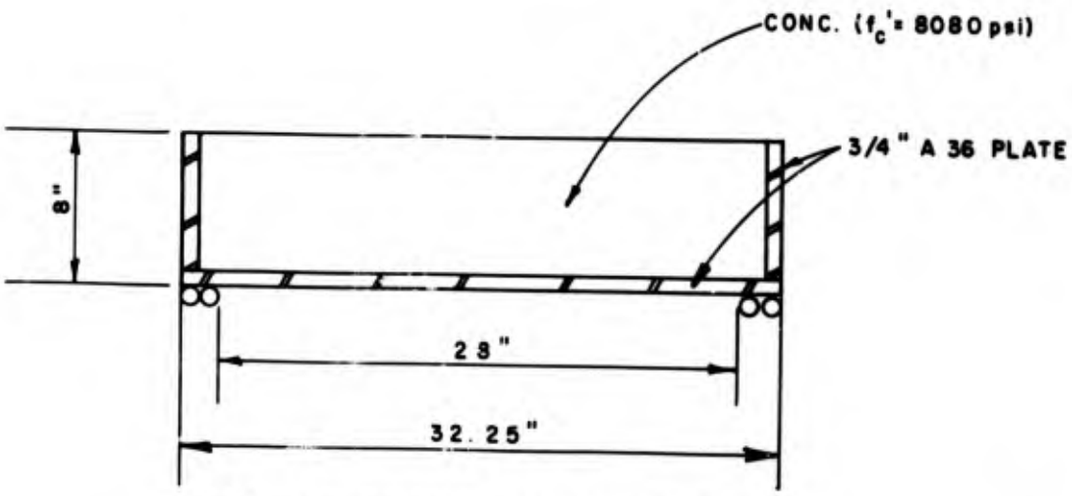

CLOSURE GEOMETRY FOR TEST 30

FIGURE 3-120

The maximum test pressure reached was 6847 psi (Figure 3-121), which does not compare well with the test pressure of 8800 psi achieved in Test 13. In light of the other test results, the observed load capacity appears too low. The failure mode is apparently somewhat different from that observed in thicker sections with the same steel plates. After the model has been observed, there may be some doubt that the specimen actually collapsed.

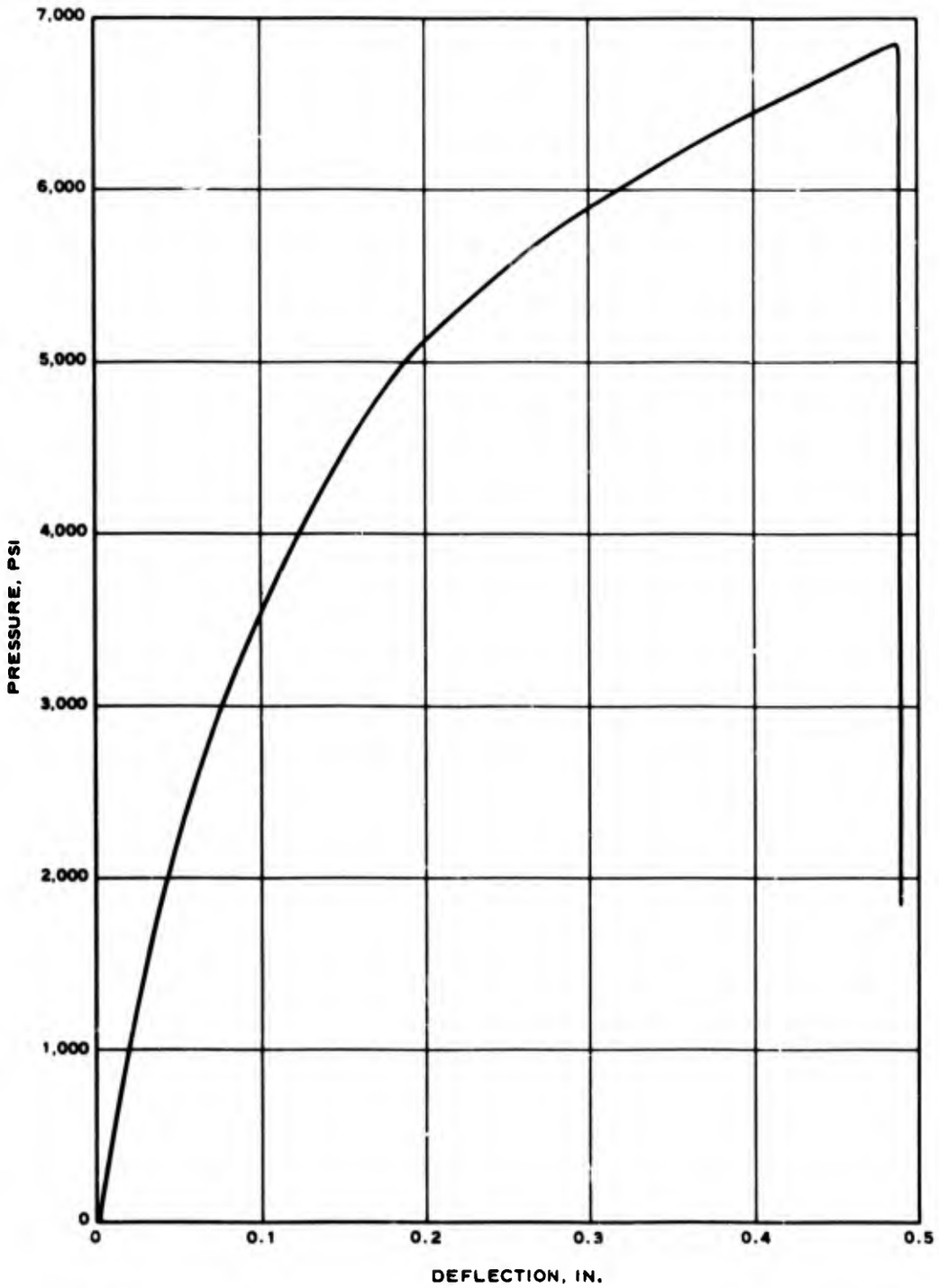

CLOSURE M130-13 TEST 30 - PRESSURE VS. DEFLECTION

FIGURE 3-121

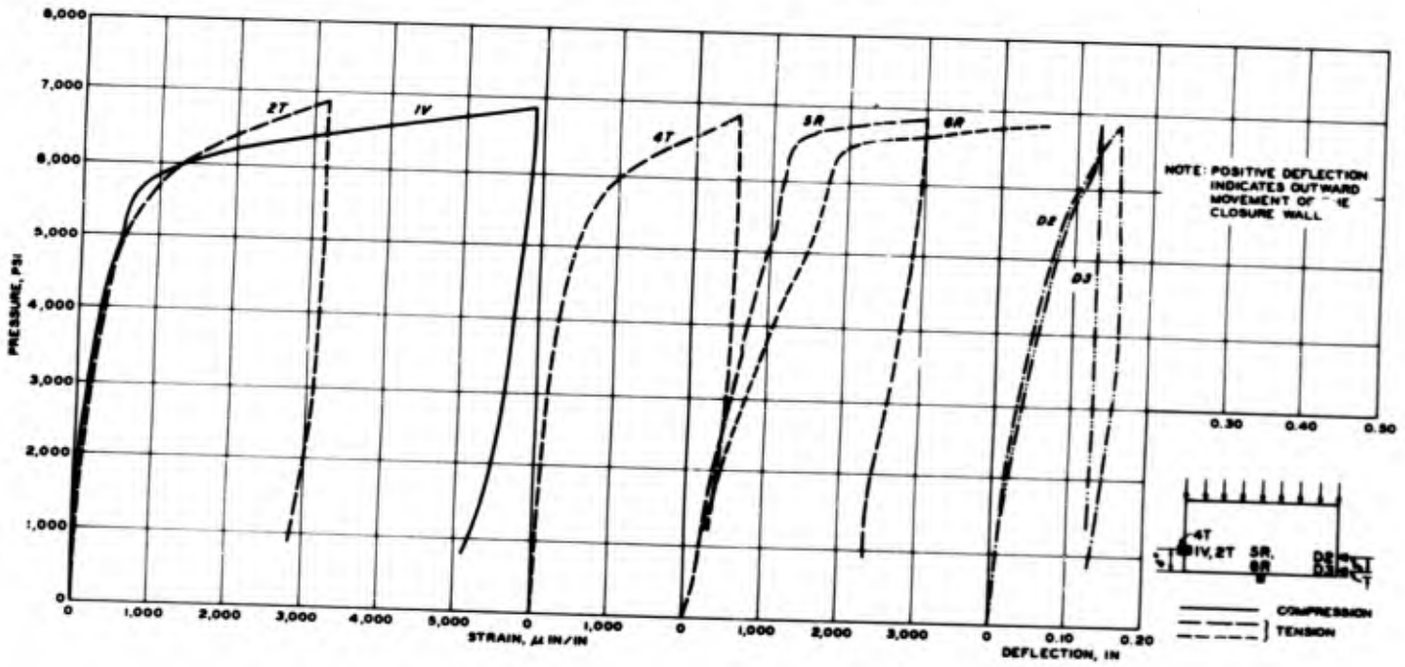

DATA PLOT - TEST 30

FIGURE 3-122

TEST 31

In Test 31 the effect of a wide bearing on total load capacity was examined. A support structure with a haunch under the bearing was also tested for the first time. It was anticipated that these parameters would influence the design approach. The model geometry for Test 31 is shown in Figure 3-123.

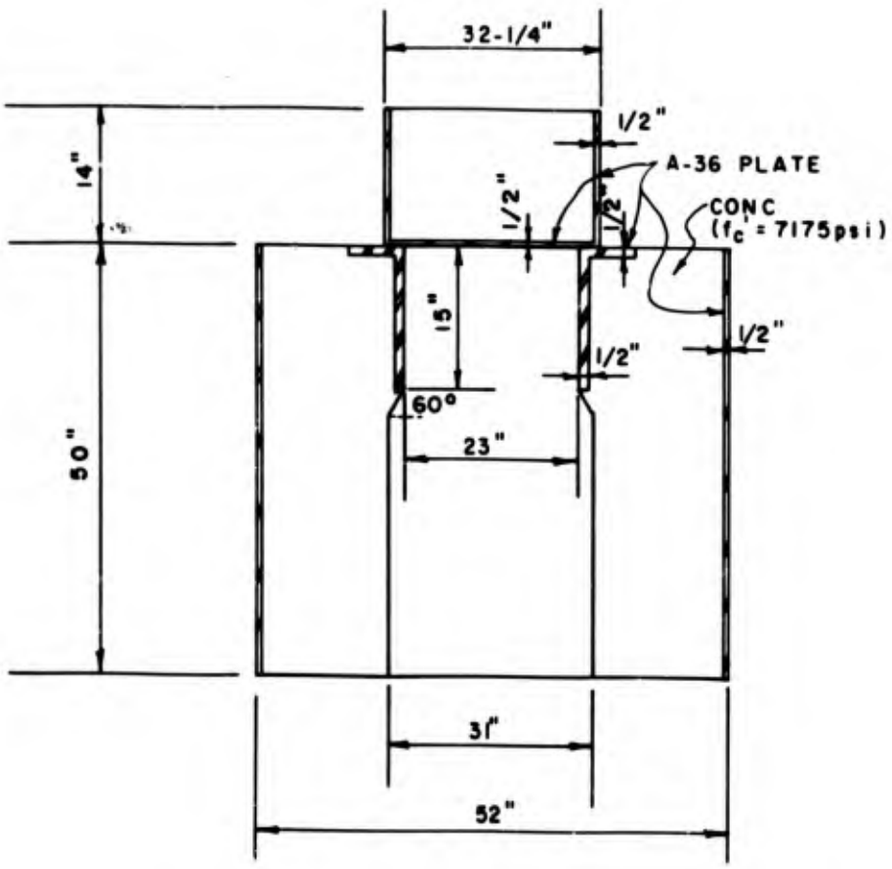

MODEL GEOMETRY FOR TEST 31

FIGURE 3-123

The collapse load for the system was 6568 psi (Figure 3-124). This load capacity may be compared with that observed in Test 8 (6375 psi) where a similar test was performed on a narrower bearing support without a haunch.

No distress was observed in the closure structure at the time of post-test inspection. The support structure failed because of a vertical shear crack propagating from the bearing to the bottom of the haunch inside the silo (Figure 3-126). Radial cracks can be seen in Figure 3-127. In Figure 3-128. which shows the bottom view of the silo looking toward the bearing area, note the circumferential crack at the base of the haunched area. There was no evident bearing distress in the support structure.

The undamaged appearance of the concrete after it was sawed (Figure 3-129) was due to the increase in bearing area provided and the fact that the shell was 1/2-inch thick (which is not shown in the photograph). No distress was observed in the closure structure at the time of post-test inspection.

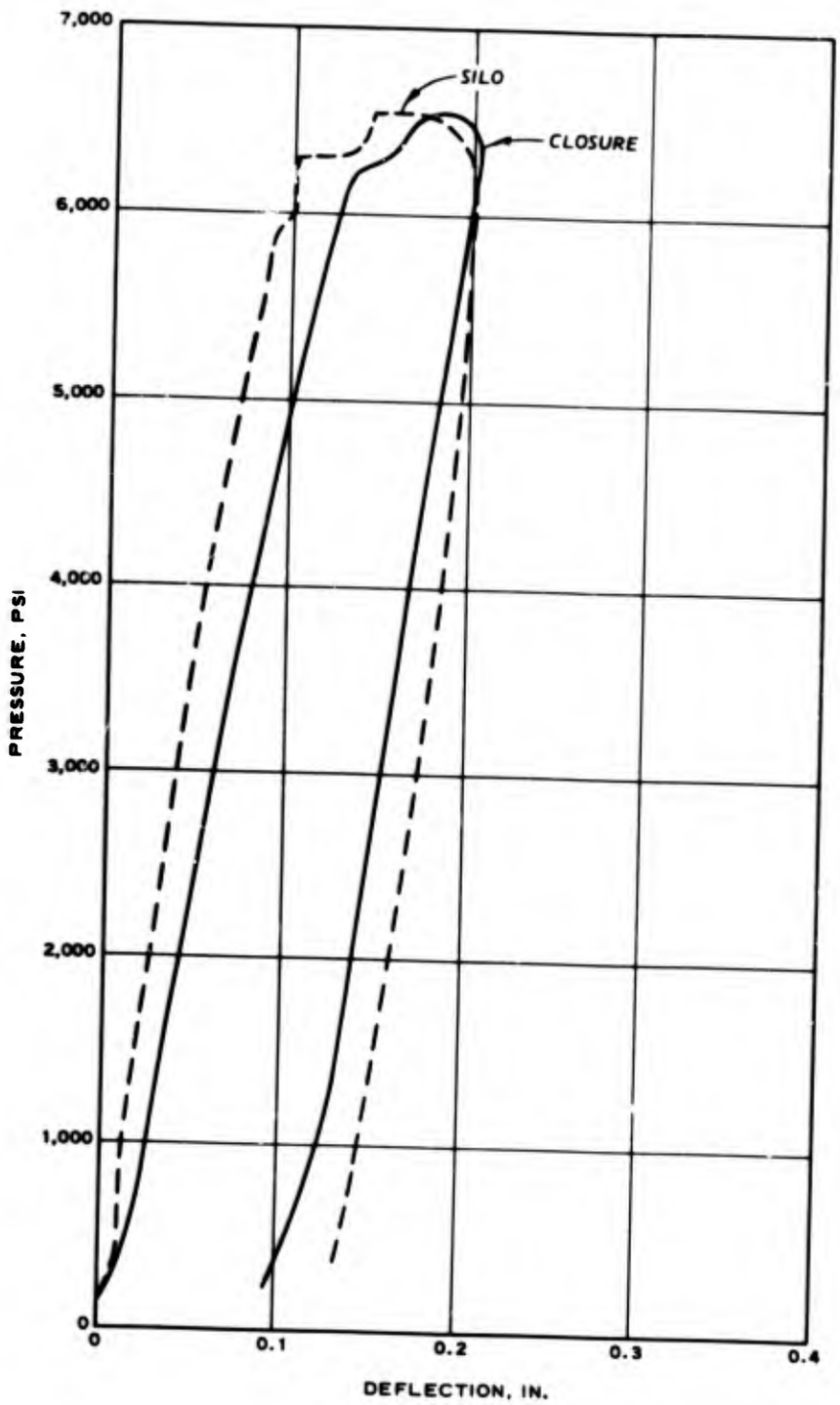

CLOSURE M130-7-1 AND SUPPORT M131-1 TEST 31 - PRESSURE VS. DEFLECTION

FIGURE 3-124

A2-158

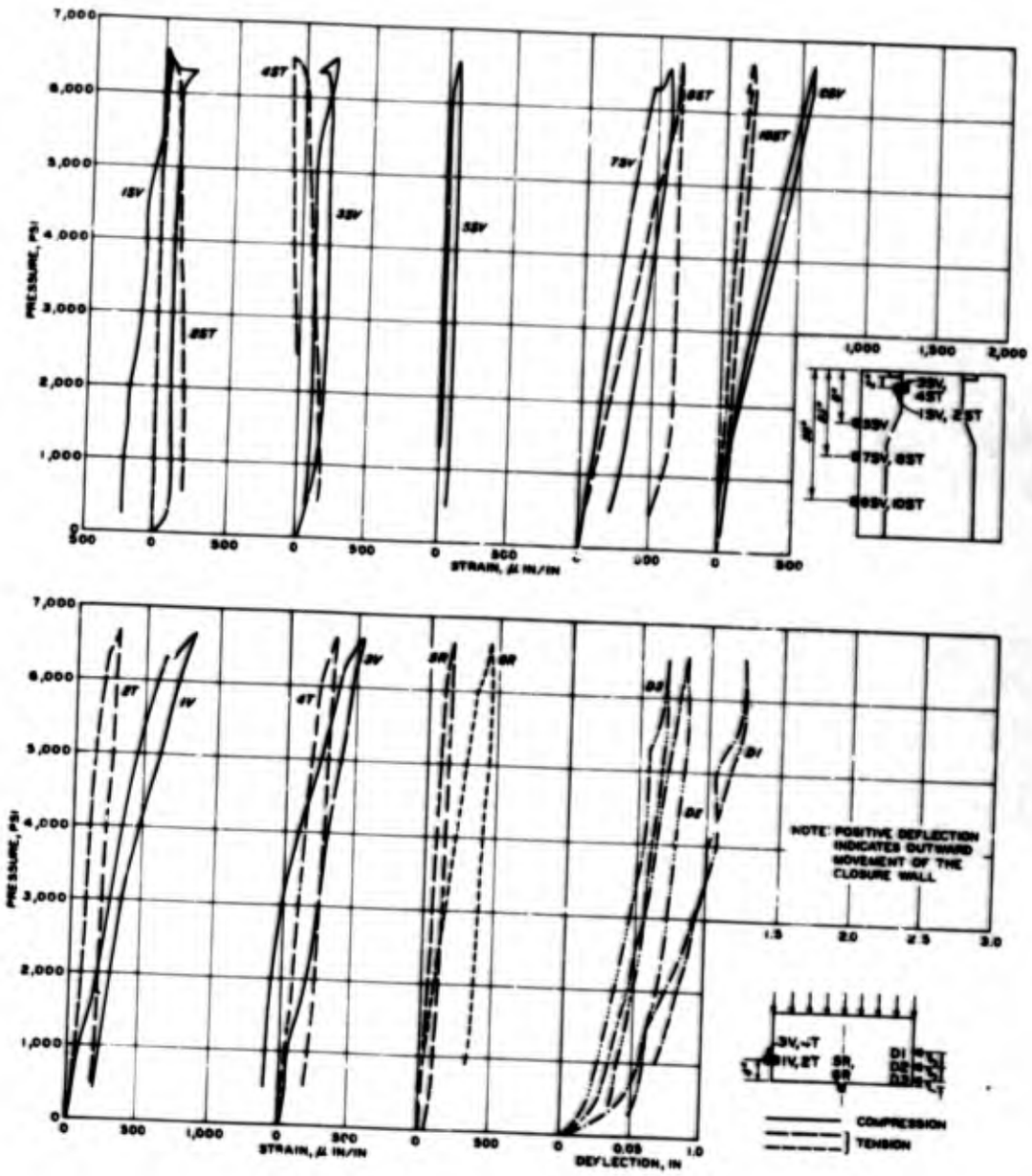

DATA PLOT - TEST 31

FIGURE 3-125

A2-159

TEST 31

FIGURE 3-126

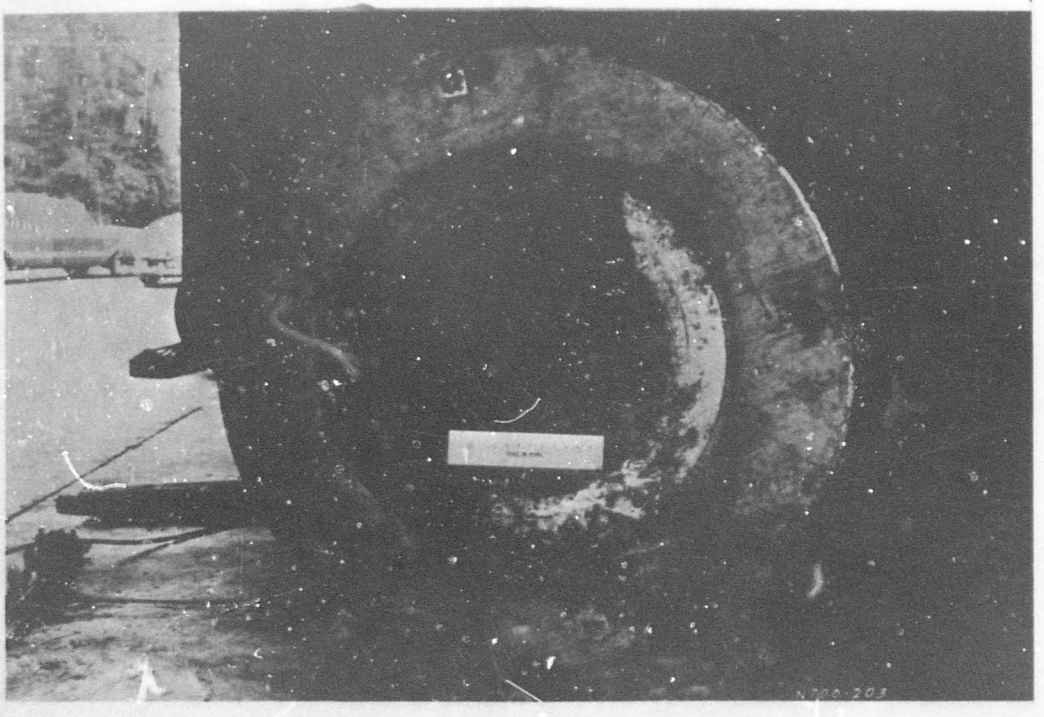

TEST 31

FIGURE 3-127

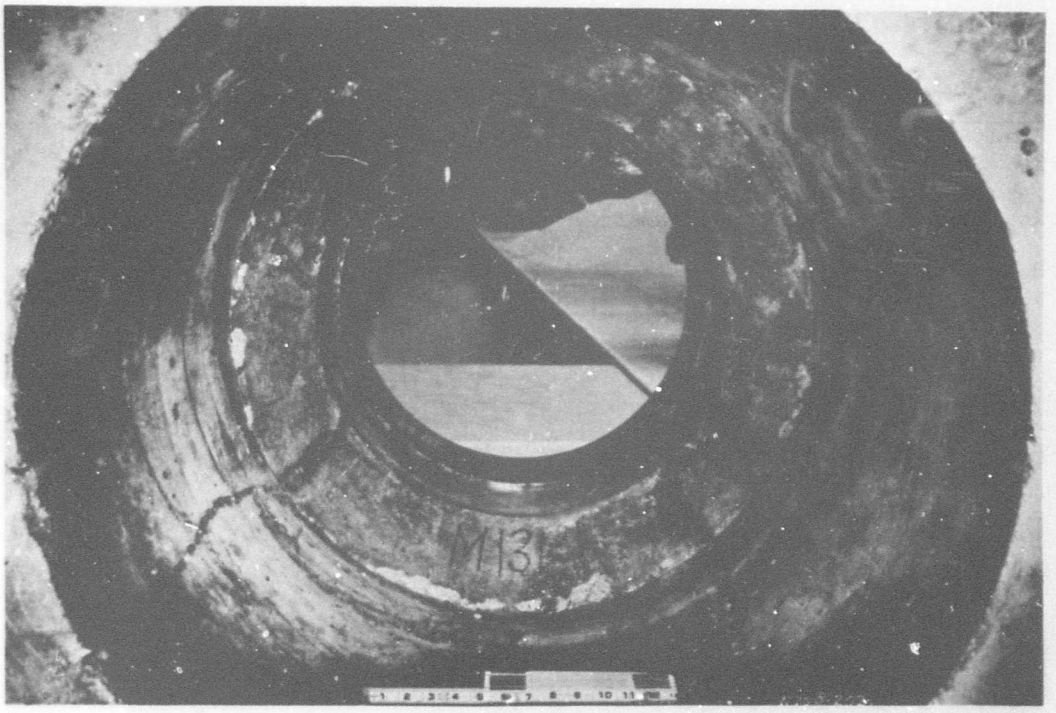

TEST 31

FIGURE 3-128

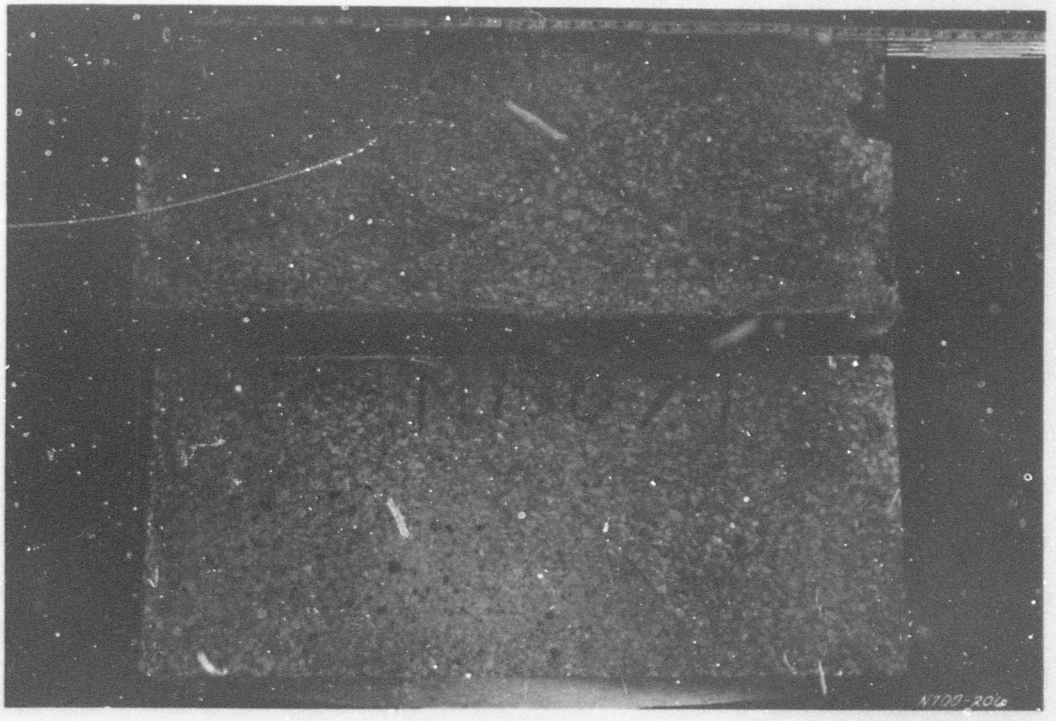

TEST 31

FIGURE 3-129

TEST 32

In Test 32 a scaled model of one of the Project Hercules test closures was loaded statically. This represented an attempt to correlate static and dynamic test data. The model geometry for Test 32 is shown in Figure 3-130.

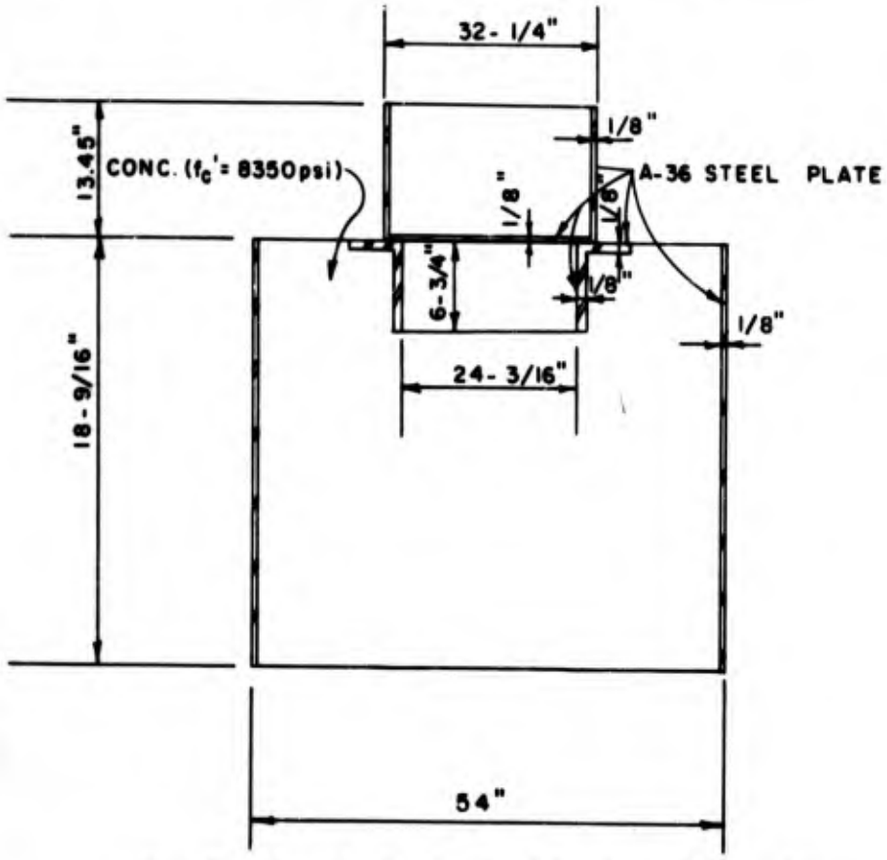

MODEL GEOMETRY FOR TEST 32 (HERCULES)

FIGURE 3-130

The closure model failed statically at 5330 psi (Figure 3-131) with no evidence of damage in the bearing structure. Pictures of the post-test closure are not available, but it is postulated that the failure was of the shear type and the high load capacity observed was due to the extremely large width of the bearing. Figure 3-133 shows the support at post-test inspection.

It has been hypothesized that the bearing strength of concrete may be expressed in terms of the unconfined concrete compressive strength and a linear function

of the confinement pressure available from the side shell of the steel. In this test the effective concrete bearing stress can be computed to be approximatly 11,000 psi, which implies that the confined bearing strength in this particular instance can be expressed as $\sigma_{concrete} = f'_c + 9.1\ \sigma_{conf.}$

This test indicates that significant reserve dynamic load capacity against the Hercules environment was present in the model from which the static specimen was scaled.

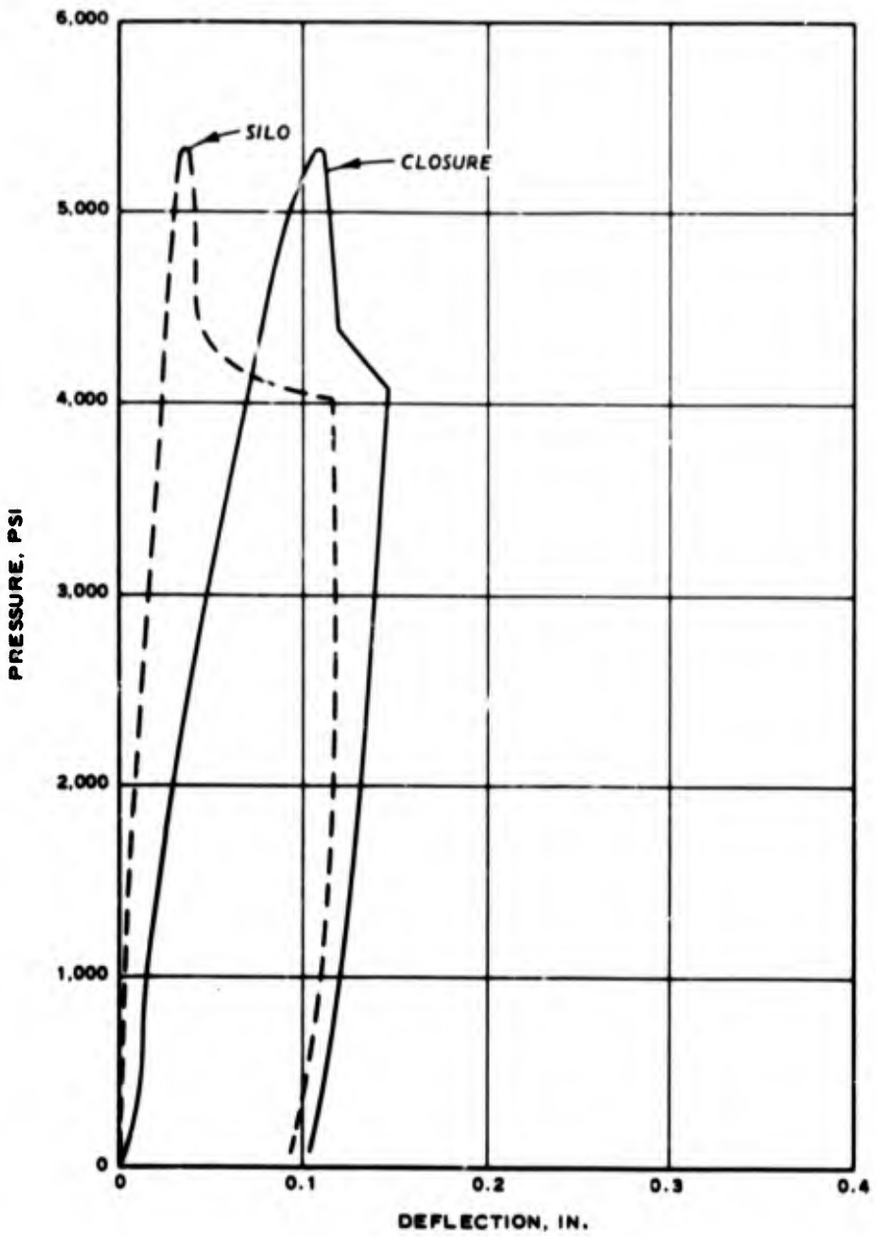

CLOSURE M130-9 AND SUPPORT M129-0 TEST 32 - PRESSURE VS. DEFLECTION

FIGURE 3-131

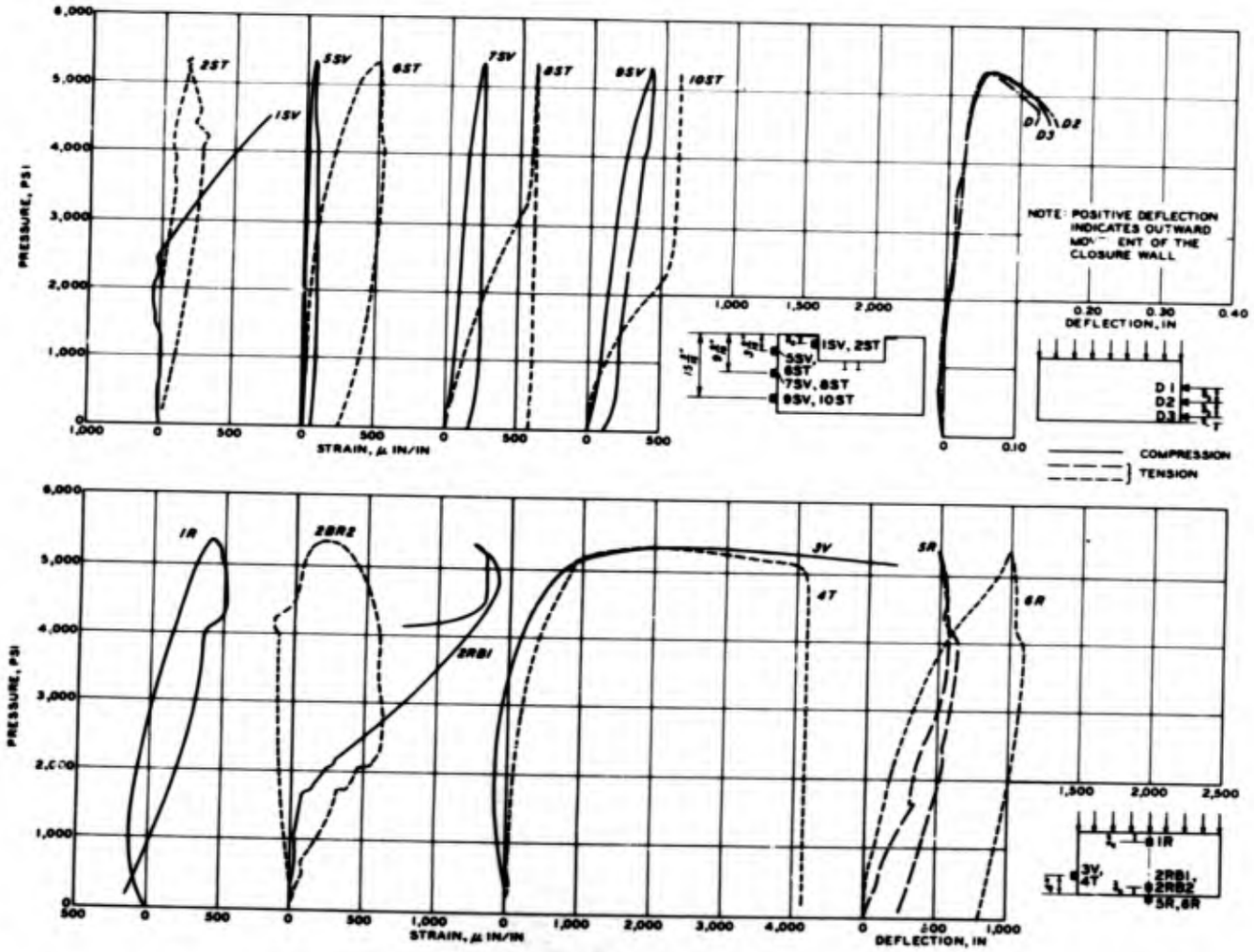

DATA PLOT - TEST 32

FIGURE 3-132

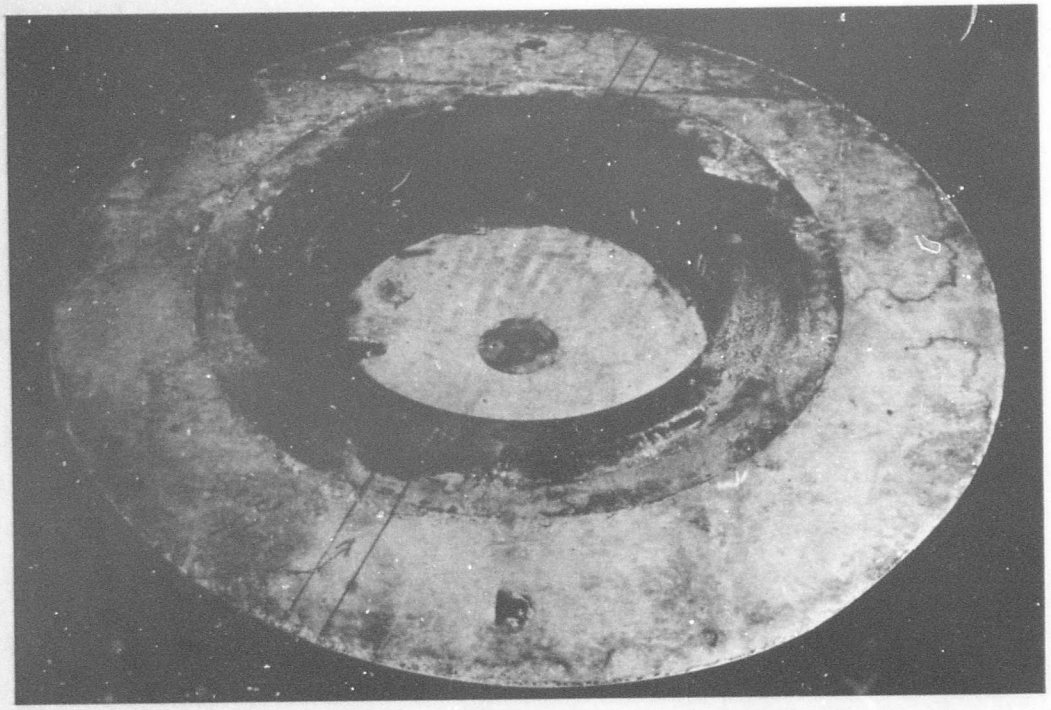

TEST 32

FIGURE 3-133

A2-166

TEST 33

In Test 33 a scaled model of the Rock Test I full size closure and support structure was loaded statically. This represented another attempt to correlate the static and dynamic test data. The model geometry is shown in Figure 3-134.

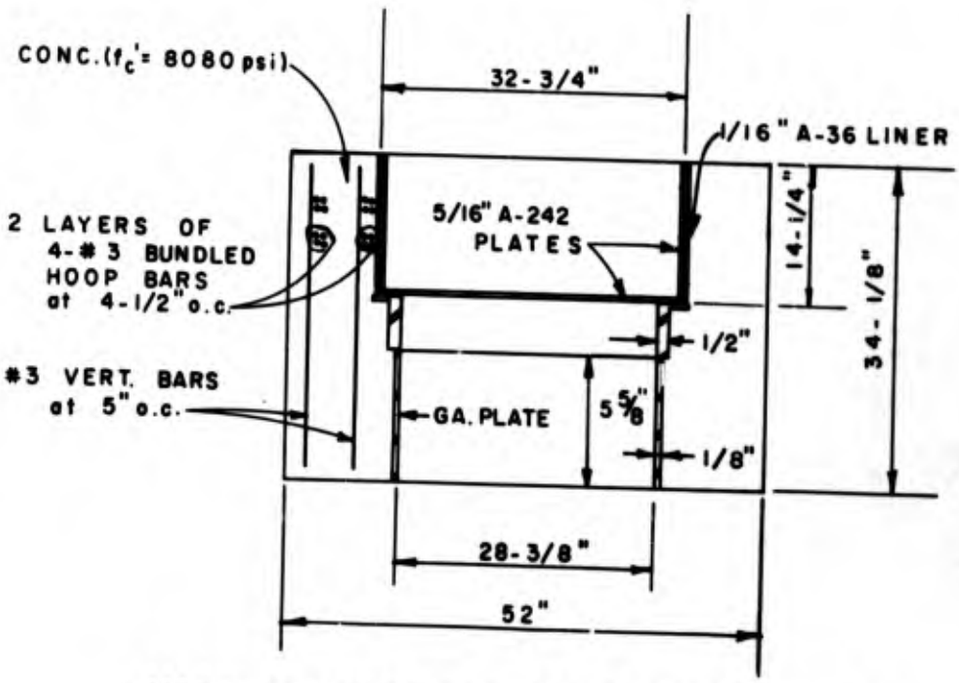

MODEL GEOMETRY FOR TEST 33 (ROCK TEST I)

FIGURE 3-134

The model failed at a static load of 4500 psi (Figure 3-135). The observed failure was in the support structure (see Figures 3-137 through 3-140). The dramatic failure of the silo support element is seen in Figure 3-137. The band of steel at the top of the silo model (on which the letter S is printed) is a 1/2-inch steel bar which provides a gasket seal area and serves no structural purpose.

The closure model was recessed into the silo support which probably accounts for the lack of radial cracking in the top support section (Figure 3-140); also, the silo support did not have enough ductility to cause the concrete to crack. As soon as it strained a small amount, the concrete spalled off the outer reinforcing bars and the test was terminated. While photographs of the closure model are not available, it would appear from the load/deflection curve that the closure was essentially undamaged.

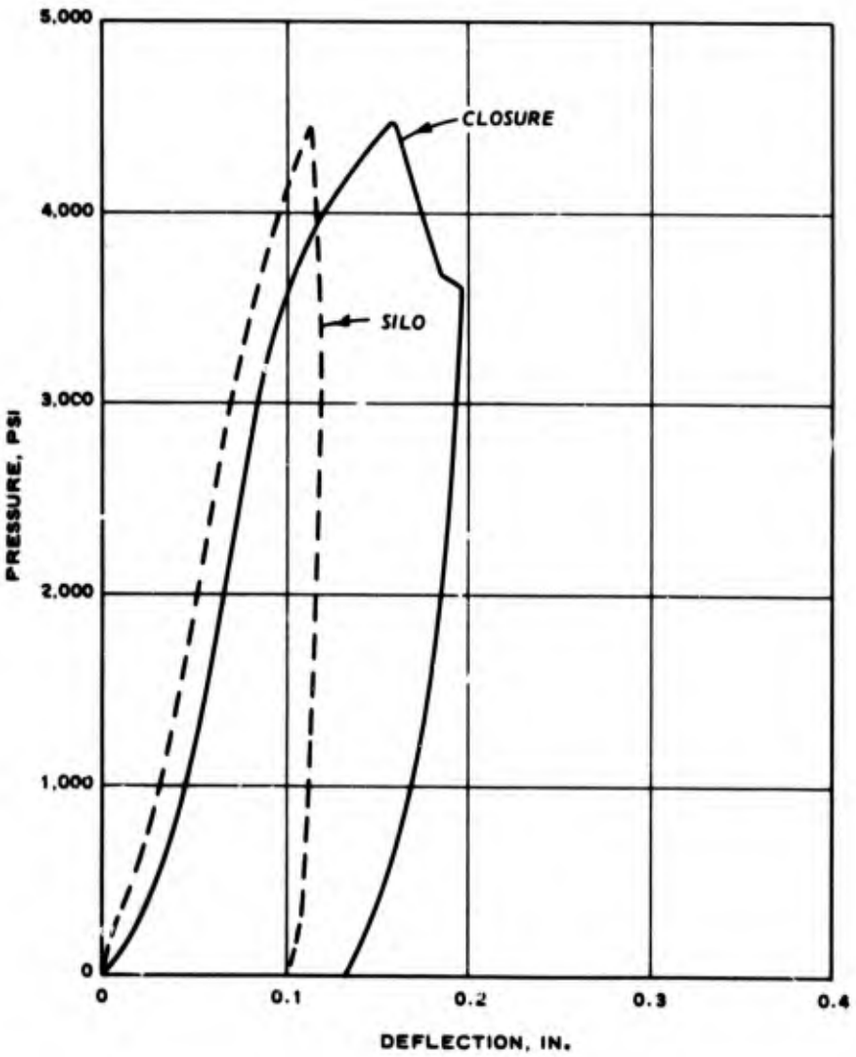

CLOSURE M130-6 AND SUPPORT M128-0 TEST 33 - PRESSURE VS. DEFLECTION

FIGURE 3-135

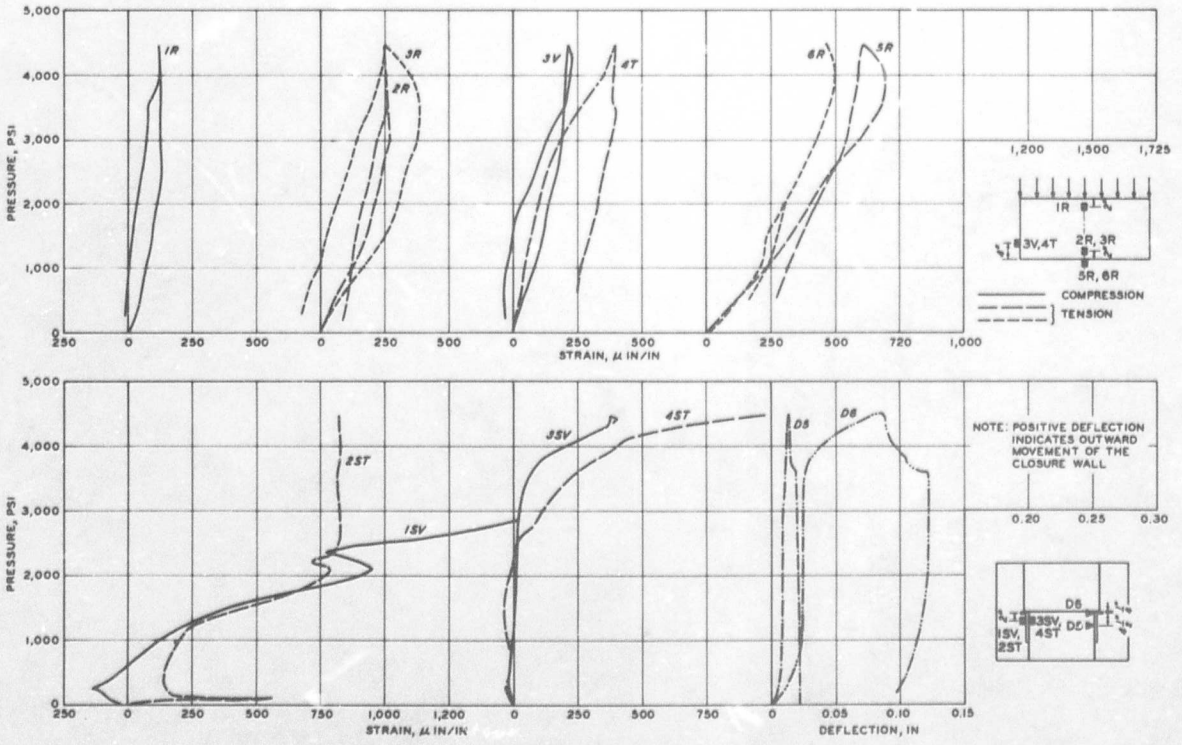

A2-169

DATA PLOT - TEST 33

FIGURE 3-136

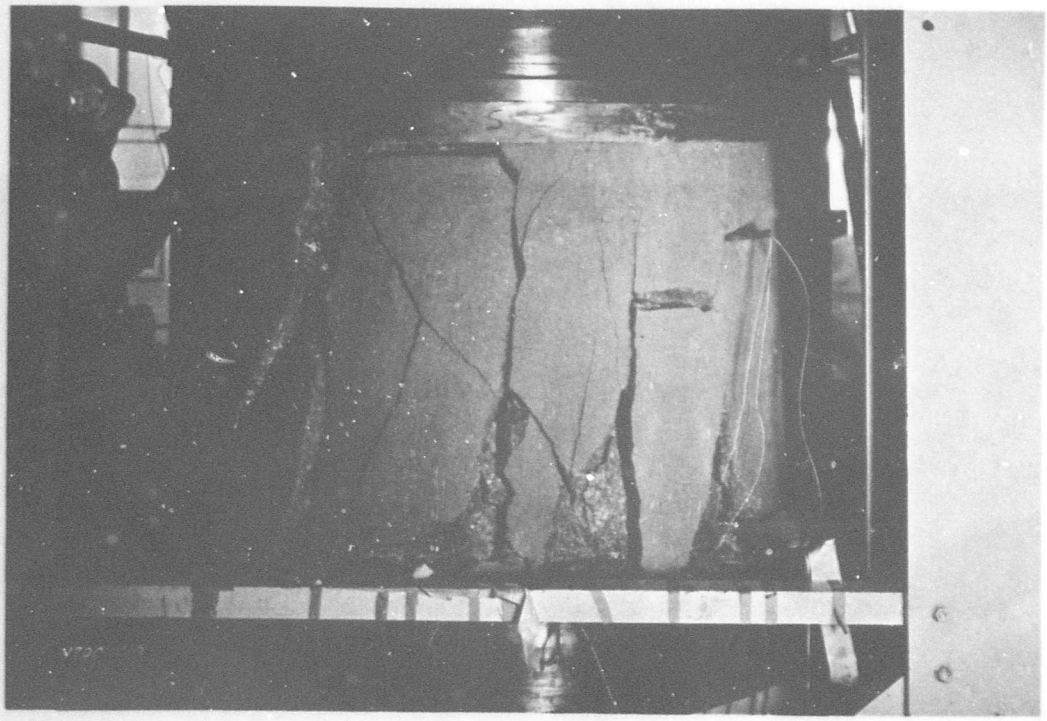

TEST 33

FIGURE 3-137

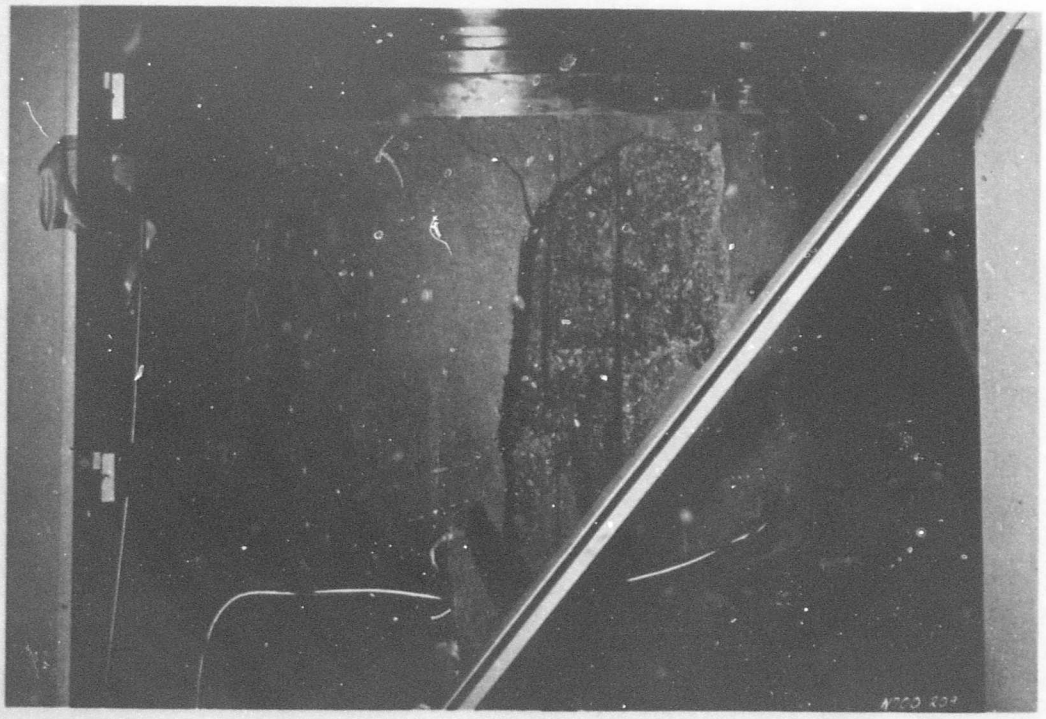

TEST 33

FIGURE 3-138

A2-170

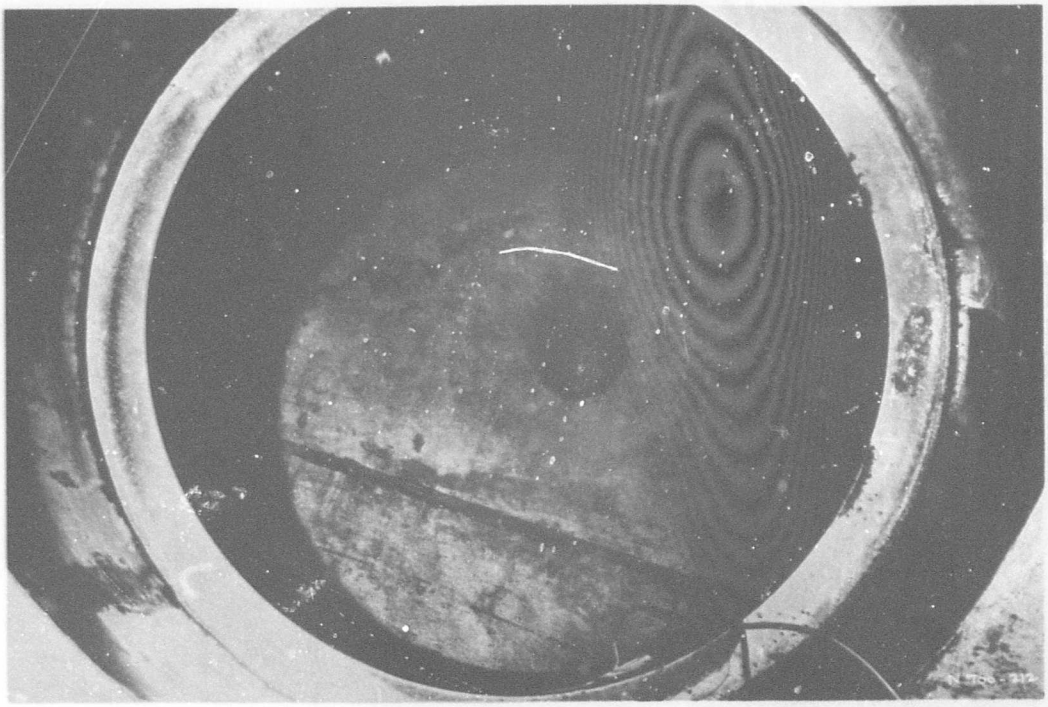

TEST 33

FIGURE 3-139

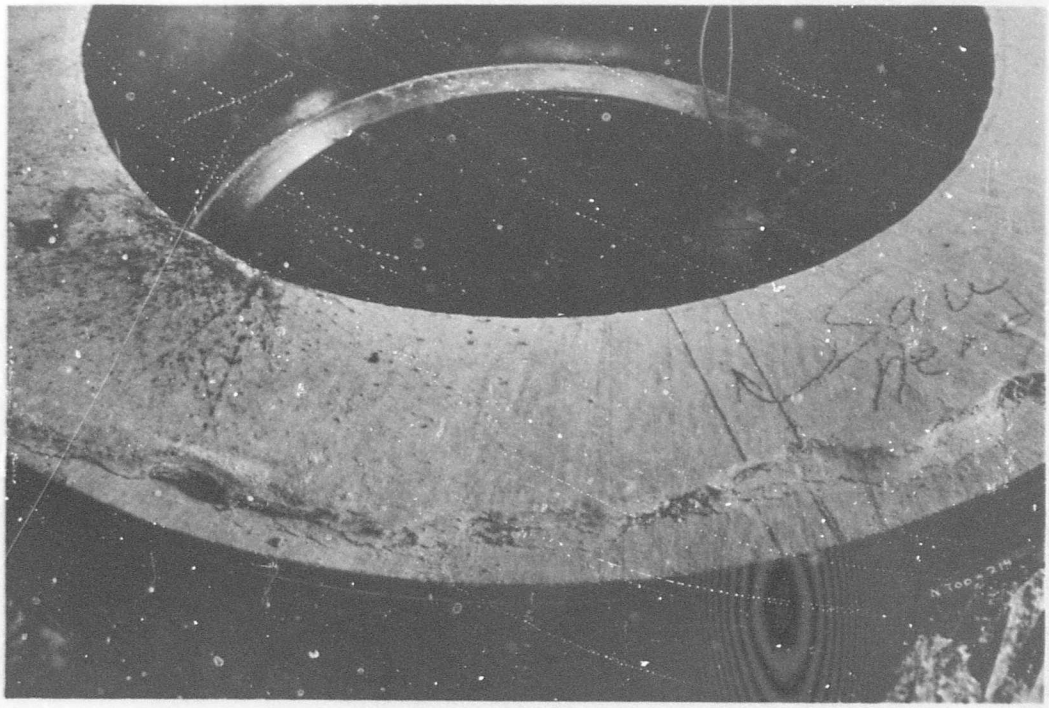

TEST 33

FIGURE 3-140

A2-171

TEST 34

In Test 34 a support with a narrow bearing was tested with a closure model identical to that used in Test 31. The test was intended to show the effect of bearing width on the total load capacity of the closure support structure. The model geometry for Test 34 is shown in Figure 3-141.

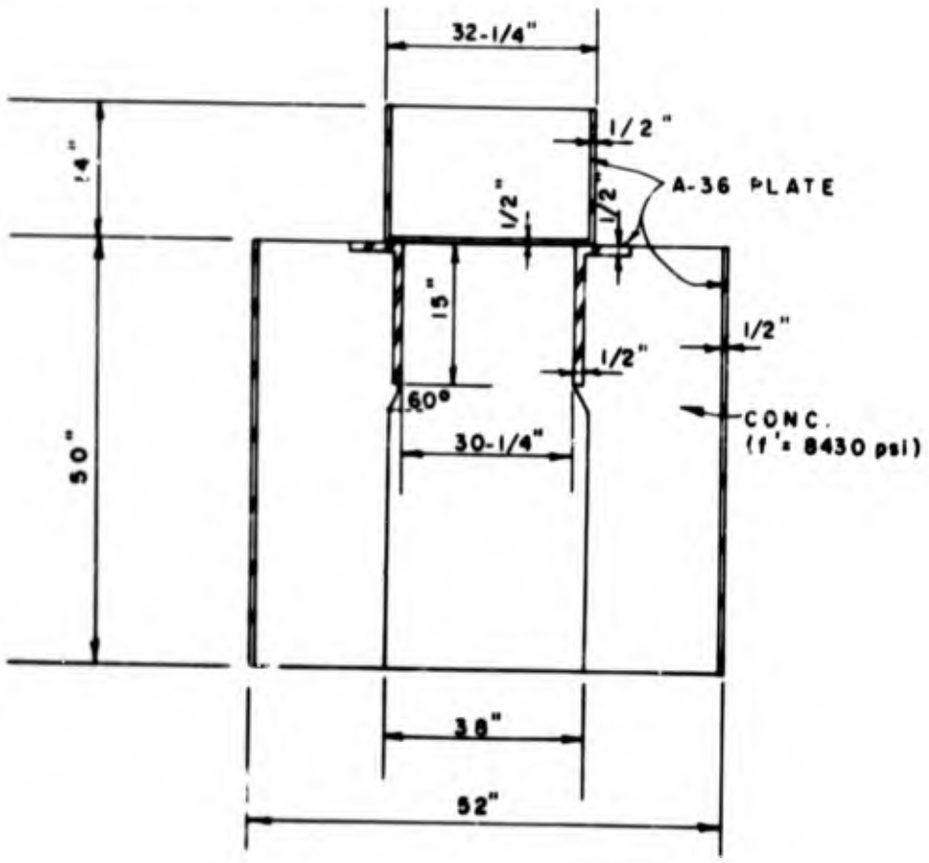

MODEL GEOMETRY FOR TEST 34

FIGURE 3-141

The collapse load for the system was 3860 psi (Figure 3-142). The failure occurred in the support structure due to excessive bearing load. Note the radial cracking and the indentation in the steel bearing ring caused by the closure bearing on the support (Figure 3-144). There was no apparent distress in the closure structure after the test.

Assuming that all the load is carried into the support structure by the confined concrete, the apparent bearing stress is computed to be approximately 30,000 psi. This implies that the confined concrete strength may be expressed as $\sigma_{concrete} = f'_c + 19.6\ \sigma_{conf.}$

In the other support structures in the second phase of the testing, failure was observed due to pure vertical shear at the haunch. This type of failure was observed in Test 31, thus no direct correlation can be made with this test.

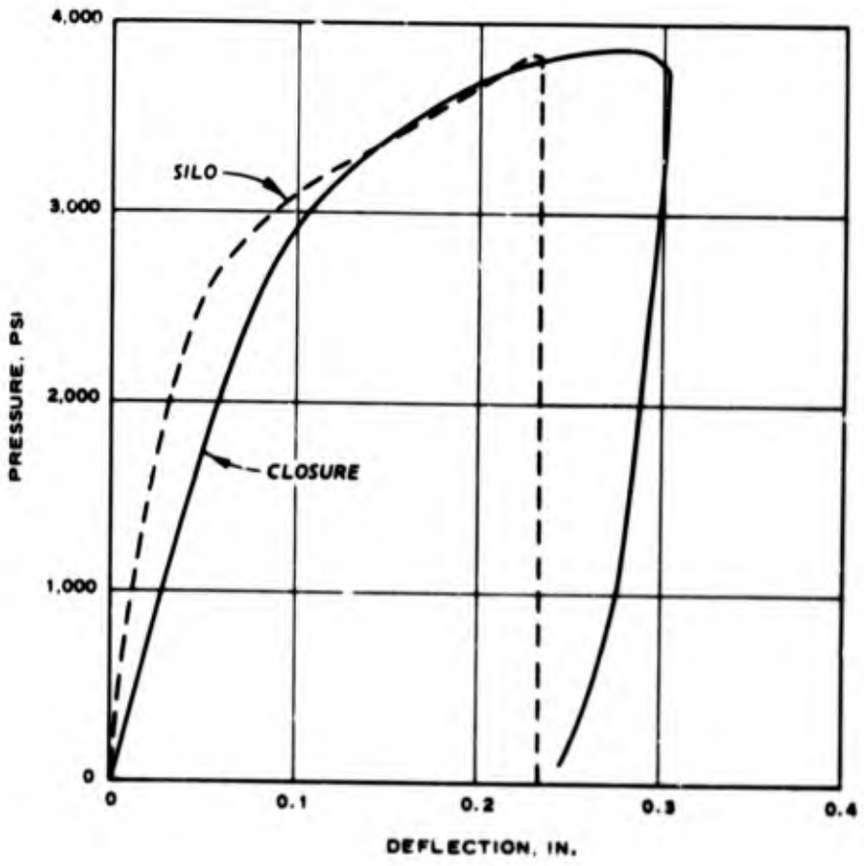

CLOSURE M130-7-2 AND SUPPORT M131-2 TEST 34 - PRESSURE VS. DEFLECTION

FIGURE 3-142

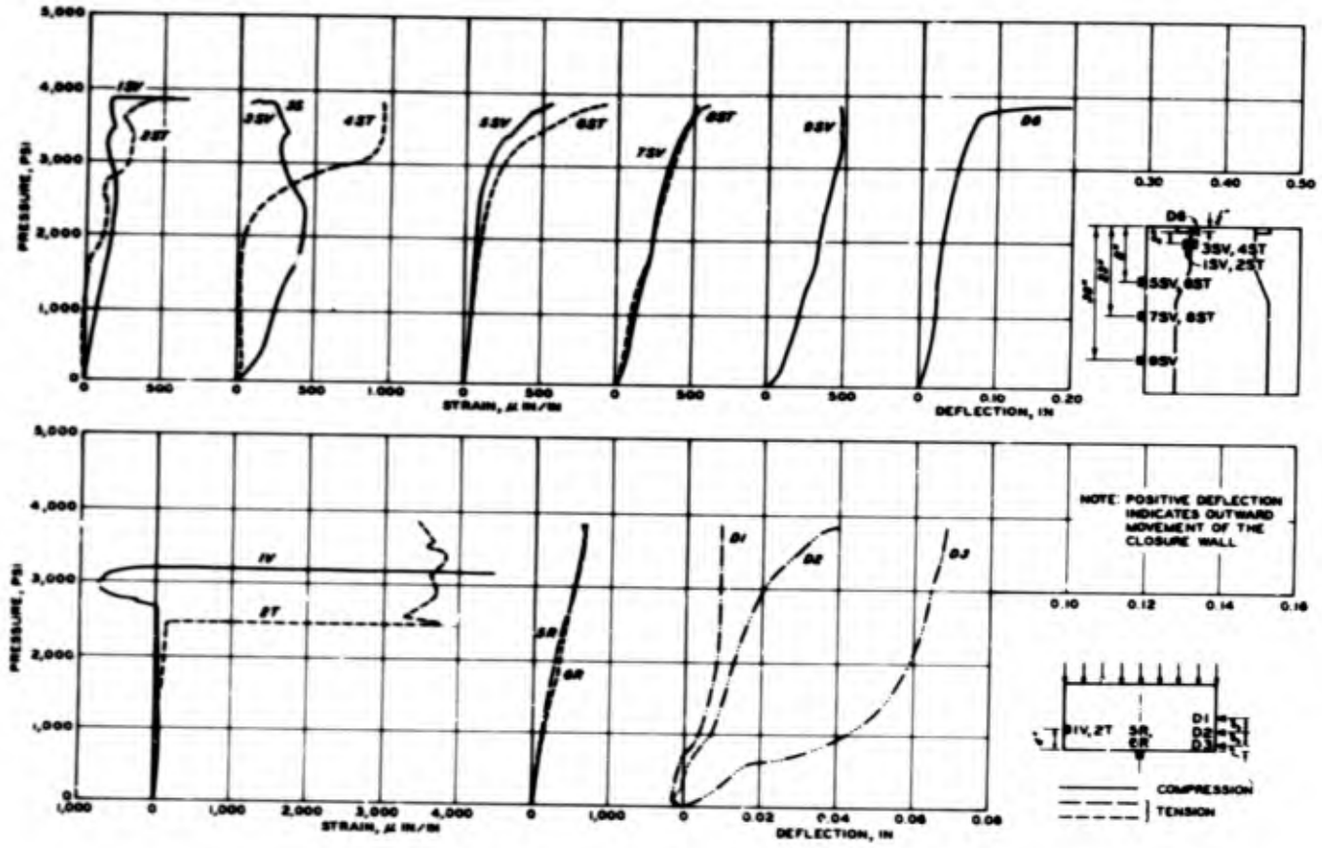

DATA PLOT - TEST 34

FIGURE 3-143

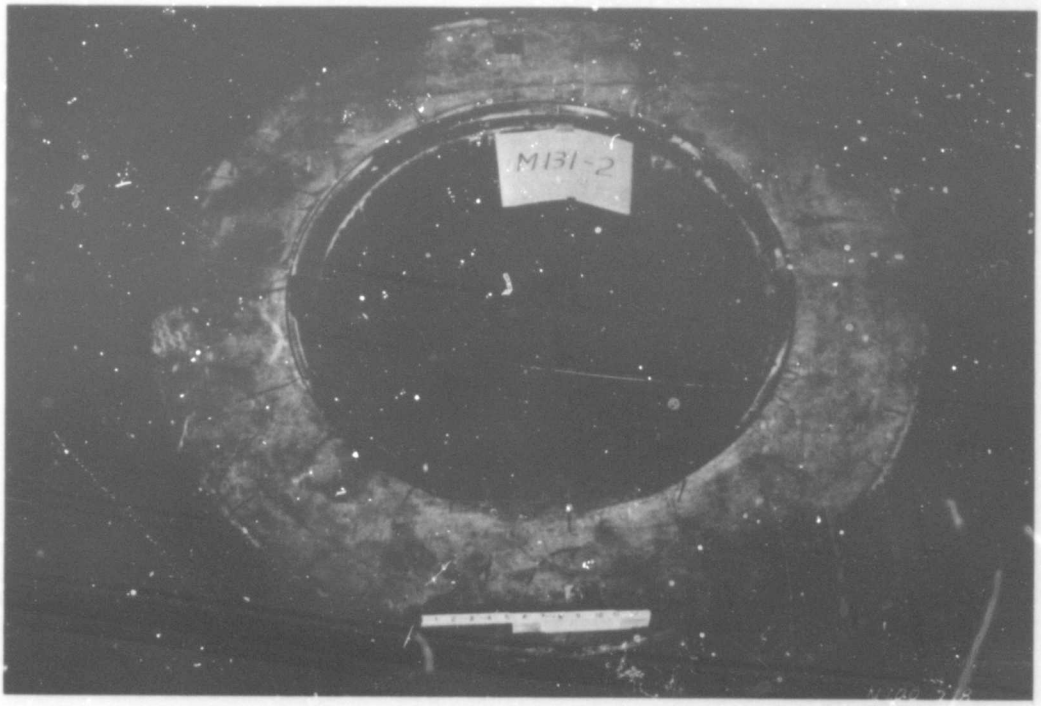

TEST 34

FIGURE 3-144

A2-175

TEST 35

In Test 35 a scaled model of a typical rise-and-rotate type (nonsymmetric) closure was tested. This test was performed in order to ascertain the increased load capacity of a nonsymmetrical structure. The model tested had a minimum outside diameter of 31 inches. The support structure had an outside diameter of 52 inches, which provided for a load as high as 6000 psi on top of the entire support and closure structure. Figure 3-145 shows the model geometry for Test 35.

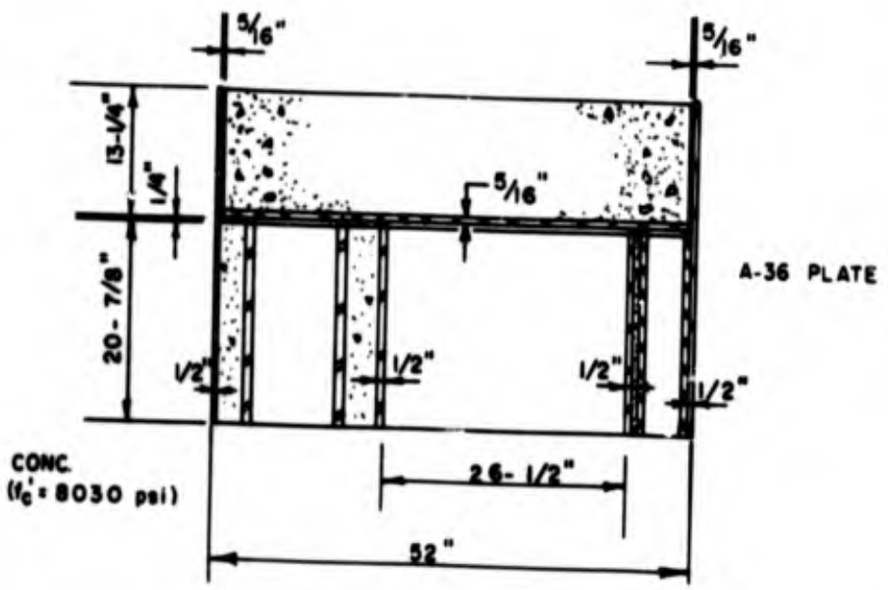

MODEL GEOMETRY FOR TEST 35 (RISE AND ROTATE)

FIGURE 3-145

The model failed at a static load of 5800 psi (Figure 3-146), illustrating the additional load capacity of a model with a large bearing area and large non-symmetical appurtenance. In Tests 3 and 4, similar symmetrical models with 1/4-inch plates were tested to ultimate load capacities on the order of 3500 psi.

The model was not sawed in half after the test was completed, and therefore the exact mode of failure is not known. However, in light of the test results, further testing of nonsymmetric closures appears feasible.

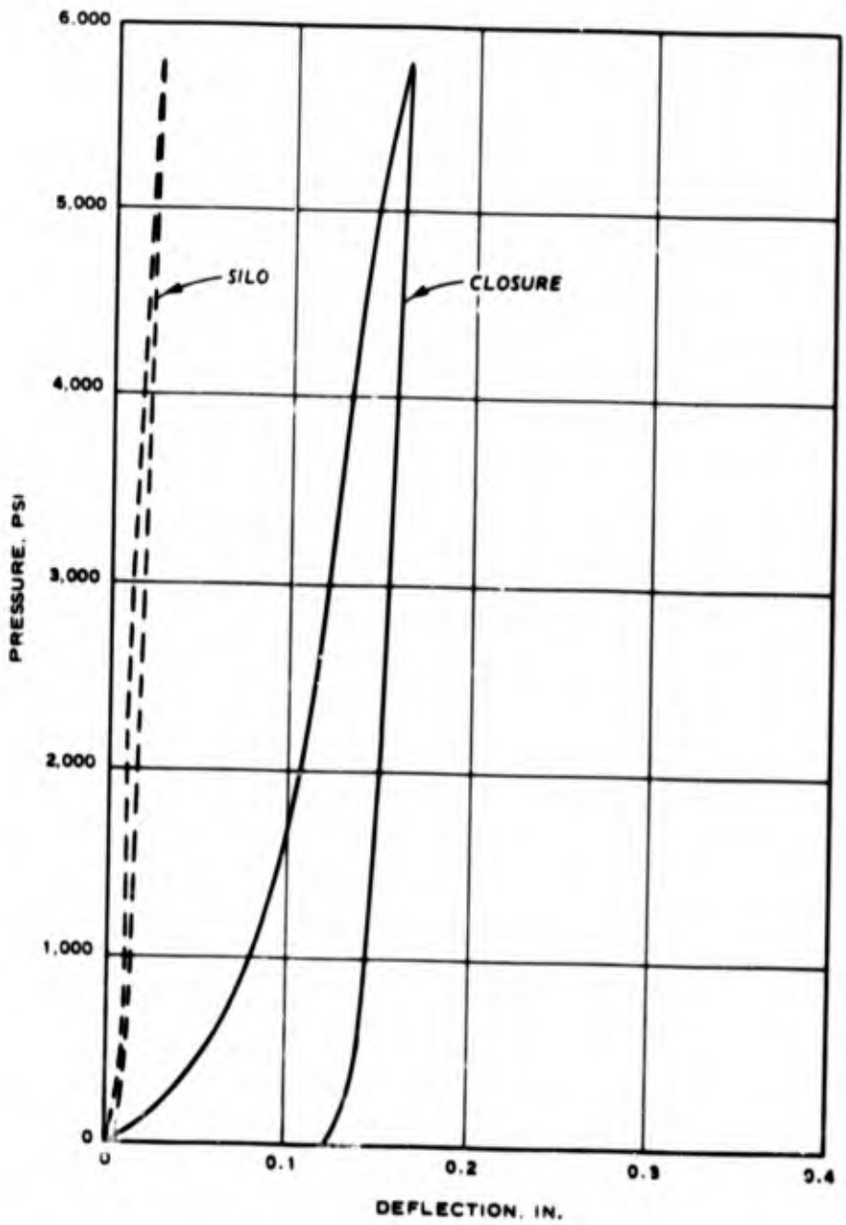

CLOSURE AND SUPPORT M127-0 TEST 35 - PRESSURE VS. DEFLECTION

FIGURE 3-146

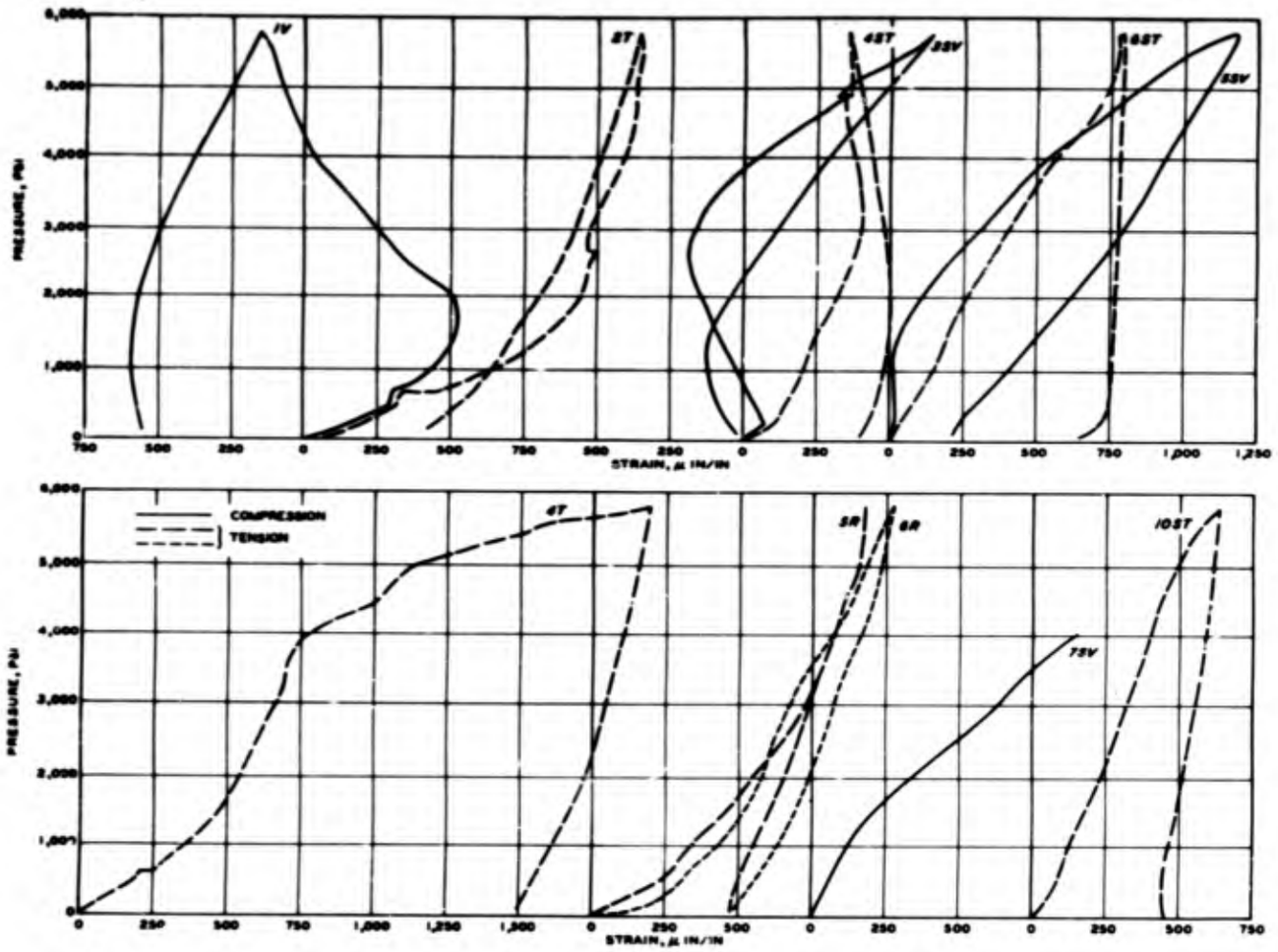

DATA PLOT - TEST 35

FIGURE 3-147

TEST 36

In Test 36 a support with a notched bearing was tested with a closure model identical to that used in several previous tests. The support was identical to that for Test 37 except that a notch, fitting the closure structure, was machined into the bearing ring. The theory was that the locking of the closure and support structure would enhance the load carrying capability of both elements. The model geometry for Test 36 in shown in Figure 3-148.

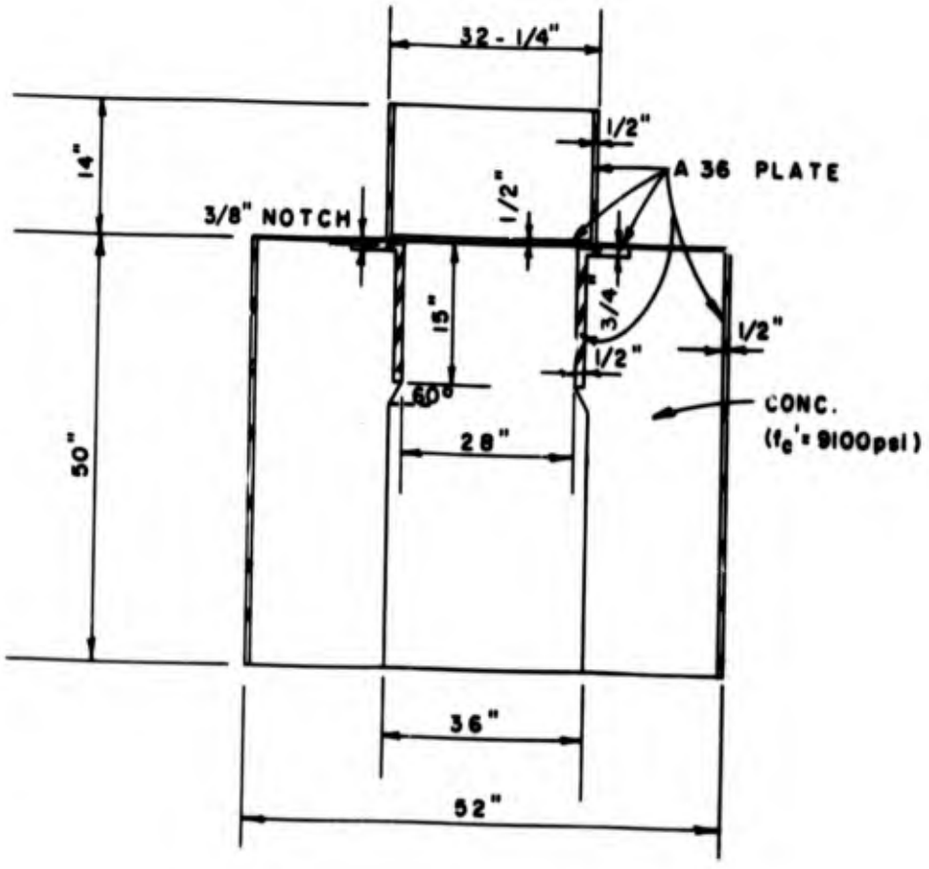

MODEL GEOMETRY FOR TEST 36

FIGURE 3-148

As shown in the pressure deflection curves (Figure 3-149), the collapse load for the system was 5293 psi, which was lower than the 6375 psi observed in Test 8. The collapse load and failure mode were nearly identical to that observed in Test 37 with the inclined bearing. The ring can be seen in Figure 3-150. In Figure 3-151, note the essentially uniform circumferential crack at the beginning of the haunched section.

Results of this test and Test 37 demonstrate that the locking effect has not been conclusively determined due to the premature failure of the support. The closure model in both tests survived essentially undamaged.

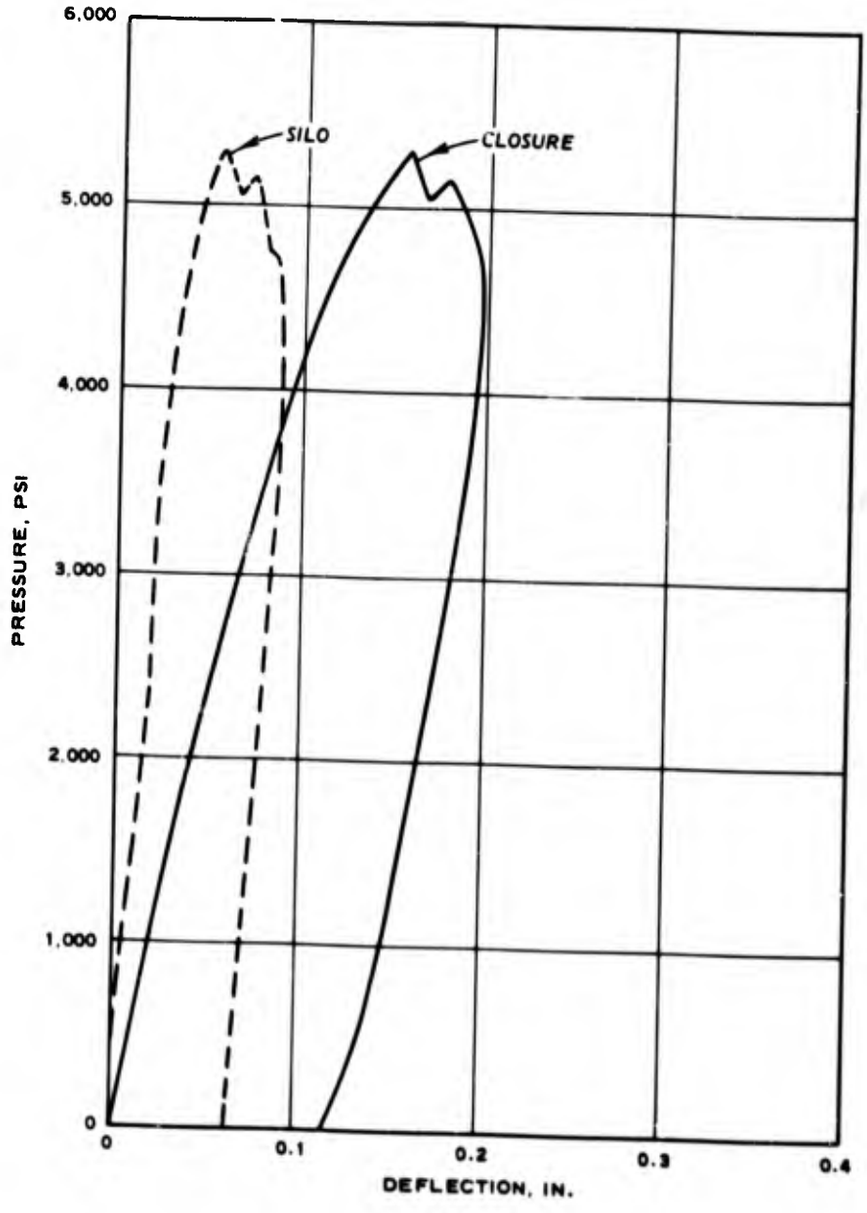

CLOSURE M130-10 AND SUPPORT M131-4 TEST 36 - PRESSURE VS. DEFLECTION

FIGURE 3-149

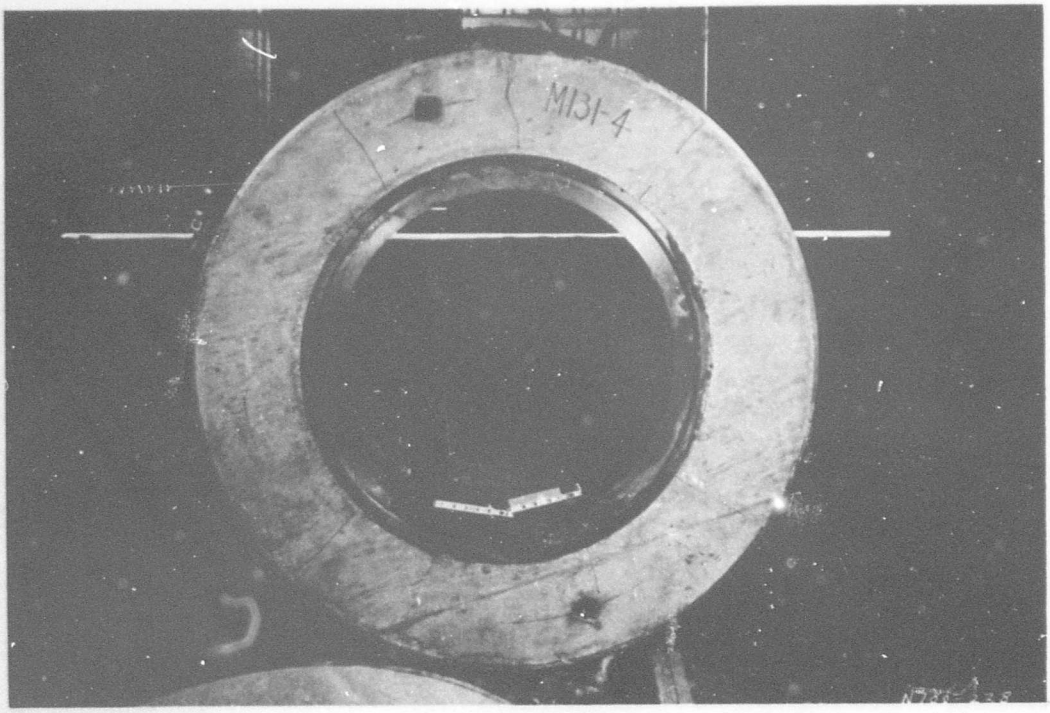

TEST 36

FIGURE 3-150

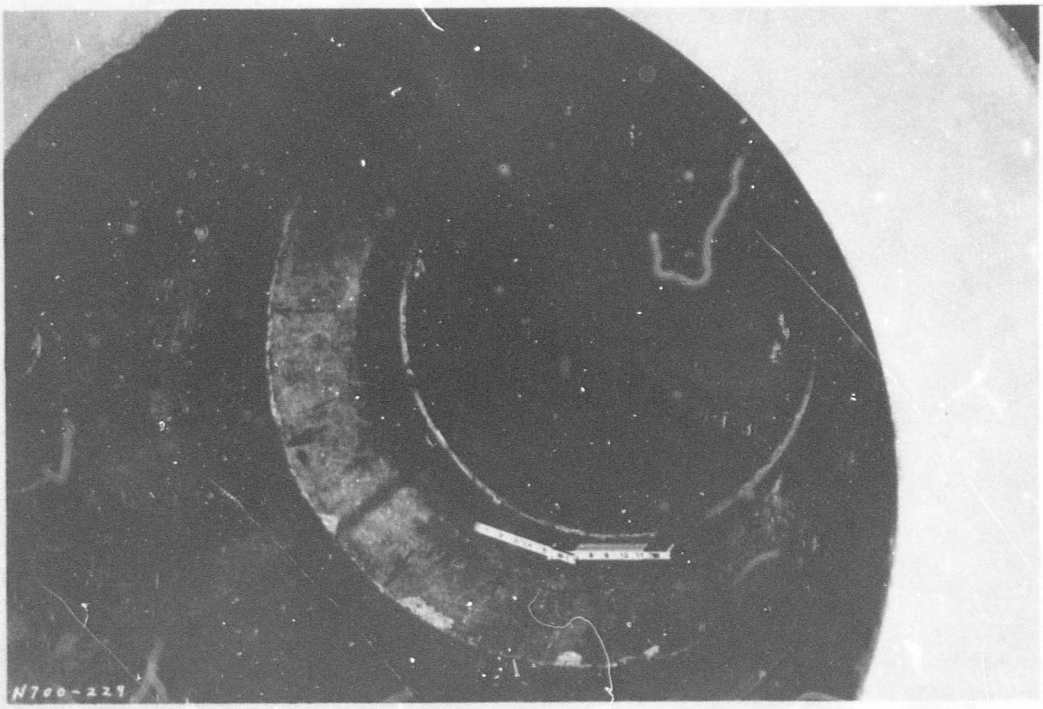

TEST 36

FIGURE 3-151

TEST 37

In Test 37 a support with an inclined bearing was tested with a closure model identical to that used in several previous tests. The test was intended to examine closure/support interaction phenomena. It was proposed that, if the stress concentration caused by the abrupt discontinuity at the inside of the bearing could be eliminated, the total load capacity of the closure structure would be enhanced.

It was anticipated that, by sloping the bearing to allow the model to rotate without concentrated bearing, the stress concentration that occurs at the edge of the bearing would be relieved. It was also expected that this type of support would provide for considerable locking between the closure and the support. The model geometry for Test 37 is shown in Figure 3-152.

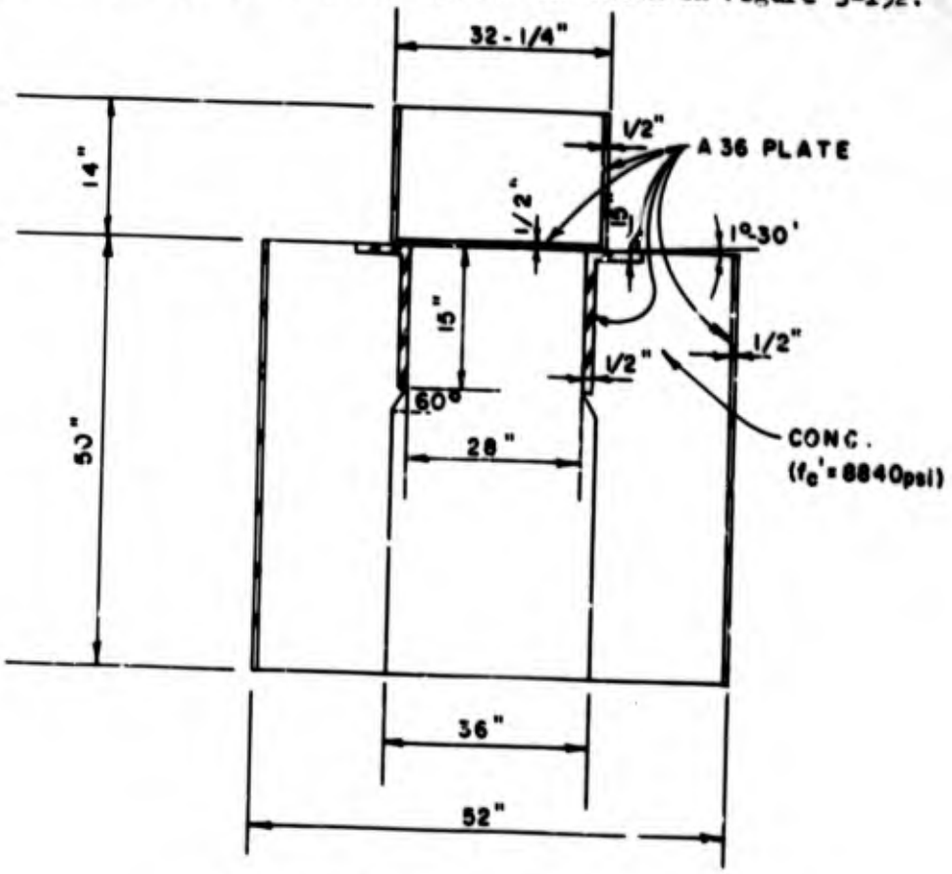

MODEL GEOMETRY FOR TEST 37

FIGURE 3-152

The ultimate load capacity for this system was 5300 psi, as indicated on the deflection curves (Figure 3-153). This was lower than the 6375 psi observed in Test 8 for a similar structure without the inclined bearing. Therefore, it is doubtful that an inclined bearing would offer any particular advantages.

In Figure 3-154 the machined area defined on the model geometry sketch (Figure 3-152) can be seen. This is not an indentation caused by the closure bearing but the actual machining that sloped the bearing ring. Figure 3-155 is a view looking upward toward the beginning of the haunch. Note the uniform crack where the haunch section was failed.

On the basis of the available shear area and the total load applied, the pure shear strength is approximately 0.21 f_c', which compares very well with the value of 0.20 f_c' established in the literature.

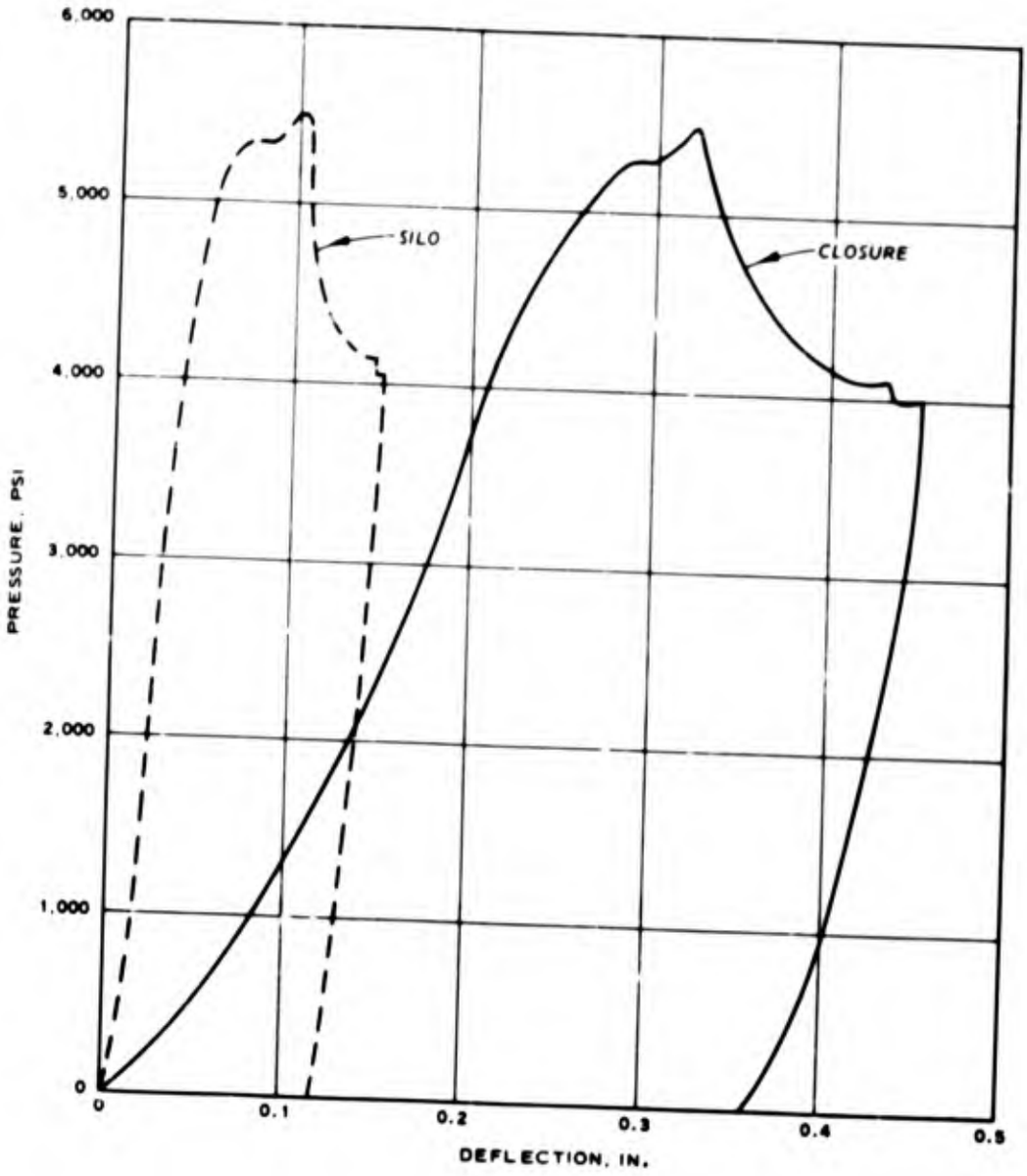

CLOSURE M130-7-3 AND SUPPORT M131-3 TEST 37 - PRESSURE VS. DEFLECTION

FIGURE 3-153

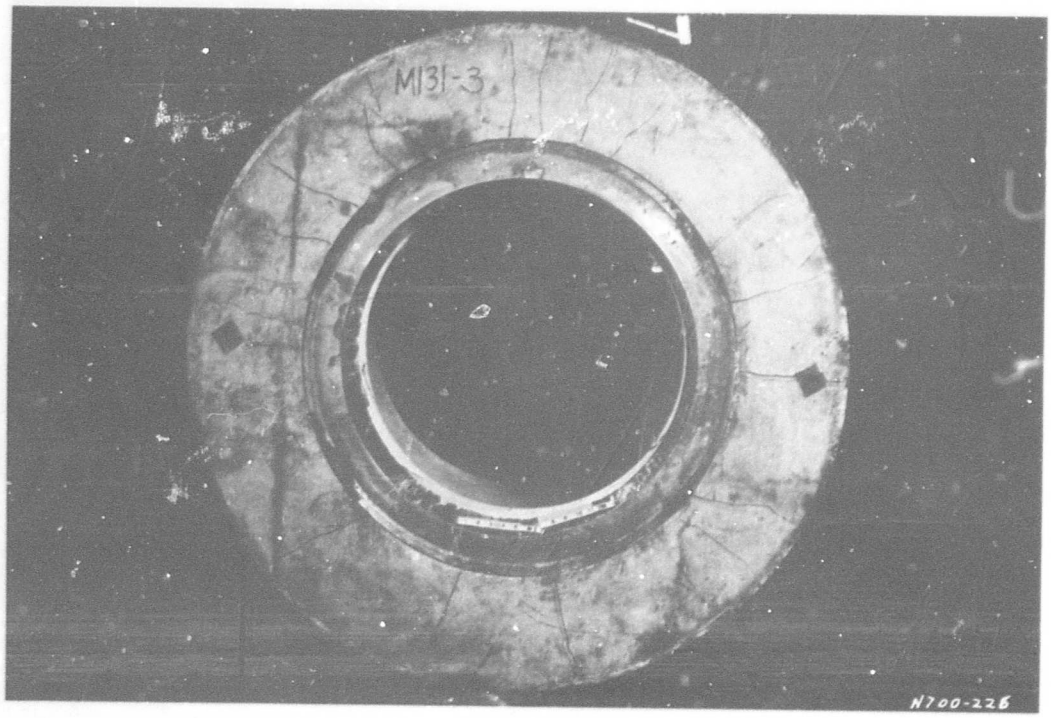

TEST 37

FIGURE 3-154

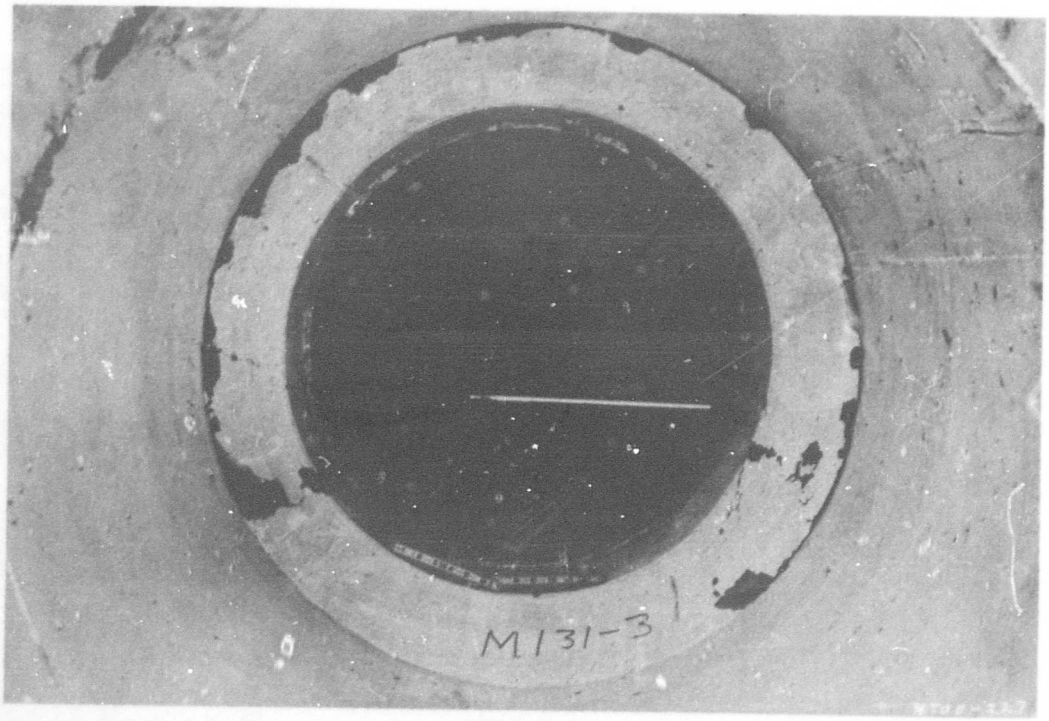

TEST 37

FIGURE 3-155

TEST 38

In Test 38 a high strength closure/closure support combination was tested. The models were designed to provide an indication of the feasibility limit for this type of structure. The model geometry for Test 38 is shown in Figure 3-156.

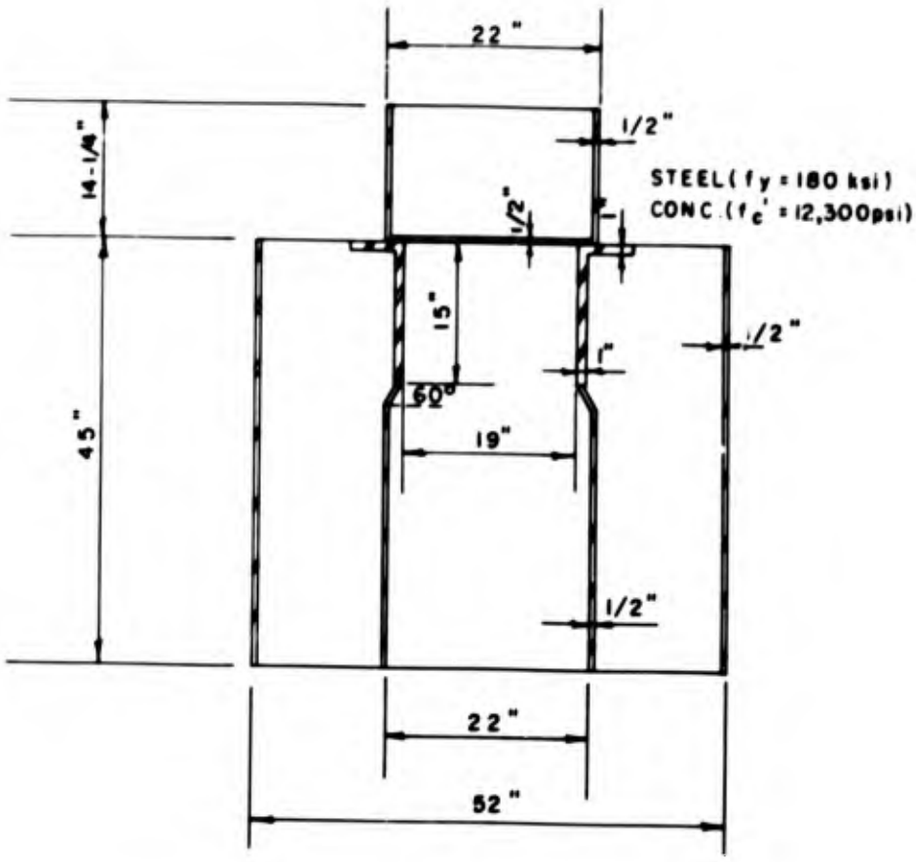

MODEL GEOMETRY FOR TEST 38

FIGURE 3-156

The test specimen attained a load capacity of 23,000 psi (Figure 3-157) and failed in an interesting manner. A crack initiated at the weld between the bottom plate and the side shell and propagated up the side shell, releasing stored energy rapidly. Figure 3-158 shows the torn section in the side of the shell and the failed weld area. This damage did not occur during the

test, but took place during the unloading cycle. The extent of the failed weld area is evident in Figure 3-159, and characteristics indicate a brittle failure. It should be pointed out that during the entire testing sequence this type of failure was apparent in only two models (Test 38 and Test 39).

The burnished area in the concrete that can be seen in Figure 3-160 is indicative of the high bearing stresses. The ratio of the load carried vertically by the 1/2-inch silo liner is insignificant compared with that carried by the concrete. No particular damage was evident in the support structure at the time of post-test inspection (Figures 3-161 and 3-162).

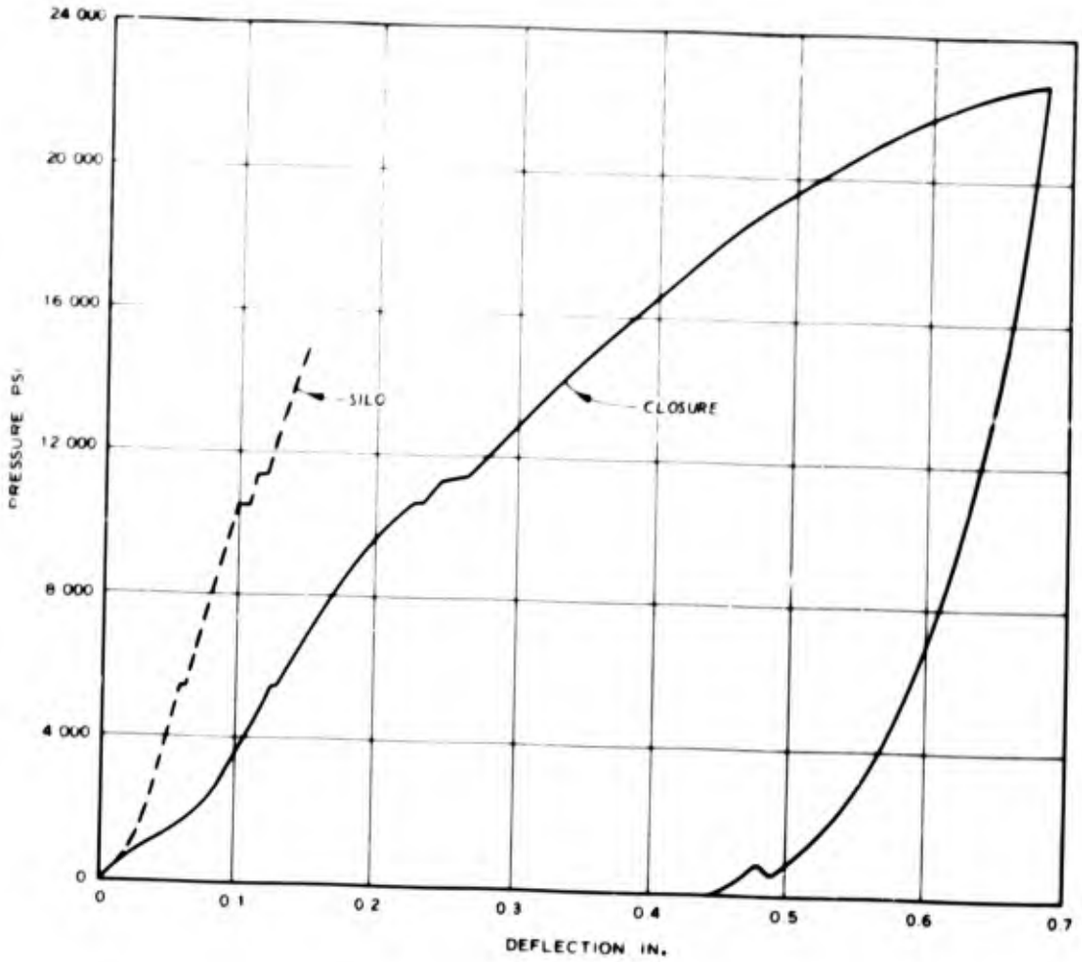

CLOSURE M130-11 AND SUPPORT M131-7 TEST 38 - PRESSURE VS. DEFLECTION

FIGURE 3-157

TEST 38

FIGURE 3-158

TEST 38

FIGURE 3-159

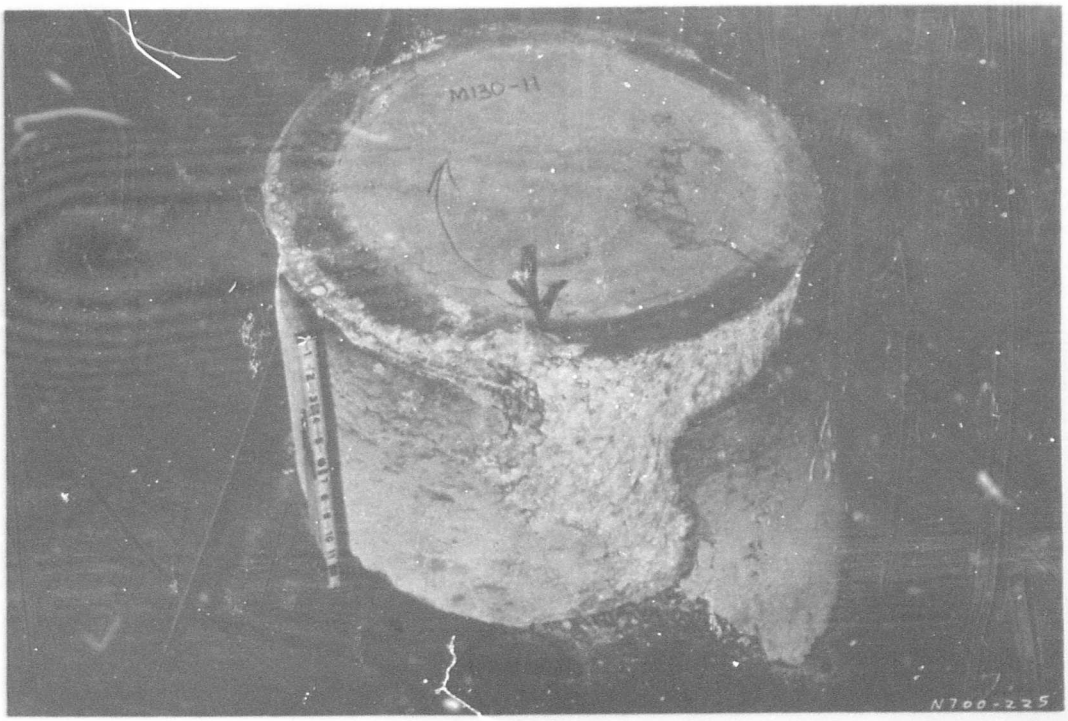

TEST 38

FIGURE 3-160

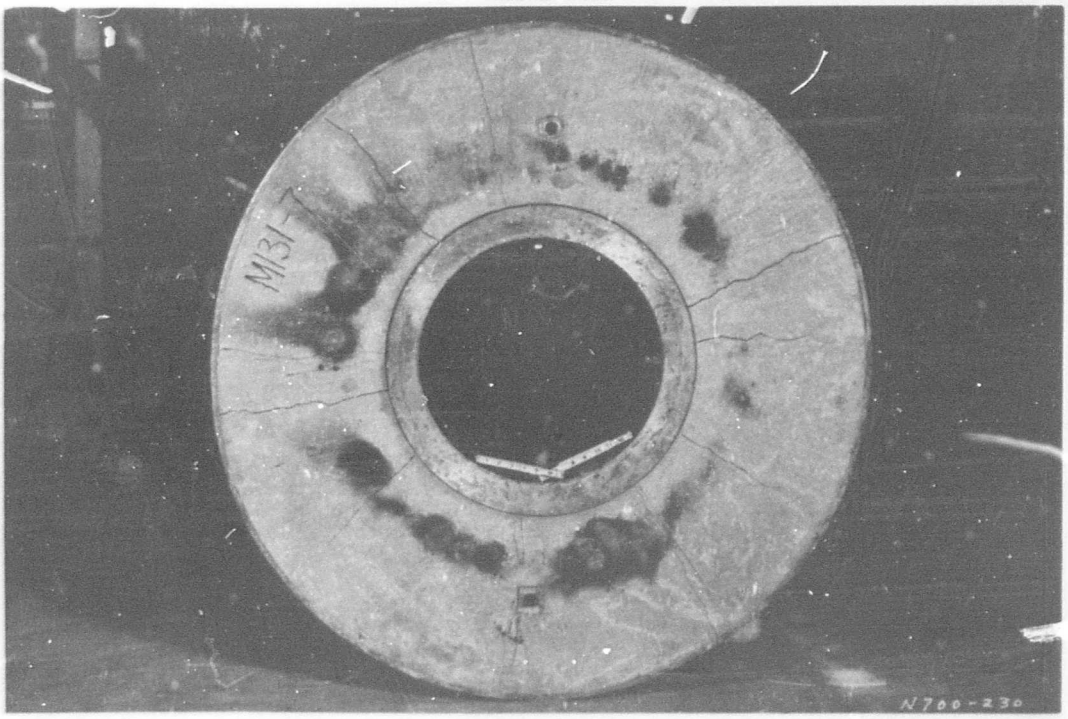

TEST 38

FIGURE 3-161

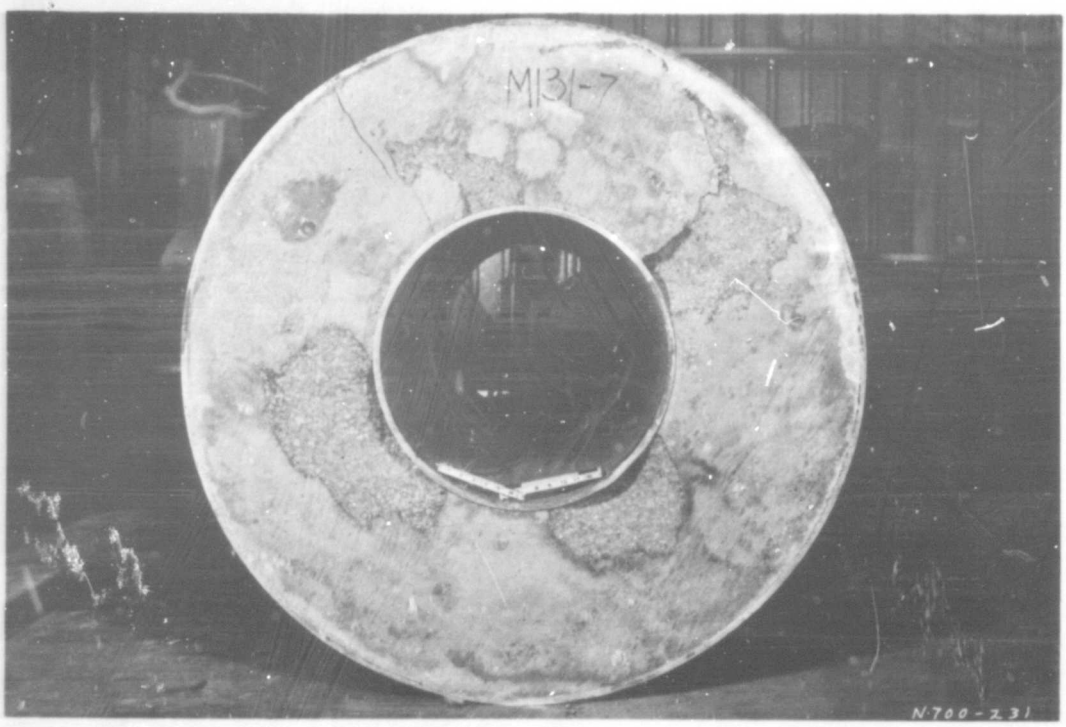

TEST 38

FIGURE 3-162
A2-192

TEST 39

In Test 39 the models were designed to illustrate the feasibility of relatively high load capacity closure structures. The model geometry for this test is shown in Figure 3-163.

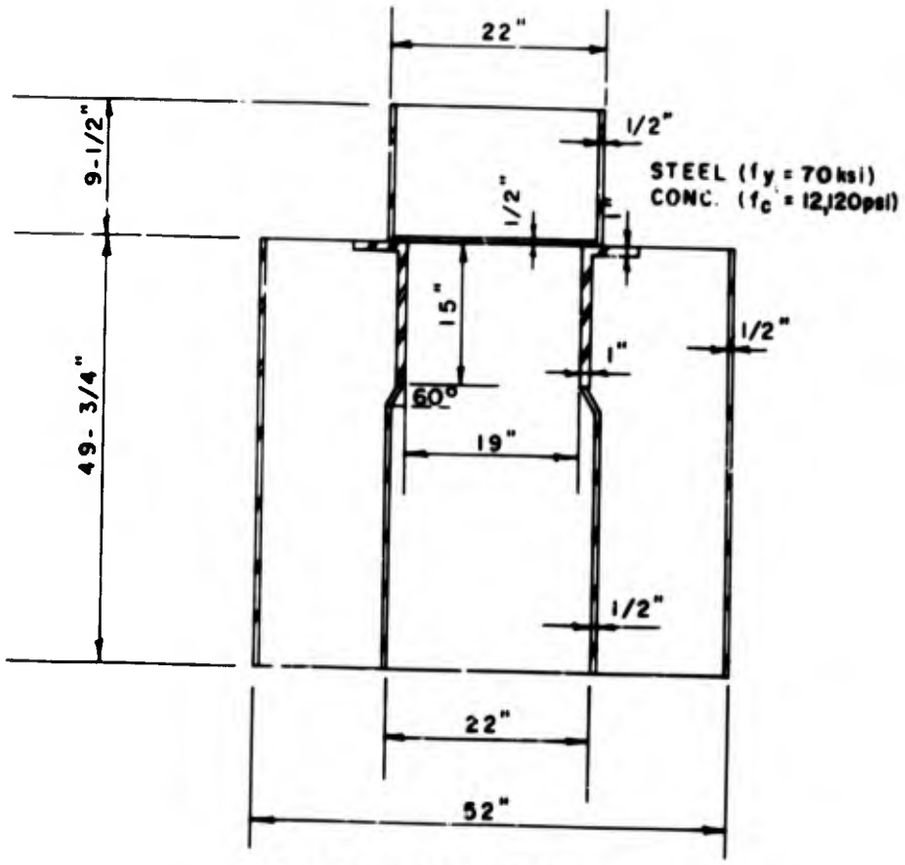

MODEL GEOMETRY FOR TEST 39

FIGURE 3-163

The specimen failed at 15,789 psi (Figure 3-164) due to a weld failure between the closure bottom plate and the side shell which can be attributed to the lack of ductility evidenced in the steel. Weld failure was experienced on only one other occasion (Test 38).

The cracked weld that led to the failure can be seen in Figure 3-165; in Figure 3-166, the cracking of the concrete inside the steel shell is evident. At the start of the tests, the concrete was level with the steel sides of the

surface; at the conclusion of the test, this amount of unrecovered deformation remained. The concrete was permanently compressed and was never recovered. The crack that is visible near the edge of the concrete in the closure model occurred above the failed surface.

It has been postulated that the bearing strength of the concrete may be expressed in terms of the unconfined concrete compressive strength and a linear function of the confinement pressure available from the side steel shell. In this particular test, calculations indicate that the effective concrete bearing stress was approximately 42,000 psi, which implies that the confined bearing strength in this case can be expressed as $\sigma_{conc.} = f'_c + 9.2\ \sigma_{conf.}$

Figure 3-166 shows the indentation in the concrete surface of the silo support which is caused by high bearing stresses. Although some distress was noted in the concrete of the silo, the support structure was adequately performing its function. The test illustrated the feasibility of designing a closure structure to withstand extremely high pressures.

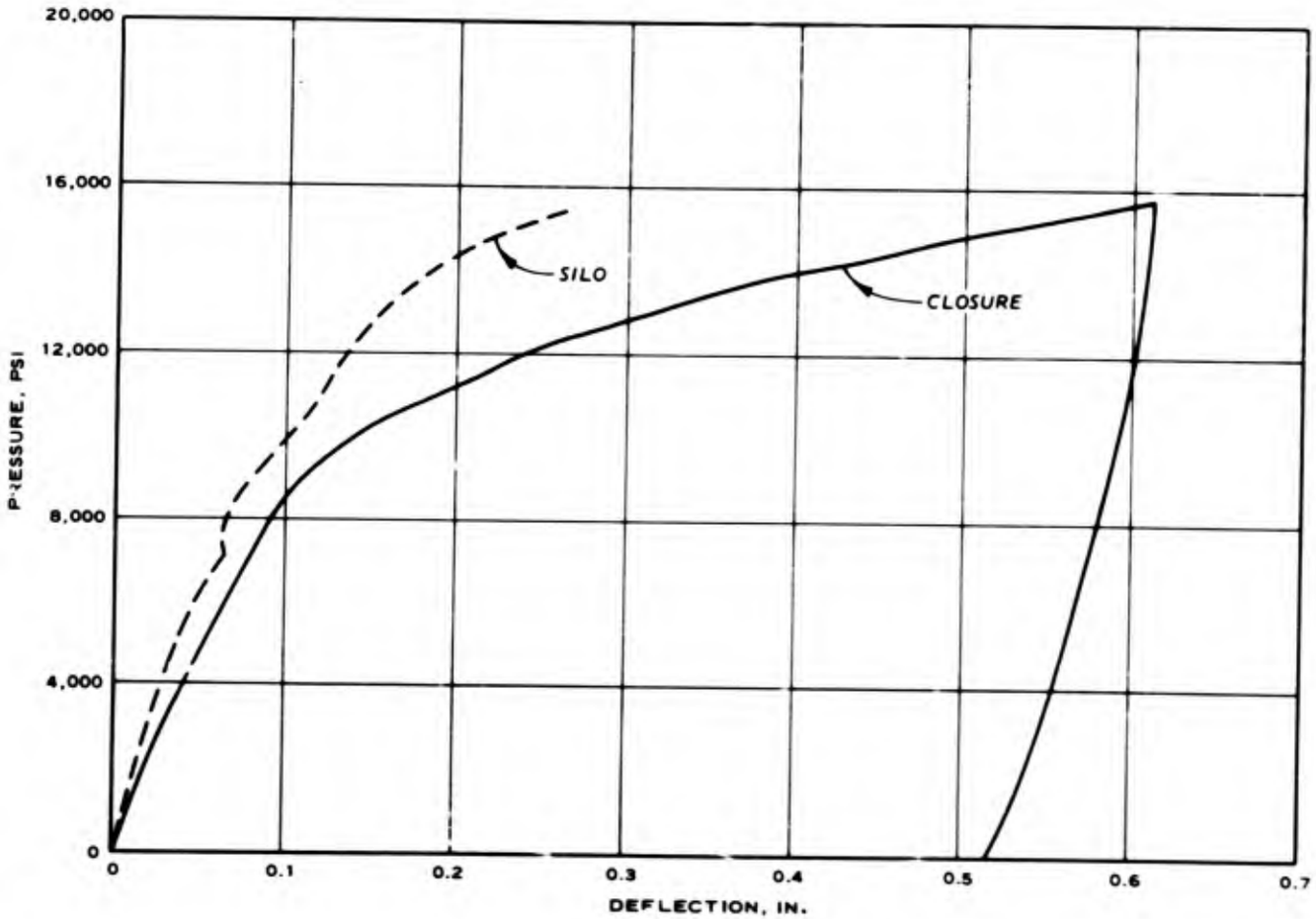

CLOSURE M130-12 AND SUPPORT M131-6 TEST 39 - PRESSURE VS. DEFLECTION

FIGURE 3-164

TEST 39

FIGURE 3-165

A2-196

TEST 39

FIGURE 3-166

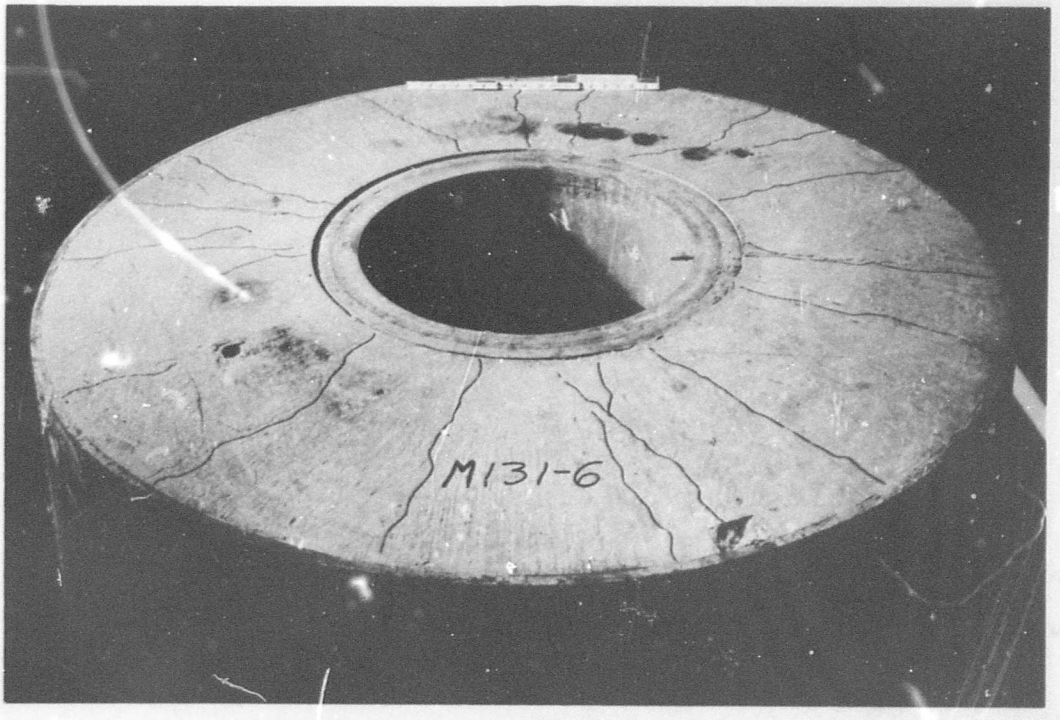

TEST 39

FIGURE 3-167

TEST 40

In Test 40 a support structure with a 1/4-inch-thick outer confinement shell was tested with a closure model identical to that used in several previous tests. A support structure that geometrically resembled those of Tests 31, 34, 36, and 37 was selected. It was anticipated that with the reduced thickness of the confinement steel the load capacity would be lower, which would be consistent with the results observed in previous support testing. The model geometry for Test 40 is shown in Figure 3-168.

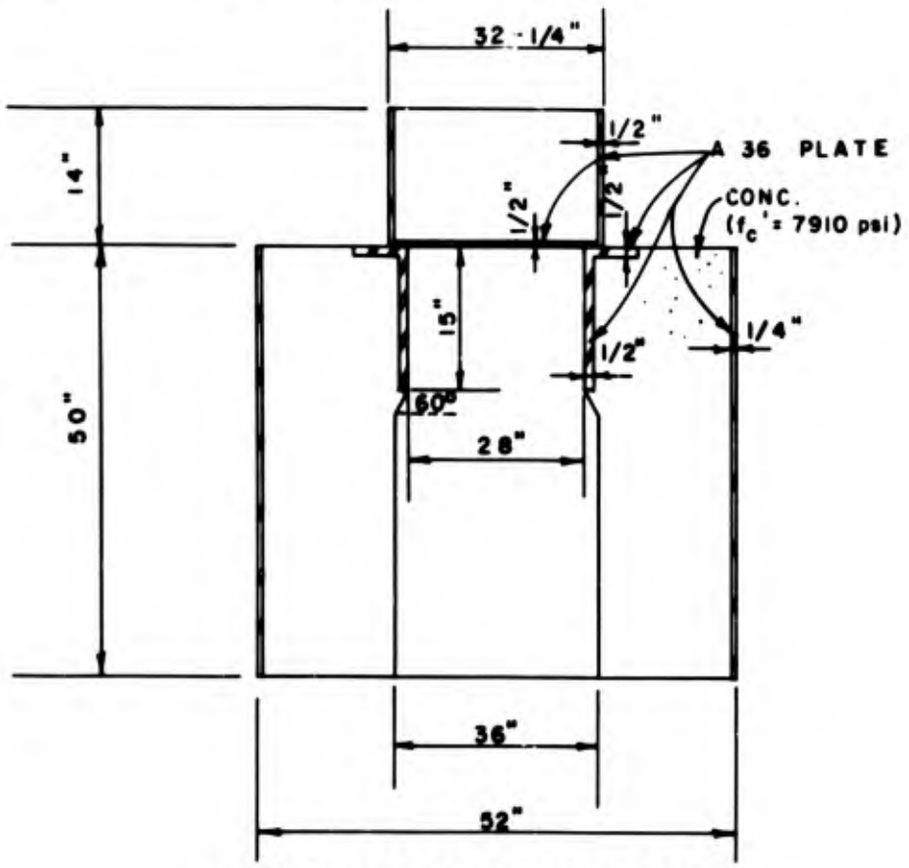

MODEL GEOMETRY FOR TEST 40

FIGURE 3-168

As shown in Figure 3-169, the system failed at the 4234-psi load level, which correlates well with all previous support data.

Post-test inspection revealed radial cracks extending down into the silo area, as well as a shear crack at the beginning of the haunch (Figure 3-170). The

vertical cracks along the sidewalls (Figure 3-171) attest to the reduced stiffness of the outer confinement ring, which allowed the section to grow, thus causing the cracks to form.

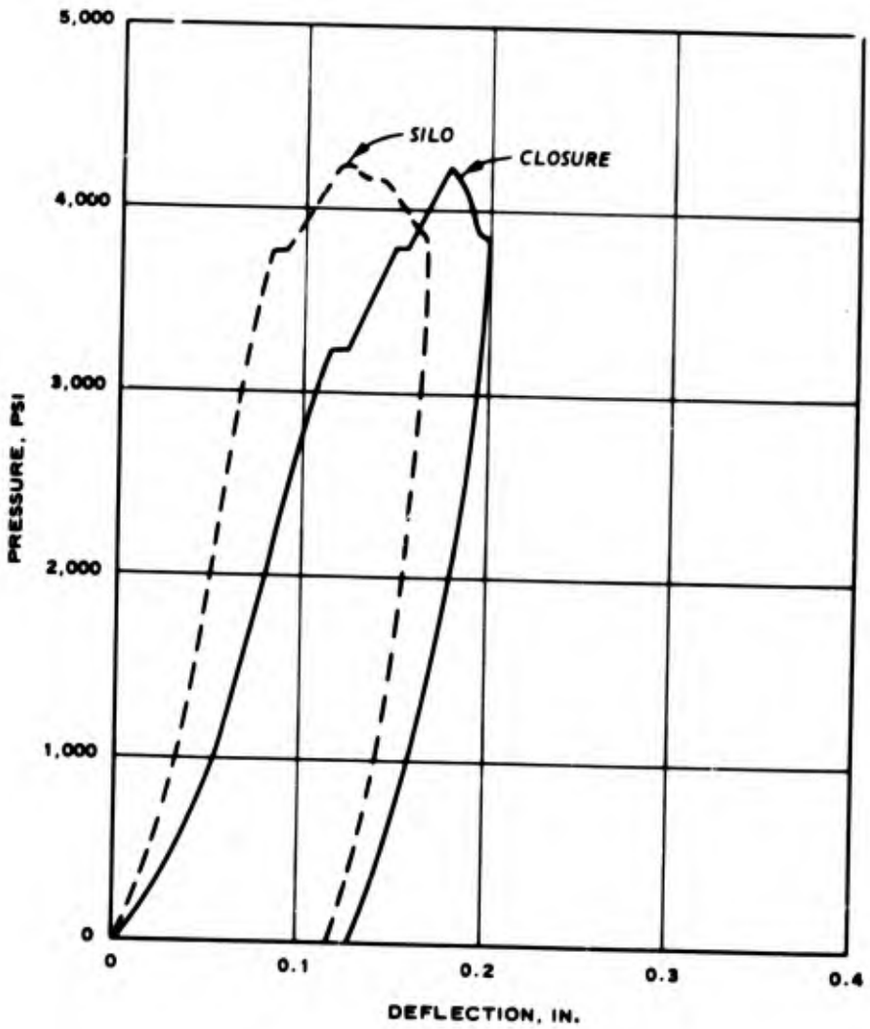

CLOSURE M130-7-6 AND SUPPORT M131-10 TEST 40 - PRESSURE VS. DEFLECTION

FIGURE 3-169
A2-199

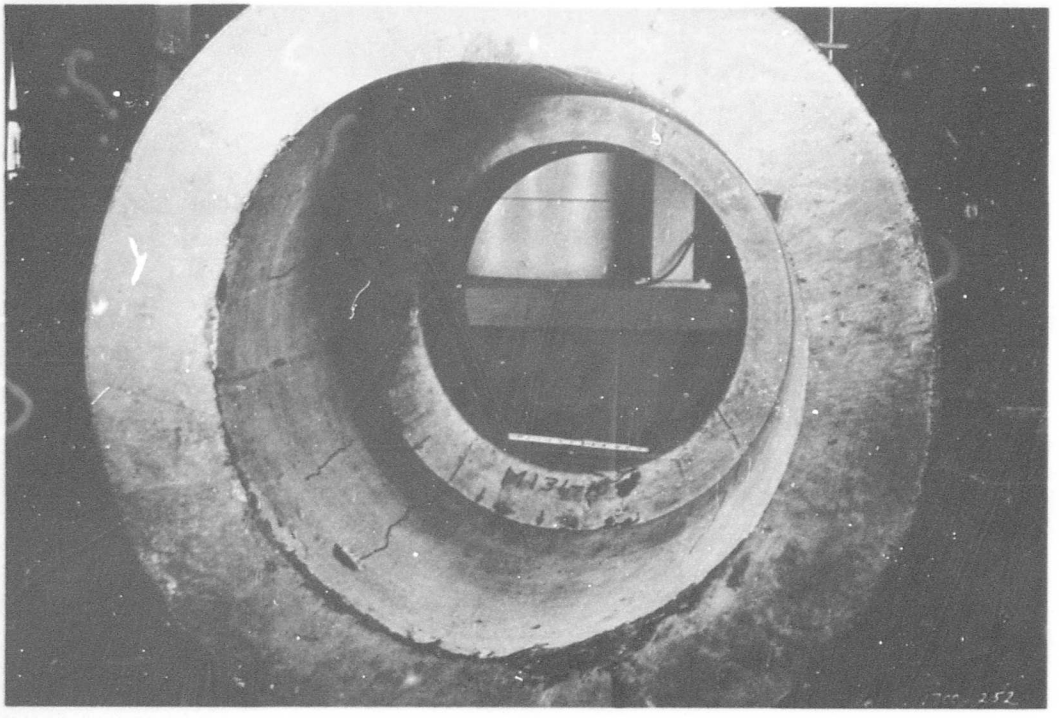

TEST 40

FIGURE 3-170

TEST 40

FIGURE 3-171

A2-200

TEST 41

In Test 41 a support structure without a bearing plate was tested with a closure model identical to that used in several previous tests. The support structure was selected so that it would resemble those of Tests 31, 34, 36 and 37. The model geometry for Test 41 is shown on Figure 3-172. It was anticipated that the load capacity of this structure would be relatively the same as in the other structures since the confined concrete below the closure bearing had previously exhibited high compressive strength characteristics.

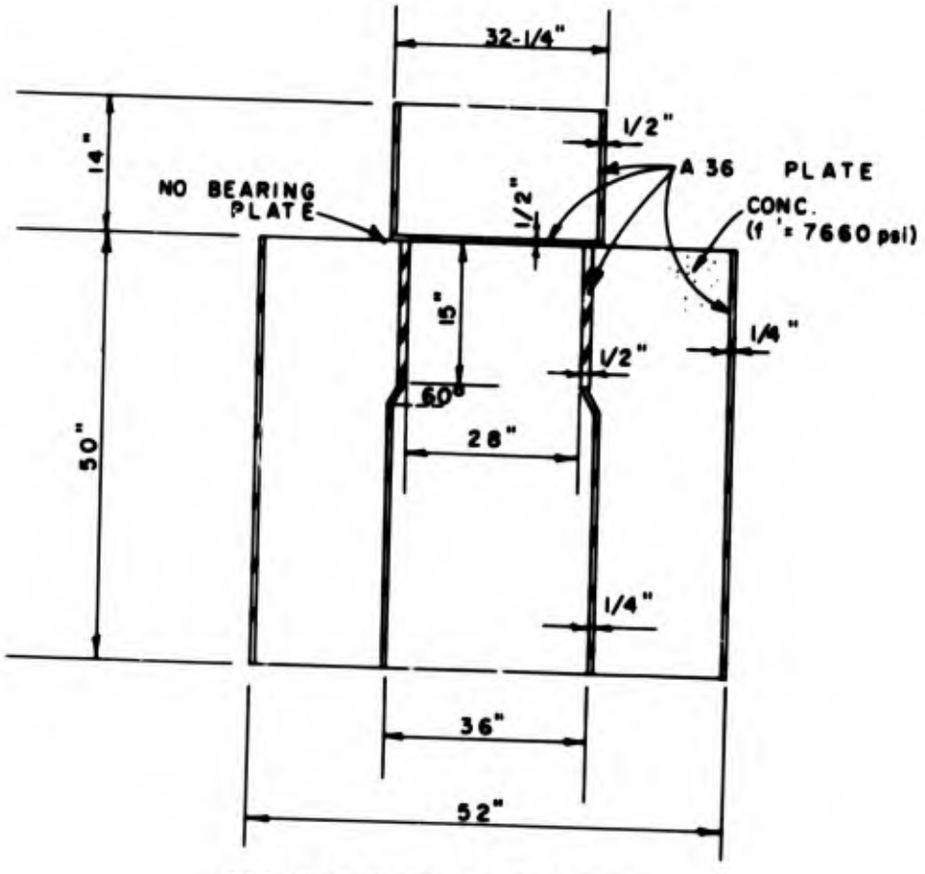

MODEL GEOMETRY FOR TEST 41

FIGURE 3-172

As shown in Figure 3-173, the collapse load for the system was 5000 psi, which compares well with the 5300- and 5500-psi load capacity observed in Tests 36 and 37, respectively. The load was lower than the 6375 psi observed in Test 8

in a similar structure with a bearing plate. This is apparently due to difference in the mode of response. In the Phase II support tests, vertical shear crack was observed at the bearing haunch which was not evident in Phase I.

It is significant that the haunched structures with similar geometric configurations all failed at approximately the same load level. Therefore it may be concluded that the capacity of the silo support is governed by the shear on the haunch section; the bearing plate below the closure structure does not contribute to any extent to the load capacity of the support structure. Pressure seals, or other system requirements, would necessitate a bearing plate in an operational support structure.

On the basis of the available shear area and the total load applied, the pure shear strength of the haunch is approximately 0.24 f'_c, which compares well with the value of 0.2 f'_c that is common in the literature.

In Figure 3-174, a local failure is evidenced by the displacement of the concrete in the area directly under the closure bearing.

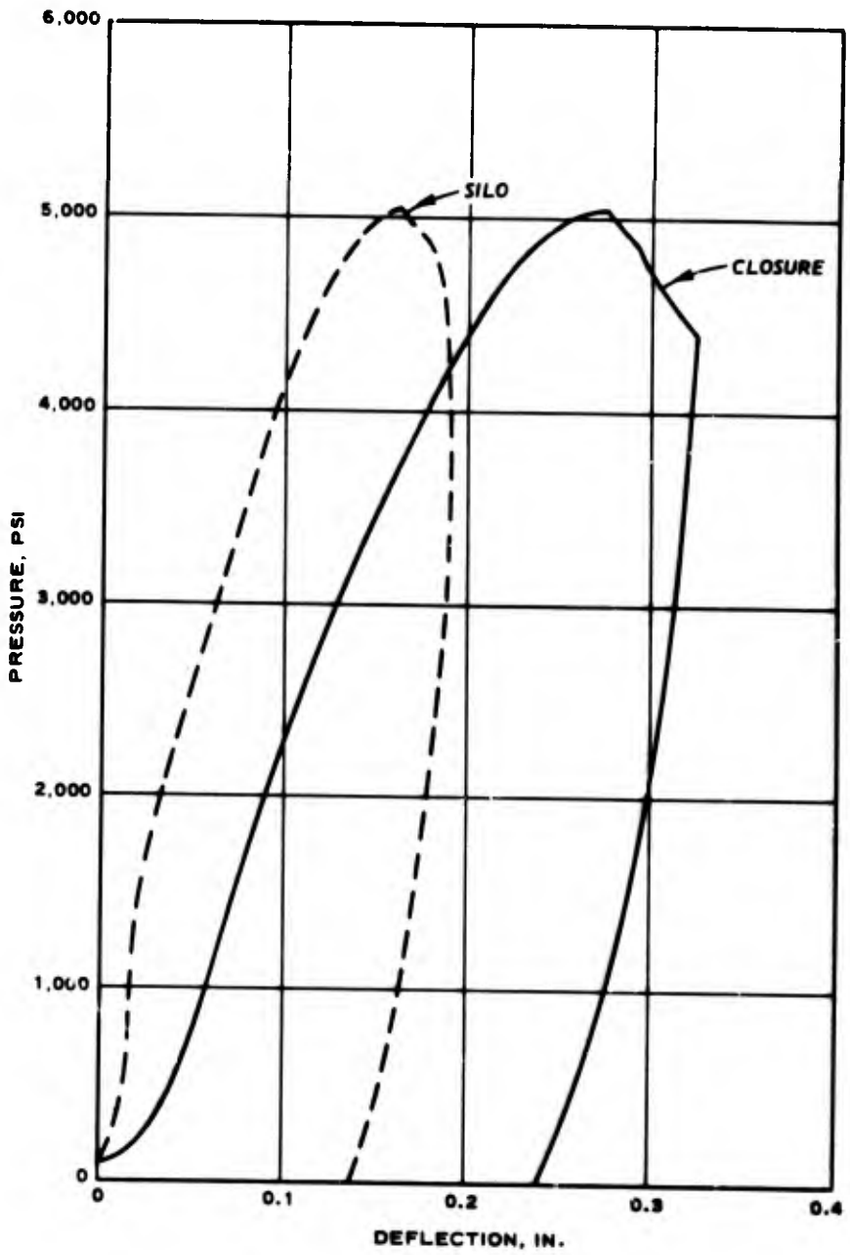

CLOSURE M130-7-5 AND SUPPORT M131-9 TEST 41 - PRESSURE VS. DEFLECTION

FIGURE 3-173

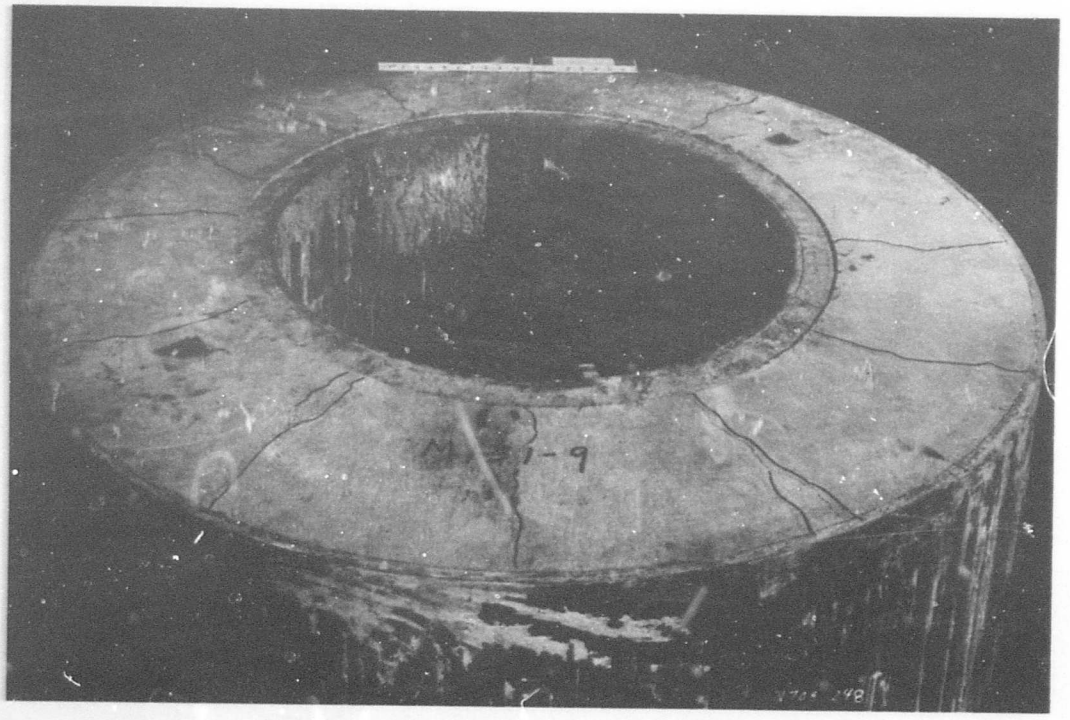

TEST 41

FIGURE 3-174

A2-204

4.0 SUMMARY AND CONCLUSIONS

4.1 Effects of Various Structural Parameters

The subscale static tests performed as part of the Closure Analysis and Test (CAT) Study covered a broad range of test parameters and variables of both closure and silo support models. In the following paragraphs, the parameters investigated and the effects of each are summarized.

4.1.1 Steel Plate Thickness

For steel of any particular yield strength, the plate thickness provided in a composite closure significantly affects the load capacity and also influences the failure mode. With thin plates, a sudden diagonal tension shear failure was observed; when the plate thickness was increased, the failure mode changed to a gradual or ductile local bearing failure which was initiated by yielding of the side steel shell.

Available strain records indicate that the most severely stressed portion of the closure is the side shell near the bearing. Large vertical strain, presumably introduced by friction load transfer from the concrete was observed, as well as large hoop strain, presumably introduced by the radial expansion of the concrete in the bearing area.

The effect of the variation in plate thickness can be seen in Tests 1 through 4, 7, 8, 13, 14, 17, 22, and 24 through 30. Figure 4-1, which is a plot of load capacity versus plate thickness/span ratio, shows that a change

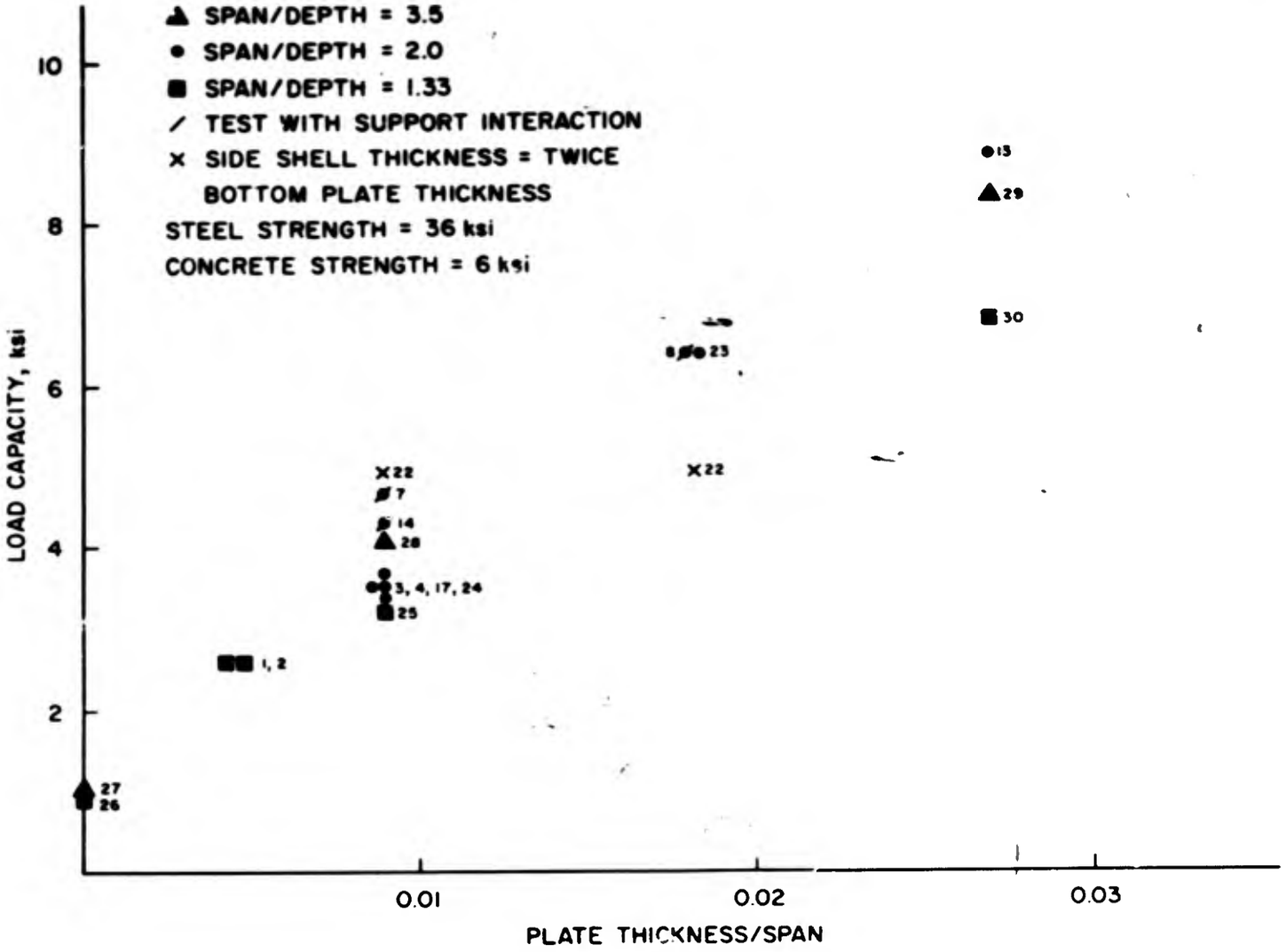

CLOSURE TEST DATA
LOAD CAPACITY VS. PLATE THICKNESS/SPAN RATIO

FIGURE 4-1

in plate thickness is of far greater significance than a change in any of the other variables tested under this study program.

4.1.2 Steel Strength

Closure models with steel plates of various yield strengths were tested to ascertain if failure could be attributed to steel strength or steel deformation. Tests 3, 4, and 16 through 21 were used to examine this test variable. It appears that, except in the case of the 150-ksi steel, the ultimate strength of the steel plate is far more significant than the thickness as such. This influence is also noted in the observed failure modes which again are a function of total plate strength rather than steel stiffness.

The influence of the steel strength may be observed in Figure 4-2, which is a plot of load capacity versus steel strength.

4.1.3 Concrete Strength

The effect of concrete strength was examined in Tests 3, 4, 16 through 20, and 24. It was hypothesized that the influence of the concrete strength would be linear since both the pure shear strength and the bearing strength of concrete vary linearly with the unconfined compressive strength. The influence of this parameter can be seen in Figure 4-3 where the load capacity versus concrete strength is plotted.

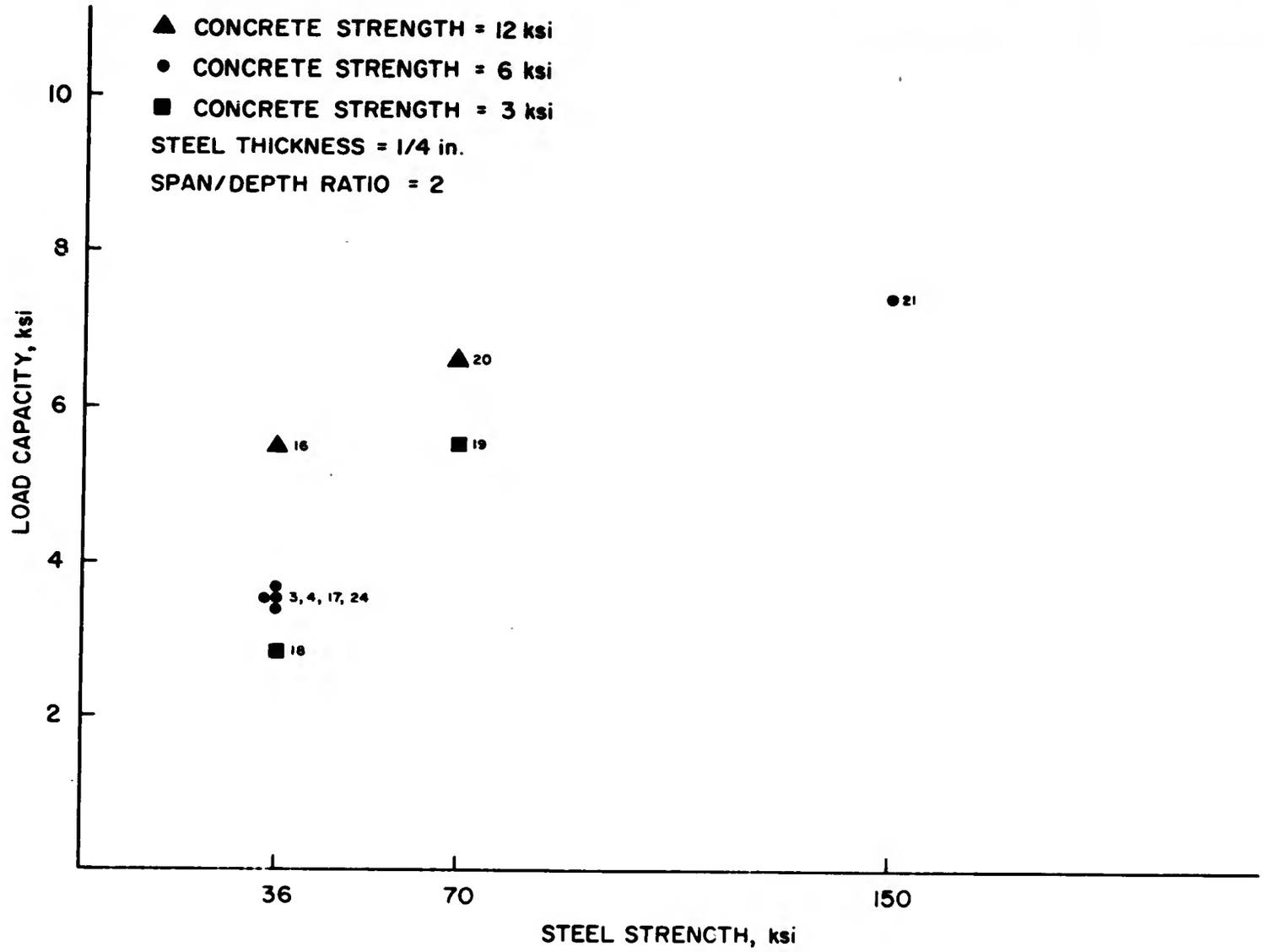

CLOSURE TEST DATA
LOAD CAPACITY VS. STEEL STRENGTH
FIGURE 4-2

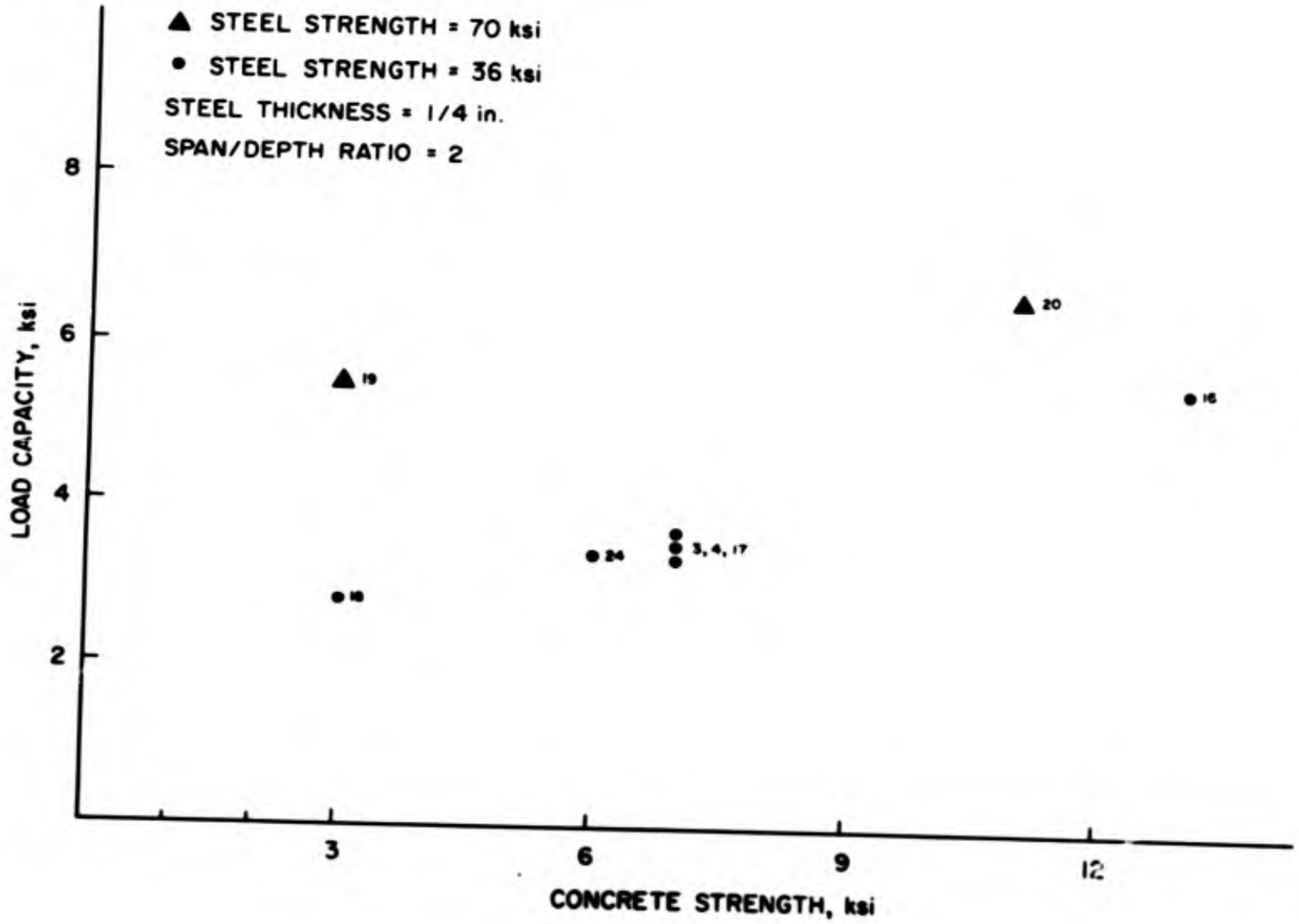

CLOSURE TEST DATA
LOAD CAPACITY VS. CONCRETE STRENGTH
FIGURE 4-3

4.1.4 Span-to-Depth Ratio

The effect of the span-to-depth ratio was examined in Tests 3, 4, 13, 17, and 24 through 30. The failure mode was essentially the same for the various ratios tested; however, in the thinner sections bending distress was evident in addition to the shear and bearing yielding more common in the thicker models. The influence of the concrete strength may be examined in Figure 4-4 where the load capacity versus span-to-depth ratio is plotted.

From these test results, it can be concluded that for practical design purposes the design thickness of the closure will be governed by radiation requirements.

4.1.5 Bearing Width

The effect of the bearing width on total load capacity of closure structures was not fully examined in this test series since the program objectives somewhat limited the study to established bearing widths. Tests 32 and 35, in which structures with wide bearings were tested, could not be correlated directly with other testing. Is is postulated that increased bearing width would yield somewhat higher load capacities for a given closure structural geometry. However, as increased bearing width poses system disadvantages because of the increased closure mass and area, and high bearing stresses can be safely resisted by proper design, no justification is seen for further examination of this variable.

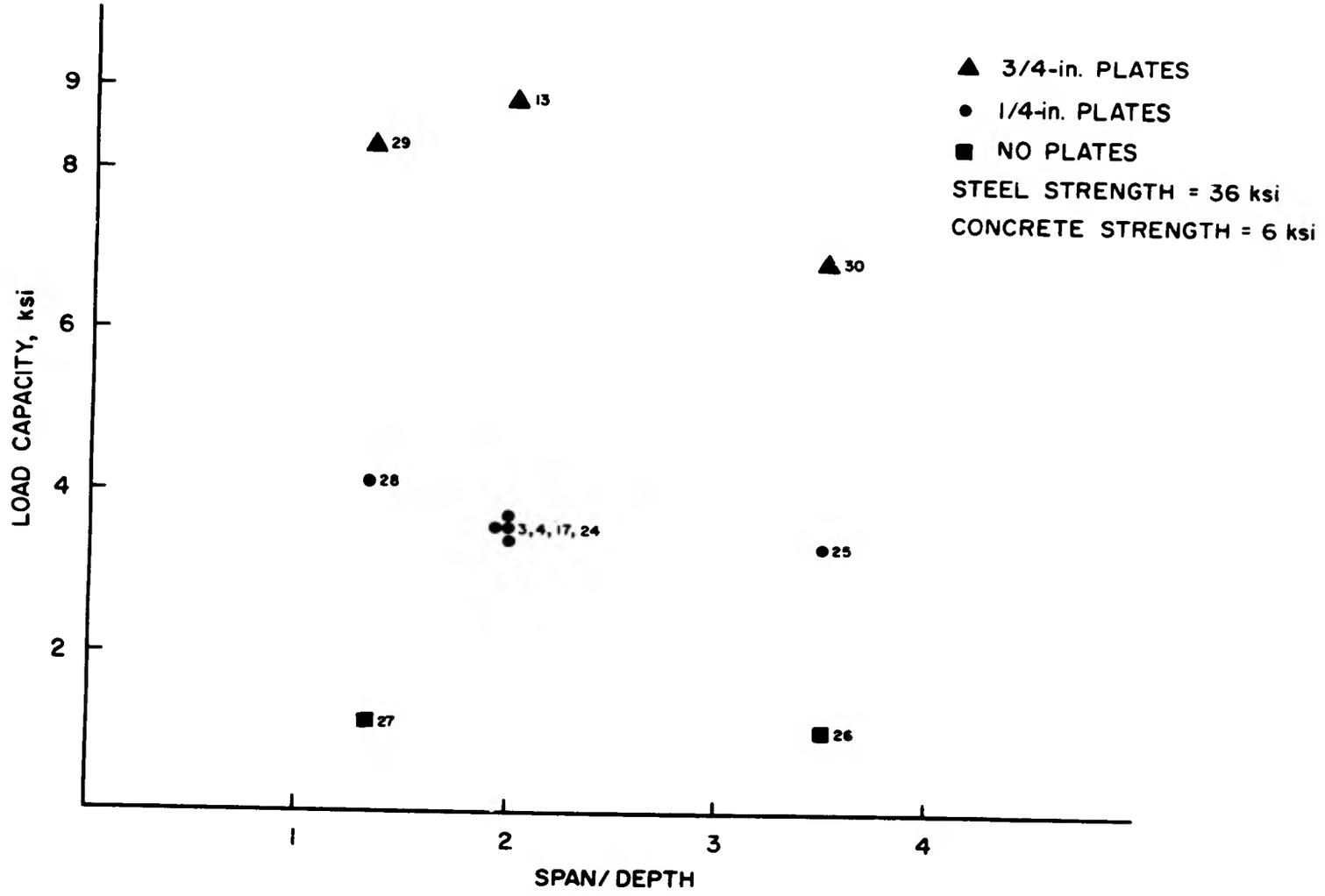

CLOSURE TEST DATA
LOAD CAPACITY VS. SPAN/DEPTH RATIO
FIGURE 4-4

4.1.6 Interaction Phenomenon

Before initiation of the static testing program, the influence of support friction on total closure/load capacity had been widely discussed, but there was actually very little known about this phenomenon. It was postulated that high friction would cause the concrete in the closure to arch across to the bearing in the form of a dome, and would thus greatly enhance the load capacity of the model.

Most of the tests were performed on a low friction support. In some cases, duplicate tests were performed on high friction bearings or on support structures where steel-to-steel bearing was available. Tests 7, 8, and 14 are of interest as they may be correlated directly with low friction tests. The load capacities obtained in Tests 7, 8 and 14 are in good agreement and indicate that support interaction through high friction can increase closure capacity by as much as 20 percent.

For practical design purposes, it is recommended that this phenomenon be ignored, since present test results indicate that it is probably of secondary importance. If future testing is performed, this parameter could then be explored in more detail.

4.1.7 Support Structure

In the first phase of testing, support structures were constructed with different bearing rings and outer shells, but the inner confinement ring thickness was held constant. In all supports collapsed during Phase I, the

failure mode was similar. Radial cracks were evident in the concrete as well as the formation of an arch to the outer steel shell. Tests 5, 6, and 8 through 11, which explored the support phenomenon, indicate that the strength of the outer confinement ring significantly influences the load capacity of the support structure. This does not imply that the inner confinement wing is not also of primary importance; however, as the vertical load is distributed at an angle of 45 degrees from the edge of the closure, the vertical stress intensity is rapidly reduced.

Figure 4-5 shows the load capacity versus outer shell thickness/outer shell diameter ratio, and Figure 4-6 shows the load capacity versus the bearing plate thickness/closure span ratio.

In the second phase of testing, support structures were constructed with haunches under the bearing area. The failure mode was essentially the same for all of these models. A pure shear crack formed at the top of the bearing surface and progressed to the haunch interface with the main structure. The value of shear along this plane at collapse compared well with the 0.2 f'_c common in the literature. This phenomenon is indicated in Tests 31, 36, 37, 40 and 41. In Test 34, where a narrow bearing was tested, a local failure was observed (as was expected), but could not be correlated with other test data.

It is recommended that the failure mode of closure support structures be thoroughly investigated in future testing efforts.

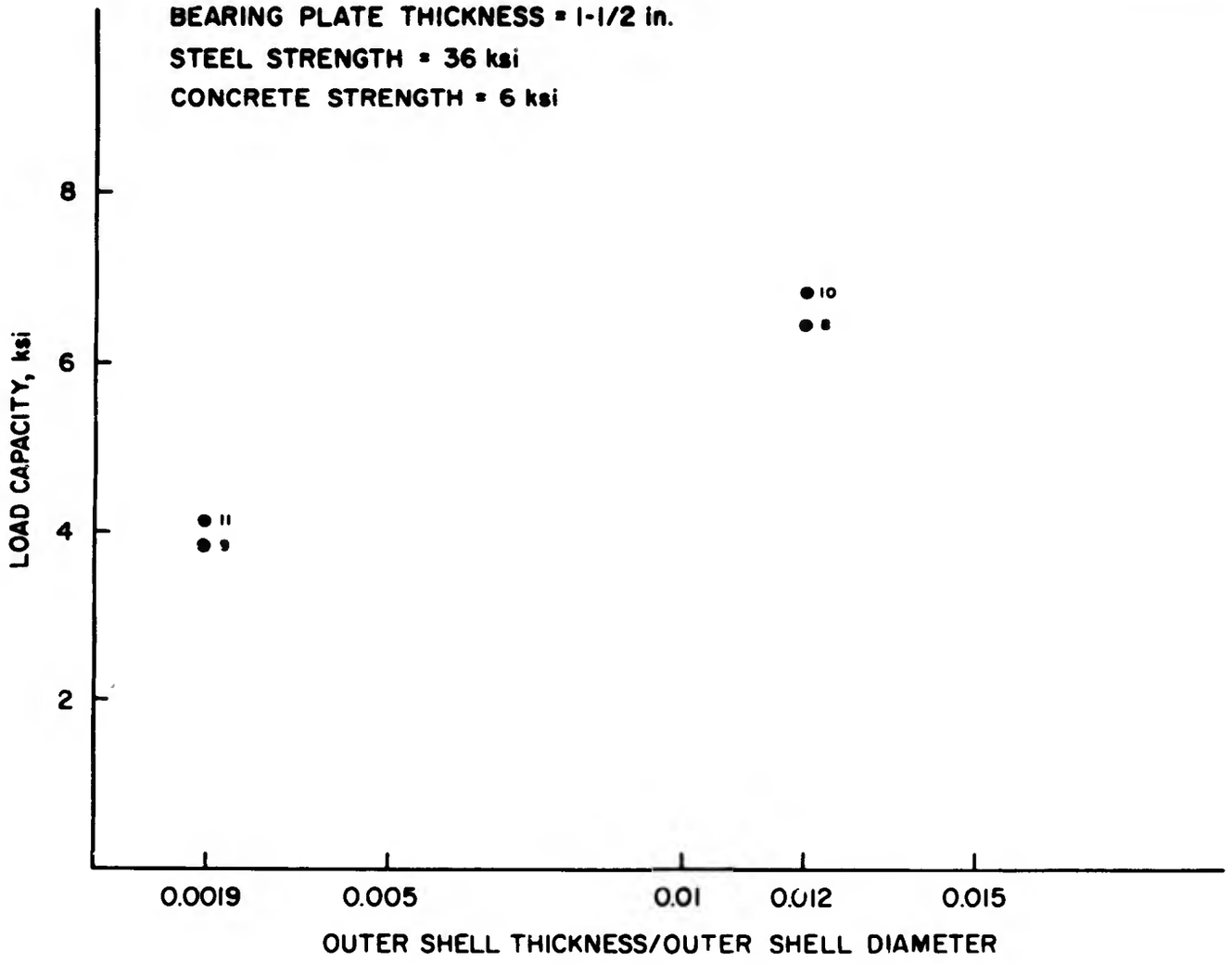

CLOSURE SUPPORT TEST DATA
LOAD CAPACITY VS. OUTER SHELL THICKNESS/OUTER SHELL DIAMETER RATIO
FIGURE 4-5

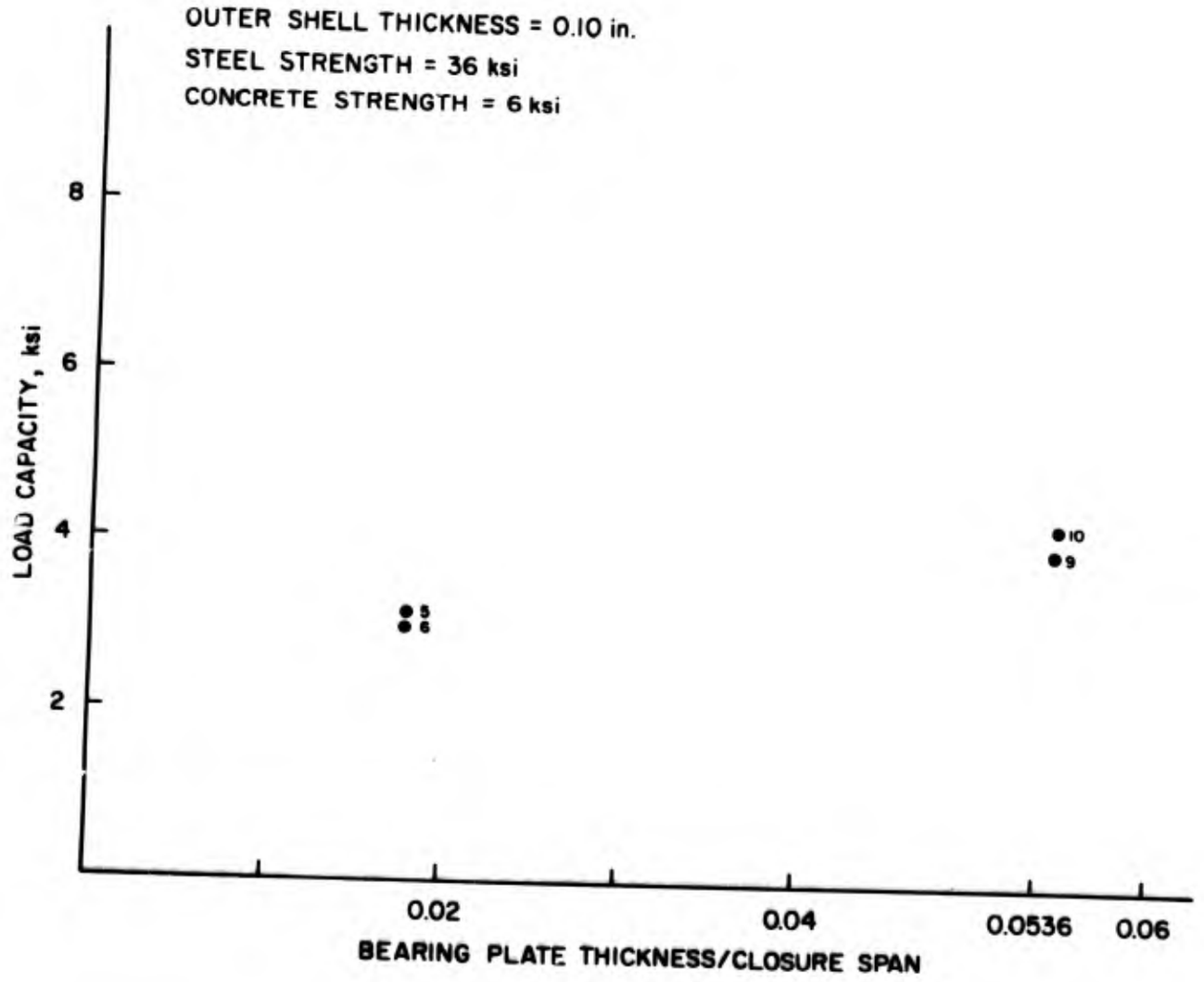

CLOSURE SUPPORT TEST DATA
LOAD CAPACITY VS. BEARING PLATE THICKNESS/CLOSURE SPAN RATIO
FIGURE 4-6

4.2 Best Representation of Closure Data

Representative closure test data were further analyzed to verify the assumed response modes. To obtain the best representation of the test data, load capacity was plotted versus a nondimensional closure geometry and steel strength parameter $(t/D)\ f_s$,

where

t = plate thickness

D = clear span

f_s = steel yield point strength

This plot is shown in Figure 4-7; here the effects of many of the parameters investigated may be observed. Examination and comparision of these parametric variations suggested that a regression analysis of the test data would be useful. This analysis is discussed in the following paragraph.

4.3 Regression Analysis of Test Data

Since the static tests explored many parameter variations in detail, a statistical model of the variation in collapse load Q with a given set of test parameters was developed to obtain an analytic expression for Q as a function of d_1, h, t_s, t_b, f'_c, and f_s for the closure structure.

From dimensional studies it became apparent that a number of parameters could be grouped as single variables; then the linear regression analysis

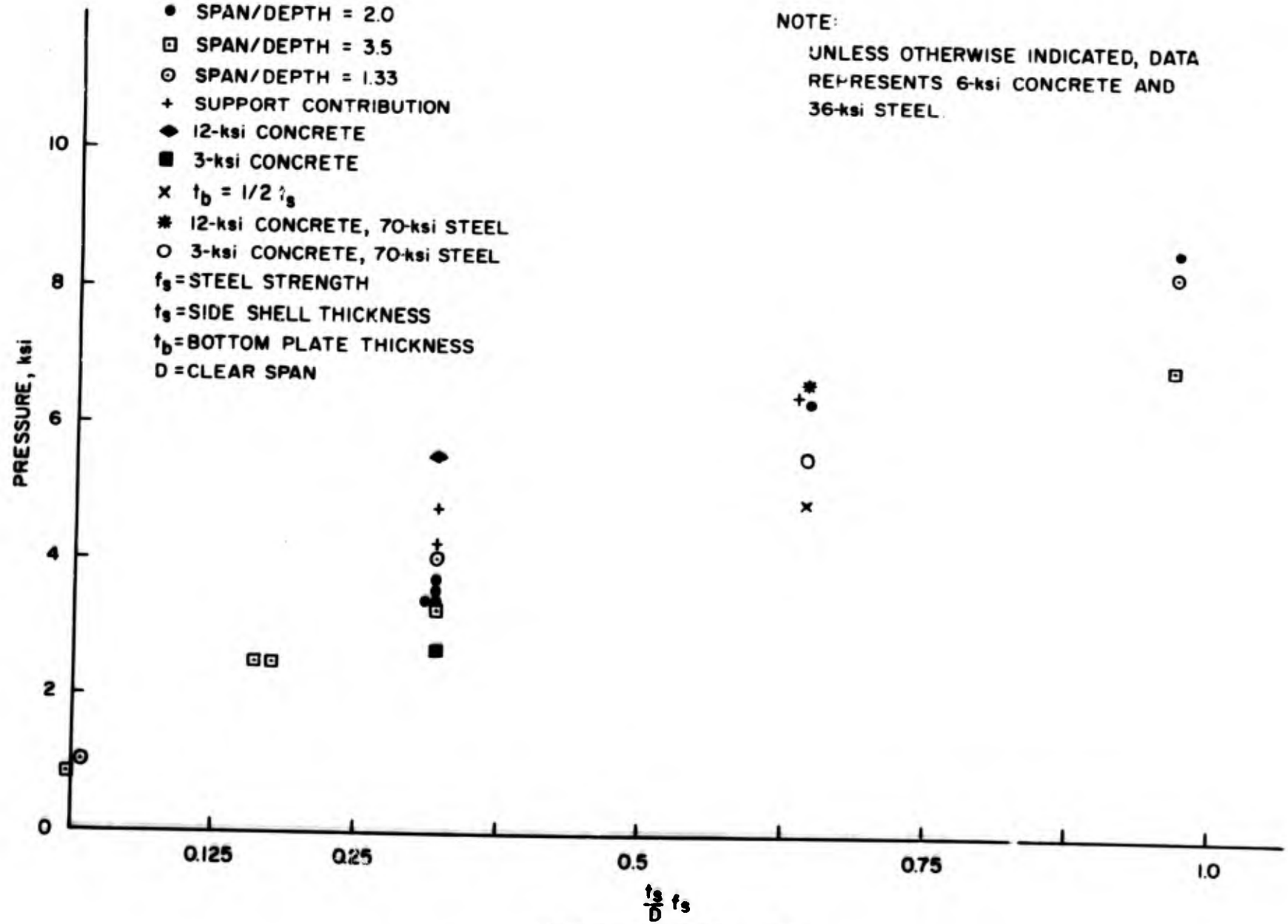

A2-217

STATIC TEST DATA LOAD
LOAD CAPACITY VS. NONDIMENSIONAL SHELL THICKNESS
FIGURE 4-7

based on these grouped variables could be used over most of the range of collapse load values. The functional model chosen was

$$Q = B_o + B_1 \left(\frac{t_s}{d_1} f_s\right) + B_2 \left(\frac{t_b}{d_1} f_s\right) + B_3 \left(f'_c\right)$$

B_o, B_1, B_2, B_3 = the linear regression coefficients

Using 23 sets of sampling data available, the regression coefficients B_o, B_1, B_2, and B_3 were determined using a multiple-regression and correlation analysis. Their values were:

$$B_o = 0.40$$

$$B_1 = 4.9$$

$$B_2 = 2.3$$

$$B_3 = 0.23$$

The above constants are to be used in conjunction with stresses in kips per square inch. The following limits must be considered in light of the experimental data available:

$$1.35 \leq \frac{h}{d} \leq 3.5$$

$$0.00 \leq \frac{t_b}{d} \text{ \& } \frac{t_s}{d} \leq 0.03$$

$$36 \text{ ksi} \leq f_s \leq 70 \text{ ksi}$$

$$3 \text{ ksi} \leq f'_c \leq 12 \text{ ksi}$$

The multiple-regression coefficient for this model was 0.9, which shows good correlation indicating that the function fits the data well.

4.4 Conclusions

- A closure/closure support structure may be designed to resist static loads significantly above the 1-kilobar pressure level. This was demonstrated in Tests 38 and 39 where closure/closure supports were tested to 23,000 psi and 16,000 psi, respectively.
- The most critical closure design parameter is the strength capacity of the closure plates.
- The total strength capacity is more important than the stiffness of the plates up to the point where the critical strain is reached in the concrete.
- The side shell is of primary design importance since it not only acts a confinement vessel for the concrete in the bearing area but also carries much of the vertical load into the bearing structure. This vertical load component is apparently introduced into the steel shell by friction between the concrete and steel.
- For a given steel bottom plate and side shell configuration, the load capacity of composite closures will vary as a function of the concrete strength. However, as our ability to define the actual material properties of concrete is still rather primitive, it is recommended that, for full-scale designs, concrete strength requirements be limited to 6000 psi.

- The span-to-depth ratio had minor effect on the total load capacity in the models tested. In the thinner section bending distress was evident, but this did not significantly influence the total load capacity.
- Support/closure interaction phenomenon such as increased friction between the model and support does not appear to increase the load capacity more than 20 percent in any situation. Therefore, it is recommended that for practical design purposes these effects be ignored.
- A closure support structure may be designed to successfully resist static loads significantly above the 1-kilobar pressure level, as was shown in Tests 38 and 39.
- Failure in the structures with haunches below the bearing was due to a pure shear failure in the haunch. In all cases where this failure was observed, the shear stress along the failure plane was computed to be near the 0.2 f'_c referenced in the literature.
- Failure in the support structures without haunches was due to radial cracks and the arch formations carrying load to the outside shell.
- In the structures tested, the load capacity was most dependent on the outer shell strength. The bearing plate thickness has only minor influence, and the inner ring does not appear critical if sufficient confinement is provided for the concrete.

A regression analysis of the test data for the closure structures yielded a simple functional representation of the failure load level in terms of closure geometric and strength parameters.

The developed function had the form of

$$Q = 0.40 + 4.9 \left(\frac{t_s}{d_1} f_s\right) + 2.3 \left(\frac{t_b}{d_1} f_s\right) + 0.23 f'_c$$

where

Q = load capacity

t_s = side shell thickness

t_b = bottom plate thickness

d_1 = closure clear span

f_s = steel yield point

f'_c = unconfined concrete compressive strength

The above constants are to be used in conjunction with stresses in kips per square inch. The following limits must be considered in light of the experimental data available:

$$1.35 \leq \frac{h}{d} \leq 3.5$$

where

h = section depth

$$0.00 \leq \frac{t_b}{d} \;\&\; \frac{t_s}{d} \leq 0.03$$

$$36 \text{ ksi} \leq f_s \leq 70 \text{ ksi}$$

$$3 \text{ ksi} \leq f'_c \leq 12 \text{ ksi}$$

Unclassified
Security Classification

DOCUMENT CONTROL DATA - R & D

(Security classification of title, body of abstract and indexing annotation must be entered when the overall report is classified)

1. ORIGINATING ACTIVITY (Corporate author)
The Ralph M. Parsons Company
617 West Seventh Street
Los Angeles, California 90017

2a. REPORT SECURITY CLASSIFICATION
Unclassified

2b. GROUP

3. REPORT TITLE
Closure Analysis and Test Study, Volume IV - Subscale Static Test Report (Appendix 2)

4. DESCRIPTIVE NOTES (Type of report and inclusive dates)
Final Report. Study period June 1, 1967 - July 31, 1969.

5. AUTHOR(S) (First name, middle initial, last name)

6. REPORT DATE
July 31, 1969

7a. TOTAL NO. OF PAGES
248

7b. NO. OF REFS

8a. CONTRACT OR GRANT NO.
F04694-67-C-0105

b. PROJECT NO.
672 A Program

c.

d.

9a. ORIGINATOR'S REPORT NUMBER(S)
Technical Report No. 4171-1

9b. OTHER REPORT NO(S) (Any other numbers that may be assigned this report)
SAMSO TR 69-213, Vol. IV

10. DISTRIBUTION STATEMENT This document is subject to special export controls and each transmittal to foreign government or foreign nationals may be made only with prior approval of SAMSO ([redacted]), Norton AFB, California 92409. The distribution of this report is limited because it contains technology restricted by U.S. Mutual Security Acts.

11. SUPPLEMENTARY NOTES

12. SPONSORING MILITARY ACTIVITY
Department of the Air Force, Space and Missile Systems Organization, Air Force Systems Command, Norton Air Force Base, California 92409

13. ABSTRACT

This report describes subscale static tests of composite silo closure and closure support models performed by The Ralph M. Parsons Company as a part of the Closure Analysis and Test Study. A total of 41 tests were performed in two phases. The effect on total load capacity caused by varying a broad range of design parameters including strength and relative thicknesses of steel shell material, span-to-depth ratio, support configuration, and concrete strength were investigated. Closure/closure support combinations with ultimate load capacities ranging from 1000 psi to 23,000 psi were tested.

Manual, empirical and finite-element design and analytical techniques are presented which will yield accurate predictions of the ultimate load capacities of full-scale composite closures.

DD FORM 1 NOV 68 1473

Unclassified
Security Classification

14

KEY WORDS	LINK A		LINK B		LINK C	
	ROLE	WT	ROLE	WT	ROLE	WT
Subscale Static Load Tests, Silo Closure						
Structural Models, Silo Closure						
Static Load Fixture, Silo Closure						
Static Test Method, Silo Closure						
Model Instrumentation, Silo Closure						

AD-855786

The Ralph M. Parsons Company

Engineers · Constructors

617 WEST SEVENTH STREET, LOS ANGELES, CALIFORNIA 90017

December 9, 1969

Department of the Air Force
Space and Missile Systems Organization (AFSC)
Norton Air Force Base, California

Vol. 1 = AD855784 *
Vol. 2 = AD855785 *
Vol. 4 = AD855786 *

ATTENTION of Lt. H. S. Yoshioka, SMQHF

SUBJECT Job No. 4171-1 - Closure Analysis & Test Study
Errata to Final Report Volumes I, II and IV

REFERENCE Contract No. F04694-67-C-0105

Gentlemen:

It is requested that the changes listed below be made in your copies of Volumes I, II and IV of Closure Analysis and Test Study, dated 31 July 1969.

On Page 4-39 of Volume I, "Project Summary and Abstract of Findings," Page 6-53 of Volume II, "Technical Report," and Page A2-218 of Volume IV, "Subscale Static Test Report," the value for the regression coefficient B_o is in error and should be corrected to read as $B_o = -0.40$, as shown below:

Incorrect	Correct
$B_o = 0.40$	$B_o = -0.40$
$B_1 = 4.9$	$B_1 = 4.9$
$B_2 = 2.3$	$B_2 = 2.3$
$B_3 = 0.23$	$B_3 = 0.23$

In addition, on Page A2-221 of Volume IV, "Subscale Static Test Report," the function "$Q = 0.40 + 4.9\left(\frac{t_s}{d_1} f_s\right) + 2.3\left(\frac{t_b}{d_1} f_s\right) + 0.23\, f_c'$" should be corrected to read as follows:

"$Q = -0.40 + 4.9\left(\frac{t_s}{d_1} f_s\right) + 2.3\left(\frac{t_b}{d_1} f_s\right) + 0.23\, f_c'$".